Oxidative Medicine and Cellular Longevity

Cardiolipin and Mitochondria-Targeted Antioxidants in Oxidative Stress, Disease, and Aging

Lead Guest Editor: Armen Y. Mulkidjanian
Guest Editors: Eugenia Mileykovskaya and Konstantin Lyamzaev

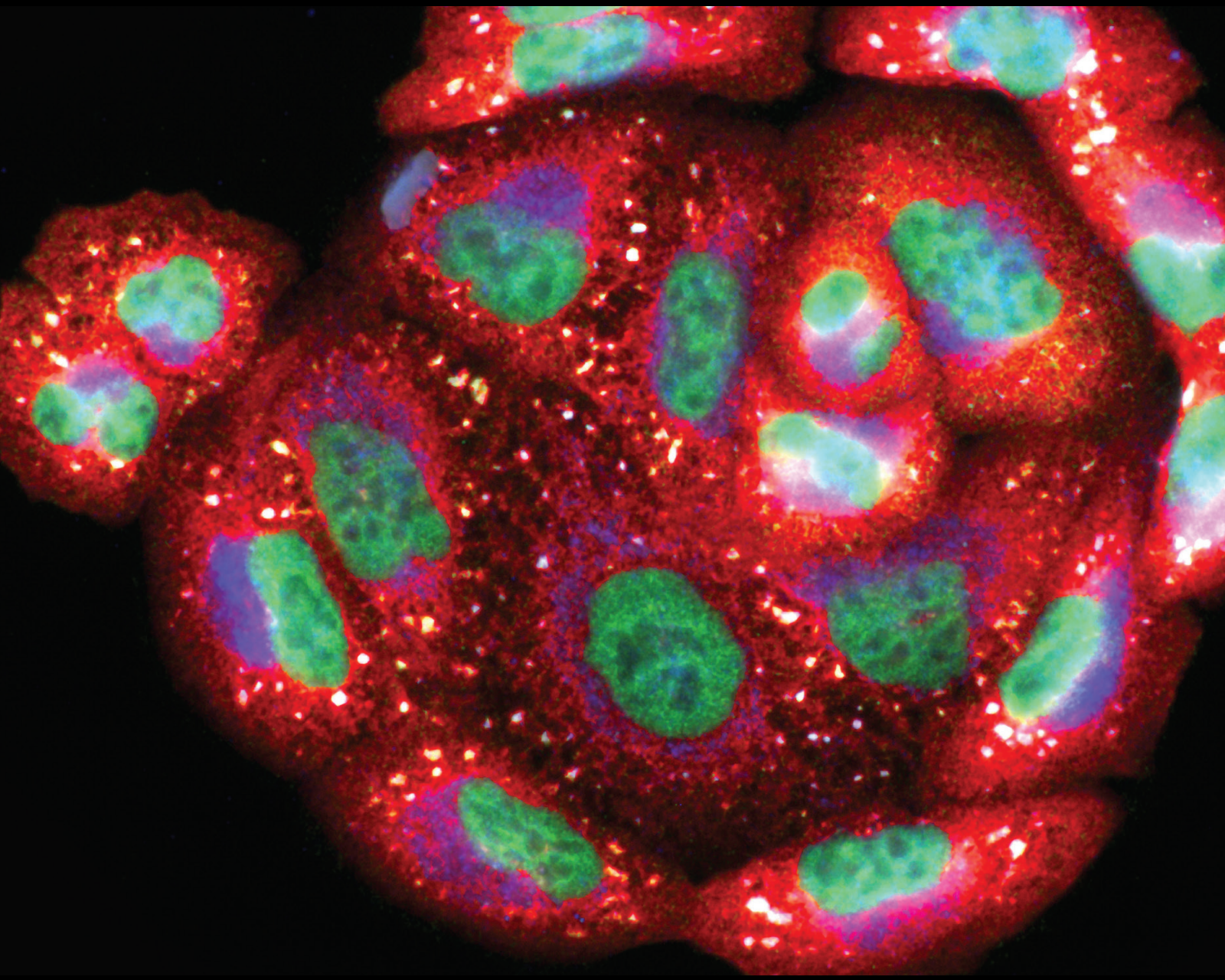

Cardiolipin and Mitochondria-Targeted Antioxidants in Oxidative Stress, Disease, and Aging

Oxidative Medicine and Cellular Longevity

Cardiolipin and Mitochondria-Targeted Antioxidants in Oxidative Stress, Disease, and Aging

Lead Guest Editor: Armen Y. Mulkidjanian
Guest Editors: Eugenia Mileykovskaya and Konstantin Lyamzaev

Contents

Hindawi
Oxidative Medicine and Cellular Longevity
Volume 2020, Article ID 1323028, 14 pages
https://doi.org/10.1155/2020/1323028

Review Article

Cardiolipin, Perhydroxyl Radicals, and Lipid Peroxidation in Mitochondrial Dysfunctions and Aging

Alexander V. Panov[1] **and Sergey I. Dikalov**[2]

[1]*Federal Scientific Center for Family Health and Human Reproduction Problems, 16 Timiryasev str., Irkutsk, 664003, Russian Federation, Russia*
[2]*Division of Clinical Pharmacology, Vanderbilt University Medical Center, Nashville, TN 37232, USA*

Correspondence should be addressed to Alexander V. Panov; alexander.panov55@gmail.com

Received 16 April 2019; Accepted 19 February 2020; Published 9 September 2020

Guest Editor: Armen Y. Mulkidjanian

Mitochondrial dysfunctions caused by oxidative stress are currently regarded as the main cause of aging. Accumulation of mutations and deletions of mtDNA is a hallmark of aging. So far, however, there is no evidence that most studied oxygen radicals are directly responsible for mutations of mtDNA. Oxidative damages to cardiolipin (CL) and phosphatidylethanolamine (PEA) are also hallmarks of oxidative stress, but the mechanisms of their damage remain obscure. CL is the only phospholipid present almost exclusively in the inner mitochondrial membrane (IMM) where it is responsible, together with PEA, for the maintenance of the superstructures of oxidative phosphorylation enzymes. CL has negative charges at the headgroups and due to specific localization at the negative curves of the IMM, it creates areas with the strong negative charge where local pH may be several units lower than in the surrounding bulk phases. At these sites with the higher acidity, the chance of protonation of the superoxide radical ($O_2^{\bullet}$), generated by the respiratory chain, is much higher with the formation of the highly reactive hydrophobic perhydroxyl radical ($HO_2^{\bullet}$). $HO_2^{\bullet}$ specifically reacts with the double bonds of polyunsaturated fatty acids (PUFA) initiating the isoprostane pathway of lipid peroxidation. Because $HO_2^{\bullet}$ is formed close to CL aggregates and PEA, it causes peroxidation of the linoleic acid in CL and also damages PEA. This causes disruption of the structural and functional integrity of the respirosomes and ATP synthase. We provide evidence that in elderly individuals with metabolic syndrome (MetS), fatty acids become the major substrates for production of ATP and this may increase several-fold generation of $O_2^{\bullet}$ and thus $HO_2^{\bullet}$. We conclude that MetS accelerates aging and the mitochondrial dysfunctions are caused by the $HO_2^{\bullet}$-induced direct oxidation of CL and the isoprostane pathway of lipid peroxidation (IPLP). The toxic products of IPLP damage not only PEA, but also mtDNA and OXPHOS proteins. This results in gradual disruption of the structural and functional integrity of mitochondria and cells.

1. Introduction

For the last five decades, the free radical theory of aging, first proposed by Harman [1–3], was regarded as one of the most important and investigated among other hypotheses of aging. Accumulation of mtDNA point mutations [4] and an exponential increase with age of mtDNA deletions [5] were considered as important hallmarks of ageing and the age-related diseases. Accumulation of mtDNA mutations with increasing age was demonstrated mainly in heart, skeletal muscles, and brain, which undergo a high range of workloads and associated metabolic activities. In the liver, which has relatively stable high rate of metabolism and high regeneration capacity, there was shown no significant accumulation of mtDNA mutations with age [6]. For decades, it was generally agreed that ROS-associated somatic mutations of mtDNA contribute to human aging and to the decline of energetic capabilities at higher age [5, 7].

In recent years, however, new experimental data have discredited to some extent the original theory of direct participation of free radicals in mtDNA mutations [8–10]. It has also been found that most common ROS species either are

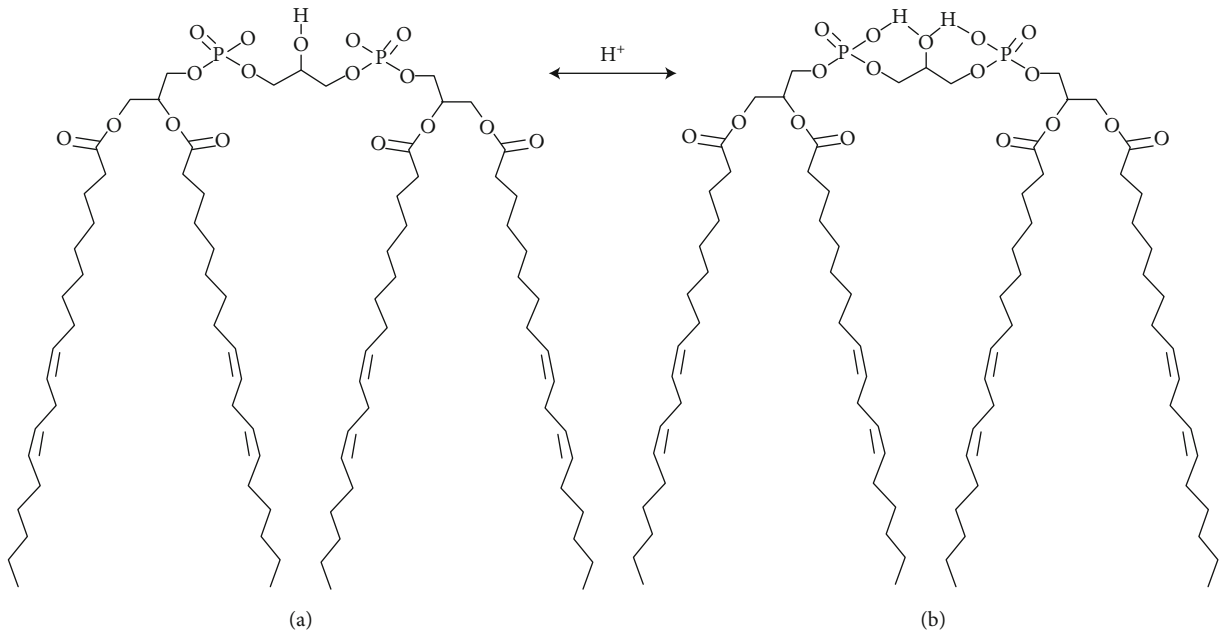

Figure 1: Cardiolipin structure. The figure depicts (for simplicity only) one of the cardiolipins–tetraoleilcardiolipin, and the two models headgroup ionization state at physiological pH 7.2. (a) Both phosphates have values of pK_{a1} of orthophosphoric acid. It is assumed that both phosphates ionize independently and the headgroup exists as a dianion. (b) Disparate pKa values of the two phosphates presume that the headgroup exists as a monoanion. The figure was adapted from [27]. Note: values for dissociation constants (pKa) of orthophosphoric acid: $pK_{a1} = 2.15$, $pK_{a2} = 7.20$, $upK_{a3} = 12.35$.

not enough chemically active ($O_2^{\bullet-}$, $^{\bullet}NO$) to initiate mutations or excessively active ($^{\bullet}OH$) and have a too short life span in order to reach mtDNA [11, 12]. Several decades ago, researchers from the Vanderbilt University have discovered the isoprostane pathway of lipid peroxidation (IPLP), which results in the formation of prostaglandin-like compounds with enormous variations in molecular positional isomerism and stereoisomerism [13–16]. Considering the chemistry of IPLP, we have proposed the mechanism of initiation of IPLP involving formation in the inner mitochondrial membrane of perhydroxyl radical ($HO_2^{\bullet}$), which is the protonated form of superoxide radical ($O_2^{\bullet-}$) [12, 17]. We suggest that the mechanisms of action of perhydroxyl radical ($HO_2^{\bullet}$) can explain the mechanism of initiation of the autoxidation of polyunsaturated fatty acids that are still part of the membrane's phospholipid. In addition, $HO_2^{\bullet}$ can be regarded as a "carrier" of the highly toxic hydroxyl radical ($^{\bullet}OH$) inside the hydrophobic core of the membrane and thus can oxidize cardiolipin. This can happen in spite the fact that normally CL contains four linoleic acids with only two double bonds, which are not substrates for IPLP. In this review, we will focus on the roles of cardiolipin in oxidative stress due to the ability of this phospholipid to create, close to the surfaces of the inner mitochondrial membrane, the narrow layer of structured water with low pH and high conductance for protons [18–20]. This facilitates conversion of $O_2^{\bullet-}$, produced by the respiratory chain, into $HO_2^{\bullet}$ that initiate IPLP [12, 17]. We consider that formation of toxic products, such as isolevuglandins (aka isoketals), produced by IPLP, as the major event in oxidative stress that is responsible for the slow but inevitable process of aging. The gradual accumulation of oxidative damages to mitochondrial enzymes and the membrane phospholipids, first of all phosphatidylethanolamine and cardiolipin, causes disruption of the structural and functional integrity of the respirosomes and ATP synthase.

2. Properties of Cardiolipin

Cardiolipin (CL) is the only phospholipid that is present almost exclusively in the inner mitochondrial membrane of all animals and in the plasma membrane of aerobic bacteria. That is in the membranes, where ATP is formed by the F_0F_1 ATP synthase [21]. CL is absent in the thylakoids of plants, where it is substituted by the plant sulfolipid (Sulfoquinovosyl dipalmitoylglycerol), probably because chloroplasts have another isoform of ATP-synthase (CF_0CF_1) [22], and, most importantly, the reversed, as compared to mitochondria, orientations of the energy-transforming enzymes, pH gradients, and electrical charges. The tight connection between the F_0F_1-ATP-syntahse and cardiolipin was proved by experiments, in which facultative anaerobes were placed into the oxygen-depleted atmosphere, and after a while, they lost not only F_0F_1-ATP-syntahse, but also cardiolipin [21].

The structure of the cardiolipin molecule was thoroughly described and discussed in [21, 23, 24]. The significance of CL specifically for the energy-transforming membranes comes from several intrinsic properties of the phospholipid, which originate from its unique structure (Figure 1). Due to the conical form, CL, together with also conical phosphatidylethanolamine (PEA), supports the superstructural organization of the respiratory chain and ATP synthase and allows accommodation of the multienzyme complexes into the

sharp curves of the inner membrane. Due to the conical form and strong negative charges at the headgroups, CL has the propensity to form inverted hexagonal (HII) structures, which are essential for activation of the respiratory chain enzymes and ATP synthesis by promoting binding and conductance of protons through the hydrophobic milieu of the inner membrane [25–28] (Figure 1).

Figure 1 does not reflect fully the fact that the shape of CL resembles that of a pyramid or cone with the broad base and a very small head, which has the length of a glycerol molecule with three C atoms. In most cardiolipins, the fatty acids have usually two double bonds and therefore are strongly bend. For this reason, CL, similar to PEA, cannot form "normal" bilayer membranes [25, 27]. The two phosphate groups give the CL molecule the ability to trap protons [29] and thereby to facilitate proton translocation along the membrane surface [30].

In general, it has been found that composition of the four fatty acids in CL has small variations in the number of double bonds for the given organism or even tissue [31]. The selection of fatty acids in CL is specific for every species and organ, but unsaturated fatty acids are most common [32]. In many animals, the "mature" CL, that is after remodeling, has four linoleic acids with two double bonds (C18:2). In the fast respiring mitochondria of animals, CL may comprise up to 20% of all lipids, and up to 80% of CL is located in the inner leaflet of the inner mitochondrial membrane [33]. In the liver mitochondria, which have relatively low respiratory activity, CL is distributed more or less evenly between the two sides of the inner membrane. The unique structure of cardiolipin results in a number of important properties [23, 34] briefly listed as follows:

(1) As the two small molecules of phosphatidic acid are located at the small "head" of the phospholipid, which is much smaller than the charged heads of other phospholipids, namely, phosphatidylcholine (PC), phosphatidylserine (PS), or phosphatidylglycerol (PG), the four fatty acids of CL are closer to each other with stronger attachments, and thus the temperature of phase transitions is higher than in the surrounding membrane. In other words, the lipids of CL are solid in comparison with the fluid lipids of surrounding phospholipids, most of which contain polyunsaturated fatty acids (PUFA). This allows protein complexes "float" being imbedded into the rafts, made of cardiolipin, and thus rearrange into functional supercomplexes, such as respirosomes

(2) Small charged heads of CL allow the phospholipid to fit proteins into negative curvatures of the inner leaflet (the matrix side) of the inner membrane

(3) Under physiological conditions, the presence of one or two negative charges at the phosphate groups allows CL to create the negatively charged regions that electrostatically interact with proteins and peptides. The excessive negative charges on the surface of rafts, comprised of many CL molecules, create the so-called antennae, when the Coulomb radii of several cardiolipins overlap and amplify a local negative charge

(4) The mobility of the head group of CL is restricted because of binding of the glycerol to two phosphatidates. Therefore, the self-shielding of phosphate groups in CL is much lower than in other phospholipids in the membrane. As a result, the phosphates of cardiolipin on the surface of the inner membrane are easily accessible for interactions with proteins, peptides, and ions, as compared with other membrane phospholipids [23]. The interactions of CL with some proteins are so strong that CL was present in the crystal structures of the isolated mitochondrial proteins, for example, complex 3 and ANT [23]. Moreover, CL is known to specifically coordinate divalent cations with high affinity [23], and the ion:-lipid stoichiometry is dependent on the CL headgroup formal charge [35].

It was suggested that distribution of the headgroup charge determines the types of nonbonding interactions that can occur among lipids, including electrostatic and hydrogen-bonding interactions [36, 37]. Clearly, for each of the above phenomena, the ionization state of CL headgroup is of fundamental importance; whether this lipid exists in the mono- or dianionic state, the charge strongly influences behavior of CL in the bilayer [27].

3. Formation of Cardiolipin Clusters with the Negatively Charged Antennae

The ability of CL to accommodate the sharp curvatures of the mitochondrial cristae explains the fact that most of CL molecules are specifically located in the inner leaflet of the inner mitochondrial membrane (IMM) and non-covalently linked to various proteins. The list of proteins linked to CL is very long and includes, first of all, the electron transport complexes of the respiratory chain, ATP-synthase, and a number of transmembrane carriers, such as ATP/ADP carrier (ANT), inorganic phosphate carrier, and uncoupling protein [26, 38]. A relatively small amount of CL, which is present in the outer leaflet of the inner mitochondrial membrane, was found to be bound to cytochrome *c*, and at the contact sites of the inner and outer membranes, CL interacts with creatine kinase and ANT [reviewed in 38].

From studies of the proteins crystals, it was deduced that CL construct bridges between proteins and thus promote existence of many proteins as dimers. It is known that all respiratory chain complexes and ATP-synthase are present in the membrane as homodimers, which, in their turn, are assembled into supercomplexes [39]. One of the consequences of the unique structure of CL is that it tends to form rafts by clustering at the sites with negative curvature of the IMM. At these sites, CL segregates laterally from other phospholipids and stabilizes the membrane, simultaneously with holding together the respirosomes [38, 40]. Although CL is the main anionic phospholipid comprising up to 20% of all phospholipids of the IMM [33], since it is located

predominantly in the inner leaflet of the IMM, particularly at the negative curves of the cristae, at some locations, concentration of CL may be high. The regions with overlapping Coulomb radii of negative charges, called antennae, are rather common all over the matrix side of the IMM [33, 41].

The phosphoester groups of most phospholipids behave as strong acids with pK_a between 1 and 3, which coincide with the pK_{a1} of the orthophosphoric acid [27]. Therefore, in the absence of the intramolecular and intermolecular interactions, which could shield the phosphates at the head of CL, it could be expected that both phosphates of CL behave similarly, and that at the neutral pH of a cell CL behaves as a dianion [27]. Indeed, some researchers observed CL as a dianion with $pK_{a1} \approx 2$ for both phosphates [27], whereas others observed large difference between $pK_{a1} \approx 2$ and $pK_{a2} \approx 8$ [21] and CL behavior as a monoanion. According to Haines [21], the reason for the discrepancies was caused by different properties of CL in the artificial membranes [27] and in the biological membranes [21].

Under normal conditions, the ΔpH between the cytosolic and the matrix sides of the inner mitochondrial membrane is close to 1.0, which is equivalent to 60 mV [42, 43]. It was suggested that one of the consequences of different dissociation of the CL phosphates may be as follows: on the cytosolic side (the outer surface of the IMM) CL traps protons, and thus converts ΔpH into $\Delta\Psi$, by enhancing the "+" charge on the outer surface of the inner membrane. On the matrix side, CL behaves as a dianion, and thus enhances the "−" charge of the $\Delta\Psi$ at the inner leaflet of the IMM [28].

CL has an important function of buffering protons, particularly on the matrix side of the inner membrane [44]. In most active mitochondria of the heart, brain, skeletal muscles, and kidney, it is hardly possible to talk about pH of the matrix because mitochondrial proteins, together with water, exist as a quasicrystalline phase [45]. Antonenko et al. [46] suggested the existence of a kinetic barrier for proton transfer from the surface of bilayer phospholipid membrane to bulk water. Thus, there is no "normal" diffusion of protons and substrates in the bulk volume of the matrix. However, close to the surface of the inner membrane bearing negative charge, there are few layers of structured water, which serve as a conductor for protons by the Grotthuss mechanism, and thus the local concentration of protons may be several orders higher than in the bulk volume of the matrix [21].

To explain the mechanisms of oxidative damage of cardiolipin and other mitochondrial phospholipids, we have suggested that low pH at the surfaces of the inner mitochondrial membrane, that is at the border between the lipid phase of the membrane and the water phases of the matrix and intermembrane compartments, is of paramount significance for the conversion of the relatively chemically inactive superoxide radical ($O_2^{\bullet-}$) to the highly active perhydroxyl radical ($HO_2^{\bullet}$) [12, 17].

4. Properties of the Perhydroxyl Radical ($HO_2^{\bullet}$)

Superoxide radicals and hydrogen peroxide are the most common oxidants produced by mitochondria [47, 48]. Superoxide radical, when formed in the mitochondrial membrane, is rapidly removed from the lipid phase into the matrix or the intermembrane space because it is anion [49]. For some time, $O_2^{\bullet-}$ was considered as the main radical responsible for oxidative stress and aging, but soon, it was discovered that $O_2^{\bullet-}$ very poorly interacts with polyunsaturated fatty acids (PUFA) and amino acids [11, 18]. Therefore, the suspects became oxidants, which may originate from superoxide radicals, such as peroxynitrite ($ONOO^-$) and hydroxyl radical ($^{\bullet}OH$). Peroxynitrite, as well as peroxynitrate (O_2NOO^-), react relatively slowly with most, but not all, biological molecules, making them rather selective oxidants. Both $ONOO^-$ and O_2NOO^- modify tyrosine in proteins, leaving a footprint detectable *in vivo* [50–52]. The most active oxidant, the $^{\bullet}OH$, indeed is so active that it reacts within 1 to 5 molecular diameters of their site of formation [53]. According to Pryor [53], $^{\bullet}OH$ reacts with free linoleate with rate constants that are nearly diffusion-controlled. The lifetime of $^{\bullet}OH$ radicals have been estimated 10^{-9} sec. It reacts indiscriminately with organic molecules/groups and, therefore, cannot reach the inner layer of lipid membrane containing the unsaturated double bonds to initiate lipid peroxidation. All of the above mentioned radicals are hydrophilic. Perhydroxyl radical is a protonated form of the superoxide radical and has molecular formula $HO_2^{\bullet}$, and it is hydrophobic and much more active chemically than $O_2^{\bullet-}$. Unlike the superoxide ($O_2^{\bullet-}$), $HO_2^{\bullet}$ is a powerful oxidant [53]. The above considerations leave us with the only plausible candidate for initiation of the autoxidation of polyunsaturated fatty acids (PUFA) and CL, the perhydroxyl radical ($HO_2^{\bullet}$) [12, 17] (Figure 2).

Perhydroxyl radical is always present in the cell due to reversible reaction $O_2^{\bullet-} + H^+ \leftrightarrow HO_2^{\bullet}$ with pKa = 4.88 [54]. Because of the low pKa, it was widely accepted that at pH 7.2 in the cytoplasm, much less than 1% of $[O_2^{\bullet}]$ is present as $HO_2^{\bullet}$ [55]. Perhaps for this reason, many researchers presumed that $HO_2^{\bullet}$ has little or no role in initiation of lipid peroxidation [56]. However, several authors pointed out that pH values in the microvolumes in the vicinity of charged membranes may be several units lower than in the bulk volume of a cell [18, 21, 57]. This may occur around the negatively charged heads of cardiolipin, and other phospholipids, such as phosphatidylserine and phosphatidylinositol that may retain protons. Thus, not the bulk pH, but local pH at the interfaces of the IMM in matrix and cytosol is critical for formation of $HO_2^{\bullet}$, and because it has no charge, $HO_2^{\bullet}$ can easily go back into the lipid core of the membrane and cross it [58]. It should be also kept in mind that on both sides of the IMM, protons have much higher mobility by the Grotthuss mechanism in the few layers of structured water molecules close to the charged surfaces of the membrane, particularly around the rafts with antennae made of cardiolipin [21, 59, 60]. It is important that interaction of $O_2^{\bullet}$ with H^+ occurs at the interfaces of the matrix and cytoplasmic sides of the IMM where CL clusters hold together respirosomes and thus where superoxide radicals are produced [47]. For this reasons, CL and PEA may be the first phospholipids with unsaturated bonds affected by $HO_2^{\bullet}$.

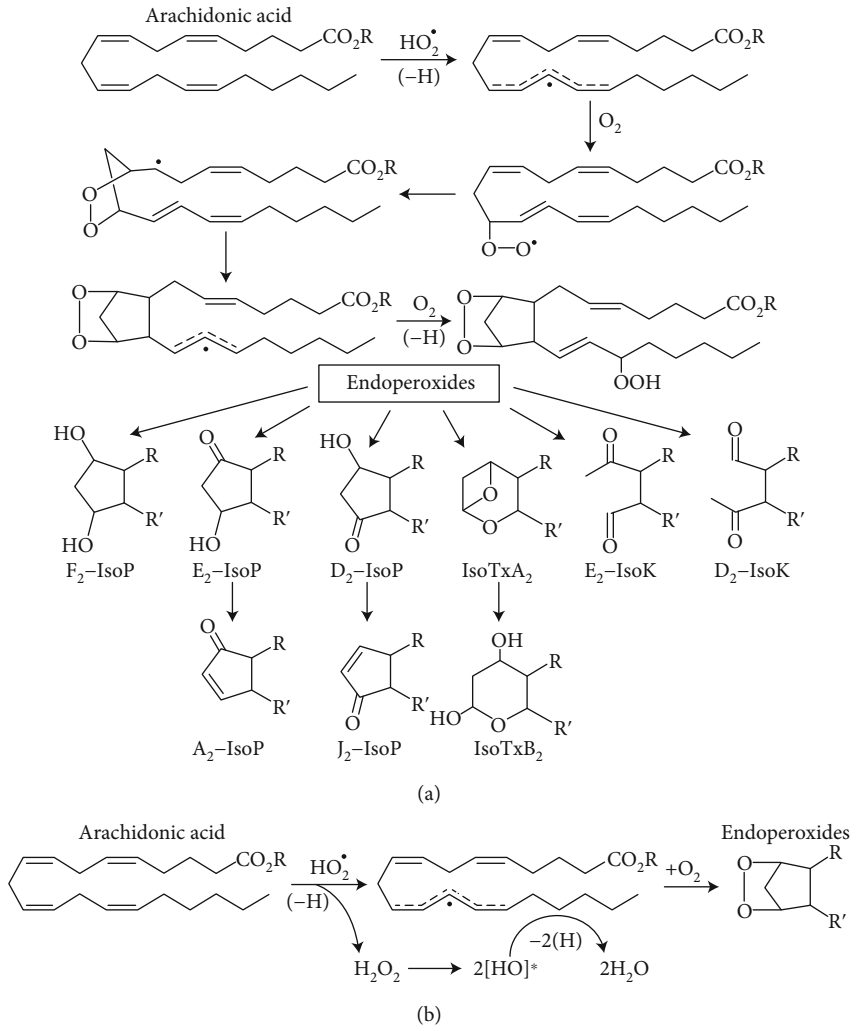

Figure 2: Autoxidation of arachidonic acid with rearrangements into different ring structures. (a) This part of Figure 2 (adapted from [81]) presents possible intermediate metabolites during autoxidation of arachidonic acid (AA) by some radical. $HO_2^\bullet$ is the only candidate to initiate autoxidation of AA that is esterified to a phospholipid [17]. (b) The proposed sequence of transformation of the $HO_2^\bullet$ and AA during IPLP [17]. Upon abstraction of the 1st H atom from AA, $HO_2^\bullet$ turns into H_2O_2, which in the hydrophobic environments undergoes homolytic decomposition into two molecules of $^\bullet OH$ radical, which instantly abstract additional two H atoms from AA, producing $2H_2O$ and the remnant of AA with complete disarranged double bonds. The extremely fast abstraction of three H atoms from any two double bonds creates a highly unstable molecule of AA, which very rapidly and randomly reacts with two molecules of O_2 and undergoes intramolecular rearrangements, which results in a large number of positional isomers and stereoisomers. The more PUFA has double bonds, the larger is the number of positional isomers and stereoisomers. Abbreviations: F_2-IsoP, E_2-IsoP, D_2-IsoP are Isoprostanes with rings, correspondingly F_2, E_2, D_2, or A_2 and J_2; $IsoTxA_2$ and $IsoTxB_2$ are isothromboxanes with rings A_2 and B_2, correspondingly, formed from Prostanglandin-H_2 (PGH_2); E_2-IsoK and D_2-IsoK are Isoketals with rings E_2 and D_2.

In comparison with other oxidants, $HO_2^\bullet$ shows high specificity in reaction with PUFA, linoleic (C18:2), and linolenic (C18:3) acids [11]. Thus, when $HO_2^\bullet$ encounters PUFA attached to a phospholipid, or two double bonds of linoleic acids (18:2) of CL, it reacts with them, with high probability and fast. This might explain why CL is one of the most sensitive phospholipids for oxidative damage [46, 61, 62]. Indeed, it has been shown that increased production of mitochondrial $HO_2^\bullet$ in cardiovascular conditions is associated with an increased cardiolipin oxidation, which represent a specific biomarker of mitochondrial oxidative stress [63]. The outcome of $HO_2^\bullet$ reaction with a different number of double bonds will be very distinct: IPLP, which requires PUFA with at least three double bonds present, produces racemic mixtures of hundreds of final products, whereas reaction with the most common fatty acid in CL, linoleic acids with two double bonds, yields "regular" lipid hydroperoxide [64].

5. The Isoprostane Pathway of Lipid Peroxidation

More than 50 years ago, it was observed that during autoxidation of linolenic acid or prolonged storage of the human blood plasma at -20°C, there were formed products similar to prostaglandins H and F_2 [65]. Roberts and Morrow at

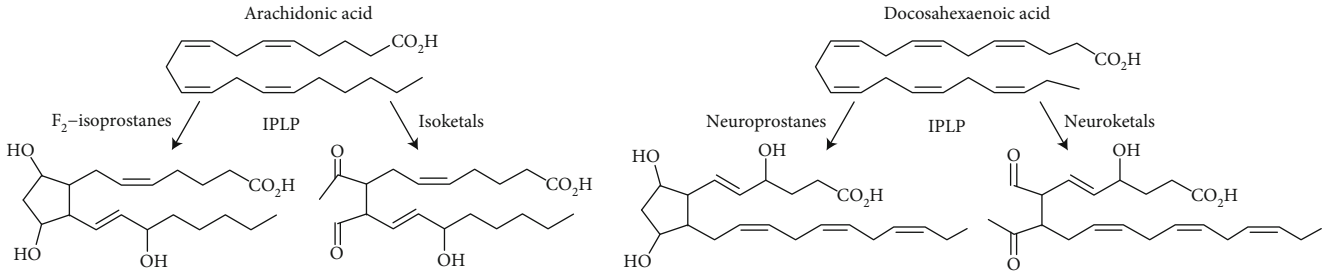

Figure 3: Examples of the parent and the corresponding product molecules resulting in the loss of two double bonds during nonenzymatic IPLP. During IPLP, the parent arachidonic and docosahexaenoic acids lose two unsaturated bonds. From AA may be produced various F2-isoprostanes and isoketals; from DHA, correspondingly, neuroprostanes and neuroketals. The images of the parent and one of the product molecules were adapted from [76].

the Vanderbilt University have shown the nonspecific autoxidative formation of prostaglandins *in vivo* [15, 16, 66–68] and discovered the nonenzymatic pathway of PUFA lipid peroxidation with racemic mixture of products possessing enormous variations in molecular positional isomerism and stereoisomerism in structure and biological activities.

A large number of products of this type of PUFA autoxidation possess high reactivities with lipids and proteins, and the resulting products may be considered as the most reliable and sensitive early markers of oxidative damages of lipids and proteins during aging and aging-associated pathologies [68–71]. The major features of the IPLP type of lipid peroxidation have been described in a number of publications [16, 66, 72]. The isoprostanes (IsoPs) that contain F-type prostane rings analogous to PGF_2 were the first class of oxidation products discovered during IPLP in abundance *in vitro* and *in vivo* [71].

IsoPs and the cyclooxygenase-derived prostaglandins (PGs) have a number of distinctions in their origin and properties, which have been discussed in a number of publications [12, 66, 71, 73–76]. Here we briefly list the most important distinctions: (1) The side chains of PGs are almost always oriented *trans* to the prostane ring whereas the products of IPLP have mostly the side chains with *cis* orientation [66, 71]. (2) The IsoPs are formed *in situ* from PUFA, which are esterified to phospholipids, while PGs are generated exclusively from the free AA and DHA [74]. (3) The products of IPLP are the racemic mixture of products with a very large number of possible stereoisomers and positional isomers, whereas the products of the enzymatically produced prostaglandins have only one optical isomer each [66, 74].

Some of the products of PUFA autoxidation, such as γ-ketoaldehydes, are highly reactive molecules, which form adducts with primary amines of the lysine-containing proteins and phosphatidylethanolamine [69]. The most active among γ-ketoaldehydes formed from AA via the IPLP are isolevuglandins (IsoLGs). IsoLGs are so reactive, that were revealed only as adducts with proteins or ethanolamine of PEA. A number of IsoPs possess potent biological activity and thus can function as mediators of the oxidant injury, or convey abnormal cellular signaling [69].

In addition to arachidonic acid (AA), which is the most common among phospholipids, other PUFA such as eicosapentaenoic acid (EPA) and docosahexaenoic acid (DHA) have been found as substrates for the IPLP [70]. Because DHA is present in a larger quantity in neurons, the products of IPLP were correspondingly named neuroprostanes and neuroketals (Figure 3).

The differences between IPLP and the "classical" lipid peroxidation have been discussed in [17]. However, the mechanisms, which are responsible for such enormous diversity of stereoisomers and positional isomers of the final product of PUFA during the IPLP, remained unknown, as well as the radical responsible for initiation of IPLP.

Figure 2(a) illustrates one of the common presentations of PUFA autoxidation. Initially, the radical that initiates autoxidation of AA was denoted as $^{\bullet}OH$ [76], Morrow and Roberts usually showed no radical at all [66, 74, 75]. The problem with hydroxyl radical is that it cannot by itself appear in the middle of the hydrophobic core of the membrane. $HO_2^{\bullet}$ is the only radical that can spontaneously come in contact with a PUFA, which is part of a phospholipid.

Recently, a hypothesis on the mechanism of initiation of IPLP by perhydroxyl radical ($HO_2^{\bullet}$) was presented [12, 17]. If we accept that it is the perhydroxyl radical that abstracts the first H atom from AA, then the product of the reaction will be hydrogen peroxide (H_2O_2). It has been shown [77, 78] that in the hydrophobic milieu, H_2O_2 undergoes homolytic splitting with formation of two hydroxyl radicals: $H_2O_2 \longrightarrow 2^{\bullet}OH$, which instantly will abstract another two H atoms, more likely from the same PUFA. This will delocalize all electrons in the double bonds with unpredictable structure of intermediate forms. Therefore, the intermediate structures of AA shown in Figure 2(a) above "endoperoxides" have no sense because nobody knows what structures will be acquired by intermediate metabolites. Therefore, in Figure 2(b), we show only the sequence of chemical intermediates for the perhydroxyl radical and show only the starting molecule AA and the possible structures of the final products. The proposed mechanism of IPLP initiation was first presented in [12, 17].

Although the abstractions of the three H atoms are shown schematically as separate and consecutive events, see Figures 2(a) and 2(b) and [77], in reality, abstraction of all hydrogen atoms occurs extremely fast, as one chain reaction, before two O_2 molecules join the remaining skeleton of AA. Rapid abstractions of three H atoms occur randomly at any double bond, this makes the molecule of PUFA highly unstable. For this reason, the O_2 molecules bind randomly with

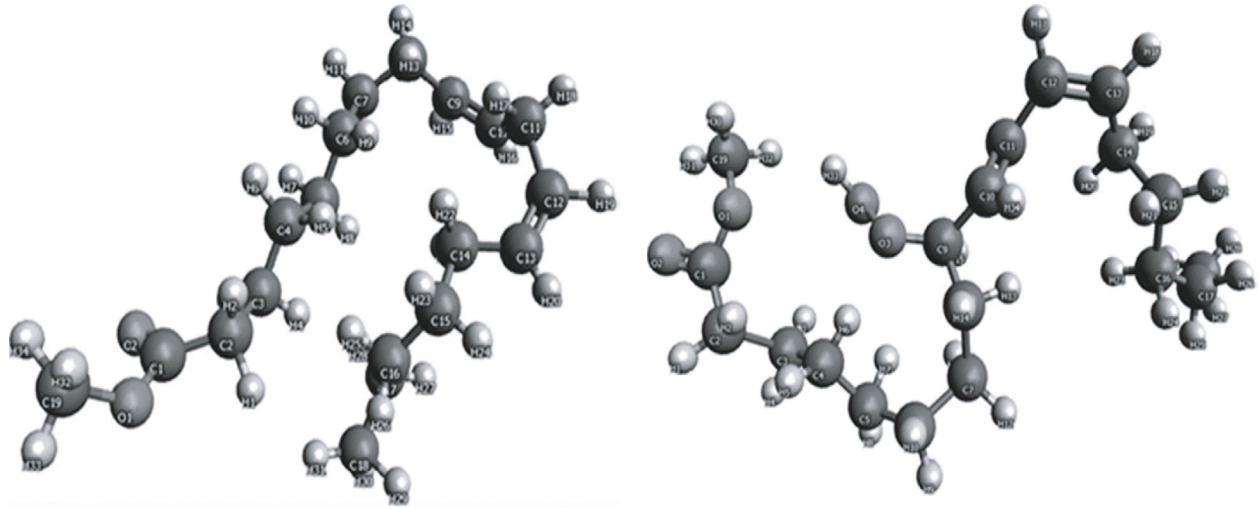

(a) (b)

Figure 4: Conformational changes of linoleate molecule upon peroxidation. Molecular dynamic simulation of (a) methyl linoleate molecule conformation and (b) methyl linoleate hydroperoxide molecule. The figure was adapted from [68].

formation of variants of regioisomers in accordance with the number of double bonds in the parent PUFA and surrounding conditions. The subsequent intramolecular rearrangements also occur randomly with the formation of different variations of the final product. Figure 3 shows a comparison of parent molecules of AA and DHA with the structures of the resulting possible products. For AA, these may be F2-isoprostanes and highly toxic isoketals, and for DHA, correspondingly, neuroprostanes and neuroketals (Figure 3). The products of IPLP have *cis* configuration relatively to the cyclopentane ring.

According to Antonenko et al. (2008) in experiments *in vitro*, cardiolipin is highly sensitive to peroxidation in the presence of $^{\bullet}OH$ [44]. The principal distinction between the *in vitro* conditions described for $^{\bullet}OH$ and $HO_2^{\bullet}$ radicals [18, 79], and the interactions of $HO_2^{\bullet}$ with AA, or $^{\bullet}OH$ with CL, is that *in vivo* reactions proceed in the completely hydrophobic environment. According to Gebicki and Bielski [18], in the water-ethanol mixture, the reactions proceed in consent with the reaction sequence of the "classical" lipid peroxidation (LP), and abstraction of the first hydrogen atom from linoleic acid results in formation of hydrogen peroxide: $LH + {}^{\bullet}HO_2 \longrightarrow L^{\bullet} + H_2O_2$, with the final formation of the stable end product linoleic hydroperoxide: $LOO^{-} + LH^{\bullet} \longrightarrow LOOH + L^{\bullet}$ [18]. Abstraction of hydrogen atom from linoleic acid by $^{\bullet}OH$ results in the conversion of the $^{\bullet}OH$ radical to water: $LH + {}^{\bullet}OH \longrightarrow L^{\bullet} + H_2O$. Bielski et al. [11] have concluded that reaction of $HO_2^{\bullet}$ radical with a double allylic H atom of a PUFA is proportional to the number of double allylic H atoms, which makes PUFAs highly specific targets with high affinity for perhydroxyl radicals [11, 18]. No selectivity was observed under similar conditions with hydroxyl radicals, which abstract H atoms randomly. According to Roberts and Morrows group [66, 74, 75], the reaction of $HO_2^{\bullet}$ with linoleic, linolenic, and arachidonic acids in water-ethanol solution, the formation of a stable products, which were the corresponding hydroperoxide [11], was relatively slow. On the contrary, studies on IPLP suggest that in the fully hydrophobic environment, reactions of $HO_2^{\bullet}$ with PUFA and linoleic acid are extremely fast, probably because of formation of hydroxyl radicals inside the hydrophobic milieu. For this reason, we can consider $^{\bullet}HO_2$ as a "carrier" of 2 $^{\bullet}OH$ inside the lipid core of the membrane.

As a result, the selective peroxidation of CL during aging, which we presume is driven to a large degree by formation of $HO_2^{\bullet}$ from the superoxide radical ($O_2^{\bullet-}$), abstraction of the first H atom from CL results in formation of hydrogen peroxide. In the hydrophobic milieu, H_2O_2 undergoes homolytic splitting into two molecules of $^{\bullet}OH$, which instantly interact with another two H atoms of the same or adjacent linoleic acid followed by interaction of O_2 with formation of the stable linoleic hydroperoxide, which is still attached to CL. Molecular dynamic simulation studies have shown that upon oxidation, the molecule of linoleic acid changes its conformation (Figure 4) [64], which may affect the ability of CL to maintain the superstructure of the mitochondrial enzyme complexes. Thus oxidatively damaged CL is a specific hallmark for the oxidative stress in mitochondria.

6. IPLP as the Mechanism of Aging

Numerous studies have demonstrated that IsoPs are the most early and reliable among available markers of lipid peroxidation *in vivo*, and recent studies provided valuable information about participation of IPLP in pathogenesis of numerous human diseases [15, 16, 68, 69]. According to our model of IPLP initiation by $HO_2^{\bullet}$, the perhydroxyl radical upon encounter with a PUFA produces one of many variants of isoPG, iso-γ-ketoacids, or iso-levuglandins. When reacting with fatty acids with two unsaturated bonds, such as linoleic acids of cardiolipin, $HO_2^{\bullet}$ produces corresponding hydroperoxides.

A large number of data proves that oxidative damages to cardiolipin [63, 80, 81] and phosphatidylethanolamine

(PEA) [82, 83] may serve as markers for the mitochondrial autoxidation caused by aging. Above, we have presented our arguments that the major mechanism of oxidative damages of fatty acids esterified with phospholipids is associated with formation of $HO_2^{\bullet}$ during "normal" production of superoxide radicals. The properties of perhydroxyl radical make it clear that regardless how small may be production of $HO_2^{\bullet}$, it will cause some direct damages to mitochondria and other cellular membranes, or via the formation of adducts with PEA and lysine-containing proteins [82, 83], and peroxidation of cardiolipin [46, 63, 80, 81]. Even though the level of $HO_2^{\bullet}$ production may be very low, it is, probably, the major mechanism of small, but persistent, accumulation of damages and regulatory signals caused by iso-prostaglandins, which, probably, often are wrong signals. Taking into consideration the crucial roles of CL and PEA in maintaining the structures of respiratory complexes and other polyenzymatic complexes, we can state that during aging the primary causes of mitochondrial dysfunctions are not limited by mutations of mtDNA, but more likely are caused by the functional and structural changes of phospholipids and proteins of mitochondria themselves.

7. The Importance of Fatty Acids Oxidation for Increased Rate of ROS Production

Mammalian mitochondria generate superoxide and hydrogen peroxide (ROS) from at least 11 different sites associated with substrates catabolism and the electron transport chain [48]. All mitochondrial sites of ROS production have very distinct properties [48, 84]. They can be divided into two groups: six sites operate at the redox potential of the $NADH/NAD^+$ isopotential pool, about -280 mV, and five sites operate at the redox potential of the ubiquinol/ubiquinone (QH_2/Q) isopotential pool, about +20 mV [48, 84].

The increased mitochondrial respiration can result in either increased production of ROS, if the accelerated respiration was caused by increased substrate supply, or in a decrease of ROS production, if the accelerated respiration was the result of increased utilization of ATP [48]. Heart, skeletal, muscles, and brain may work at very different workloads. In order to produce more ATP during high workloads, the mitochondria must receive the correspondingly increased supply of electrons into the respiratory chain. The commonly used substrates, often regarded as complex I substrates, such as glutamate and pyruvate, have relatively low rates of respiration because the NADH dehydrogenase of complex I is the rate limiting step [85]. The accelerated rates of respiration may be achieved by activation of glutamate and pyruvate transamination, or by the use of substrates mixtures, such as pyruvate + glutamate + malate (for the brain). Under these conditions, activation of transaminase reactions in mitochondria produce, in addition to NADH, 2-oxoglutarate, which is then converted to succinate in the TCA cycle [85–87]. Brand has stressed the importance of fatty acids oxidation for the bioenergetics of the skeletal muscle and heart mitochondria [48, 89]. During β-oxidation of fatty acids by the multienzyme complexes, the electron-transferring flavoprotein-ETF:Q oxidoreductase system reduces the membrane's pool of ubiquinone. In the presence of palmitoylcarnitine and other substrates (glutamate, pyruvate or succinate), there is no inhibition of SDH (complex II) [88], and thus electrons enter the respiratory chain both through the $NADH/NAD^+$ and QH_2/Q pathways allowing at high workloads fast production of ATP [48, 89, 90]. If consumption of ATP is limited, the excessive electrons activate at high membrane potential the reverse electron transport, which results in increased production of superoxide and H_2O_2 [48, 89]. We have suggested that in people with metabolic syndrome, which is characterized by increased utilization of fatty acids for production of energy, aging of the heart and brain may be accelerated [88, 90]. Indeed, recent studies support the cross-talk between the oxidative stress and metabolic conditions in mitochondria [91].

8. Oxidative Stress and the Mitochondrial Membrane Integrity

Mitochondria, particularly the inner membrane, contain very large amount of proteins, many of them in hundreds and thousands copies. Between proteins are located phospholipids, which comprise only around 20–25% of the total mass. Cardiolipin is located almost exclusively in the inner membrane of mitochondria (IMM). However, only phosphatidylcholine, together with few other phospholipids, form a biological membrane. Interactions of phosphatidylethanolamine (PEA) and cardiolipin (CL) with proteins allow integration of large proteins and multiprotein complexes into numerous curves of the inner membrane. PEA has a conical form because at C2, this phospholipid has a polyunsaturated fatty acid, usually arachidonic acid (C20:4, ω-6) or docosahexaenoic acid (C22:6, ω3), which have a curved shape. During oxidative stress, due to the high affinity of $HO_2^{\bullet}$ to polyunsaturated fatty acids, PEA also undergoes peroxidation as well as the linoleic acid of cardiolipins. These two phospholipids are located close to each other because they share the function of maintaining the structural integrity of the IMM and multienzyme complexes. Therefore, oxidative damages to CL and PEA result in the malfunctions of the lipid-protein interactions and dysfunction of proteins. Accumulation of oxidized PEA and CL and their depletion are mitochondrial hallmarks of aging [80, 92, 93]. Recently, it has been shown that during aging and diabetes, the fatty acid composition of CL may undergo remodeling when C18:2 fatty acids can be replaced by arachidonic acid (C20:4, ω-6) or docosahexaenoic acid (C22:6, ω3) [94, 96], which are substrates for IPLP [13, 14]. Because CL is directly involved in formation of $HO_2^{\bullet}$, it may explain why CL and PEA are particularly sensitive to oxidative damages [62, 92, 93].

It is conceivable that oxidative damages of even small amounts of CL and PEA may cause significant dysfunctions in energy production by mitochondria because both phospholipids are responsible for the superstructural organization of proteins involved in oxidative phosphorylation [96, 97]. In addition, CL is tightly bound with the transmembrane carriers of respiratory substrates, cytochrome *c*, and ANT. In the absence of CL, the electron transport between the respiratory complexes becomes disrupted, the membrane

potential drops significantly, and the synthesis of ATP becomes inhibited [98, 99].

In comparison with CL, the effects of PEA on mitochondrial functions are less studied. However, it was established that in the absence of PEA, the transport and assembly of proteins are also abnormal, only in this case, with the presence of only CL, the proteins tend to form unusually large superstructures, which result in the loss of membrane potential and ATP synthesis [98, 99]. Normal structural organization and functioning of respiratory chain and ATP-synthase requires coordinated interactions between CL and PEA.

9. Aging, Oxidative Stress, and Metabolic Syndrome

Oxidative stress is regarded as the main cause of aging, mitochondrial dysfunctions, and thus is one of the main pathogenic mechanisms of many diseases [100–105]. This is particularly true for those diseases, which are associated with the metabolic syndrome that develops at the certain stage of aging in humans [100–102]. It is clear, however, that the metabolic syndrome is not the result of only accumulated errors and dysfunctions in the course of life for whatever reason. From the point of view of the normal ontogenesis of an individual after birth, development of the metabolic syndrome represents a normal metabolic transition from the reproductive to post productive state of an individual.

Recently, we have shown that the full-scale oxidation of fatty acids by synaptic brain and heart mitochondria at all metabolic states occurs synergistically in the presence of other mitochondrial substrates, such as pyruvate, glutamate, or succinate [88]. We have also shown that oxidation of fatty acids may cause a several-fold increase in production of ROS [88, 90]. Figure 5 illustrates how simultaneous oxidation of palmitoyl-carnitine and other substrates affects production of ROS.

One of the important features of the metabolic syndrome is a dramatic increase in utilization of fatty acids for production of energy by mitochondria, particularly in women after menopause [106, 107]. From Figure 5, we can deduce that in aged individuals with metabolic syndrome, increased utilization of fatty acids may cause increased oxidative stress and thus accelerate the rate of aging.

10. The Rate of Aging is Proportional to the Rate of Superoxide Radical Production

Formation of $HO_2^\bullet$ is proportional to the level of $O_2^{\bullet-}$ present at the interfaces of the inner membrane with the matrix and intermembrane spaces, where concentration of $O_2^{\bullet-}$ at any moment is determined by the rates of its production and elimination [48]. Taking into consideration that $HO_2^\bullet$ is extremely reactive and dangerous, it is understandable that removal of superoxide radicals is very important for protecting cells from the deleterious effects of its protonated form as $^\bullet HO_2$. The activities of SOD2 and SOD1 are of most importance for the heart and the central nerve system, where the alternative antioxidant systems are relatively weak, whereas the contents of AA and DHA are the highest [33]. Because $HO_2^\bullet$ interacts with PUFA and CL inside the membranes, any type of antioxidants, including superoxide dismutases, will have no effect on the aging caused by $HO_2^\bullet$ but will have effects on aging processes caused by other radicals. This means that the rate of $HO_2^\bullet$ formation is strictly dependent on the rate of superoxide radical formation. As we have discussed above, at old age, when fatty acids become the predominant substrates for energy provision, the rate of aging may also increase. Thus, to delay aging, first of all, it is necessary to delay production of superoxide radical, and secondly, to diminish conversion of superoxide into $^\bullet HO_2$. Local cellular conditions also affect the amount of $O_2^{\bullet-}$ converted to $HO_2^\bullet$, for example, accumulation of lactic acid during high physical loads or mild hypoxia may increase oxidative damages to skeletal muscle cells or cardiomyocytes due to the acidification-induced higher levels of $HO_2^\bullet$ production [17]. From this point of view, of particular interest for our discussions are recent publications of the Skulachev's school of researchers on the effects of the mitochondria-targeted antioxidants with plastoquinone as an electron acceptor [46, 98–111].

Summarizing the data of several publications of the Skulachev's research team, it has been concluded [98] that the plastoquinone-based mitochondria-targeted antioxidants operate in two quite different ways: (i) by preventing peroxidation of cardiolipin [46, 99] and (ii) by mild uncoupling of mitochondria resulting from fatty acid cycling that inhibits the formation of reactive oxygen species in mitochondria [111].

Shabalina et al. (2017) used the mtDNA mutator mice, which exhibit marked features of premature aging. The authors have suggested that accelerated aging was caused by the increased mitochondrial ROS that interact with polyunsaturated fatty acids in cardiolipin, releasing malondialdehyde and 4-hydroxynonenal that form protein adducts and thus diminish mitochondrial functions [109]. Treatment of animals with accelerated aging with SkQ1 counteracted these changes as it scavenges mitochondrial ROS. As the results, the normal mitochondrial ultrastructure was preserved in liver and heart; the phosphorylation capacity of skeletal muscle mitochondria as well as the thermogenic capacity of brown adipose tissue also improved. The SkQ1-treated mice lived significantly longer (335 versus 290 days) [109].

11. Conclusions

In this review, we examined the unique structure of cardiolipin and how this structure is reflected in several unique functions of this phospholipid. Cardiolipin (CL), together with phosphatidylethanolamine (PEA), maintain the superstructural organization of the enzymes that perform the most important function of mitochondria–oxidative phosphorylation. Both CL and PEA are not capable to build up a flat biological membrane, but they accommodate the functional complexes of proteins into the sharp curves of the inner mitochondrial membrane. At some regions of the IMM, cardiolipin creates regions with a strong negative charge, where local pH may be several units lower than in the

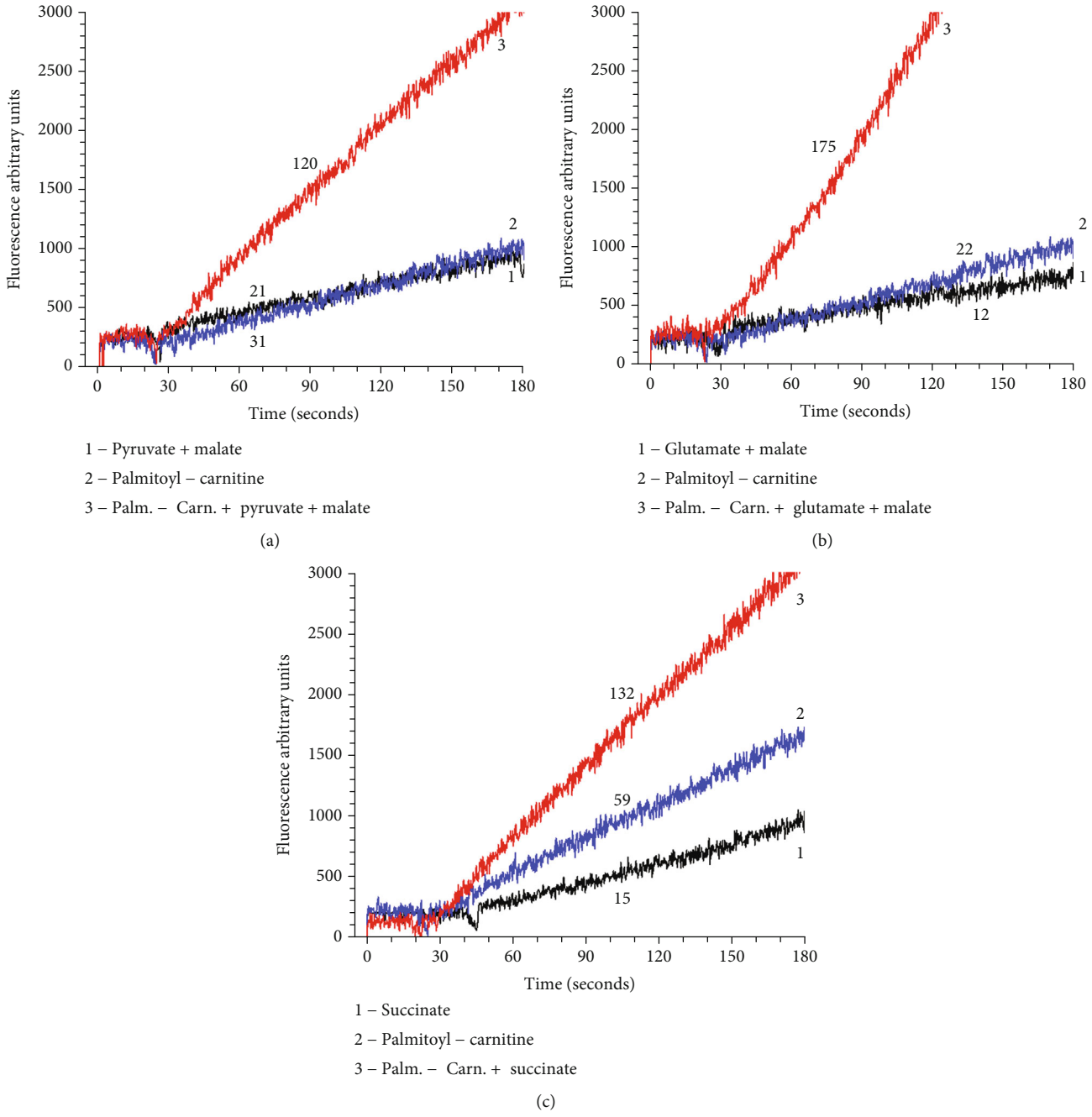

FIGURE 5: Production of superoxide radicals by rat heart mitochondria-oxidizing palmitoyl-carnitine. Designations: 1. supporting substrate only; 2. palmitoyl-carnitine only, and 3. palmitoyl – carnitine + supporting substrate. Substrates: Figure 5(a) (pyruvate 2.5 mM + malate 2 mM), Figure 5(b) (glutamate 5 mM + malate 2 mM), and Figure 5(c). (succinate 5 mM). Experimental conditions are described in [93]. The incubation medium contained Amplex Red 2 μM, horse radish peroxidase 2 units, substrates as indicated above, and volume 1 ml. The reaction was initiated by addition of 50 μg of mitochondria. Initial rates were measured for 3 minutes. Numbers at the traces are the rates of H_2O_2 production in picomol H_2O_2/min/mg protein RHM. The rates were corrected for the time control rate with RHM incubated without added substrates. The figure was taken from [95].

bulk phase of a compartment. We suggest that at these regions, the probability of protonation of the superoxide radical is relatively high. The resulting molecule of perhydroxyl radical is hydrophobic and specifically reacts with the double bonds of PUFA and linoleic acid of cardiolipin, producing correspondingly racemic mixture of isoprostanes and isoketals from PUFA and linoleate hydroperoxide. This explains why CL and PEA are the most common markers of the specific oxidative damages in mitochondria. Damages to CL and PEA cause gradual disarrangement of the structural organization of the functional complexes of oxidative phosphorylation as well as other enzymes of the

mitochondria. For this reasons, we consider that oxidative damages to CL and PEA are the primary cause of aging and the age-associated diseases. Therefore, developments of the mitochondria-targeted antioxidant drugs, similar to SkQ, are very promising in finding and making a reality the existence of the mythical "Elixir of Youth."

Abbreviations

AA: Arachidonic acid (C20:4 ω6)
ANT: Adenine nucleotide translocase
CL: Cardiolipin
COX: Cyclooxygenase
DHA: Docosahexaenoic acid (C22:6 ω3)
$HO_2^{\bullet}$: Perhydroxyl radical
IMM: Inner mitochondrial membrane
IsoPs: Isoprostanes
IPLP: Isoprostane pathway of lipid peroxidation
LOX: Lipoxygenases
LP: Lipid peroxidation
MetS: Metabolic syndrome
mtDNA: Mitochondrial deoxyribonucleic acid
NO: Nitric oxide radical
$O_2^{\bullet-}$: Superoxide radical
OH: Hydroxyl radical
OMM: Outer mitochondrial membrane
$ONOO^-$: Peroxynitrite
O_2NOO^-: Peroxynitrate
OXPHOS: Oxidative phosphorylation
PEA: Phosphatidylethanolamine
PGF_2: Isoprostanes containing F-type prostane rings
PGs: Prostaglandins
PUFA: Polyunsaturated fatty acids
RET: Reverse electron transport
ROS: Reactive oxygen species
SOD: Superoxide dismutase
SOD1: Cytoplasmic isoform of Cu,Zn-SOD
SOD2: Mitochondrial isoform of Mn-SOD.

Conflicts of Interest

The authors declare that there is no conflict of interest regarding the publication of this paper.

Acknowledgments

This work was supported by R01HL124116 and R01HL144943 National Institutes of Health grants.

References

[1] D. Harman, "The aging process," *Proceedings of the National Academy of Sciences of the United States of America*, vol. 78, no. 11, pp. 7124–7128, 1981.

[2] D. Harman, "Free radical theory of aging: consequences of mitochondrial aging," *Age*, vol. 6, no. 3, pp. 86–94, 1983.

[3] D. Harman, "Free radical theory of aging: an update: increasing the functional life span," *Annals of the New York Academy of Sciences*, vol. 1067, pp. 10–21, 2006.

[4] A. Chomyn and G. Attardi, "MtDNA mutations in aging and apoptosis," *Biochemical and Biophysical Research Communications*, vol. 304, no. 3, pp. 519–529, 2003.

[5] B. Kadenbach, C. Münscher, V. Frank, J. Müller-Höcker, and J. Napiwotzki, "Human aging is associated with stochastic somatic mutations of mitochondrial DNA," *Mutation Research/DNAging*, vol. 338, no. 1-6, pp. 161–172, 1995.

[6] R. M. Anson, E. Hudson, and V. A. Bohr, "Mitochondrial endogenous oxidative damage has been overestimated," *The FASEB Journal*, vol. 14, no. 2, pp. 355–360, 2000.

[7] D. C. Wallace, "Mitochondrial genetics: a paradigm for aging and degenerative diseases?," *Science*, vol. 256, no. 5057, pp. 628–632, 1992.

[8] M. Pinto and C. T. Moraes, "Mechanisms linking mtDNA damage and aging," *Free Radical Biology and Medicine*, vol. 85, pp. 250–258, 2015.

[9] K. Szczepanowska and A. Trifunovic, "Origins of mtDNA mutations in ageing," *Essays in Biochemistry*, vol. 61, no. 3, pp. 325–337, 2017.

[10] K. L. DeBalsi, K. E. Hoff, and W. C. Copeland, "Role of the mitochondrial DNA replication machinery in mitochondrial DNA mutagenesis, aging and age-related diseases," *Ageing Research Reviews*, vol. 33, pp. 89–104, 2017.

[11] B. H. Bielski, R. L. Arudi, and M. W. Sutherland, "A study of the reactivity of HO_2/O_2- with unsaturated fatty acids," *The Journal of Biological Chemistry*, vol. 258, no. 8, pp. 4759–4761, 1983.

[12] A. Panov, "Mitochondrial production of perhydroxyl radical (HO2•) as inducer of aging and related pathologies," *Journal of Biochemical and Biophysical*, vol. 1, 2017.

[13] L. Jackson Roberts II, T. J. Montine, W. R. Markesbery et al., "Formation of isoprostane-like compounds (neuroprostanes) in vivo from docosahexaenoic acid," *The Journal of Biological Chemistry*, vol. 273, no. 22, pp. 13605–13612, 1998.

[14] J. D. Morrow, J. A. Awad, H. J. Boss, I. A. Blair, and L. J. Roberts 2nd, "Non-cyclooxygenase-derived prostanoids (F2-isoprostanes) are formed in situ on phospholipids," *Proceedings of the National Academy of Sciences of the United States of America*, vol. 89, no. 22, pp. 10721–10725, 1992.

[15] P. Montuschi, P. J. Barnes, and L. Jackson Roberts II, "Isoprostanes: markers and mediators of oxidative stress," *The FASEB Journal*, vol. 18, no. 15, pp. 1791–1800, 2004.

[16] S. S. Davies and L. Jackson Roberts II, "F_2-isoprostanes as an indicator and risk factor for coronary heart disease," *Free Radical Biology and Medicine*, vol. 50, no. 5, pp. 559–566, 2011.

[17] A. Panov, "Perhydroxyl radical ($HO_2^{\bullet}$) as inducer of the isoprostane lipid peroxidation in mitochondria," *Molecular Biology*, vol. 52, no. 3, pp. 295–305, 2018.

[18] J. M. Gebicki and B. H. J. Bielski, "Comparison of the capacities of the perhydroxyl and the superoxide radicals to initiate chain oxidation of linoleic acid," *Journal of the American Chemical Society*, vol. 103, no. 23, pp. 7020–7022, 1981.

[19] D. A. Cherepanov, B. A. Feniouk, W. Junge, and A. Y. Mulkidjanian, "Low dielectric permittivity of water at the membrane interface: effect on the energy coupling mechanism in biological membranes," *Biophysical Journal*, vol. 85, no. 2, pp. 1307–1316, 2003.

[20] A. D. N. J. de Grey, "HO2•: the forgotten radical," *DNA and Cell Biology*, vol. 21, no. 4, pp. 251–257, 2002.

[21] T. H. Haines, "A new look at Cardiolipin," *Biochimica et Biophysica Acta*, vol. 1788, no. 10, pp. 1997–2002, 2009.

[22] A. A. Benson, H. Daniel, and R. Wiser, "A sulfolipid in plants," *Proceedings of the National Academy of Sciences of the United States of America*, vol. 45, no. 11, pp. 1582–1587, 1959.

[23] R. N. A. H. Lewis and R. N. McElhaney, "The physicochemical properties of cardiolipin bilayers and cardiolipin- containing lipid membranes," *Biochimica et Biophysica Acta*, vol. 1788, no. 10, pp. 2069–2079, 2009.

[24] R. H. Houtkooper and F. M. Vaz, "Cardiolipin, the heart of mitochondrial metabolism," *Cellular and Molecular Life Sciences*, vol. 65, no. 16, pp. 2493–2506, 2008.

[25] J. Jouhet, "Importance of the hexagonal lipid phase in biological membrane organization," *Frontiers in Plant Science*, vol. 4, 2013.

[26] C. Arnarez, S. J. Marrink, and X. Periole, "Identification of cardiolipin binding sites on cytochrome _c_ oxidase at the entrance of proton channels," *Scientific Reports*, vol. 3, no. 1, 2013.

[27] M. Sathappa and N. N. Alder, "The ionization properties of cardiolipin and its variants in model bilayers," *Biochimica et Biophysica Acta*, vol. 1858, no. 6, pp. 1362–1372, 2016.

[28] T. H. Haines and N. A. Dencher, "Cardiolipin: a proton trap for oxidative phosphorylation," *FEBS Letters*, vol. 528, no. 1-3, pp. 35–39, 2002.

[29] M. Kates, J. Y. Syz, D. Gosser, and T. H. Haines, "pH-dissociation characteristics of cardiolipin and its $2'$-deoxy analogue," *Lipids*, vol. 28, no. 10, pp. 877–882, 1993.

[30] T. H. Haines, "Anionic lipid headgroups as a proton-conducting pathway along the surface of membranes: a hypothesis," *Proceedings of the National Academy of Sciences of the United States of America*, vol. 80, no. 1, pp. 160–164, 1983.

[31] M. Schlame, M. Ren, Y. Xu, M. L. Greenberg, and I. Haller, "Molecular symmetry in mitochondrial cardiolipins," *Chemistry and Physics of Lipids*, vol. 138, no. 1-2, pp. 38–49, 2005.

[32] C. Ye, Z. Shen, and M. L. Greenberg, "Cardiolipin remodeling: a regulatory hub for modulating cardiolipin metabolism and function," *Journal of Bioenergetics and Biomembranes*, vol. 48, no. 2, pp. 113–123, 2016.

[33] S. E. Horvath and G. Daum, "Lipids of mitochondria," *Progress in Lipid Research*, vol. 52, no. 4, pp. 590–614, 2013.

[34] J. M. Seddon, "Structure of the inverted hexagonal (H_{II}) phase, and non-lamellar phase transitions of lipids," *Biochimica et Biophysica Acta*, vol. 1031, no. 1, pp. 1–69, 1990.

[35] J. A. Cohen and M. Cohen, "Adsorption of monovalent and divalent cations by phospholipid membranes. The monomer-dimer problem," *Biophysical Journal*, vol. 36, no. 3, pp. 623–651, 1981.

[36] T. J. Pinheiro, A. A. Duralski, and A. Watts, "Phospholipid headgroup–headgroup electrostatic interactions in mixed bilayers of cardiolipin with phosphatidylcholines studied by 2H NMR," *Biochemistry*, vol. 33, no. 16, pp. 4896–4902, 1994.

[37] J. M. Boggs, "Lipid intermolecular hydrogen bonding: influence on structural organization and membrane function," *Biochimica et Biophysica Acta*, vol. 906, no. 3, pp. 353–404, 1987.

[38] M. Schlame, D. Rua, and M. L. Greenberg, "The biosynthesis and functional role of cardiolipin," *Progress in Lipid Research*, vol. 39, no. 3, pp. 257–288, 2000.

[39] H. Schagger, "Respiratory chain supercomplexes," *IUBMB Life*, vol. 52, no. 3-5, pp. 119–128, 2001.

[40] F. L. Hoch, "Cardiolipins and mitochondrial proton-selective leakage," *Journal of Bioenergetics and Biomembranes*, vol. 30, no. 6, pp. 511–532, 1998.

[41] P. Adelroth and P. Brzezinski, "Surface-mediated proton-transfer reactions in membrane-bound proteins," *Biochimica et Biophysica Acta*, vol. 1655, no. 1-3, pp. 102–115, 2004.

[42] V. P. Skulachev, "Chemiosmotic systems and the basic principles of cell energetics," in *Molecular Mechanisms in Bioenergetics*, L. Ernster, Ed., pp. 37–73, Elsevier, Amsterdam, London, New York, Tokyo, 1992.

[43] V. P. Skulachev, "Chemiosmotic concept of the membrane bioenergetics: what is already clear and what is still waiting for elucidation?," *Journal of Bioenergetics and Biomembranes*, vol. 26, no. 6, pp. 589–598, 1994.

[44] M. Schlame and M. Ren, "The role of cardiolipin in the structural organization of mitochondrial membranes," *Biochimica et Biophysica Acta*, vol. 1788, no. 10, pp. 2080–2083, 2009.

[45] P. A. Srere, "Protein crystals as a model for mitochondrial matrix proteins," *Trends in Biochemical Sciences*, vol. 6, pp. 4–7, 1981.

[46] Y. N. Antonenko, A. V. Avetisyan, L. E. Bakeeva et al., "Mitochondria-targeted plastoquinone derivatives as tools to interrupt execution of the aging program. 1. Cationic plastoquinone derivatives: synthesis and in vitro studies," *Biochemistry*, vol. 73, no. 12, pp. 1273–1287, 2008.

[47] M. D. Brand, "The sites and topology of mitochondrial superoxide production," *Experimental Gerontology*, vol. 45, no. 7-8, pp. 466–472, 2010.

[48] M. D. Brand, "Mitochondrial generation of superoxide and hydrogen peroxide as the source of mitochondrial redox signaling," *Free Radical Biology and Medicine*, vol. 100, pp. 14–31, 2016.

[49] M. P. Murphy, "How mitochondria produce reactive oxygen species," *The Biochemical Journal*, vol. 417, no. 1, pp. 1–13, 2009.

[50] J. S. Beckman and W. H. Koppenol, "Nitric oxide, superoxide, and peroxynitrite: the good, the bad, and ugly," *The American Journal of Physiology*, vol. 271, pp. C1424–C1437, 1996.

[51] W. A. Pryor and G. L. Squadrito, "The chemistry of peroxynitrite: a product from the reaction of nitric oxide with superoxide," *The American Journal of Physiology*, vol. 268, pp. L699–L722, 1995.

[52] W. A. Pryor, K. N. Houk, C. S. Foote et al., "Free radical biology and medicine: it's a gas, man!," *American Journal of Physiology-Regulatory, Integrative and Comparative Physiology*, vol. 291, no. 3, pp. R491–R511, 2006.

[53] W. A. Pryor, "Oxy-radicals and related species: their formation, lifetimes and reactions," *Annual Review of Physiology*, vol. 48, pp. 657–667, 1986.

[54] B. H. J. Bielski, "Reevaluation of the spectral and kinetic properties of HO2AND O2-FREE radicals," *Photochemistry and Photobiology*, vol. 28, no. 4-5, pp. 645–649, 1978.

[55] J. M. McCord and I. Fridovich, "Superoxide dismutase. An enzymic function for erythrocuprein (hemocuprein)," *The Journal of Biological Chemistry*, vol. 244, pp. 6049–6055, 1978.

[56] J. M. Gutteridge, "Lipid peroxidation and antioxidants as biomarkers of tissue damage," *Clinical Chemistry*, vol. 41, pp. 1819–1828, 1995.

[57] J. Barber, "Membrane surface charges and potentials in relation to photosynthesis," *Biochimica et Biophysica Acta*, vol. 594, no. 4, pp. 253–308, 1980.

[58] R. A. Gus'kova, I. I. Ivanov, V. K. Kol'tover, V. V. Akhobadze, and A. B. Rubin, "Permeability of bilayer lipid membranes for superoxide (O_2^-) radicals," *Biochimica et Biophysica Acta*, vol. 778, no. 3, pp. 579–585, 1984.

[59] S. Serowy, S. M. Saparov, Y. N. Antonenko, W. Kozlovsky, V. Hagen, and P. Pohl, "Structural proton diffusion along lipid bilayers," *Biophysical Journal*, vol. 84, no. 2, pp. 1031–1037, 2003.

[60] C. A. Wraight, "Chance and design-proton transfer in water, channels and bioenergetic proteins," *Biochimica et Biophysica Acta*, vol. 1757, no. 8, pp. 886–912, 2006.

[61] E. J. Lesnefsky and C. L. Hoppel, "Oxidative phosphorylation and aging," *Ageing Research Reviews*, vol. 5, no. 4, pp. 402–433, 2006.

[62] E. J. Lesnefsky and C. L. Hoppel, "Cardiolipin as an oxidative target in cardiac mitochondria in the aged rat," *Biochimica et Biophysica Acta*, vol. 1777, no. 7-8, pp. 1020–1027, 2008.

[63] S. Dikalov, H. Itani, B. Richmond et al., "Tobacco smoking induces cardiovascular mitochondrial oxidative stress, promotes endothelial dysfunction, and enhances hypertension," *American Journal of Physiology. Heart and Circulatory Physiology*, vol. 316, no. 3, pp. H639–H646, 2019.

[64] M. Soloviev, I. Moskalenko, and E. Pliss, "Quantum chemical evaluation of the role of $HO_2^•$ radicals in the kinetics of the methyl linoleate oxidation in micelles," *Reaction Kinetics, Mechanisms and Catalysis*, vol. 127, no. 2, pp. 561–581, 2019.

[65] W. A. Pryor, J. P. Stanley, and E. Blair, "Autoxidation of polyunsaturated fatty acids: II. A suggested mechanism for the formation of TBA-reactive materials from prostaglandin-like endoperoxides," *Lipids*, vol. 11, no. 5, pp. 370–379, 1976.

[66] J. D. Morrow, K. E. Hill, R. F. Burk, T. M. Nammour, K. F. Badr, and L. J. Roberts 2nd, "A series of prostaglandin F2-like compounds are produced in vivo in humans by a non-cyclooxygenase, free radical-catalyzed mechanism," *Proceedings of the National Academy of Sciences of the United States of America*, vol. 87, no. 23, pp. 9383–9387, 1990.

[67] L. Jackson Roberts II and J. P. Fessel, "The biochemistry of the isoprostane, neuroprostane, and isofuran pathways of lipid peroxidation," *Chemistry and Physics of Lipids*, vol. 128, no. 1-2, pp. 173–186, 2004.

[68] C. J. Brame, O. Boutaud, S. S. Davies et al., "Modification of proteins by isoketal-containing oxidized phospholipids," *The Journal of Biological Chemistry*, vol. 279, no. 14, pp. 13447–13451, 2004.

[69] T. J. Montine and J. D. Morrow, "Fatty acid oxidation in the pathogenesis of Alzheimer's disease," *The American Journal of Pathology*, vol. 166, no. 5, pp. 1283–1289, 2005.

[70] G. L. Milne, H. Yin, and J. D. Morrow, "Human biochemistry of the isoprostane pathway," *The Journal of Biological Chemistry*, vol. 283, no. 23, pp. 15533–15537, 2008.

[71] E. S. Musiek, H. Yin, G. L. Milne, and J. D. Morrow, "Recent advances in the biochemistry and clinical relevance of the isoprostane pathway," *Lipids*, vol. 40, no. 10, pp. 987–994, 2005.

[72] D. F. Wendelborn, K. Seibert, and L. J. Roberts II, "Isomeric prostaglandin F2 compounds arising from prostaglandin D2: a family of icosanoids produced in vivo in humans," *Proceedings of the National Academy of Sciences of the United States of America*, vol. 85, no. 2, pp. 304–308, 1988.

[73] H. Yin, L. Gao, H. H. Tai, L. J. Murphey, N. A. Porter, and J. D. Morrow, "Urinary prostaglandin F2alpha is generated from the isoprostane pathway and not the cyclooxygenase in humans," *The Journal of Biological Chemistry*, vol. 282, no. 1, pp. 329–336, 2007.

[74] L. Jackson Roberts II and G. L. Milne, "Isoprostanes," *Journal of Lipid Research*, vol. 50, pp. S219–S223, 2009.

[75] J. D. Morrow, L. J. Roberts, V. C. Daniel et al., "Comparison of Formation of D_2/E_2-Isoprostanes and F_2-Isoprostanes *in Vitro* and *in Vivo* – Effects of Oxygen Tension and Glutathione," *Archives of Biochemistry and Biophysics*, vol. 353, no. 1, pp. 160–171, 1998.

[76] W. Christie, *Isoprostanes*, 2006, http://lipidlibrary.aocs.org/Primer/content.cfm? ItemNumber =39314.

[77] B. Halliwell and J. M. C. Gutteridge, "Oxygen toxicity, oxygen radicals, transition metals and disease," *The Biochemical Journal*, vol. 219, no. 1, pp. 1–14, 1984.

[78] M. C. Owen, B. Viskolcz, and I. G. Csizmadia, "Quantum Chemical Analysis of the Unfolding of a Penta-alanyl 310-Helix Initiated by HO•, HO2• and O2–•," *The Journal of Physical Chemistry B*, vol. 115, no. 24, pp. 8014–8023, 2011.

[79] S. E. Fridovich and N. A. Porter, "Oxidation of arachidonic acid in micelles by superoxide and hydrogen peroxide," *The Journal of Biological Chemistry*, vol. 256, no. 1, pp. 260–265, 1981.

[80] G. Paradies, G. Petrosillo, V. Paradies, and F. M. Ruggiero, "Role of cardiolipin peroxidation and Ca^{2+} in mitochondrial dysfunction and disease," *Cell Calcium*, vol. 45, no. 6, pp. 643–650, 2009.

[81] G. Paradies, G. Petrosillo, V. Paradies, and F. M. Ruggiero, "Mitochondrial dysfunction in brain aging: role of oxidative stress and cardiolipin," *Neurochemistry International*, vol. 58, no. 4, pp. 447–457, 2011.

[82] L. Guo, Z. Chen, B. E. Cox et al., "Phosphatidylethanolamines modified by γ-ketoaldehyde (γKA) induce endoplasmic reticulum stress and endothelial activation," *The Journal of Biological Chemistry*, vol. 286, no. 20, pp. 18170–18180, 2011.

[83] C. B. Sullivan, E. Matafonova, L. J. Roberts II, V. Amarnath, and S. S. Davies, "Isoketals form cytotoxic phosphatidylethanolamine adducts in cells," *Journal of Lipid Research*, vol. 51, no. 5, pp. 999–1009, 2010.

[84] C. L. Quinlan, I. V. Perevoshchikova, M. Hey-Mogensen, A. L. Orr, and M. D. Brand, "Sites of reactive oxygen species generation by mitochondria oxidizing different substrates," *Redox Biology*, vol. 1, no. 1, pp. 304–312, 2013.

[85] A. Panov, S. Dikalov, N. Shalbuyeva, R. Hemendinger, J. T. Greenamyre, and J. Rosenfeld, "Species- and tissue-specific relationships between mitochondrial permeability transition and generation of ROS in brain and liver mitochondria of rats and mice," *American Journal of Physiology. Cell Physiology*, vol. 292, no. 2, pp. C708–C718, 2007.

[86] A. Panov, P. Schonfeld, S. Dikalov, R. Hemendinger, H. L. Bonkovsky, and B. R. Brooks, "The Neuromediator glutamate, through specific substrate interactions, enhances mitochondrial ATP production and reactive oxygen species generation

in nonsynaptic brain mitochondria," *The Journal of Biological Chemistry*, vol. 284, no. 21, pp. 14448–14456, 2009.

[87] A. Panov, Z. Orynbayeva, V. Vavilin, and V. Lyakhovich, "Fatty Acids in Energy Metabolism of the Central Nervous System," *BioMed Research International*, vol. 2014, Article ID 472459, 22 pages, 2014.

[88] I. V. Perevoshchikova, C. L. Quinlan, A. L. Orr, A. A. Gerencser, and M. D. Brand, "Sites of superoxide and hydrogen peroxide production during fatty acid oxidation in rat skeletal muscle mitochondria," *Free Radical Biology & Medicine*, vol. 61, pp. 298–309, 2013.

[89] A. V. Panov, "Synergistic oxidation of fatty acids, glucose and amino acids metabolites by isolated rat heart mitochondria EC," *Cardiology*, vol. 5, pp. 198–208, 2018.

[90] A. V. Panov and S. I. Dikalov, "Mitochondrial metabolism and the age-associated cardiovascular diseases," *EC Cardiology*, vol. 5, pp. 750–769, 2018.

[91] S. I. Dikalov and A. E. Dikalova, "Crosstalk between mitochondrial hyperacetylation and oxidative stress in vascular dysfunction and hypertension," *Antioxidants & Redox Signaling*, vol. 31, no. 10, pp. 710–721, 2019.

[92] T. Sen, N. Sen, S. Jana, F. H. Khan, U. Chatterjee, and S. Chakrabarti, "Depolarization and cardiolipin depletion in aged rat brain mitochondria: relationship with oxidative stress and electron transport chain activity," *Neurochemistry International*, vol. 50, no. 5, pp. 719–725, 2007.

[93] G. Petrosillo, N. Moro, V. Paradies, F. M. Ruggiero, and G. Paradies, "Increased susceptibility to Ca(2+)-induced permeability transition and to cytochrome *c* release in rat heart mitochondria with aging: effect of melatonin," *Journal of Pineal Research*, vol. 48, no. 4, pp. 340–346, 2010.

[94] H. J. Lee, J. Mayette, S. I. Rapoport, and R. P. Bazinet, "Selective remodeling of cardiolipin fatty acids in the aged rat heart," *Lipids in Health and Disease*, vol. 5, no. 1, p. 2, 2006.

[95] X. Han, J. Yang, K. Yang, Z. Zhao, D. R. Abendschein, and R. W. Gross, "Alterations in myocardial cardiolipin content and composition occur at the very earliest stages of diabetes: a shotgun lipidomics study," *Biochemistry*, vol. 46, no. 21, pp. 6417–6428, 2007.

[96] K. Beyer and M. Klingenberg, "ADP/ATP carrier protein from beef heart mitochondria has high amounts of tightly bound cardiolipin, as revealed by 31P nuclear magnetic resonance," *Biochemistry*, vol. 24, no. 15, pp. 3821–3826, 1985.

[97] M. Schlame, K. Beyer, M. Hayer-Hartl, and M. Klingenberg, "Molecular species of cardiolipin in relation to other mitochondrial phospholipids: is there an acyl specificity of the interaction between cardiolipin and the ADP/ATP carrier?," *European Journal of Biochemistry*, vol. 199, no. 2, pp. 459–466, 1991.

[98] J. B. Bultema, H.-P. Braun, E. J. Boekema, and R. Kouril, "Megacomplex organization of the oxidative phosphorylation system by structural analysis of respiratory supercomplexes from potato," *Biochimica et Biophysica Acta*, vol. 1787, no. 1, pp. 60–67, 2009.

[99] I. Wittig and H. Schägger, "Supramolecular organization of ATP synthase and respiratory chain in mitochondrial membranes," *Biochimica et Biophysica Acta (BBA) - Bioenergetics*, vol. 1787, no. 6, pp. 672–680, 2009.

[100] S. M. Grundy, "Metabolic syndrome: a multiplex cardiovascular risk factor," *Journal of Clinical Endocrinology and Metabolism*, vol. 92, no. 2, pp. 399–404, 2007.

[101] G. Gastaldi, J. P. Giacobino, and J. Ruiz, "Metabolic syndrome, a mitochondrial disease?," *Revue Médicale Suisse*, vol. 4, no. 160, pp. 1387-1388, 2008.

[102] S. H. Kwak, K. S. Park, K. U. Lee, and H. K. Lee, "Mitochondrial metabolism and diabetes," *Journal of Diabetes Investigation*, vol. 1, no. 5, pp. 161–169, 2010.

[103] T. Doenst, T. D. Nguyen, and E. D. Abel, "Cardiac metabolism in heart failure: implications beyond ATP production," *Circulation Research*, vol. 113, no. 6, pp. 709–724, 2013.

[104] S. Judge and C. Leeuwenburgh, "Cardiac mitochondrial bioenergetics, oxidative stress, and aging," *American Journal of Physiology. Cell Physiology*, vol. 292, no. 6, pp. C1983–C1992, 2007.

[105] E. Murphy, H. Ardehali, R. S. Balaban et al., "Mitochondrial function, biology, and role in Disease," *Circulation Research*, vol. 118, no. 12, pp. 1960–1991, 2016.

[106] E. J. Anderson, M. E. Lustig, K. E. Boyle et al., "Mitochondrial H_2O_2 emission and cellular redox state link excess fat intake to insulin resistance in both rodents and humans," *The Journal of Clinical Investigation*, vol. 119, no. 3, pp. 573–581, 2009.

[107] M. C. Carr, "The emergence of the metabolic syndrome with menopause," *The Journal of Clinical Endocrinology & Metabolism*, vol. 88, no. 6, pp. 2404–2411, 2003.

[108] V. P. Skulachev, Y. N. Antonenko, D. A. Cherepanov et al., "Prevention of cardiolipin oxidation and fatty acid cycling as two antioxidant mechanisms of cationic derivatives of plastoquinone (SkQs)," *Biochimica et Biophysica Acta*, vol. 1797, no. 6-7, pp. 878–889, 2010.

[109] I. G. Shabalina, M. Y. Vyssokikh, N. Gibanova et al., "Improved health-span and lifespan in mtDNA mutator mice treated with the mitochondrially targeted antioxidant SkQ1," *Aging*, vol. 9, no. 2, pp. 315–339, 2017.

[110] Y. N. Antonenko, V. A. Roginsky, A. A. Pashkovskaya et al., "Protective effects of mitochondria-targeted antioxidant SkQ in aqueous and lipid membrane environments," *The Journal of Membrane Biology*, vol. 222, no. 3, pp. 141–149, 2008.

[111] F. F. Severin, I. I. Severina, Y. N. Antonenko et al., "Penetrating cation/fatty acid anion pair as a mitochondria-targeted protonophore," *Proceedings of the National Academy of Sciences of the United States of America*, vol. 107, no. 2, pp. 663–668, 2010.

Hindawi
Oxidative Medicine and Cellular Longevity
Volume 2020, Article ID 6813405, 20 pages
https://doi.org/10.1155/2020/6813405

Review Article

Wheel and Deal in the Mitochondrial Inner Membranes: The Tale of Cytochrome *c* and Cardiolipin

Antonio Díaz-Quintana, Gonzalo Pérez-Mejías, Alejandra Guerra-Castellano, Miguel A. De la Rosa, and Irene Díaz-Moreno

Instituto de Investigaciones Químicas (IIQ), Centro de Investigaciones Científicas Isla de la Cartuja (cicCartuja), Universidad de Sevilla – Consejo Superior de Investigaciones Científicas (CSIC), Avda. Américo Vespucio 49, Seville 41092, Spain

Correspondence should be addressed to Antonio Díaz-Quintana; qzaida@us.es and Irene Díaz-Moreno; idiazmoreno@us.es

Received 29 July 2019; Accepted 28 February 2020; Published 22 April 2020

Guest Editor: Armen Y. Mulkidjanian

Cardiolipin oxidation and degradation by different factors under severe cell stress serve as a trigger for genetically encoded cell death programs. In this context, the interplay between cardiolipin and another mitochondrial factor—cytochrome *c*—is a key process in the early stages of apoptosis, and it is a matter of intense research. Cytochrome *c* interacts with lipid membranes by electrostatic interactions, hydrogen bonds, and hydrophobic effects. Experimental conditions (including pH, lipid composition, and post-translational modifications) determine which specific amino acid residues are involved in the interaction and influence the heme iron coordination state. In fact, up to four binding sites (A, C, N, and L), driven by different interactions, have been reported. Nevertheless, key aspects of the mechanism for cardiolipin oxidation by the hemeprotein are well established. First, cytochrome *c* acts as a pseudoperoxidase, a process orchestrated by tyrosine residues which are crucial for peroxygenase activity and sensitivity towards oxidation caused by protein self-degradation. Second, flexibility of two weakest folding units of the hemeprotein correlates with its peroxidase activity and the stability of the iron coordination sphere. Third, the diversity of the mode of interaction parallels a broad diversity in the specific reaction pathway. Thus, current knowledge has already enabled the design of novel drugs designed to successfully inhibit cardiolipin oxidation.

1. Introduction

Mitochondria—the so-called powerhouses of the cell—are responsible for a broad assortment of metabolic processes. Their key role in cells is reflected by the cornucopia of proteins involved in its function. In total, more than 1150 genes related to organelle function are recorded in the human MitoCarta. Furthermore, 1 in every 5000 people are effected by a mitochondrial disorder [1].

Mitochondria play a significant role in cell homeostasis by helping to modulate cell signaling pathways. On one hand, the activity of the electron transport chain (ETC) is related to the release of reactive oxygen species (ROS) [2] which are strong modifiers of cell constituents such as proteins, nucleic acids, and lipids. Dysregulation of ROS can lead to oxidative stress which in turn can initiate cell death programs [3, 4], in which lipid peroxidation and their products play a key role [5].

Cardiolipin (CL) oxidation by cytochrome *c* (C*c*) at the onset of apoptosis is a decisive step [6]. During homeostasis, the soluble cationic hemeprotein is located in the mitochondrial intermembrane space, shuttling electrons between complexes III (CIII) and IV (CIV) in the ETC. Indeed, C*c* is a key Janus catalyst of CL signaling rather than a passive messenger. Its ability to oxidize superoxide anions ($O_2^{-\bullet}$) to molecular O_2 along with its peroxidase activity in solution reduce the damage caused by oxidative stress [7–12]. However, rearrangement of the mitochondrial membrane triggered by t-Bid upon severe stress makes CL available to bind C*c* [13] on the outer leaflet of the IMM. Thus, acyl chains of CL are oxidized due to the oxygenase activity of the hemeprotein [14]. In fact, oxygenase activity of C*c* rises substantially in

C*c*-CL complexes [15]. Subsequent CL oxidation favors the release of C*c* into the cytosol where it triggers apoptosis [16–18]. Furthermore, an array of products from C*c*-mediated CL oxidation—e.g., hydroxy-, oxo-, and peroxipolyunsaturated fatty acids—act as cell fate decision signals [19].

Although major features of cell death signaling pathways converging on CL metabolism have been thoroughly characterized, understanding the intimate mechanism of CL oxidation by C*c* remains challenging. Both CL-containing membranes and C*c* display complex behaviors that depend on different factors, including experimental conditions and post-translational modifications (PTM) of the protein.

This review article aims to provide the readers with an overview of the interaction between C*c* and CL and how it affects the peroxidase and oxygenase activities of the hemeprotein. Particular emphasis will be made on the conformational plasticity of C*c*, which enables its Janus functionality. In addition, we will discuss free oxidation of CL, regulation of C*c* activity, and its relationship with a diverse range of human diseases and recent strategies to combat them.

2. Cardiolipin: Properties and Role in the Mitochondrial Membranes

Cardiolipins (1,3-bis(*sn*-3′-phosphatidyl)-*sn*-glycerol) are a group of anionic phospholipids found in the plasma membrane of various bacteria and the inner mitochondrial membrane of eukaryotic cells [20]. These lipids contain two 1,2-diacyl-*sn*-glycero-3-phos-phoryl moieties bridged by a glycerol molecule. The two phosphatidyl groups are stereochemically nonequivalent, being respectively in *pro-R* and *pro-S* positions with respect to carbon 2 in the bridge [21]. The presence of 4 acylation sites—a fifth one at the central carbon of the glycerol bridge is also possible—would be consistent with a diverse range of CL species according to the distinct acyl chains available in a given organism. In humans, for instance, we would expect 14^4 CL derivatives. This contrasts with the rather lower diversity of CL compounds found in each organism [22].

Despite the presence of two phosphate groups in CL, it is thought that the single anionic species predominates. In this species, one proton is shared through a bicyclic resonance structure involving the central hydroxyl group [23]. In membranes, the glycerol hydroxyl forms intra- and interlipid hydrogen bonds with oxygen atoms from phosphate, not with carbonyl groups [24]. Early measurements of ionization constants yielded a first pK_A value of 2.8 and a second one in the range between 7.5 and 9.5. A recent fourier transform infrared spectroscopy (FT-IR) analysis on liposomes also suggests two ionization steps with pK_A values 4.7 and 7.9 [25, 26]. Density functional theory level computations indicate a wide gap between the two pK_A values [27]. Other results indicate the opposite: both behave as strong dibasic acids with pK_A values within the pH range 2-3 in solution [28] and membrane preparations [29, 30]. According to this data, membrane-embedded CL carries two negative charges at physiological pH values.

The behavior of CL-containing membranes is complex and strongly dependent on the composition [31] and experimental/simulation conditions [32]. For instance, the selected CL protonation state in deterministic simulations can influence results. Thermodynamic analyses with lipid mono- and bilayers indicate a decrease in the area compressibility modulus [33]. According to molecular dynamics (MD) simulations, their thickness—measured as interphosphate distances—decreases with CL content, as the electron density does [24, 34]. Furthermore, small-angle X-ray scattering (SAXS) and neutron scattering (SANS) have confirmed that CL-containing bilayers have a lower thickness. This may reflect the smaller head-group volume per phosphate. However, these membranes show larger distances between electron density maxima and a thicker hydrocarbon moiety [24]. Comparison of different MD trajectories of bilayers with PDB files suggests conformational selection takes place when CLs bind to membrane proteins [34]. The negative charge of CL and its four acyl groups strongly affect the phase preference of the lipid, which varies from lamellar ($L\alpha$) to inverted hexagonal (H_{II}) depending on pH [30, 32].

CL is essential for the functionality of mitochondrial membranes and processes taking place therein—e.g., protein import and electron transport [6]. It represents between 5% and 20% of the total lipid content of the inner mitochondrial membrane (IMM) and is more abundant in the internal leaflet [35, 36] (Figure 1(a)). CL acts on membrane components of the ETC, aiding the assembly of the so-called respiratory supercomplexes [37, 38]. Supercomplexes modulate the performance of mitochondrial electron transport and oxidative phosphorylation [39]. Reportedly, CL is able to trap protons [40, 41], and it has been hypothesized to be important in the mechanism of CIII and IV acting as a proton exchanger [42–44]. The absence and/or modification of CL cause the development of several pathologies such as Barth's syndrome [37, 45–48]. Indeed, alteration of the IMM due to a decrease in the content of CL disrupts the ETC, increasing the generation of ROS [49] (Figure 1(b)). Remarkably, CL can be oxidized directly by ROS such as hydroxyl radicals and singlet oxygen, acting the products as proapoptotic signals [50].

CL is a mitochondrial stress-signaling factor in mitophagy and both the intrinsic and extrinsic apoptotic pathways [6, 51]. Under stress conditions (e.g., treatment with rotenone, staurosporine or cyclosporine A, and autophagic or apoptotic stimuli), CL molecules flip from the IMM to the outer mitochondrial membrane (OMM) [52–54] (Figure 1(b)). When eliciting the extrinsic apoptotic pathway in lymphoblastoid cells (type II cells) derived from Barth's syndrome patients and tafazzin knock-down HeLa cells, CL microdomains on the OMM recruit procaspase-8 to promote its activation [55, 56]. When caspase-8 becomes active, it cleaves the proapoptotic factor Bid, a BH3-only member of the Bcl-2 family [56]. The active C-terminal fragment of the Bid (t-Bid) targets CL or its degradation product monolyso-CL (MLCL) in mitochondria [57–60] and promotes OMM permeabilization [61]. During this process, the peroxidase activity of C*c* results in the

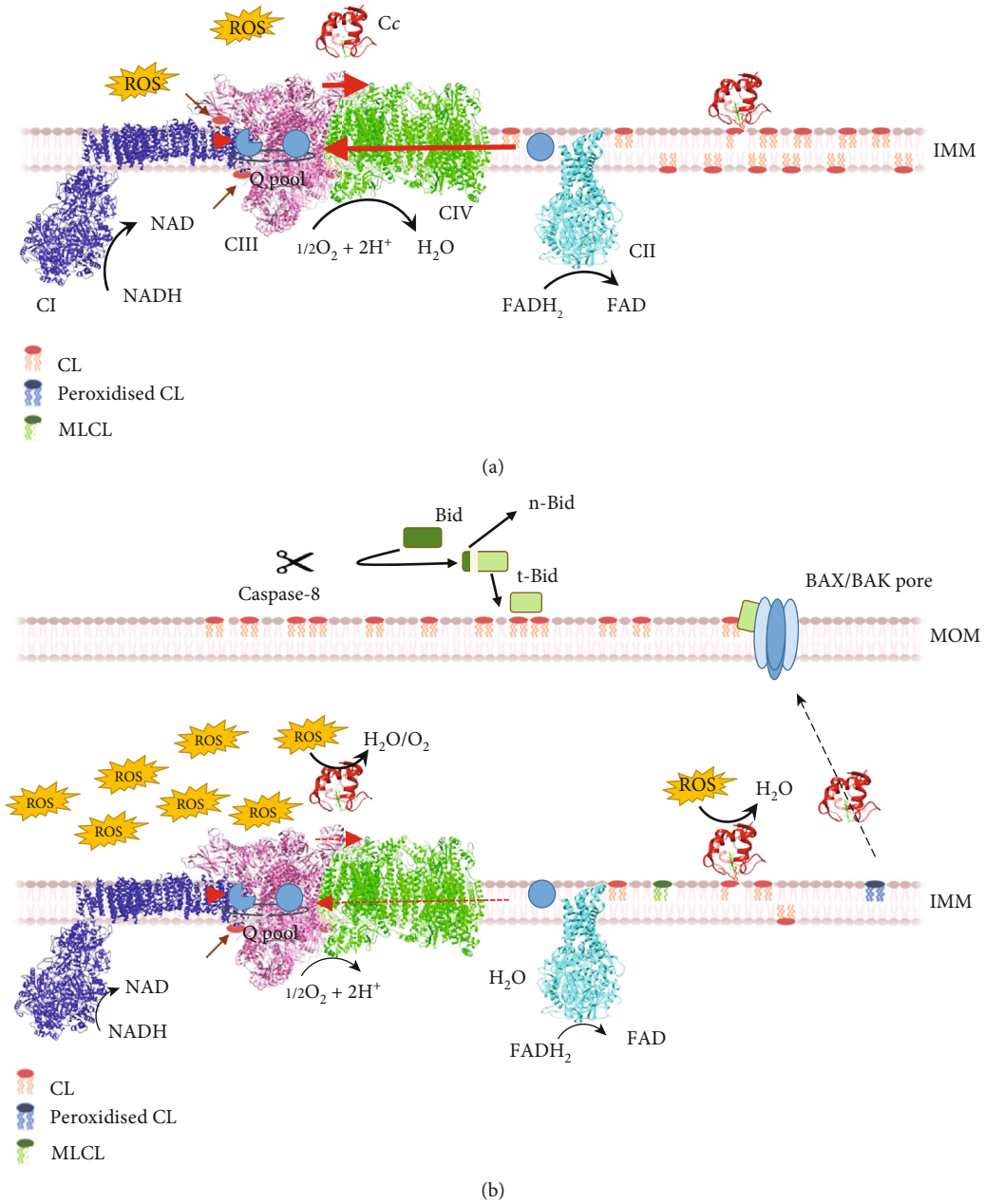

Figure 1: Role of cardiolipin in cell homeostasis and apoptosis. (a) Under homeostatic conditions, cardiolipin (CL) facilitates the assembly of respiratory supercomplexes (brown arrows) and maintains a population of C*c* bound to the inner mitochondrial membrane (IMM). The efficiency of electron transfer is high (thick red arrow). (b) Under apoptotic stimuli, procaspase-8 is recruited to CL-enriched microdomains in the outer mitochondrial membrane (OMM). The activation of caspase-8 involves cleavage of the BID proapoptotic factor into two domains, namely, the N-terminal (n-Bid) and C-terminal fragments (t-Bid). Dissociation of these two fragments is required for the interaction of t-Bid with CL. Then, t-Bid promotes the formation of mitochondrial pores by assembling BAX–BAK oligomers. At the same time, ROS production increases and C*c* acts as a ROS scavenger and pseudoperoxidase. C*c* peroxidase activity results in oxidation of CL acyl chains, to which the hemeprotein is anchored, freeing C*c* from the IMM, facilitating its subsequent release into the cytosol upon OMM permeabilization. The efficiency of electron transfer is low (dashed red arrow). In addition, CL can be degraded in part, losing one of its acyl chains, giving rise to monolysocardiolipin (MLCL).

oxidation of CL (to which it is anchored) facilitating the release of C*c* from the IMM and subsequent massive release into the cytosol at the onset of apoptosis [18, 62]. Extramitochondrial C*c* molecules interact with a variety of targets in the cytosol and nucleus, leading to a point of no return in the programmed cell death regulation [63–77].

3. Cytochrome *c* Binds Cardiolipin: A Tale of Grooves, Cavities, and Melting

C*c* belongs to the class I single-heme cytochrome *c* family, displaying the four typical α-helices conserved in the whole domain family [78]. In addition, C*c* displays three Ω-loops,

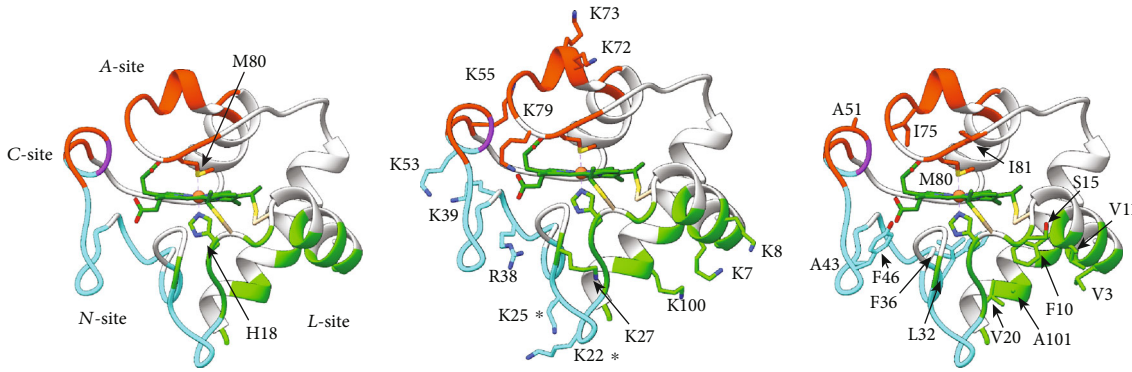

FIGURE 2: Cardiolipin-binding sites in cytochrome *c*. (a) Ribbon representation of oxidized human C*c* (PDB 2N9J) [92]. CL-binding sites are highlighted in orange (*A*-site or distal productive), green (*L*-site or proximal productive), purple (*C*-site), and cyan (*N*-site or proximal unproductive). The heme axial ligands H18 and M80 are highlighted as well. (b) Side chain representation of the positively charged C*c* residues involved in the formation of the C*c*-CL complex. Residues marked with an asterisk are reported to constitute the *L*- and *N*-sites. (c) Side chain representation of hydrophobic C*c* residues, which ensure the tight interaction between C*c* and CL acyl chains.

two of them providing axial ligands for the heme iron. His18 at the proximal side of the heme provides the imidazole ligand conserved among the class I family. At physiological pH values, Met80 thioether acts as a distal ligand. The heme porphyrin ring is covalently bound to the protein backbone by thioether bonds between the vinyl groups of the porphyrin and conserved cysteine residues in the CXXCH motif. For human C*c*, conserved cysteine residues are Cys14 and Cys17. According to hydrogen exchange (HX) experiments, the apparently simple structure hides five folding units (called foldons) with different stabilities [79]. The most stable one (I) comprises the N- and C-terminal α-helices. Foldon II comprises Ω_{I} (from Thr19 to Phe36) and α-helix 3, which comes before Ω_{III}. Foldon III (a.k.a. neck) comprises two short amino acid stretches with an extended conformation flanking the Ω_{II}-loop. Notably, the latter faces heme propionates and is the least stable foldon (V), followed by the Ω_{III} region (IV) containing Met80.

The low stability of the loop containing Met80, comprising the sixth iron ligand, has a crucial role in C*c* physiology. Recent ultrafast X-ray spectroscopy analyses have highlighted the weakness of the Met80-S_{δ}-Fe^{+2} bond and the lack of stability ($4\,kJ\,mol^{-1}$) provided by the protein matrix, most likely via hydrogen bonding [80].

At physiological pH, C*c* has a net charge of +8 from its unevenly distributed ionizable groups [81, 82]. This favors interactions with negatively charged molecules, such as the polar head of phospholipids, including CL. This interaction was first analyzed by Kimelberg and Lee, using lecithin-CL vesicles [83]. Their analysis together with early HX measurements by solid-state nuclear magnetic resonance (ssNMR) indicated that C*c* preferentially binds with CL [84]. They also suggested that during this interaction, CL destabilizes or unfolds the hemeprotein. Further relaxation time measurements by ^{31}P NMR showed that C*c* impacts CL dynamics [85]. Surface plasmon resonance and electrochemical experiments on planar lipid bilayers allowed Salamon and Tollin to propose a two-step mechanism [86–88]. According to their proposal, C*c* first binds to membranes through electrostatic interactions and, subsequently, through hydrophobic interactions to promote changes in both the structure of C*c* and the membrane. Then, electron paramagnetic resonance (EPR) and magnetic circular dichroism (MCD) analyses showed that C*c* undergoes structural changes which affect Fe coordination and result in the appearance of a radical at high liposome concentrations [89]. Hence, mixing C*c* with lipids may yield several species, found in recent fluorescence anisotropy analyses [90].

Apparently at odds with this proposed model, paramagnetic-quenching EPR experiments on horse heart C*c*, spin-labelled at different lysine positions, indicated that the hemeprotein can weakly interact with 1,2-dioleoyl-*sn*-glycero-3-phosphoglycerol (DOPG) bilayers [91]. This study highlighted three lysine residues at Ω_{III} (K72, K86, and K87, a.k.a *A*-site; Figure 2(a)) adjacent to the DOPG membrane. Further fluorescence studies using vesicles containing fluorescent lipid probes identified a secondary CL-binding site at low pH values [93]. Contrary to the *A*-site, CL association at this novel region (a.k.a. *C*-site; Figure 2(a)) is unaffected by ionic strength or the presence of ATP. Data suggested CL binds to this site via hydrogen bonds at N52, and a single acyl chain of the phospholipid inserts into a nearby hydrophobic pocket while the others remain in the bilayer [94]. This proposed interaction mechanism is known as the extended lipid anchorage model and is supported by studies on the ability of natural and engineered phospholipids to quench the fluorescence of Zn-substituted C*c* [95, 96]. Consistently, a N52I mutation heavily impacts the kinetics of the interaction between C*c* and CL in CL-containing liposomes [97].

While, a combination of lysine modification, tryptic digestion, and MALDI-TOF analysis unveiled that horse heart C*c* promotes the fusion of lipid vesicles via an interaction at a second positive patch. This region (*L*-site) comprises K22, K25, K27, H26, and H33, besides the previously reported *A*- and *C*-sites (Figure 2(a)) [98].

An additional UV-Vis analysis showed slight differences in the binding kinetics within a set of yeast C*c* mutants [99]. Based on their own data and the solution structure of

the protein (PDB 1AKK; [100]), the authors proposed a cleft defined by the Ω_{III} residues K72, K73, K86, and R91, matching *A*-site. Building on from this data, the ability of site-directed mutants of horse heart C*c* to bind CL-containing liposomes was tested [101]. Notably, substituting K73 and K79 with asparagine alters the affinity of C*c* towards these liposomes, whereas the same mutation at position 72 does not.

A common feature of these binding sites is the presence of several positively charged and hydrophobic residues (Figures 2(b) and 2(c)). In line with Tollin and Salamon's early postulates [88], the interaction between the positively charged residues of C*c* and negatively charged phosphate groups of CL initiates the formation of the C*c*-CL complex driven by electrostatic interactions [101–104]. After the initiation of the complex, hydrophobic C*c* residues play a key role in the interaction with CL acyl chains, thereby establishing a tight binding between C*c* and CL [15, 105].

A strong piece of evidence supporting the extended anchorage hypothesis is the presence of a channel formed by residues 52 to 74 in the tuna C*c* XRD structure [81], where the highlighted cavities are only visible in the 4 Å model. An attempt to manually dock CL inside the structure of horse heart C*c* yielded two acyl chains within the backbone [97]. Any assessment of clashes of these two acyl chains with internal residues was missing. Nevertheless, none of the two cavities in this structure appear in the updated structure at 1.5 Å resolution (PDB 5CYT; unpublished). Hence, the extended lipid anchorage model demands that C*c* must undergo a substantial conformation change when interacting with lipid vesicles. A low-resolution analysis using monoclonal antibodies suggested that lipid-bound C*c* displayed an alkaline-like conformation [106]. The alkaline form of oxidized C*c* presents a conformation different to that of the native species, which relates to an exchange between the Met thioether ligand and a Lys amine. However, to our knowledge, the only C*c* alkaline structure available (PDB 1LMS; [107]) lacks a channel in which the acyl chain may be lodged, although the heme moiety is more accessible to solvent than the native structure. Another possibility is the formation of C*c* oligomers by domain swapping [108, 109]. Although these structures are highly variable depending on how the domain swapping is triggered by experimental conditions, a recent analysis has shown they are capable of encompassing an acyl chain [110]. Furthermore, Tyr67 in these structures would face C_{11} of docked linoleic ($18:2^{\Delta 9,12}$) acid, a finding in agreement with peroxidation mechanisms. However, evidence of C*c* oligomerization in the presence of membranes remains unavailable.

Many of the studies above report the loss of the Met80 coordination and at least partial denaturation—or transition to a molten globule state—of C*c* when binding to CL-containing vesicles or liposomes [15, 84, 93, 95–97, 109–111]. Aside from CL, some other lipids can elicit similar such structural changes in C*c* [105]. This makes the heme moiety more accessible to small substrates such as carbon monoxide or nitric oxide [105, 111]. Moreover, time-resolved fluorescence resonance energy transfer (trFRET) experiments show labelled residues—not previously reported to bind CL—moving further away from the heme group in the presence of CL-containing liposomes [103, 112]. Furthermore, changes in the CD spectra and Trp59 fluorescence indicate unfolding of at least the lowest energy foldons. Consistent with the loss of Met80 coordination, substantial negative shifts in the midpoint potential of C*c* are observable in the presence of lipid vesicles [113, 114]. Disruption of the Fe-Met80 bond also correlates with a substantial increase in C*c* peroxidase activity when C*c* interacts with CL-containing vesicles [15, 105, 113]. An illustration of conformational changes, adapted from Muenzner et al. [112], is available in Figure 3(a).

The current understanding of the effects of lipid binding on C*c* structure (as described above) is controversial. For instance, depending on the nature of the CL-rich membrane preparations and experimental setup, the shift in redox potential can be positive [86] or negative [113, 114]. Recently, Wand and collaborators demonstrated that the mitochondrial crypts are concave surfaces, opposed to the convex lipoic vesicles often used in the analyses. They then analyzed the solution structure of oxidized horse heart C*c* encapsulated in reverse lipid micelles by NMR [115]. They utilized pseudocontact shifts as experimental restraints, which are highly sensitive to distances and orientation with respect to the main axes of the iron coordination sphere. An overlay of the structures of free [100] and encapsulated horse C*c* [115] (PDB 1AKK [100] and 2N3B [115], respectively) are shown in Figure 3(b). Notably, the structure of C*c* remains unaltered, and the chemical-shift perturbation map [115] resembles that observed for interactions between C*c* and its protein targets [116] and other class I single-heme cytochrome *c* family members [117]. In fact, this patch includes a novel region (*N*-site), not previously reported, comprising F36, G37, T58, W59, and K60, besides the known residues of the *A*- and *L*-sites (Figure 2(a)). Surprisingly, ssNMR spectra tracking the interaction between C*c* and small unilamellar (convex) vesicles showed no feature indicating formation of either a molten globule or unfolding [118]. Consistently, solution HSQC (NMR) spectra of horse heart C*c* in the presence and absence of similar vesicles overlapped quite well [119]. Although some signals broaden, while others were displaced—as expected for this interaction—no features of unfolding are apparent. Therefore, the overall curvature or the membrane may be irrelevant for the stability of bound C*c*. Previous data on C*c* unfolding in the presence of lipid vesicles might be reviewed in regard to membrane composition, lipid stability, and experimental setup. For instance, the dynamics of C*c* can change depending on buffer conditions [119]. Similarly, the ionization state of CL also affects C*c* binding [120].

Understanding the entire landscape of the data requires the rationale underpinning the studies to be taken into account. An equilibrium between unbounded native C*c* species and membrane-bound populations—by either weak electrostatic interactions, hydrogen bonding, or hydrophobic interactions—can be observed. The relative weights of such populations vary with experimental conditions. Furthermore, our ability to detect different species relies on the sensitivity of each biophysical approach. As recently pointed out,

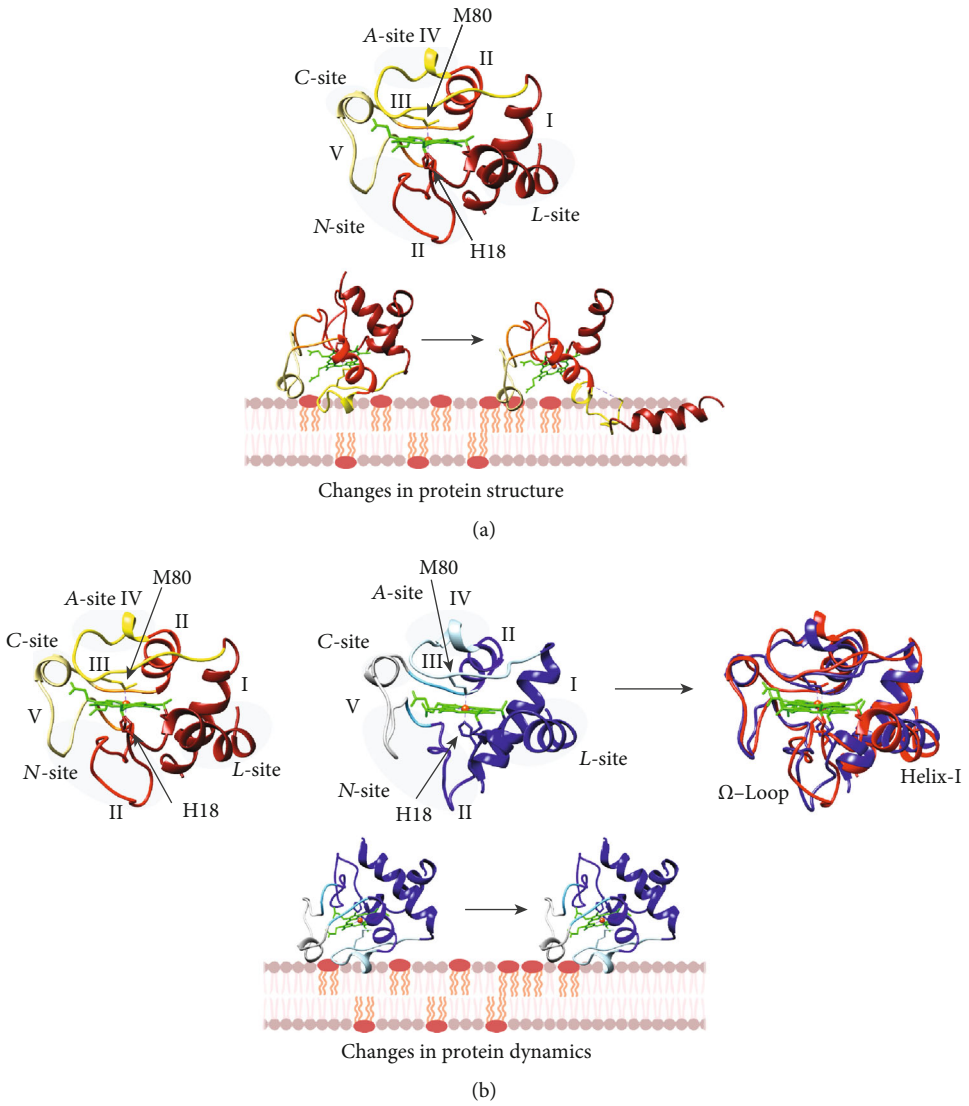

Figure 3: Proposed model for the interaction of cytochrome *c* with cardiolipin at pH values above 7. (a) Upper: structure of free C*c* showing the foldon units (in red scale, PDB 1AKK [100]). Lower: the C*c*-CL interaction promotes unfolding of the metalloprotein and dissociation of the axial ligand M80, thus increasing accessibility to the heme crevice. (b) Upper: structural comparison of free (in red scale, PDB 1AKK [100]) and CL-bound C*c* (in blue scale, PDB 2N3B [115]). Lower: interaction of C*c* with CL yields a slight difference in dynamics at the level of the Ω-loops and helix-I. The different foldon units of C*c* are colored as a gradient from the most stable (dark colors) to the weakest region (light colors). The heme group is in green, and the iron atom in orange.

many of the analyses above suffer from low-resolution data or the introduction of probes that could partially alter results [118]. Therefore, full understanding requires complete knowledge of experimental conditions.

4. Interplay between Lipid and Cytochrome *c* Dynamics: The Compact/Extended Model

C*c* can undergo several structural transitions triggered by changes in experimental conditions such as pH [89, 90, 121–123]. For example, low-spin ($S = 0$) Fe^{II} species may turn into high-spin ($S = 2$) species in the presence of liposomes, as shown by EPR and MCD spectroscopies [89]. Notably, ionic strength and lipid-to-protein (L/P) ratio strongly influence the populations of the distinct species [15, 110, 124, 125]. These ratios relate to lipid surface coverage by C*c* molecules [125, 126]. At low L/P ratios the C*c*-coated micelles undergo coalescence—forming giant unilamellar vesicles—and precipitate. Whereas at moderate L/P ratios, C*c* promotes interactions between small unilamellar vesicles [125, 127].

The dynamic of the C*c* heme group is highly sensitive to spin state, axial ligand strength, and conformational changes. Therefore, Raman spectroscopy studies have been key in unveiling the complexity of C*c* conformation equilibria under different conditions [123, 125–128]. Hildebrandt and collaborators detected native (B1; His-Met coordination) and altered (B2) states in the presence of DOPG vesicles [125]. The B2 state comprises different species: a low-spin (B2[6cLS]), His-His-coordinated species, and two high-spin

species (a pentacoordinated (B2[5cHS]) and a hexacoordinated species (B2[6cHS])) in which a water molecule acts as the sixth ligand. The populations of the different states change according to the L/P ratio. The B2 species predominates at high L/P ratios, whereas native B1 and His-His-coordinated B2[6cLS] coexist at lower ratios. These states are also detectable by MCD [114]. The B2 bis-His-coordinated species is detectable when C*c* is absorbed onto self-assembled monolayers, with and without CL [129]. At increasing concentrations of DOPC/tetraoleoylcardiolipin (TOCL) micelles, the population of bis-His species increases, as confirmed by His-by-Asn mutations and spectroscopic analyses [130].

In addition to the L/P ratio, the content of CL and its composition influence C*c* affinity and dynamics in the bound state. Fluorescence data has indeed revealed that increasing amounts of CL favors C*c* binding to membranes [120]. The theoretical analysis therein suggests that the protonation state of CL may have a strong influence on populations of distinct membrane-bound C*c* species. However, the authors acknowledge that the formalism does not include the effects that C*c* exerts on CL distribution or membrane state (see below). Indeed, kinetic investigations have shown that the exchange rate between a native-like, compact (C) and the "extended" (E) conformations correlates with the amount of CL in the vesicles [131]. A more recent spectroscopic analysis on titration experiments by Pandiscia and Schweitzer-Stenner resulted in similar conclusions [90]. Additionally, the study highlighted that the L/P ratio also affects the relative weight of electrostatic interactions, hydrogen bonds, and hydrophobic interactions—according to ionic strength series. In summary, besides governing C*c* conformational states, the L/P ratio modulates the nature of bilayer-protein interactions. Notably, all the studies highlighted above hint at a rather peripheral binding model, with little or no embedding of C*c* into the membrane [90, 123, 125, 126, 128, 129, 131].

On the other hand, C*c* does exert a strong influence on lipid head-group dynamics, as revealed by early ^{31}P ssNMR studies which demonstrated an increase in acyl chains dynamics and a restraint in the polar head groups of phospholipids [132, 133]. Interestingly, C*c* has little impact on the ^{31}P ssNMR "powder" spectra of dioleoyl-phosphatidylcholine (DOPC), dioleoyl-phosphatidylethanolamine (DOPE), or DOPC/DOPE vesicles not containing CL [134]. Indeed, NMR data strongly supported CL undergoing phase separation—to form CL rafts—within mixed DOPC/CL preparations upon the addition of C*c* [132, 135]. Further, freeze-fracture electron microscopy images highlighted the ability of C*c* to promote the transition of phospholipid bilayers containing CL into non-bilayer structures, including inverted tubular (H_{II}) states [133, 134]. A full isotropic signal in the ^{31}P ssNMR spectra of phospholipid preparations in the presence of C*c* evinced the formation of vesicular or micellar structures when the vesicles contained CL [132, 136]. Similarly, a downfield broad signal indicated that CL mediates the formation of the H_{II} phase upon the addition of C*c*. In this sense, molecular dynamics simulations in which C*c* is in contact with a DOPC/CL membrane highlight the ability of this protein to recruit CL into rafts [118]. In addition, C*c* can induce local changes in membrane curvature when the ratio of CL increases up to 20%. Furthermore, C*c* induces pore formation in DOPC/CL giant unilamellar vesicles (GUV), as shown by confocal microscopy [137]. These pores are wide enough to allow C*c* and dextran molecules to cross the membrane.

Nevertheless, the ability of C*c* to induce membrane changes seems to be secondary regarding the activation of peroxidase activity. Addition of C*c* to large DOPC/CL unilamellar vesicles at a ca. 6 CL/C*c* ratio promotes peroxidase activity without substantially affecting ^{31}P ssNMR spectra or the ^{13}C frequencies of the lipid glycerol signals [138]. The major population—those accounting for less than 10% of the protein are not detectable—of C*c* in these experiments displays the same structure as the native protein *in solution*. Chemical-shift perturbation analysis revealed that residues affected include the Ω_{III}-loop and some nearby residues (including *A*-site residues). However, changes in the dynamics of the Ω_{III}-loop as it couples with bilayer motions are observable. This, rather than an overall unfolding, is sufficient to trigger the peroxidase activity under these conditions. In accordance with this finding, the perturbation pattern shifts when the temperature is changed or when the vesicle phospholipids are unsaturated.

The formation of C*c*-CL complex requires approximately 6 molecules of CL per C*c* molecule [15, 112, 119, 138, 139]. The values of the apparent dissociation equilibrium constant for the C*c*-CL-reduced complex are in the low micromolar range (1.4 μM at pH 8.1 and 2.2 μM at pH 6.5) [140], whereas in the oxidized form, they are in the high micromolar range in a two-step reaction (20 μM and 42 μM) [102]. Nevertheless, binding constants depend on CL composition. The affinity of C*c* towards tetrastearyl-cardiolipin-containing vesicles is several fold higher than that for TOCL ones [102], whereas tetra-myristoyl-cardiolipin barely interacts C*c* [15]. Notably, the measured affinities correlate well with the peroxidase activity of C*c* in the presence of the respective vesicles, rather than the degree of unsaturation in the acyl chains [102].

5. Cardiolipin Oxidation by Cytochrome *c*

CL is particularly sensitive to auto-oxidation processes—those directly initiated by inducers, such as ROS. The proximity of its four unsaturated acyl chains allow "arm-to-arm" propagation, enhancing its reactivity [141]. Auto-oxidation takes place in several steps. A free radical (e.g., a ROS molecule) contains an unpaired electron, and this semioccupied orbital is a sink for a second electron. Polyunsaturated fatty acids (PUFA), such as linoleic or linolenic composing CL, are particularly sensitive to ROS-induced oxidation due to conjugative effects. Radicals such as superoxide, peroxyl ($ROO^{\bullet}$), or hydroxyl ($HO^{\bullet}$) sequester a hydrogen atom from the α-methylene carbon with respect to the first (di-) vinyl group. The resulting radical reacts immediately with O_2 to generate a peroxyl radical. The variation of electron vacancy in the lipid radical underlies the diversity of reaction products. No matter how the lipid radical originates, it tends to propagate via

a reaction with molecular oxygen, water, or other lipids. Within the process of CL signaling, there are several reactions which stand out including the addition of oxygen (to form peroxides), transfer of hydrogen atoms, addition of peroxyl radicals, and intramolecular peroxide substitution [142].

Oxidative phosphorylation and certain mitochondrial enzymes are sources of $O_2^{-\bullet}$ radicals [143]. Superoxide is highly soluble in lipids but can be reduced within membranes by tocopherol and quinone and eliminated by superoxide dismutase (SOD), which transforms two superoxide molecules into a molecular oxygen and hydrogen peroxide [144]. In fact, enzymes like SOD, catalase, and peroxidases take part in active cell defense against oxidative stress [144]. H_2O_2 is a strong oxidant—the reduction potential for the H_2O_2/H_2O pair is +1.35 V, at pH 7—but kinetically inefficient. However, the presence of iron chelates under certain pathological conditions can enhance H_2O_2 efficiency through Haber-Weiss-like reactions (see Equations (1)–(3)) [145]:

$$Fe^{3+} + H_2O_2 \longrightarrow Fe^{2+} + O_2^{-\bullet} + 2H^+ \quad (1)$$

$$Fe^{2+} + H_2O_2 \longrightarrow Fe^{3+} + HO^- + HO^{\bullet} \left(\text{Fenton's reaction}\right) \quad (2)$$

$$O_2^{-\bullet} + Fe^{3+} \longrightarrow Fe^{2+} + O_2 \quad (3)$$

The hydroxyl radical product is highly reactive, sequestering hydrogen atoms from available substrates. The resulting carbon-centered radicals may react with molecular oxygen to generate (hydro-) peroxides (Equations (4)–(6)):

$$HO^{\bullet} + RH \longrightarrow H_2O + R^{\bullet} \quad (4)$$

$$R^{\bullet} + O_2 \longrightarrow RO_2^{\bullet} \quad (5)$$

$$RO_2^{\bullet} + H^+ + Fe^{2+} \longrightarrow ROOH + Fe^{3+} \quad (6)$$

Nevertheless, homeostatic cells exert a tight control over metal chelation to avoid Fenton's reactions. Indeed, a set of antioxidant agents prevent a surge in the levels of ROS. Hence, except for pathological conditions, H_2O_2 requires the activity of peroxidases to function efficiently as an oxidant. Within the IMM, C*c* displays both peroxidase and oxygenase activities, the latter promoting CL oxidation, while sparing other phospholipids [18, 146]. This event is crucial for the release of mitochondrial proapoptotic factors into the cytoplasm [18].

5.1. Peroxidase and Oxygenase Activities of Cytochrome c (Dr. Jeckyll and Mr. Hyde). Heme peroxidases constitute a vital and ubiquitous group of heme enzymes catalyzing the two-electron oxidation of substrates using H_2O_2 as the ultimate electron acceptor [147, 148]. In canonical peroxidases, H_2O_2 is added to the pentacoordinated, high-spin Fe^{III}. The resulting state—Compound I—is two oxidation equivalents above the resting state and is reduced back to the resting configuration in two steps through Compound II. Both states, Compounds I and II, are high valence oxoferryl (Fe^{IV}) derivatives, but the first comprises an additional π-cation radical (see Equations (7)–(9)) (Figure 4) [147].

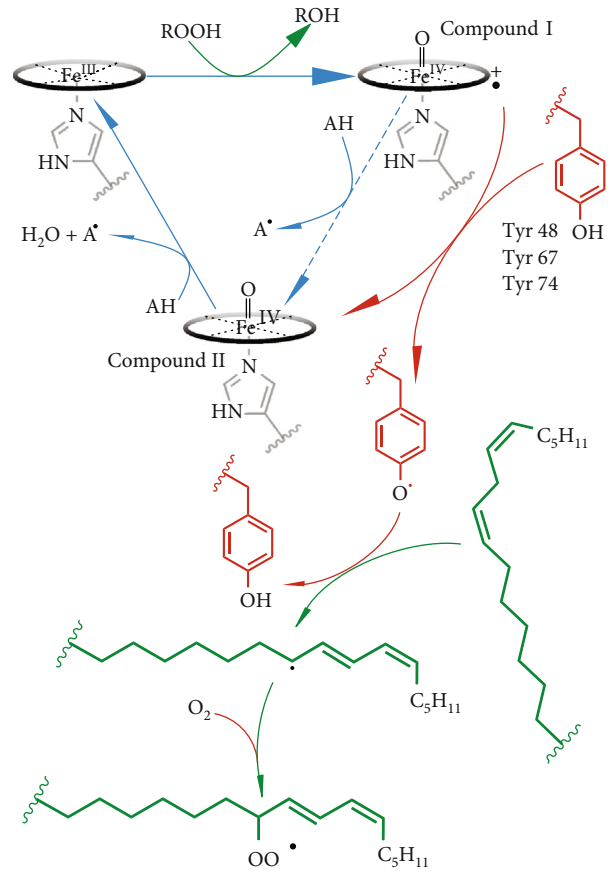

Figure 4: Peroxidase and oxygenase activities of cytochrome *c*. Reaction model merging the proposal from Kagan and collaborators [149] and the adapted catalytic model of cyclooxygenases as reviewed by Marnett [150]. Blue arrows correspond to the canonical peroxidase cycle [146]. Heterolytic cleavage of a peroxide substrate—preferentially for C*c*, a lipid hydroperoxide—yields the corresponding hydroxyl derivative (or water when the substrate is H_2O_2) and Compound I, which is reduced back to the resting ferric state in two sequential single-electron transfers from A substrate. Red and green arrows indicate the reactions purportedly leading to oxygenase activity according to the literature. Spin trap experiments have detected Y48 radicals [151]. Dimers of tyrosines 67 and 74 and oxidation products of Y48 are detectable even in the absence of H_2O_2 [152]. The tyrosyl radical sequesters a hydrogen atom from an unsaturated fatty acid. Finally, O_2 reacts with the alkyl radical to form an alkyl peroxide radical as an initial product undergoing further reactions.

$$\text{Heme}\left[Fe^{III}\right]_{RS} + H_2O_2 \longrightarrow \text{Heme}\left[O = Fe^{IV} - R^{\bullet+}\right]_{CompI} + H_2O \quad (7)$$

$$\text{Heme}\left[O = Fe^{IV} - R^{\bullet+}\right]_{CompI} + AH_2 \longrightarrow \text{Heme}\left[O = Fe^{IV}\right]_{CompII} + AH^{\bullet} \quad (8)$$

$$\text{Heme}\left[O = Fe^{IV}\right]_{CompII} + AH_2 \longrightarrow \text{Heme}\left[Fe^{III}\right]_{RS} + AH^{\bullet\bullet} + H_2O \quad (9)$$

In true peroxidases, a histidine residue acts as an acid-base catalyst at the distal side of the heme ring, while a highly conserved arginine residue stabilizes the alkoholate leaving group to favor the heterolytic cleavage of the peroxide O–O bond [153]. The orientation of these residues and the hydrogen-bond network at the heme distal side are critical for efficient formation of Compound I [154]. As recently pointed out by Vlasova [148], the composition of a true peroxidase active site prevents its damage by highly oxidizing intermediate compounds.

C*c* and other hemeproteins can act as pseudoperoxidases; that is, under only certain stimuli they show peroxidase activity [148, 155]. Contrary to true peroxidases, the surroundings of heme moiety are unprotected against oxidation, so the peroxidase activity ends up damaging the protein. In the early 1990s, Radi and collaborators reported the ability of C*c* to oxidize small compounds in solution [145] and to carry out lipid peroxidation [146] in the presence of H_2O_2. Nevertheless, the reactivity of C*c* towards H_2O_2 was low, as it requires the absence of the sixth ligand. Thus, the K_m value for H_2O_2 was very high—ca. 65 mM. In this sense, oxidative reactions showed a time lag after the addition of H_2O_2, indicative of an activation step. Moreover, peroxidase activity in solution decayed at pH values higher than 8 [145]. Poor reactivity may also result from the absence of histidine at the distal site (*vide infra*), as it is an acid-base residue "pumping" the heterolytic cleavage of H_2O_2 during Compound I formation. Based on chemiluminescence analyses of the reaction, Chance and coworkers proposed a homolytic reaction mechanism (Equations (10)–(12)) [156], supported by EPR spin trap studies of small organic hydroperoxides [157].

$$\text{Heme}\left[\text{Fe}^{\text{III}}\right] + \text{H}_2\text{O}_2 \longrightarrow \text{Heme}\left[\text{HO}^{\bullet} - \text{Fe}^{\text{III}}\right] \quad (10)$$

$$\text{HO}^{\bullet} + \text{H}_2\text{O}_2 \longrightarrow \text{H}_2\text{O} + \text{HO}_2^{\bullet} \quad (11)$$

$$\text{Heme}\left[\text{HO}^{\bullet} - \text{Fe}^{\text{III}}\right] + \text{HO}_2^{\bullet} \longrightarrow \text{Heme}\left[\text{Fe}^{\text{III}}\right] + \text{O}_2 + \text{H}_2\text{O} \quad (12)$$

However, EPR spin trap experiments highlighted the generation of C*c* tyrosine radicals upon treatment with H_2O_2 [18, 151, 155, 158]. Furthermore, spin trap experiments detecting radical products resulting from oxidation of different substrates by H_2O_2 strongly suggested the reaction being mediated by an oxoferryl [O=Fe^{IV}] intermediate [155]. Analysis of the orientation of this radical within the native state identified a tyrosine residue at the Ω_{II}-loop—namely, Y48 in horse heart C*c* and either Y46 or Y48 in human C*c* [159]. The peroxidase activity of C*c* in the presence of CL increases by three orders of magnitude when the driving oxidant is a lipid peroxide instead of H_2O_2 [149]. Spin trap analysis of reaction products by Kagan and collaborators indicates a diversity of catalytic mechanisms depending on the binding site of the substrate, namely, a homolytic peroxide cleavage minority mechanism and a major, heterolytic mechanism. Notably, the small hydroperoxide substrates involved in this pathway dock near R38 and H33. However, how the docked structure undergoes conformational changes to fulfil all geometrical constraints needed for Compound I formation remains unclear (Figure 4).

Binding of hydrogen peroxide to the heme iron is a key step in the reaction mechanism underlying peroxidase activity. The reactive species need to displace the thioether axial ligand. This takes place when a strong interaction between C*c* and a membrane induce a substantial conformational change in the hemeprotein [15, 84, 93, 95–97, 109, 111]. Nevertheless, Kagan and coworkers also detected peroxidase activity in C*c* at low CL/C*c* ratios—at which the most interactions are weak electrostatic [15]. Furthermore, they found that the energy required to activate peroxidase activity is lower than that required for partial unfolding of the protein. In fact, as pointed out before, the bond joining iron to the thioether ligand is quite weak [160]. Thus, "breathing" fluctuations of Ω_{II}- and Ω_{III}-loops may facilitate the replacement of the thioether ligand by small reactants—such as cyanide, carbon monoxide, water, or hydrogen peroxide—without demanding major structural changes. In fact, C*c* peroxidase activity rises in the presence of H_2O_2 as the concentration of denaturant increases, as previously observed in a similar analysis with bacterial cytochrome c_{550} [161]. Statistical analysis of activity and unfolding slopes indicate that increasing the motions of the weakest Ω-loops correlates well with peroxidase activity in the "compact" C*c* species [162].

The peroxidase activity of C*c* can exert a protective role in mitochondria under certain conditions [11]. Indeed, reduction of lipoid hydroperoxide compounds to hydroxyl ones provides a way of relieving oxidative stress in the mitochondrial membrane while generating signaling molecules [149]. Moreover, $O_2^{-\bullet}$ reduces nitric oxide ($^{\bullet}$NO) generated in mitochondria under stress to form peroxynitrite (HOONO), a highly reactive species. C*c*-CL complexes have been proposed to aid peroxynitrite detoxification to yield either nitrate or nitrite through an oxoferryl state [163].

Conversely, the peroxidase activity of C*c* has been implicated in certain pathologies. For instance, oxidation of sulfite to its radical $SO_3^{-\bullet}$ is a key mechanism in sulfite toxicity [164]. Moreover, C*c* mediates the formation of tyrosine radicals responsible for α-synuclein dimerization [66, 165], which leads to the development of the Lewy body diseases.

Canonical peroxidase activity involves two sequential one-electron oxidation steps and no transfer of oxygen from the oxoferryl complexes to the substrate [146]. Nevertheless, Compound I in certain heme enzymes—such as cytochrome P450—can transfer oxygen to certain substrates yielding hydroxy-derivatives. Interestingly, hydroxy-derivatives of CL cannot undergo peroxidation and inhibit the release of C*c* [166]. Altogether, considering the findings above concerning tyrosyl radicals in C*c* [151], Kagan and collaborators proposed that C*c* acts as an oxygenase to produce CL peroxidation [167]. This activity would also be responsible for phosphatidylserine peroxidation affecting the plasma membrane during apoptosis [65]. This hypothesis suggests that hydrogen is transferred to Compound I from a nearby tyrosine residue to yield oxoferryl Compound II and the aforementioned tyrosyl radical (Figure 4). This mechanism is similar to that proposed for cyclooxygenases, in which a hydrogen atom is sequestered from an acyl chain, generating

a carbon-centered radical capable of reacting with molecular oxygen [150].

Unlike true peroxidases, the environment of the heme moiety is unprotected from highly oxidizing species arising during the catalytic cycle [148]. When reacting with H_2O_2, degradation of the heme porphyrin often becomes apparent by a diminution of the Soret band intensity [146, 156]. A thorough mass spectrometry analysis of C*c* residue adducts derived from H_2O_2 has been carried out by Flemmig and collaborators [152]. Several oxidation reactions can occur to produce a methyl-sulfoxide derivative from the methionine thioether, a sulfonic acid derivative from cysteines and 2-oxohistidine from histidine. While tyrosine residues can covalently cross-link or undergo oxidation to dihydroxyphenylalanine (DOPA) and subsequently to quinones, lysine residues can undergo carbonylation [152, 168, 169]. These changes occur when H_2O_2 is added to C*c* samples [80, 152, 170–173].

Remarkably, different regions in the protein display different sensitivities to oxidation depending on the environment. For instance, specific M80 oxidation takes place in the presence of DOPC/DOPE micelles [174]. The Ω_{III}-loop is the first to be affected, whereas foldon I (helices I and IV) is the least affected by oxidation. Notably, the peroxidase activity of C*c* increases in a time-dependent manner upon the addition of H_2O_2. Such increments in peroxidase activity may result from successive oxidation of M80 and lysine residues, as proposed by Yin and Konermann [80, 170]. Indeed, M80 oxidation promotes conformation exchange in C*c* which impacts on heme ligation. With time, oxidative damage extends to the porphyrin ring, releasing iron capable of performing Fenton's reactions [173]. Finally, it is worth noting that CL peroxides can induce at least some of these oxidative PTM [152].

5.2. The Alkaline Transition of Cytochrome c and Peroxidase Activity. As mentioned above, previous data obtained using monoclonal antibodies highlighted that an alkaline-like conformation could interact with CL and exit mitochondria during apoptosis [106]. These antibodies also recognize the M80A mutant in the cell nucleus [175]. Notably, this mutant displays enhanced peroxidase activity. In addition, the peroxidase activity of C*c* is somewhat pH dependent [145, 176]. Indeed, for horse heart C*c*, peroxidase activity increases at acidic pH values [177] and slows beyond pH 8 [145]. Furthermore, the ability of C*c* to oxidize $O_2^{-\bullet}$ falls at pH values above 7 [7]. The affinity of C*c* towards membranes and the interaction patch involved also depend on pH [15, 98, 120, 127]. These effects illustrate how pH-dependent conformation changes modulate the different activities performed by C*c*.

A number of mutations and PTM have been reported to simultaneously affect the peroxidase activity of C*c* while bringing the so-called alkaline transition to lower even physiological pH values [178–182]. Loss of M80 coordination is evident from NMR spectra and UV-Vis spectra in all these studies. C*c* peroxidase activity requires the heme iron to be pentacoordinated; the relationship with the pK_A of the alkaline transition could be attributable to the lysine amine being weaker than methionine thioether in the ligand. However, at a neutral pH, lysine is a stronger ligand than methionine [183]. In fact, horse heart and human C*c* show lower peroxidase activities at alkaline pH values [145, 182]. Moreover, mutation M100K in *P. versutus* cytochrome c_{550} makes the protein more stable at neutral pH while decreasing its peroxidase activity 20-fold [183].

Nevertheless, the shift in the alkaline transition towards lower pH values indicates destabilization or higher dynamics in the Ω_{II}- and Ω_{III}-loops in the Met-coordinated species. Given the weakness of the thioether ligand bond towards iron, increasing fluctuations of these loops will increase the population of high-spin species and/or alternative low-spin (e.g., bis-His) species below the pK_A value of the transition. This is observable in phosphomimic mutants, as well as in nitrated species of C*c* [178–180, 184–186]. Furthermore, enhanced dynamics facilitate the access of small substrates to the heme iron [162].

5.3. Control of Cardiolipin Oxidation by Post-translational Modification of Cytochrome c. Protein PTM regulate tightly controlled cellular processes and increase the functional diversity of proteins, often acting as a cell response switch. Several post-translational modifications modulate C*c* structure and functionality, such as sulfoxidation [187], carbonylation [152], homocysteinylation [188], nitration [179, 180], and phosphorylation [189] (Figure 5). Phosphorylation of tyrosine residues is associated with many human pathologies including cancer, ischemia, asthma, and sepsis. As highlighted earlier, tyrosine radicals are key for the oxygenase activity of C*c* [157]. Thus, the amount of hydroxyl products from TOCL oxidation is lower when Y48E phosphomimic species instead of WT C*c* acts as a catalyst [190]. Additionally, tyrosine phosphorylation impairs the formation of radicals, preventing dimerization [191]. This fact may be critical in pathological processes such as Parkinson's disease [66]. Therefore, the PTM that affect these residues are key in regulating C*c* activity.

Given the difficulty in preserving the phosphorylation state of C*c* outside of cell extracts, a common strategy to investigate consequences of phosphorylation is to mimic the modification by site-directed mutagenesis. All phosphomimetic C*c* species, except a mutant at position 97, display altered affinity towards cardiolipin [178, 186, 190, 192–195]. The peroxidase activity of both free C*c* and C*c*-CL complexes increases in the phosphomimetic T28D and Y48*p*CMF. However, for the Y48E species, the increase only occurs with the free protein (Table 1) [178, 190, 192, 194]. In addition, at a high CL/lipid ratio, the peroxidase activity of the T28E mutant decreases [195]. A possible explanation may be that the greater population of CL versus other lipids in the liposome composition promote unfolding of the hemeprotein, acting as an off switch (Table 1) [131]. Hence, the negative charge at these positions could induce structural changes in the heme crevice which allow greater accessibility for hydrogen peroxide (Figure 5).

Peroxynitrite generated during nitrooxidative stress is a powerful amino acid modifier, affecting tyrosine residues among others [201]. Common products of the reaction

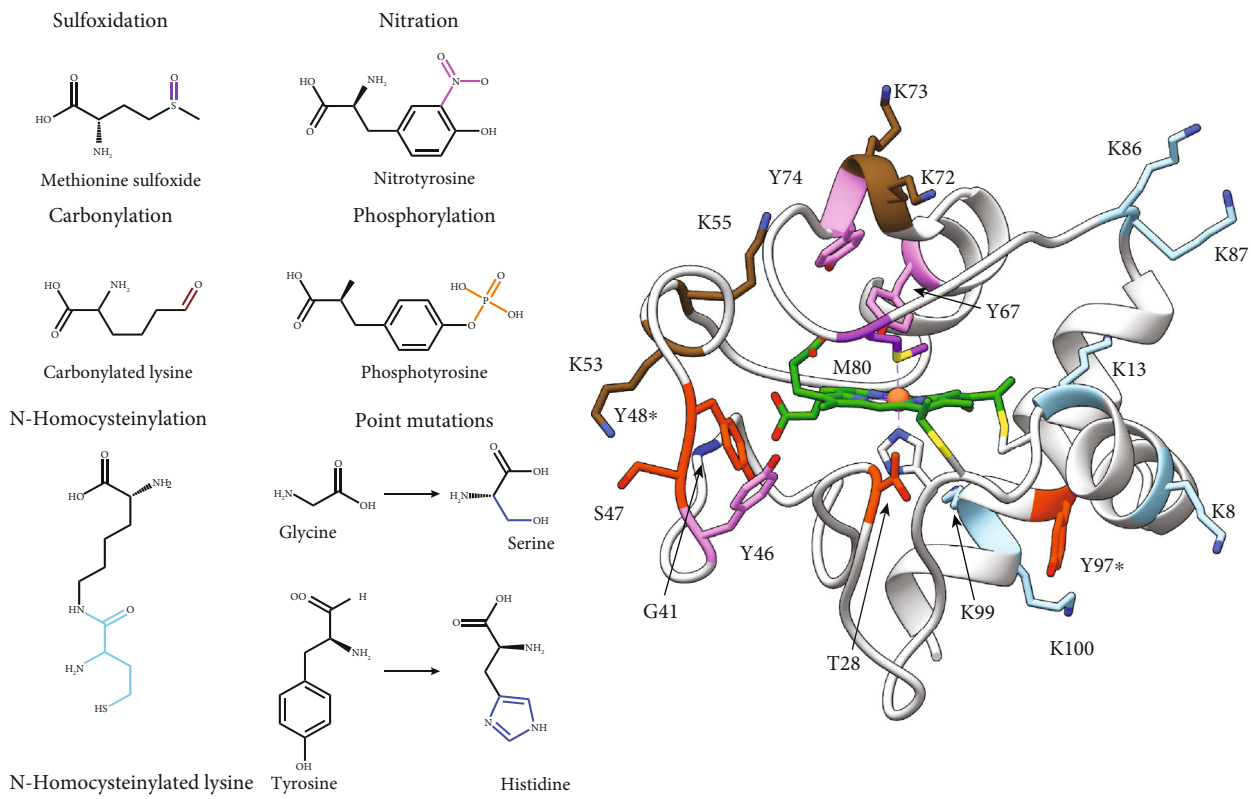

FIGURE 5: Functional implications of PTM and mutations of cytochrome *c*. Left: chemical modifications of cytochrome *c* residues. Right: ribbon representation of oxidized human C*c* (PDB 2N9J) [92]. Residues are colored by type of PTM: pink for nitration, purple for sulfoxidation, orange for phosphorylation, brown for carbonylation, cyan for N-homocysteinylation, and blue for point mutations. Y48 (asterisk) can be either phosphorylated, nitrated, or mutated for histidine, while Y97 (asterisk) can be phosphorylated or nitrated.

between tyrosine and HOONO are 3,5-dinitrotyrosine, 3-nitrotyrosine, tyrosine radicals, and dityrosine. Nevertheless, treatment of C*c* in vitro with peroxynitrite yields its 3-nitrotyrosine adducts, with the nitro group attaching to one of the C_ε of the aromatic ring [202]. Nitration affects the redox potential of C*c* as well as its electron-exchange kinetics, depending on the residue involved [203]. The nitration of Y46, Y48, Y74, and Y97 residues also increases the peroxidase activity of C*c* and lowers the pK_A value of the alkaline transition besides other functional properties [179, 180, 183, 185, 197, 204, 205] (Table 1). Nitration of C*c* has been associated with several diseases, including chronic nephropathy [206].

All modifications/mutations of S47 and Y67 alter the peroxidase activity of C*c* [79, 179, 185, 192, 195, 197]. Y67 is located close to Met80 and is part of the hydrophobic pocket which houses the acyl chains of CL. This residue is also key for the stability of the Ω_{III} – loop (Table 1).

Homocysteinylation is a PTM that involves the covalent bonding of a homocysteine thiolactone—an intermediate metabolite of methionine metabolism—with a lysine residue [188]. Upregulation of this PTM is implicated in several human pathologies including cancer and cardiopathies [198, 207]. The degree of homocysteinylation, as well as the rate at which this modification occurs in the presence of homocysteine thiolactone, is related to the number of lysine residues [188]. Human C*c* displays a lysine content of 17.1% in its amino acid composition, which makes it sensitive to homocysteinylation. Homocysteinylation of surface lysines on C*c* causes aggregation of the protein. However, N-homocysteinylated lysines adjacent to the heme cavity produce conformational changes, disrupt the coordination of the M80 axial ligand, and alter the redox state of C*c*, reducing the iron of the heme group [196, 208]. These conformational changes increase C*c* peroxidase activity (Table 1) [209].

As discussed before, C*c* is modulated by several oxidative modifications due to its activity, eventually leading to changes in iron coordination. One oxidative modification is the carbonylation of lysine residues, which affects residues 72 and 73, both of which are involved in the alkaline transition of C*c* [170] (Figure 5). Reportedly, successive carbonylation events at K53, K55, K72, and K73 lead to the formation of the pentacoordinated C*c* species, resulting in increased C*c* peroxidase activity (Table 1) [170]. Similarly, the sulfoxidation of M80 facilitates the formation of a Compound I-type intermediate that initiates the activity of C*c* peroxidase (Table 1) [171, 210].

5.4. Peroxidase Activity of Cytochrome c and Diseases. Since the peroxidase activity of C*c* relates to the activation of apoptosis, it is a clear target for the development of more efficient

Table 1: Effect of PTM and point mutations on cytochrome *c* peroxidase activity.

C*c* PTMs/mutation		Effect on peroxidase activity	References
Sulfoxidation[a]			
M80		↑	[168, 187, 196]
Nitration[b]			
Y46		↑	[184]
Y48		↑	[184]
Y67		↑	[185, 197]
Y74		↑	[185, 197]
Y97		↑	[185, 197]
Carbonylation[c]			
K53		↑	[152]
K55		↑	[152]
K72		↑	[152]
K73		↑	[152]
Phosphorylation			
T28	T28D	↑	[192]
T28	T28E	↓	[195]
S47	S47D	≈	[192]
Y48	Y48E	↑/↓	[176, 190]
	Y48pCMF	↑	[194]
Y97	Y97E	≈	[176]
	Y97*p*CMF	≈	[193]
N-Homocysteinylation[d]			
K8/K13		↑	[198]
K86/87		↑	[198]
K99		↑	[198]
K100		↑	[198]
Point mutation			
G41S		↑	[181, 199]
Y48H		↑	[181, 200]

[a]Determined under oxidative stress. [b]Determined after peroxynitrite treatment. [c]Determined after chloramine-T treatment. [d]Determined after homocysteine thiolactone treatment.

therapies against certain diseases or pathologies. There are several examples in the literature that shed light on this topic.

The point mutations Y48H and G41S in C*c* cause the appearance of a special type of thrombocytopenia (thrombocytopenia 4) which is an asymptomatic disorder [199, 200]. Thrombocytopenia 4 is notable for normal platelet production. However, in thrombocytopenia platelets are not transported to the bone marrow and remain in the matrix, causing the effective platelet content to be lower. Both mutations cause an increase in peroxidase activity, which is related to an increase in the population of C*c* in the pentacoordinated heme state [181, 211, 212] (Table 1).

Most neurodegenerative diseases are associated with cellular stress and apoptotic processes. Due to the double role played by C*c* in the electron transport chain and apoptosis, it represents an amenable target for the development of therapies against neurodegenerative pathologies. For example, post-translational phosphorylation of C*c* at Y97 is an excellent neuroprotective strategy following brain injury as it increases the efficiency of electron transport during hypoxic conditions [193, 213]. Moreover, C*c* has been implicated in the development of Parkinson's disease—as it colocalizes with α-synuclein in the Lewy bodies [214]. In fact, the peroxidase activity of C*c* plays an important role in the aggregation of α-synuclein by tyrosine dimerization [66, 174].

Minocycline is an antibiotic functional against both Gram-positive and Gram-negative bacteria. Additionally, it displays neuroprotective properties [215]. The antibiotic minocycline impairs the interaction between C*c* and CL, inhibiting the activation of peroxidase activity and the consequent release of C*c* into the cytosol to trigger apoptosis [216–218].

Nitric oxide is a well-known inhibitor of C*c* peroxidase activity and thus may downregulate apoptosis [219, 220]. Flavonoids are excellent antioxidants that prevent cellular aging by ROS scavenger activity. In addition, they can inhibit C*c* peroxidase activity, preventing proapoptotic events [221].

The protection of healthy cells during radiotherapy is a hot topic. In fact, novel synthetic compounds—e.g., imidazole-substituted fatty acids—are currently being trialed in order to preserve healthy cells by inhibiting the peroxidase activity of C*c* during the irradiation process [222, 223]. These de novo compounds, mainly imidazole conjugates, block access to the heme crevice preventing the activation of peroxidase activity.

Finally, the activation of proapoptotic events, such as the release of C*c* after the peroxidation of CL, may be a good target for the development of more efficient and specific therapies against cancer [224, 225].

6. Concluding Remarks

In this review, we have outlined major advances and hypotheses regarding the oxidation of CL by C*c*. CL oxidation is a crucial event at the onset of a diverse range of pathologies, and thus, controlling it has become a key objective of current research. Targeting C*c*—a key player in CL oxidation—has emerged as an important task.

Since its discovery last century, C*c* has displayed great functional complexity despite its apparently simple structure. Indeed, its highly dynamic architecture, which enables conformation changes critical in regulating metabolism, signaling, and cell fate, still amazes the scientific community. C*c* interacts with membranes in different ways depending on their composition and curvature, being able of modifying the latter. When the hemeprotein interacts with lipids, it may undergo subtle changes in the dynamics of its most flexible foldons or may even unfold. A plethora of factors, including PTM, control these phenomena.

The chemical activity of this protein ranges from the simplest reactions to diverse and complex reaction mechanisms to drive the oxidation of substrates including CL. In the recent years, we have witnessed concerted effort to unveil the intimate chemistry of this process. Solving this

conundrum will require us to discriminate minority conformations in functional assays and elucidate how this activity is tuned under distinct conditions. Nevertheless, knowledge has already amassed on the subject enabling us to examine the inhibition of CL oxidation, which will aid the development of translational approaches.

Conflicts of Interest

The authors declare that there is no conflict of interest regarding the publication of this review article.

Acknowledgments

This work was supported by the Ministry of Science and Innovation/FEDER–National Research Agency (PGC2018-096049-B-I00), European Social Fund, Andalusian Government (BIO-198, US-1257019, and US-1254317), and TA Instruments. G.P.M. was awarded a PhD fellowship from the Spanish Ministry of Education, Culture and Sport (FPU17/04604). Molecular graphics and analyses were performed with the UCSF Chimera software, developed by the Resource for Biocomputing, Visualization and Informatics at the University of California, San Francisco, with support from NIH (P41-GM103311).

References

[1] Y. M. Lee, "Mitochondrial diseases," *Journal of Epilepsy Research*, vol. 2, no. 1, pp. 1–4, 2012.

[2] J. F. Turrens, "Mitochondrial formation of reactive oxygen species," *The Journal of Physiology*, vol. 552, no. 2, pp. 335–344, 2003.

[3] Y. Y. Tyurina, C. M. St Croix, S. C. Watkins et al., "Redox (phospho)lipidomics of signaling in inflammation and programmed cell death," *Journal of Leukocyte Biology*, vol. 106, no. 1, pp. 57–81, 2019.

[4] N. Kajarabille and G. O. Latunde-Dada, "Programmed cell-death by ferroptosis: antioxidants as mitigators," *International Journal of Molecular Sciences*, vol. 20, no. 19, p. 4968, 2019.

[5] V. E. Kagan, Y. Y. Tyurina, W. Y. Sun et al., "Redox phospholipidomics of enzymatically generated oxygenated phospholipids as specific signals of programmed cell death," *Free Radical Biology and Medicine*, vol. 147, pp. 231–241, 2020.

[6] J. Dudek, "Role of cardiolipin in mitochondrial signaling pathways," *Frontiers in Cell and Developmental Biology*, vol. 5, p. 90, 2017.

[7] J. Butler, G. G. Jayson, and A. J. Swallow, "The reaction between the superoxide anion radical and cytochrome c," *Biochimica et Biophysica Acta (BBA) - Bioenergetics*, vol. 408, no. 3, pp. 215–222, 1975.

[8] A. Atlante, P. Calissano, A. Bobba, A. Azzariti, E. Marra, and S. Passarella, "Cytochrome c is released from mitochondria in a reactive oxygen species (ROS)-dependent fashion and can operate as a ROS scavenger and as a respiratory substrate in cerebellar neurons undergoing excitotoxic death," *Journal of Biological Chemistry*, vol. 275, no. 47, pp. 37159–37166, 2000.

[9] M. O. Pereverzev, T. V. Vygodina, A. A. Konstantinov, and V. P. Skulachev, "Cytochrome c, an ideal antioxidant," *Biochemical Society Transactions*, vol. 31, no. 6, pp. 1312–1315, 2003.

[10] P. Pasdois, J. E. Parker, E. J. Griffiths, and A. P. Halestrap, "The role of oxidized cytochrome c in regulating mitochondrial reactive oxygen species production and its perturbation in ischaemia," *Biochemical Journal*, vol. 436, no. 2, pp. 493–505, 2011.

[11] E. Sedlak, M. Fabian, N. C. Robinson, and A. Musatov, "Ferricytochrome c protects mitochondrial cytochrome c oxidase against hydrogen peroxide-induced oxidative damage," *Free Radical Biology and Medicine*, vol. 49, no. 10, pp. 1574–1581, 2010.

[12] S. S. Korshunov, B. F. Krasnikov, M. O. Pereverzev, and V. P. Skulachev, "The antioxidant functions of cytochromec," *FEBS Letters*, vol. 462, no. 1-2, pp. 192–198, 1999.

[13] V. A. Tyurin, Y. Y. Tyurina, A. N. Osipov et al., "Interactions of cardiolipin and lyso-cardiolipins with cytochrome *c* and tBid: conflict or assistance in apoptosis," *Cell Death & Differentiation*, vol. 14, no. 4, pp. 872–875, 2007.

[14] M. Huttemann, P. Pecina, M. Rainbolt et al., "The multiple functions of cytochrome c and their regulation in life and death decisions of the mammalian cell: from respiration to apoptosis," *Mitochondrion*, vol. 11, no. 3, pp. 369–381, 2011.

[15] N. A. Belikova, Y. A. Vladimirov, A. N. Osipov et al., "Peroxidase activity and structural transitions of cytochrome c bound to cardiolipin-containing membranes," *Biochemistry*, vol. 45, no. 15, pp. 4998–5009, 2006.

[16] Y. Shidoji, K. Hayashi, S. Komura, N. Ohishi, and K. Yagi, "Loss of molecular interaction between cytochrome c and cardiolipin due to lipid peroxidation," *Biochemical and Biophysical Research Communications*, vol. 264, no. 2, pp. 343–347, 1999.

[17] G. Petrosillo, F. M. Ruggiero, and G. Paradies, "Role of reactive oxygen species and cardiolipin in the release of cytochrome c from mitochondria," *The FASEB Journal*, vol. 17, no. 15, pp. 2202–2208, 2003.

[18] V. E. Kagan, V. A. Tyurin, J. Jiang et al., "Cytochrome *c* acts as a cardiolipin oxygenase required for release of proapoptotic factors," *Nature Chemical Biology*, vol. 1, no. 4, pp. 223–232, 2005.

[19] Y. Y. Tyurina, S. M. Poloyac, V. A. Tyurin et al., "A mitochondrial pathway for biosynthesis of lipid mediators," *Nature Chemistry*, vol. 6, no. 6, pp. 542–552, 2014.

[20] M. Schlame, "Thematic review series: glycerolipids. Cardiolipin synthesis for the assembly of bacterial and mitochondrial membranes," *Journal of Lipid Research*, vol. 49, no. 8, pp. 1607–1620, 2008.

[21] G. L. Powell and J. Jacobus, "nonequivalence of the phosphorus atoms in cardiolipin," *Biochemistry*, vol. 13, no. 19, pp. 4024–4026, 1974.

[22] M. Schlame, M. Ren, Y. Xu, M. L. Greenberg, and I. Haller, "Molecular symmetry in mitochondrial cardiolipins," *Chemistry and Physics of Lipids*, vol. 138, no. 1-2, pp. 38–49, 2005.

[23] M. Kates, J. Y. Syz, D. Gosser, and T. H. Haines, "pH-dissociation characteristics of cardiolipin and its $2'$-deoxy analogue," *Lipids*, vol. 28, no. 10, pp. 877–882, 1993.

[24] J. Pan, X. Cheng, M. Sharp, C. S. Ho, N. Khadka, and J. Katsaras, "Structural and mechanical properties of cardiolipin lipid bilayers determined using neutron spin echo, small

angle neutron and X-ray scattering, and molecular dynamics simulations," *Soft Matter*, vol. 11, no. 1, pp. 130–138, 2015.

[25] W. Hübner, H. H. Mantsch, and M. Kates, "Intramolecular hydrogen bonding in cardiolipin," *Biochimica et Biophysica Acta (BBA) - Biomembrane*, vol. 1066, no. 2, pp. 166–174, 1991.

[26] R. Hielscher, T. Wenz, C. Hunte, and P. Hellwig, "Monitoring the redox and protonation dependent contributions of cardiolipin in electrochemically induced FTIR difference spectra of the cytochrome bc1 complex from yeast," *Biochimica et Biophysica Acta (BBA) - Bioenergetics*, vol. 1787, no. 6, pp. 617–625, 2009.

[27] M. Dahlberg, A. Marini, B. Mennucci, and A. Maliniak, "Quantum chemical modeling of the cardiolipin headgroup," *The Journal of Physical Chemistry A*, vol. 114, no. 12, pp. 4375–4387, 2010.

[28] G. Olofsson and E. Sparr, "Ionization constants pK_a of cardiolipin," *PLoS ONE*, vol. 8, no. 9, article e73040, 2013.

[29] J. M. Seddon, R. D. Kaye, and D. Marsh, "Induction of the lamellar-inverted hexagonal phase transition in cardiolipin by protons and monovalent cations," *Biochimica et Biophysica Acta (BBA) - Biomembranes*, vol. 734, no. 2, pp. 347–352, 1983.

[30] E. E. Kooijman, L. A. Swim, Z. T. Graber, Y. Y. Tyurina, H. Bayır, and V. E. Kagan, "Magic angle spinning 31P NMR spectroscopy reveals two essentially identical ionization states for the cardiolipin phosphates in phospholipid liposomes," *Biochimica et Biophysica Acta (BBA) - Biomembranes*, vol. 1859, no. 1, pp. 61–68, 2017.

[31] T. Róg, H. Martinez-Seara, N. Munck, M. Oresic, M. Karttunen, and I. Vattulainen, "Role of cardiolipins in the inner mitochondrial membrane: insight gained through atom-scale simulations," *The Journal of Physical Chemistry B*, vol. 113, no. 11, pp. 3413–3422, 2009.

[32] M. Dahlberg, "Polymorphic phase behavior of cardiolipin derivatives studied by coarse-grained molecular dynamics," *The Journal of Physical Chemistry B*, vol. 111, no. 25, pp. 7194–7200, 2007.

[33] S. Nichols-Smith, S. Y. Teh, and T. L. Kuhl, "Thermodynamic and mechanical properties of model mitochondrial membranes," *Biochimica et Biophysica Acta (BBA) - Biomembranes*, vol. 1663, no. 1-2, pp. 82–88, 2004.

[34] M. Dahlberg and A. Maliniak, "Molecular dynamics simulations of cardiolipin bilayers," *The Journal of Physical Chemistry B*, vol. 112, no. 37, pp. 11655–11663, 2008.

[35] D. Ardail, J. P. Privat, M. Egret-Charlier, C. Levrat, F. Lerme, and P. Louisot, "Mitochondrial contact sites. Lipid composition and dynamics," *Journal of Biological Chemistry*, vol. 265, no. 31, pp. 18797–18802, 1990.

[36] J. J. Krebs, H. Hauser, and E. Carafoli, "Asymmetric distribution of phospholipids in the inner membrane of beef heart mitochondria," *Journal of Biological Chemistry*, vol. 254, pp. 5309–5316, 1979.

[37] V. Raja and M. L. Greenberg, "The functions of cardiolipin in cellular metabolism–potential modifiers of the Barth syndrome phenotype," *Chemistry and Physics of Lipids*, vol. 179, pp. 49–56, 2014.

[38] M. Zhang, E. Mileykovskaya, and W. Dowhan, "Gluing the respiratory chain Together," *Journal of Biological Chemistry*, vol. 277, no. 46, pp. 43553–43556, 2002.

[39] K. Pfeiffer, V. Gohil, R. A. Stuart et al., "Cardiolipin stabilizes respiratory chain supercomplexes," *Journal of Biological Chemistry*, vol. 278, no. 52, pp. 52873–52880, 2003.

[40] T. H. Haines, "Anionic lipid headgroups as a proton-conducting pathway along the surface of membranes: a hypothesis," *Proceedings of the National Academy of Sciences*, vol. 80, no. 1, pp. 160–164, 1983.

[41] T. H. Haines and N. A. Dencher, "Cardiolipin: a proton trap for oxidative phosphorylation," *FEBS Letters*, vol. 528, no. 1-3, pp. 35–39, 2002.

[42] C. Lange, J. H. Nett, B. L. Trumpower, and C. Hunte, "Specific roles of protein-phospholipid interactions in the yeast cytochrome bc_1 complex structure," *The EMBO Journal*, vol. 20, no. 23, pp. 6591–6600, 2001.

[43] A. Namslauer and P. Brzezinski, "Structural elements involved in electron-coupled proton transfer in cytochrome c oxidase," *FEBS Letters*, vol. 567, no. 1, pp. 103–110, 2004.

[44] C. Arnarez, S. J. Marrink, and X. Periole, "Identification of cardiolipin binding sites on cytochrome *c* oxidase at the entrance of proton channels," *Scientific Reports*, vol. 3, no. 1, 2013.

[45] M. Schlame and M. Ren, "Barth syndrome, a human disorder of cardiolipin metabolism," *FEBS Letters*, vol. 580, no. 23, pp. 5450–5455, 2006.

[46] A. Saric, K. Andreau, A. S. Armand, I. M. Møller, and P. X. Petit, "Barth Syndrome: from mitochondrial dysfunctions associated with aberrant production of reactive oxygen species to pluripotent stem cell studies," *Frontiers in Genetics*, vol. 6, p. 359, 2016.

[47] F. Gonzalvez, M. D'Aurelio, M. Boutant et al., "Barth syndrome: cellular compensation of mitochondrial dysfunction and apoptosis inhibition due to changes in cardiolipin remodeling linked to tafazzin (TAZ) gene mutation," *Biochimica et Biophysica Acta (BBA) - Molecular Basis of Disease*, vol. 1832, no. 8, pp. 1194–1206, 2013.

[48] G. Wang, M. L. McCain, L. Yang et al., "Modeling the mitochondrial cardiomyopathy of Barth syndrome with induced pluripotent stem cell and heart-on-chip technologies," *Nature Medicine*, vol. 20, no. 6, pp. 616–623, 2014.

[49] G. Paradies, V. Paradies, V. De Benedictis, F. M. Ruggiero, and G. Petrosillo, "Functional role of cardiolipin in mitochondrial bioenergetics," *Biochimica et Biophysica Acta (BBA) - Bioenergetics*, vol. 1837, no. 4, pp. 408–417, 2014.

[50] H. Yin and M. Zhu, "s," *Free Radical Research*, vol. 46, no. 8, pp. 959–974, 2012.

[51] J. J. Maguire, Y. Y. Tyurina, D. Mohammadyani et al., "Known unknowns of cardiolipin signaling: the best is yet to come," *Biochimica et Biophysica Acta (BBA) - Molecular and Cell Biology of Lipids*, vol. 1862, no. 1, pp. 8–24, 2017.

[52] C. T. Chu, J. Ji, R. K. Dagda et al., "Cardiolipin externalization to the outer mitochondrial membrane acts as an elimination signal for mitophagy in neuronal cells," *Nature Cell Biology*, vol. 15, no. 10, pp. 1197–1205, 2013.

[53] G. de Arriba, M. Calvino, S. Benito, and T. Parra, "Cyclosporine A-induced apoptosis in renal tubular cells is related to oxidative damage and mitochondrial fission," *Toxicology Letters*, vol. 218, no. 1, pp. 30–38, 2013.

[54] M. Garcia Fernandez, L. Troiano, L. Moretti et al., "Early changes in intramitochondrial cardiolipin distribution during apoptosis," *Cell Growth & Differentiation*, vol. 13, no. 9, pp. 449–455, 2002.

[55] F. Gonzalvez, Z. T. Schug, R. H. Houtkooper et al., "Cardiolipin provides an essential activating platform for caspase-8 on mitochondria," *Journal of Cell Biology*, vol. 183, no. 4, pp. 681–696, 2008.

[56] O. Jalmar, L. François-Moutal, A. J. García-Sáez et al., "Caspase-8 binding to cardiolipin in giant unilamellar vesicles provides a functional docking platform for Bid," *PLoS ONE*, vol. 8, no. 2, article e55250, 2013.

[57] M. Lutter, M. Fang, X. Luo, M. Nishijima, X. S. Xie, and X. Wang, "Cardiolipin provides specificity for targeting of tBid to mitochondria," *Nature Cell Biology*, vol. 2, no. 10, pp. 754–756, 2000.

[58] M. D. Esposti, I. M. Cristea, S. J. Gaskell, Y. Nakao, and C. Dive, "Proapoptotic Bid binds to monolysocardiolipin, a new molecular connection between mitochondrial membranes and cell death," *Cell Death & Differentiation*, vol. 10, no. 12, pp. 1300–1309, 2003.

[59] F. Gonzalvez, F. Pariselli, O. Jalmar et al., "Mechanistic issues of the interaction of the hairpin-forming domain of tBid with mitochondrial cardiolipin," *PLoS ONE*, vol. 5, no. 2, article e9342, 2010.

[60] P. X. Petit, P. Dupaigne, F. Pariselli et al., "Interaction of the alpha-helical H6 peptide from the pro-apoptotic protein tBid with cardiolipin," *FEBS Journal*, vol. 276, no. 21, pp. 6338–6354, 2009.

[61] E. Raemy and J. C. Martinou, "Involvement of cardiolipin in tBID-induced activation of BAX during apoptosis," *Chemistry and Physics of Lipids*, vol. 179, pp. 70–74, 2014.

[62] M. Ott, J. D. Robertson, V. Gogvadze, B. Zhivotovsky, and S. Orrenius, "Cytochrome c release from mitochondria proceeds by a two-step process," *Proceedings of the National Academy of Sciences*, vol. 99, no. 3, pp. 1259–1263, 2002.

[63] P. Li, D. Nijhawan, I. Budihardjo et al., "Cytochrome c and dATP-dependent formation of Apaf-1/caspase-9 complex initiates an apoptotic protease cascade," *Cell*, vol. 91, no. 4, pp. 479–489, 1997.

[64] H. Zou, Y. Li, X. Liu, and X. Wang, "An APAF-1.cytochrome c multimeric complex is a functional apoptosome that activates procaspase-9," *Journal of Biological Chemistry*, vol. 274, no. 17, pp. 11549–11556, 1999.

[65] H. Bayir, B. Fadeel, M. J. Palladino et al., "Apoptotic interactions of cytochrome c: redox flirting with anionic phospholipids within and outside of mitochondria," *Biochimica et Biophysica Acta (BBA) - Bioenergetics*, vol. 1757, no. 5-6, pp. 648–659, 2006.

[66] A. Kumar, D. Ganini, and R. P. Mason, "Role of cytochrome *c* in α-synuclein radical formation: implications of α-synuclein in neuronal death in Maneb- and paraquat-induced model of Parkinson's disease," *Molecular Neurodegeneration*, vol. 11, no. 1, pp. 70–82, 2016.

[67] C. A. Elena-Real, A. Díaz-Quintana, K. González-Arzola et al., "Cytochrome *c* speeds up caspase cascade activation by blocking 14-3-3 ε-dependent Apaf-1 inhibition," *Cell Death & Disease*, vol. 9, no. 3, pp. 365–377, 2018.

[68] J. Martínez-Fábregas, I. Díaz-Moreno, K. González-Arzola et al., "New Arabidopsis thaliana cytochrome c partners: a look into the elusive role of cytochrome c in programmed cell death in plants," *Molecular & Cellular Proteomics*, vol. 12, no. 12, pp. 3666–3676, 2013.

[69] J. Martínez-Fábregas, I. Díaz-Moreno, K. González-Arzola, A. Díaz-Quintana, and M. A. De la Rosa, "A common signalosome for programmed cell death in humans and plants," *Cell Death & Disease*, vol. 5, no. 7, p. e1314, 2014.

[70] J. Martínez-Fábregas, I. Díaz-Moreno, K. González-Arzola et al., "Structural and functional analysis of novel human cytochrome c targets in apoptosis," *Molecular & Cellular Proteomics*, vol. 13, no. 6, pp. 1439–1456, 2014.

[71] K. González-Arzola, I. Díaz-Moreno, A. Cano-González et al., "Structural basis for inhibition of the histone chaperone activity of SET/TAF-Iβ by cytochrome c," *Proceedings of the National Academy of Sciences*, vol. 112, no. 32, pp. 9908–9913, 2015.

[72] K. González-Arzola, A. Díaz-Quintana, F. Rivero-Rodríguez, A. Velázquez-Campoy, M. A. de la Rosa, and I. Díaz-Moreno, "Histone chaperone activity of Arabidopsis thaliana NRP1 is blocked by cytochrome c," *Nucleic Acids Research*, vol. 45, no. 4, pp. 2150–2165, 2017.

[73] I. Díaz-Moreno, A. Velázquez-Cruz, S. Curran-French, A. Díaz-Quintana, and M. A. De la Rosa, "Nuclear cytochrome c - a mitochondrial visitor regulating damaged chromatin dynamics," *FEBS Letters*, vol. 592, no. 2, pp. 172–178, 2018.

[74] A. Nur-E-Kamal, S. R. Gross, Z. Pan, Z. Balklava, J. Ma, and L. F. Liu, "Nuclear translocation of cytochrome *c* during apoptosis," *Journal of Biological Chemistry*, vol. 279, no. 24, pp. 24911–24914, 2004.

[75] R. Zalk, A. Israelson, E. S. Garty, H. Azoulay-Zohar, and V. Shoshan-Barmatz, "Oligomeric states of the voltage-dependent anion channel and cytochrome c release from mitochondria," *Biochemical Journal*, vol. 386, no. 1, pp. 73–83, 2005.

[76] F. Nolin, J. Michel, L. Wortham et al., "Stage-specific changes in the water, Na+, Cl- and K+ contents of organelles during apoptosis, demonstrated by a targeted cryo correlative analytical approach," *PLoS ONE*, vol. 11, no. 2, article e0148727, 2016.

[77] K. González-Arzola, A. Velázquez-Cruz, A. Guerra-Castellano et al., "New moonlighting functions of mitochondrial cytochrome c in the cytoplasm and nucleus," *FEBS Letters*, vol. 593, no. 22, pp. 3101–3119, 2019.

[78] I. Bertini, G. Cavallaro, and A. Rosato, "Cytochrome c: occurrence and functions," *Chemical Reviews*, vol. 106, no. 1, pp. 90–115, 2006.

[79] H. Maity, M. Maity, and S. Walter Englander, "How cytochrome c folds, and why: submolecular foldon units and their stepwise sequential stabilization," *Journal of Molecular Biology*, vol. 343, no. 1, pp. 223–233, 2004.

[80] V. Yin, G. S. Shaw, and L. Konermann, "Cytochromecas a peroxidase: activation of the precatalytic native state by H_2O_2-induced covalent modifications," *Journal of the American Chemical Society*, vol. 139, no. 44, pp. 15701–15709, 2017.

[81] R. E. Dickerson, T. Takano, D. Eisenberg et al., "Ferricytochrome c. I. General features of the horse and bonito proteins at 2.8 A resolution," *Journal of Biological Chemistry*, vol. 246, no. 5, pp. 1511–1535, 1971.

[82] W. H. Koppenol and E. Margoliash, "The asymmetric distribution of charges on the surface of horse cytochrome c. Functional implications," *Journal of Biological Chemistry*, vol. 257, no. 8, pp. 4426–4437, 1982.

[83] H. K. Kimelberg and C. P. Lee, "Binding and electron transfer to cytochrome c in artificial phospholipid membranes,"

Biochemical and Biophysical Research Communications, vol. 34, no. 6, pp. 784–790, 1969.

[84] P. J. R. Spooner and A. Watts, "Reversible unfolding of cytochrome c upon interaction with cardiolipin bilayers. I. Evidence from deuterium NMR measurements," *Biochemistry*, vol. 30, no. 16, pp. 3871–3879, 1991.

[85] P. J. Spooner, A. A. Duralski, S. E. Rankin, T. J. Pinheiro, and A. Watts, "Dynamics in a protein-lipid complex: nuclear magnetic resonance measurements on the headgroup of cardiolipin when bound to cytochrome c," *Biophysical Journal*, vol. 65, no. 1, pp. 106–112, 1993.

[86] Z. Salamon and G. Tollin, "Interaction of horse heart cytochrome c with lipid bilayer membranes: effects on redox potentials," *Journal of Bioenergetics and Biomembranes*, vol. 29, no. 3, pp. 211–221, 1997.

[87] Z. Salamon and G. Tollin, "Surface plasmon resonance studies of complex formation between cytochrome c and bovine cytochrome c oxidase incorporated into a supported planar lipid bilayer. II. Binding of cytochrome c to oxidase-containing cardiolipin/phosphatidylcholine membranes," *Biophysical Journal*, vol. 71, no. 2, pp. 858–867, 1996.

[88] Z. Salamon and G. Tollin, "Surface plasmon resonance studies of complex formation between cytochrome c and bovine cytochrome c oxidase incorporated into a supported planar lipid bilayer. I. Binding of cytochrome c to cardiolipin/phosphatidylcholine membranes in the absence of oxidase," *Biophysical Journal*, vol. 71, no. 2, pp. 848–857, 1996.

[89] I. L. Nantes, M. R. Zucchi, O. R. Nascimento, and A. Faljoni-Alario, "Effect of heme iron valence state on the conformation of cytochrome c and its association with membrane interfaces. A CD and EPR investigation," *Journal of Biological Chemistry*, vol. 276, no. 1, pp. 153–158, 2001.

[90] L. A. Pandiscia and R. Schweitzer-Stenner, "Coexistence of native-like and non-native partially unfolded ferricytochrome c on the surface of cardiolipin-containing liposomes," *The Journal of Physical Chemistry B*, vol. 119, no. 4, pp. 1334–1349, 2015.

[91] A. Kostrzewa, T. Páli, W. Froncisz, and D. Marsh, "Membrane location of spin-labeled cytochrome c determined by paramagnetic relaxation agents," *Biochemistry*, vol. 39, no. 20, pp. 6066–6074, 2000.

[92] M. Imai, T. Saio, H. Kumeta, T. Uchida, F. Inagaki, and K. Ishimori, "Investigation of the redox-dependent modulation of structure and dynamics in human cytochrome *c*," *Biochemical and Biophysical Research Communications*, vol. 469, no. 4, pp. 978–984, 2016.

[93] M. Rytomaa and P. K. Kinnunen, "Evidence for two distinct acidic phospholipid-binding sites in cytochrome c," *Journal of Biological Chemistry*, vol. 269, no. 3, pp. 1770–1774, 1994.

[94] M. Rytomaa and P. K. J. Kinnunen, "Reversibility of the binding of cytochrome c to liposomes. Implications for lipid-protein interactions," *Journal of Biological Chemistry*, vol. 270, no. 7, pp. 3197–3202, 1995.

[95] E. K. J. Tuominen, K. Zhu, C. J. A. Wallace et al., "ATP induces a conformational change in lipid-bound cytochrome c," *Journal of Biological Chemistry*, vol. 276, no. 22, pp. 19356–19362, 2001.

[96] E. K. J. Tuominen, C. J. A. Wallace, and P. K. J. Kinnunen, "Phospholipid-CytochromecInteraction," *Journal of Biological Chemistry*, vol. 277, no. 11, pp. 8822–8826, 2002.

[97] F. Sinibaldi, B. D. Howes, M. C. Piro et al., "Extended cardiolipin anchorage to cytochrome c: a model for protein-mitochondrial membrane binding," *JBIC Journal of Biological Inorganic Chemistry*, vol. 15, no. 5, pp. 689–700, 2010.

[98] C. Kawai, F. M. Prado, G. L. C. Nunes, P. di Mascio, A. M. Carmona-Ribeiro, and I. L. Nantes, "pH-dependent interaction of cytochrome c with mitochondrial mimetic membranes: the role of an array of positively charged amino acids," *Journal of Biological Chemistry*, vol. 280, no. 41, pp. 34709–34717, 2005.

[99] E. Kalanxhi and C. J. A. Wallace, "Cytochrome c impaled: investigation of the extended lipid anchorage of a soluble protein to mitochondrial membrane models," *Biochem J*, vol. 407, no. 2, pp. 179–187, 2007.

[100] L. Banci, I. Bertini, H. B. Gray et al., "Solution structure of oxidized horse heart cytochrome c," *Biochemistry*, vol. 36, no. 32, pp. 9867–9877, 1997.

[101] F. Sinibaldi, B. D. Howes, E. Droghetti et al., "Role of lysines in cytochrome c-cardiolipin interaction," *Biochemistry*, vol. 52, no. 26, pp. 4578–4588, 2013.

[102] M. Abe, R. Niibayashi, S. Koubori, I. Moriyama, and H. Miyoshi, "Molecular mechanisms for the induction of peroxidase activity of the cytochrome c-cardiolipin complex," *Biochemistry*, vol. 50, no. 39, pp. 8383–8391, 2011.

[103] J. Hanske, J. R. Toffey, A. M. Morenz, A. J. Bonilla, K. H. Schiavoni, and E. V. Pletneva, "Conformational properties of cardiolipin-bound cytochrome c," *Proceedings of the National Academy of Sciences*, vol. 109, no. 1, pp. 125–130, 2012.

[104] J. Hong, K. Huang, W. Wang et al., "Direct electrochemistry of artificial peroxidase based on self-assembled cytochrome c-sds-nano-micelle," *Analytical Letters*, vol. 45, no. 15, pp. 2221–2235, 2012.

[105] A. A. Kapralov, I. V. Kurnikov, I. I. Vlasova et al., "The hierarchy of structural transitions induced in cytochrome c by anionic phospholipids determines its peroxidase activation and selective peroxidation during apoptosis in cells," *Biochemistry*, vol. 46, no. 49, pp. 14232–14244, 2007.

[106] R. Jemmerson, J. Liu, D. Hausauer, K. P. Lam, A. Mondino, and R. D. Nelson, "A conformational change in cytochrome c of apoptotic and necrotic cells is detected by monoclonal antibody binding and mimicked by association of the native antigen with synthetic phospholipid vesicles," *Biochemistry*, vol. 38, no. 12, pp. 3599–3609, 1999.

[107] M. Assfalg, I. Bertini, A. Dolfi et al., "Structural model for an alkaline form of ferricytochrome c," *Journal of the American Chemical Society*, vol. 125, no. 10, pp. 2913–2922, 2003.

[108] S. Hirota, Y. Hattori, S. Nagao et al., "Cytochrome c polymerization by successive domain swapping at the C-terminal helix," *Proceedings of the National Academy of Sciences*, vol. 107, no. 29, pp. 12854–12859, 2010.

[109] S. Hirota, N. Yamashiro, Z. Wang, and S. Nagao, "Effect of methionine80 heme coordination on domain swapping of cytochrome c," *JBIC Journal of Biological Inorganic Chemistry*, vol. 22, no. 5, pp. 705–712, 2017.

[110] L. J. McClelland, H. B. B. Steele, F. G. Whitby et al., "Cytochrome c can form a well-defined binding pocket for hydrocarbons," *Journal of the American Chemical Society*, vol. 138, no. 51, pp. 16770–16778, 2016.

[111] S. M. Kapetanaki, G. Silkstone, I. Husu, U. Liebl, M. T. Wilson, and M. H. Vos, "Interaction of carbon monoxide with

the apoptosis-inducing cytochrome c-cardiolipin complex," *Biochemistry*, vol. 48, no. 7, pp. 1613–1619, 2009.

[112] J. Muenzner, J. R. Toffey, Y. Hong, and E. V. Pletneva, "Becoming a peroxidase: cardiolipin-induced unfolding of cytochrome c," *The Journal of Physical Chemistry B*, vol. 117, no. 42, pp. 12878–12886, 2013.

[113] L. V. Basova, I. V. Kurnikov, L. Wang et al., "Cardiolipin switch in mitochondria: shutting off the reduction of cytochrome c and turning on the peroxidase activity," *Biochemistry*, vol. 46, no. 11, pp. 3423–3434, 2007.

[114] J. M. Bradley, G. Silkstone, M. T. Wilson, M. R. Cheesman, and J. N. Butt, "Probing a complex of cytochrome c and cardiolipin by magnetic circular dichroism spectroscopy: implications for the initial events in apoptosis," *Journal of the American Chemical Society*, vol. 133, no. 49, pp. 19676–19679, 2011.

[115] E. S. O'Brien, N. V. Nucci, B. Fuglestad, C. Tommos, and A. J. Wand, "Defining the apoptotic trigger the interaction of cytochrome c and cardiolipin," *Journal of Biological Chemistry*, vol. 290, no. 52, pp. 30879–30887, 2015.

[116] I. Díaz-Moreno, J. M. García-Heredia, A. Díaz-Quintana, and M. A. De la Rosa, "Cytochrome c signalosome in mitochondria," *European Biophysics Journal*, vol. 40, no. 12, pp. 1301–1315, 2011.

[117] I. Díaz-Moreno, A. Díaz-Quintana, M. Ubbink, and M. A. De la Rosa, "An NMR-based docking model for the physiological transient complex between cytochrome f and cytochrome c6," *FEBS Letters*, vol. 579, no. 13, pp. 2891–2896, 2005.

[118] A. Mandal, C. L. Hoop, M. DeLucia et al., "Structural Changes and Proapoptotic Peroxidase Activity of Cardiolipin-Bound Mitochondrial Cytochrome c," *Biophysical Journal*, vol. 109, no. 9, pp. 1873–1884, 2015.

[119] D. Mohammadyani, N. Yanamala, A. K. Samhan-Arias et al., "Structural characterization of cardiolipin-driven activation of cytochrome c into a peroxidase and membrane perturbation," *Biochimica et Biophysica Acta (BBA) - Biomembrane*, vol. 1860, no. 5, pp. 1057–1068, 2018.

[120] G. P. Gorbenko, J. G. Molotkovsky, and P. K. J. Kinnunen, "Cytochrome c interaction with cardiolipin/phosphatidylcholine model membranes: effect of cardiolipin protonation," *Biophysical Journal*, vol. 90, no. 11, pp. 4093–4103, 2006.

[121] J. B. Robinson Jr., J. M. Strottmann, and E. Stellwagen, "A globular high spin form of ferricytochrome c," *Journal of Biological Chemistry*, vol. 258, no. 11, pp. 6772–6776, 1983.

[122] P. Tonge, G. R. Moore, and C. W. Wharton, "Fourier-transform infra-red studies of the alkaline isomerization of mitochondrial cytochrome c and the ionization of carboxylic acids," *Biochemical Journal*, vol. 258, no. 2, pp. 599–605, 1989.

[123] R. Schweitzer-Stenner, "Internal electric field in cytochrome c explored by visible electronic circular dichroism spectroscopy," *The Journal of Physical Chemistry B*, vol. 112, no. 33, pp. 10358–10366, 2008.

[124] L. A. Pandiscia and R. Schweitzer-Stenner, "Salt as a catalyst in the mitochondria: returning cytochrome c to its native state after it misfolds on the surface of cardiolipin containing membranes," *Chemical Communications*, vol. 50, no. 28, pp. 3674–3676, 2014.

[125] S. Oellerich, S. Lecomte, M. Paternostre, T. Heimburg, and P. Hildebrandt, "Peripheral and integral binding of Cytochromecto phospholipids vesicles," *The Journal of Physical Chemistry B*, vol. 108, no. 12, pp. 3871–3878, 2004.

[126] S. Oellerich, H. Wackerbarth, and P. Hildebrandt, "Spectroscopic characterization of nonnative conformational states of Cytochromec," *The Journal of Physical Chemistry B*, vol. 106, no. 25, pp. 6566–6580, 2002.

[127] B. Milorey, D. Malyshka, and R. Schweitzer-Stenner, "pH dependence of ferricytochrome c conformational transitions during binding to cardiolipin membranes: evidence for histidine as the distal ligand at neutral pH," *The Journal of Physical Chemistry*, vol. 8, no. 9, pp. 1993–1998, 2017.

[128] R. Schweitzer-Stenner, "Relating the multi-functionality of cytochrome c to membrane binding and structural conversion," *Biophysical Reviews*, vol. 10, no. 4, pp. 1151–1185, 2018.

[129] A. Ranieri, D. Millo, G. di Rocco et al., "Immobilized cytochrome c bound to cardiolipin exhibits peculiar oxidation state-dependent axial heme ligation and catalytically reduces dioxygen," *JBIC Journal of Biological Inorganic Chemistry*, vol. 20, no. 3, pp. 531–540, 2015.

[130] D. A. Capdevila, S. Oviedo Rouco, F. Tomasina et al., "Active site structure and peroxidase activity of oxidatively modified cytochrome c species in complexes with cardiolipin," *Biochemistry*, vol. 54, no. 51, pp. 7491–7504, 2015.

[131] Y. Hong, J. Muenzner, S. K. Grimm, and E. V. Pletneva, "Origin of the conformational heterogeneity of cardiolipin-bound cytochrome c," *ournal of the American Chemical Society*, vol. 134, no. 45, pp. 18713–18723, 2012.

[132] P. J. R. Spooner and A. Watts, "Cytochrome c interactions with cardiolipin in bilayers: a multinuclear magic-angle spinning NMR study," *Biochemistry*, vol. 31, no. 41, pp. 10129–10138, 1992.

[133] A. Rietveld, P. Sijens, A. J. Verkleij, and B. de Kruijff, "Interaction of cytochrome c and its precursor apocytochrome c with various phospholipids," *EMBO Journal*, vol. 2, no. 6, pp. 907–913, 1983.

[134] B. de Kruijff and P. R. Cullis, "Cytochrome c specifically induces non-bilayer structures in cardiolipin- containing model membranes," *Biochimica et Biophysica Acta (BBA) - Biomembranes*, vol. 602, no. 3, pp. 477–490, 1980.

[135] L. R. Brown and K. Wüthrich, "NMR and ESR studies of the interactions of cytochrome c with mixed cardiolipin-phosphatidylcholine vesicles," *Biochimica et Biophysica Acta (BBA) - Biomembranes*, vol. 468, no. 3, pp. 389–410, 1977.

[136] T. J. T. Pinheiro and A. Watts, "Lipid specificity in the interaction of cytochrome c with anionic phospholipid bilayers revealed by solid-state ^{31}P NMR," *Biochemistry*, vol. 33, no. 9, pp. 2451–2458, 1994.

[137] C. L. Bergstrom, P. A. Beales, Y. Lv, T. K. Vanderlick, and J. T. Groves, "Cytochrome c causes pore formation in cardiolipin-containing membranes," *Proceedings of the National Academy of Sciences*, vol. 110, no. 16, pp. 6269–6274, 2013.

[138] M. Li, A. Mandal, V. A. Tyurin et al., "Surface-binding to cardiolipin nanodomains triggers cytochrome c pro-apoptotic peroxidase activity via localized dynamics," *Structure*, vol. 27, no. 5, pp. 806–815.e4, 2019.

[139] G. G. Borisenko, A. A. Kapralov, V. A. Tyurin, A. Maeda, D. A. Stoyanovsky, and V. E. Kagan, "Molecular design of new inhibitors of peroxidase activity of cytochrome c/cardiolipin complexes: fluorescent oxadiazole-derivatized cardiolipin," *Biochemistry*, vol. 47, no. 51, pp. 13699–13710, 2008.

[140] P. Ascenzi, M. Marino, F. Polticelli, R. Santucci, and M. Coletta, "Cardiolipin modulates allosterically the nitrite reductase activity of horse heart cytochrome c," *BIC Journal of Biological Inorganic Chemistry*, vol. 19, no. 7, pp. 1195–1201, 2014.

[141] H. Yin and M. Zhu, "Free radical oxidation of cardiolipin: chemical mechanisms, detection and implication in apoptosis, mitochondrial dysfunction and human diseases," *Free Radical Research*, vol. 46, no. 8, pp. 959–974, 2012.

[142] H. Yin, L. Xu, and N. A. Porter, "Free radical lipid peroxidation: mechanisms and analysis," *Chemical Reviews*, vol. 111, no. 10, pp. 5944–5972, 2011.

[143] H. P. Indo, H.-C. Yen, I. Nakanishi et al., "A mitochondrial superoxide theory for oxidative stress diseases and aging," *Journal of Clinical Biochemistry and Nutrition*, vol. 56, no. 1, pp. 1–7, 2015.

[144] C. Michiels, M. Raes, O. Toussaint, and J. Remacle, "Importance of SE-glutathione peroxidase, catalase, and CU/ZN-SOD for cell survival against oxidative stress," *Free Radical Biology and Medicine*, vol. 17, no. 3, pp. 235–248, 1994.

[145] R. Radi, L. Thomson, H. Rubbo, and E. Prodanov, "Cytochrome c-catalyzed oxidation of organic molecules by hydrogen peroxide," *Archives of Biochemistry and Biophysics*, vol. 288, no. 1, pp. 112–117, 1991.

[146] R. Radi, J. F. Turrens, and B. A. Freeman, "Cytochrome c-catalyzed membrane lipid peroxidation by hydrogen peroxide," *Archives of Biochemistry and Biophysics*, vol. 288, no. 1, pp. 118–125, 1991.

[147] J. Dawson, "Probing structure-function relations in heme-containing oxygenases and peroxidases," *Science*, vol. 240, no. 4851, pp. 433–439, 1988.

[148] I. Vlasova, "Peroxidase activity of human hemoproteins: keeping the fire under control," *Molecules*, vol. 23, no. 10, p. 2561, 2018.

[149] N. A. Belikova, Y. Y. Tyurina, G. Borisenko et al., "Heterolytic reduction of fatty acid hydroperoxides by cytochrome c/cardiolipin complexes: antioxidant function in mitochondria," *Journal of the American Chemical Society*, vol. 131, no. 32, pp. 11288-11289, 2009.

[150] L. J. Marnett, "Cyclooxygenase mechanisms," *Current Opinion in Chemical Biology*, vol. 4, no. 5, pp. 545–552, 2000.

[151] S. Y. Qian, Y. R. Chen, L. J. Deterding et al., "Identification of protein-derived tyrosyl radical in the reaction of cytochrome c and hydrogen peroxide: characterization by ESR spin-trapping, HPLC and MS," *Biochemical Journal*, vol. 363, no. 2, pp. 281–288, 2002.

[152] U. Barayeu, M. Lange, L. Méndez et al., "Cytochrome c autocatalyzed carbonylation in the presence of hydrogen peroxide and cardiolipins," *Journal of Biological Chemistry*, vol. 294, no. 6, pp. 1816–1830, 2019.

[153] T. L. Poulos and J. Kraut, "The stereochemistry of peroxidase catalysis," *Journal of Biological Chemistry*, vol. 255, no. 17, pp. 8199–8205, 1980.

[154] L. Banci, P. Carloni, A. Díaz, and G. G. Savellini, "Molecular dynamics calculations on peroxidases: the effect of calcium ions on protein structure," *JBIC Journal of Biological Inorganic Chemistry*, vol. 1, no. 3, pp. 264–272, 1996.

[155] A. Lawrence, C. M. Jones, P. Wardman, and M. J. Burkitt, "Evidence for the role of a peroxidase compound I-type intermediate in the oxidation of glutathione, NADH, ascorbate, and dichlorofluorescin by cytochrome c/H_2O_2. Implications for oxidative stress during apoptosis," *Journal of Biological Chemistry*, vol. 278, no. 32, pp. 29410–29419, 2003.

[156] E. Cadenas, A. I. Varsavsky, B. Alberto, and C. Britton, "Low level chemiluminescence of the cytochrome c-catalyzed decomposition of hydrogen peroxide," *FEBS Letters*, vol. 113, no. 2, pp. 141–144, 1980.

[157] D. P. Barr and R. P. Mason, "Mechanism of radical production from the reaction of cytochrome c with organic hydroperoxides. An ESR spin trapping investigation," *Journal of Biological Chemistry*, vol. 270, no. 21, pp. 12709–12716, 1995.

[158] D. P. Barr, M. R. Gunther, L. J. Deterding, K. B. Tomer, and R. P. Mason, "ESR spin-trapping of a protein-derived tyrosyl radical from the reaction of cytochrome c with hydrogen peroxide," *Journal of Biological Chemistry*, vol. 271, no. 26, pp. 15498–15503, 1996.

[159] B. S. Rajagopal, A. N. Edzuma, M. A. Hough et al., "The hydrogen-peroxide-induced radical behaviour in human cytochrome c-phospholipid complexes: implications for the enhanced pro-apoptotic activity of the G41S mutant," *Biochemical Journal*, vol. 456, no. 3, pp. 441–452, 2013.

[160] M. W. Mara, R. G. Hadt, M. E. Reinhard et al., "Metalloprotein entatic control of ligand-metal bonds quantified by ultrafast X-ray spectroscopy," *Science*, vol. 356, no. 6344, pp. 1276–1280, 2017.

[161] R. E. M. Diederix, M. Ubbink, and G. W. Canters, "Peroxidase activity as a tool for studying the folding of c-type cytochromes," *Biochemistry*, vol. 41, no. 43, pp. 13067–13077, 2002.

[162] N. Tomaskova, R. Varhac, V. Lysakova, A. Musatov, and E. Sedlak, "Peroxidase activity of cytochrome c in its compact state depends on dynamics of the heme region," *Biochimica et Biophysica Acta (BBA) - Proteins and Proteomics*, vol. 1866, no. 11, pp. 1073–1083, 2018.

[163] P. Ascenzi, M. Coletta, M. T. Wilson et al., "Cardiolipin-cytochrome c complex: switching cytochrome c from an electron-transfer shuttle to a myoglobin- and a peroxidase-like heme-protein," *IUBMB Life*, vol. 67, no. 2, pp. 98–109, 2015.

[164] M. Velayutham, C. F. Hemann, A. J. Cardounel, and J. L. Zweier, "Sulfite oxidase activity of cytochrome c: role of hydrogen peroxide," *Biochemistry and Biophysics Reports*, vol. 5, pp. 96–104, 2016.

[165] H. Bayır, A. A. Kapralov, J. Jiang et al., "Peroxidase mechanism of lipid-dependent cross-linking of synuclein with cytochrome c: protection against apoptosis versus delayed oxidative stress in Parkinson disease," *Journal of Biological Chemistry*, vol. 284, no. 23, pp. 15951–15969, 2009.

[166] K. Nomura, H. Imai, T. Koumura, T. Kobayashi, and Y. Nakagawa, "Mitochondrial phospholipid hydroperoxide glutathione peroxidase inhibits the release of cytochrome c from mitochondria by suppressing the peroxidation of cardiolipin in hypoglycaemia-induced apoptosis," *Biochemical Journal*, vol. 351, no. 1, pp. 183–193, 2000.

[167] V. E. Kagan, G. G. Borisenko, Y. Y. Tyurina et al., "Oxidative lipidomics of apoptosis: redox catalytic interactions of cytochrome c with cardiolipin and phosphatidylserine," *Free Radical Biology and Medicine*, vol. 37, no. 12, pp. 1963–1985, 2004.

[168] N. H. Kim, M. S. Jeong, S. Y. Choi, and J. H. Kang, "Oxidative modification of cytochrome c by hydrogen peroxide," *Molecules and Cells*, vol. 22, no. 2, pp. 220–227, 2006.

[169] A. D. Nugraheni, C. Ren, Y. Matsumoto, S. Nagao, M. Yamanaka, and S. Hirota, "Oxidative modification of

methionine80 in cytochrome c by reaction with peroxides," *Journal of Inorganic Biochemistry*, vol. 182, pp. 200–207, 2018.

[170] V. Yin, S. H. Mian, and L. Konermann, "Lysine carbonylation is a previously unrecognized contributor to peroxidase activation of cytochromecby chloramine-T," *Chemical Science*, vol. 10, no. 8, pp. 2349–2359, 2019.

[171] R. D. Parakra, T. Kleffmann, G. N. L. Jameson, and E. C. Ledgerwood, "The proportion of Met80-sulfoxide dictates peroxidase activity of human cytochrome c," *Dalton Transactions*, vol. 47, no. 27, pp. 9128–9135, 2018.

[172] F. Zhong and E. V. Pletneva, "Ligation and reactivity of methionine-oxidized Cytochromec," *Inorganic Chemistry*, vol. 57, no. 10, pp. 5754–5766, 2018.

[173] S. Harel, M. A. Salan, and J. Kanner, "Iron release from metmyoglobin, methaemoglobin and cytochrome c by a system generating hydrogen peroxide," *Free Radical Research Communications*, vol. 5, no. 1, pp. 11–19, 1998.

[174] D. A. Capdevila, W. A. Marmisollé, F. Tomasina et al., "Specific methionine oxidation of cytochrome c in complexes with zwitterionic lipids by hydrogen peroxide: potential implications for apoptosis," *Chemical Science*, vol. 6, no. 1, pp. 705–713, 2015.

[175] L. C. Godoy, C. Muñoz-Pinedo, L. Castro et al., "Disruption of the M80-Fe ligation stimulates the translocation of cytochrome c to the cytoplasm and nucleus in nonapoptotic cells," *Proceedings of the National Academy of Sciences*, vol. 106, no. 8, pp. 2653–2658, 2009.

[176] L. J. McClelland, T.-C. Mou, M. E. Jeakins-Cooley, S. R. Sprang, and B. E. Bowler, "Structure of a mitochondrial cytochrome c conformer competent for peroxidase activity," *Proceedings of the National Academy of Sciences*, vol. 111, no. 18, pp. 6648–6653, 2014.

[177] G. Balakrishnan, Y. Hu, O. F. Oyerinde, J. Su, J. T. Groves, and T. G. Spiro, "A conformational switch to β-sheet structure in cytochrome c leads to heme exposure. Implications for cardiolipin peroxidation and apoptosis," *Journal of the American Chemical Society*, vol. 129, no. 3, pp. 504-505, 2007.

[178] J. M. García-Heredia, A. Díaz-Quintana, M. Salzano et al., "Tyrosine phosphorylation turns alkaline transition into a biologically relevant process and makes human cytochrome c behave as an anti-apoptotic switch," *JBIC Journal of Biological Inorganic Chemistry*, vol. 16, no. 8, pp. 1155–1168, 2011.

[179] L. A. Abriata, A. Cassina, V. Tórtora et al., "Nitration of solvent-exposed tyrosine 74 on CytochromecTriggers heme iron-methionine 80 bond disruption," *Journal of Biological Chemistry*, vol. 284, no. 1, pp. 17–26, 2008.

[180] A. M. Cassina, R. Hodara, J. M. Souza et al., "Cytochrome c nitration by peroxynitrite," *Journal of Biological Chemistry*, vol. 275, no. 28, pp. 21409–21415, 2000.

[181] O. M. Deacon, D. A. Svistunenko, G. R. Moore, M. T. Wilson, and J. A. R. Worrall, "Naturally occurring disease-related mutations in the 40-57 Ω-loop of human cytochrome c control triggering of the alkaline isomerization," *Biochemistry*, vol. 57, no. 29, pp. 4276–4288, 2018.

[182] S. M. Nold, H. Lei, T. C. Mou, and B. E. Bowler, "Effect of a K72A mutation on the structure, stability, dynamics, and peroxidase activity of human cytochrome c," *Biochemistry*, vol. 56, no. 26, pp. 3358–3368, 2017.

[183] J. A. R. Worrall, A. M. M. van Roon, M. Ubbink, and G. W. Canters, "The effect of replacing the axial methionine ligand with a lysine residue in cytochrome c-550 from Paracoccus versutus assessed by X-ray crystallography and unfolding," *FEBS Journal*, vol. 272, no. 10, pp. 2441–2455, 2005.

[184] I. Díaz-Moreno, J. M. García-Heredia, A. Díaz-Quintana, M. Teixeira, and M. A. De la Rosa, "Nitration of tyrosines 46 and 48 induces the specific degradation of cytochrome c upon change of the heme iron state to high-spin," *Biochimica et Biophysica Acta (BBA) - Bioenergetics*, vol. 1807, no. 12, pp. 1616–1623, 2011.

[185] J. M. García-Heredia, I. Díaz-Moreno, P. M. Nieto et al., "Nitration of tyrosine 74 prevents human cytochrome c to play a key role in apoptosis signaling by blocking caspase-9 activation," *Biochimica et Biophysica Acta (BBA) - Bioenergetics*, vol. 1797, no. 6-7, pp. 981–993, 2010.

[186] A. Guerra-Castellano, A. Díaz-Quintana, B. Moreno-Beltrán et al., "Mimicking tyrosine phosphorylation in human cytochrome cby the evolved tRNA synthetase technique," *Chemistry*, vol. 21, no. 42, pp. 15004–15012, 2015.

[187] K. M. Ivanetich, J. J. Bradshaw, and L. S. Kaminsky, "Methionine sulfoxide cytochrome c," *Biochemistry*, vol. 15, no. 5, pp. 1144–1153, 1976.

[188] H. Jakubowski, "Protein homocysteinylation: possible mechanism underlying pathological consequences of elevated homocysteine levels," *FASEB Journal*, vol. 13, no. 15, pp. 2277–2283, 1999.

[189] H. A. Kalpage, J. Wan, P. T. Morse et al., "Cytochrome c phosphorylation: control of mitochondrial electron transport chain flux and apoptosis," *The International Journal of Biochemistry & Cell Biology*, vol. 121, p. 105704, 2020.

[190] P. Pecina, G. G. Borisenko, N. A. Belikova et al., "Phosphomimetic substitution of cytochrome c tyrosine 48 decreases respiration and binding to cardiolipin and abolishes ability to trigger downstream caspase activation," *Biochemistry*, vol. 49, no. 31, pp. 6705–6714, 2010.

[191] B. M. K. Gmeiner and C. C. C. Seelos, "Tyrosine phosphorylation blocks tyrosine free radical formation and, hence, the hormonogenic iodination reaction," *Free Radical Biology and Medicine*, vol. 21, no. 3, pp. 349–351, 1996.

[192] A. Guerra-Castellano, I. Díaz-Moreno, A. Velázquez-Campoy, M. A. De la Rosa, and A. Díaz-Quintana, "Structural and functional characterization of phosphomimetic mutants of cytochrome c at threonine 28 and serine 47," *Biochimica et Biophysica Acta (BBA) - Bioenergetics*, vol. 1857, no. 4, pp. 387–395, 2016.

[193] A. Guerra-Castellano, A. Díaz-Quintana, G. Pérez-Mejías et al., "Oxidative stress is tightly regulated by cytochromecphosphorylation and respirasome factors in mitochondria," *Proceedings of the National Academy of Sciences*, vol. 115, no. 31, pp. 7955–7960, 2018.

[194] B. Moreno-Beltrán, A. Guerra-Castellano, A. Díaz-Quintana et al., "Structural basis of mitochondrial dysfunction in response to cytochromecphosphorylation at tyrosine 48," *Proceedings of the National Academy of Sciences*, vol. 114, no. 15, pp. E3041–E3050, 2017.

[195] G. Mahapatra, A. Varughese, Q. Ji et al., "Phosphorylation of cytochrome c threonine 28 regulates electron transport chain activity in kidney: implications for AMP kinase," *Journal of Biological Chemistry*, vol. 292, no. 1, pp. 64–79, 2017.

[196] R. K. Shervedani and M. S. Foroushani, "Direct electrochemistry of cytochrome c immobilized on gold electrode surface via Zr(IV) ion glue and its activity for ascorbic acid," *Bioelectrochemistry*, vol. 98, pp. 53–63, 2014.

[197] C. Batthyány, J. M. Souza, R. Durán, A. Cassina, C. Cerveñansky, and R. Radi, "Time course and site(s) of cytochrome *c* tyrosine nitration by peroxynitrite†," *Biochemistry*, vol. 44, no. 22, pp. 8038–8046, 2005.

[198] T. Hasan, R. Arora, A. K. Bansal, R. Bhattacharya, G. S. Sharma, and L. R. Singh, "Disturbed homocysteine metabolism is associated with cancer," *Experimental & Molecular Medicine*, vol. 51, no. 2, pp. 1–13, 2019.

[199] I. M. Morison, E. M. Cramer Bordé, E. J. Cheesman et al., "A mutation of human cytochrome *c* enhances the intrinsic apoptotic pathway but causes only thrombocytopenia," *Nature Genetics*, vol. 40, no. 4, pp. 387–389, 2008.

[200] D. de Rocco, C. Cerqua, P. Goffrini et al., "Mutations of cytochrome c identified in patients with thrombocytopenia THC4 affect both apoptosis and cellular bioenergetics," *Biochimica et Biophysica Acta (BBA) - Molecular Basis of Disease*, vol. 1842, no. 2, pp. 269–274, 2014.

[201] B. Alvarez and R. Radi, "Peroxynitrite reactivity with amino acids and proteins," *Amino Acids*, vol. 25, no. 3-4, pp. 295–311, 2003.

[202] I. Díaz-Moreno, P. M. Nieto, R. del Conte et al., "A non-damaging method to analyze the configuration and dynamics of nitrotyrosines in proteins," *Chemistry*, vol. 18, no. 13, pp. 3872–3878, 2012.

[203] V. Rodríguez-Roldán, J. M. García-Heredia, J. A. Navarro, M. A. De la Rosa, and M. Hervás, "Effect of nitration on the physicochemical and kinetic features of wild-type and monotyrosine mutants of human respiratory Cytochromec†," *Biochemistry*, vol. 47, no. 47, pp. 12371–12379, 2008.

[204] J. M. García-Heredia, I. Díaz-Moreno, A. Díaz-Quintana et al., "Specific nitration of tyrosines 46 and 48 makes cytochrome c assemble a non-functional apoptosome," *FEBS Letters*, vol. 586, no. 2, pp. 154–158, 2012.

[205] H. K. Ly, T. Utesch, I. Díaz-Moreno, J. M. García-Heredia, M. A. De La Rosa, and P. Hildebrandt, "Perturbation of the redox site structure of cytochrome c variants upon tyrosine nitration," *The Journal of Physical Chemistry B*, vol. 116, no. 19, pp. 5694–5702, 2012.

[206] L. A. MacMillan-Crow, D. L. Cruthirds, K. M. Ahki, P. W. Sanders, and J. A. Thompson, "Mitochondrial tyrosine nitration precedes chronic allograft nephropathy," *Free Radical Biology and Medicine*, vol. 31, no. 12, pp. 1603–1608, 2001.

[207] J. Beltowski, "Protein homocysteinylation: a new mechanism of atherogenesis?," *Postępy Higieny i Medycyny Doświadczalnej*, vol. 59, pp. 392–404, 2005.

[208] J. Perła-Kaján, L. Marczak, Ł. Kaján, P. Skowronek, T. Twardowski, and H. Jakubowski, "Modification by homocysteine thiolactone affects redox status of cytochrome c," *Biochemistry*, vol. 46, no. 21, pp. 6225–6231, 2007.

[209] G. S. Sharma and L. R. Singh, "Conformational status of cytochrome c upon N-homocysteinylation: implications to cytochrome c release," *Archives of Biochemistry and Biophysics*, vol. 614, pp. 23–27, 2017.

[210] Z. Wang, Y. Ando, A. D. Nugraheni, C. Ren, S. Nagao, and S. Hirota, "Self-oxidation of cytochrome c at methionine80 with molecular oxygen induced by cleavage of the Met-heme iron bond," *Molecular BioSystems*, vol. 10, no. 12, pp. 3130–3137, 2014.

[211] A. I. Karsisiotis, O. M. Deacon, M. T. Wilson et al., "Increased dynamics in the 40-57 Ω-loop of the G41S variant of human cytochrome *c* promote its pro-apoptotic conformation," *Scientific Reports*, vol. 6, no. 1, pp. 30447–30459, 2016.

[212] O. M. Deacon, A. I. Karsisiotis, T. Moreno-Chicano et al., "Heightened dynamics of the oxidized Y48H variant of human CytochromecIncreases its peroxidatic activity," *Biochemistry*, vol. 56, no. 46, pp. 6111–6124, 2017.

[213] T. H. Sanderson, G. Mahapatra, P. Pecina et al., "Cytochrome c is tyrosine 97 phosphorylated by neuroprotective insulin treatment," *PLoS ONE*, vol. 8, no. 11, article e78627, 2013.

[214] M. Hashimoto, A. Takeda, L. J. Hsu, T. Takenouchi, and E. Masliah, "Role of Cytochromecas a stimulator of α-synuclein aggregation in lewy body disease," *Journal of Biological Chemistry*, vol. 274, no. 41, pp. 28849–28852, 1999.

[215] N. Garrido-Mesa, A. Zarzuelo, and J. Gálvez, "Minocycline: far beyond an antibiotic," *British Journal of Pharmacology*, vol. 169, no. 2, pp. 337–352, 2013.

[216] T. M. Scarabelli, A. Stephanou, E. Pasini et al., "Minocycline inhibits caspase activation and reactivation, increases the ratio of XIAP to smac/DIABLO, and reduces the mitochondrial leakage of cytochrome c and smac/DIABLO," *Journal of the American College of Cardiology*, vol. 43, no. 5, pp. 865–874, 2004.

[217] A. Patriarca, F. Polticelli, M. C. Piro et al., "Conversion of cytochrome c into a peroxidase: inhibitory mechanisms and implication for neurodegenerative diseases," *Archives of Biochemistry and Biophysics*, vol. 522, no. 1, pp. 62–69, 2012.

[218] A. M. Firsov, E. A. Kotova, and Y. N. Antonenko, "Minocycline prevents peroxidative permeabilization of cardiolipin-containing bilayer lipid membranes mediated by cytochrome c," *Biochemical and Biophysical Research Communications*, vol. 507, no. 1-4, pp. 510–513, 2018.

[219] I. I. Vlasova, V. A. Tyurin, A. A. Kapralov et al., "Nitric oxide inhibits peroxidase activity of cytochrome c-cardiolipin complex and blocks cardiolipin oxidation," *Journal of Biological Chemistry*, vol. 281, no. 21, pp. 14554–14562, 2006.

[220] G. Silkstone, S. M. Kapetanaki, I. Husu, M. H. Vos, and M. T. Wilson, "Nitric oxide binding to the cardiolipin complex of ferric cytochrome c," *Biochemistry*, vol. 51, no. 34, pp. 6760–6766, 2012.

[221] R. Lagoa, A. K. Samhan-Arias, and C. Gutiérrez-Merino, "Correlation between the potency of flavonoids for cytochrome c reduction and inhibition of cardiolipin-induced peroxidase activity," *BioFactors*, vol. 43, no. 3, pp. 451–468, 2017.

[222] J. Atkinson, A. A. Kapralov, N. Yanamala et al., "A mitochondria-targeted inhibitor of cytochrome *c* peroxidase mitigates radiation-induced death," *Nature Communications*, vol. 2, no. 1, 2011.

[223] A. Bakan, A. A. Kapralov, H. Bayir, F. Hu, V. E. Kagan, and I. Bahar, "Inhibition of peroxidase activity of Cytochromec: de novo compound discovery and validation," *Molecular Pharmacology*, vol. 88, no. 3, pp. 421–427, 2005.

[224] V. E. Kagan, H. A. Bayır, N. A. Belikova et al., "Cytochrome c/cardiolipin relations in mitochondria: a kiss of death," *Free Radical Biology and Medicine*, vol. 46, no. 11, pp. 1439–1453, 2009.

[225] Y. A. Vladimirov, E. V. Proskurnina, and A. V. Alekseev, "Molecular mechanisms of apoptosis. Structure of cytochrome c-cardiolipin complex," *Biochemistry*, vol. 78, no. 10, pp. 1086–1097, 2013.

Hindawi
Oxidative Medicine and Cellular Longevity
Volume 2020, Article ID 3631272, 11 pages
https://doi.org/10.1155/2020/3631272

Research Article

Novel Fluorescent Mitochondria-Targeted Probe MitoCLox Reports Lipid Peroxidation in Response to Oxidative Stress *In Vivo*

Konstantin G. Lyamzaev,[1] **Alisa A. Panteleeva**,[1] **Anna A. Karpukhina**,[2] **Ivan I. Galkin**,[1] **Ekatherina N. Popova**,[1] **Olga Yu. Pletjushkina**,[1] **Bettina Rieger**,[3] **Karin B. Busch**,[3,4] **Armen Y. Mulkidjanian**,[1,2,5] **and Boris V. Chernyak**[1]

[1]*Belozersky Institute of Physico-Chemical Biology, Lomonosov Moscow State University, Moscow 119992, Russia*
[2]*Department of Bioengineering and Bioinformatics, Lomonosov Moscow State University, Moscow 119992, Russia*
[3]*Institute of Molecular Cell Biology, Department of Biology, University of Muenster, D-48149 Muenster, Germany*
[4]*Mitochondrial Dynamics Group, Department of Biology, Osnabrueck University, D-49069 Osnabrueck, Germany*
[5]*Department of Physics, Osnabrueck University, D-49069 Osnabrueck, Germany*

Correspondence should be addressed to Armen Y. Mulkidjanian; amulkid@uni-osnabrueck.de
and Boris V. Chernyak; bchernyak1@gmail.com

Received 1 July 2019; Accepted 22 November 2019; Published 10 February 2020

Academic Editor: Maria Isaguliants

A new mitochondria-targeted probe MitoCLox was designed as a starting compound for a series of probes sensitive to cardiolipin (CL) peroxidation. Fluorescence microscopy reported selective accumulation of MitoCLox in mitochondria of diverse living cell cultures and its oxidation under stress conditions, particularly those known to cause a selective cardiolipin oxidation. Ratiometric fluorescence measurements using flow cytometry showed a remarkable dependence of the MitoCLox dynamic range on the oxidation of the sample. Specifically, MitoCLox oxidation was induced by low doses of hydrogen peroxide or organic hydroperoxide. The mitochondria-targeted antioxidant 10-(6′-plastoquinonyl)decyltriphenyl-phosphonium (SkQ1), which was shown earlier to selectively protect cardiolipin from oxidation, prevented hydrogen peroxide-induced MitoCLox oxidation in the cells. Concurrent tracing of MitoCLox oxidation and membrane potential changes in response to hydrogen peroxide addition showed that the oxidation of MitoCLox started without a delay and was complete during the first hour, whereas the membrane potential started to decay after 40 minutes of incubation. Hence, MitoCLox could be used for splitting the cell response to oxidative stress into separate steps. Application of MitoCLox revealed heterogeneity of the mitochondrial population; in living endothelial cells, a fraction of small, rounded mitochondria with an increased level of lipid peroxidation were detected near the nucleus. In addition, the MitoCLox staining revealed a specific fraction of cells with an increased level of oxidized lipids also in the culture of human myoblasts. The fraction of such cells increased in high-density cultures. These specific conditions correspond to the initiation of spontaneous myogenesis *in vitro*, which indicates that oxidation may precede the onset of myogenic differentiation. These data point to a possible participation of oxidized CL in cell signalling and differentiation.

1. Introduction

Cardiolipin (CL) is a unique diphosphatidylglycerol phospholipid with four acyl chains. In eukaryotic cells, it is exclusively located in the inner mitochondrial membrane where it constitutes about 18% of phospholipids. CL supports the functional activity of mitochondria by shaping the membrane curvature and defining the crista morphology [1], stabilizing respiratory supercomplexes [2–5], mediating proton transfer to energy-converting enzymes [6–8], and preventing

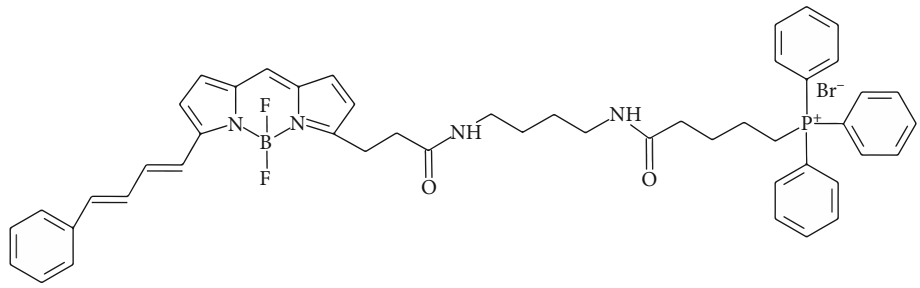

Figure 1: Chemical structure of MitoCLox.

proton leakage [9]. Almost all membrane energy-converting enzymes contain tightly bound CL molecules as important structural components [10–12].

In intact mitochondria, CL is located exclusively in the inner membrane, but various mitochondria-damaging agents induce translocation of CL to the outer mitochondrial membrane [13]. It was found that nucleoside diphosphate kinase D (NDPK-D) binds CL in the intermembrane space and facilitates its redistribution [13, 14]. The externalized CL can interact with the dynamin-related GTPase Drp1 and stimulate its oligomerization, which is critical for the fission of mitochondria [15]. Interestingly, the other dynamin-related GTPase OPA1, which stimulates the inner membrane fusion, also interacts with CL [13, 16]. In addition, CL molecules exposed at the surface of fragmented mitochondria can be recognized by receptors of autophagosomes including LC3, which induces the engulfment of damaged organelles (mitophagy) followed by their digestion in lysosomes [17]. The other important partners of externalized CL are inflammasome NLRP3 [18] and caspase-1 [18]. It was suggested that independent interactions of the NLRP3 and caspase-1 with CL at the outer mitochondrial membrane contribute to the proinflammatory activation of macrophages [19]. These findings indicate that CL is an important player in the regulation of mitochondrial dynamics and in the mechanisms of quality control.

The content of unsaturated fatty acids in CL is significantly higher than that in other mitochondrial phospholipids. In combination with the proximity to respiratory enzymes, which are potential sources of reactive oxygen species (ROS), the high content of unsaturated fatty acids makes CL especially sensitive to oxidation. It was found that a small respiratory protein cytochrome *c*, after its binding to oxidized CL at the outer surface of the inner mitochondrial membrane, can catalyze CL peroxidation, which induces the cytochrome *c* release from mitochondria and apoptosis [20, 21]. Oxidation and age-dependent loss of CL were suggested to contribute to age-related cardiac [22] and neurodegenerative [23] diseases, as well as to diabetes [24]. It was suggested that the protective effects of mitochondria-targeted peptide SS-20 owe to its binding to CL and preventing cytochrome *c*-dependent CL peroxidation [25]. Imidazole-substituted analogs of fatty acids that were conjugated with TPP^+ inhibited cytochrome *c*-dependent CL peroxidation and protected mouse embryonic cells exposed to ionizing irradiation [26]. As argued elsewhere, the protective and antiaging effects of mitochondria-targeted antioxidants with various cationic maieties could be due to the specific protection of CL against peroxidation [27, 28].

Elsewhere, we have described MitoCLox, a new mitochondria-targeted fluorescence probe for tracing cardiolipin (CL) oxidation [29]. In MitoCLox, similar to the previously introduced MitoPerOx [30], a BODIPY (581/591) fluorophore is linked with a triphenylphosphonium cation (TPP^+). However, the linker in MitoCLox is longer than the linker of MitoPerOx and contains not one but two peptide bonds (see Figure 1). The flexible linker was chosen as a mimic of the SS-20 peptide from Ref. [25]; this long linker has a capacity to accommodate additional positively charged moieties.

It was shown that MitoCLox can report CL oxidation in liposomes but did not react with organic hydroperoxides even in the presence of ferric ions [29]. Based on results of molecular dynamic simulations, it was suggested that MitoCLox and its derivatives, owing to the positive charge(s), could be selectively sensitive to oxidation of cardiolipin, the dominant negatively charged phospholipid in the inner mitochondrial membrane [29].

Here, we have used MitoCLox for tracing peroxidation of mitochondrial lipids in living cells. MitoCLox selectively accumulated in their mitochondria and reported lipid peroxidation induced by exogenous prooxidants or by internal redox changes.

2. Materials and Methods

2.1. Chemicals. MitoCLox was synthesized as described in [29]. SkQ1 was synthesized, as described in [31]. Other reagents were from Sigma-Aldrich (USA).

2.2. Cell Cultures. Human carcinoma cell line RKO (ATCC CRL-2577), human fetal lung fibroblasts MRC5 transformed with SV-40 (MRC5 SV2, EcACC Cat. No. 84100401), and human endothelial cell line EA.hy926 (ATCC CRL-2922) were cultured in DMEM medium (Dulbecco's modified Eagle's medium) (Gibco, USA) supplemented with 2 mM glutamine and 10% fetal bovine serum (FBS) (HyClone, USA) and 100 U/ml streptomycin and 100 U/ml penicillin (all from Gibco, CA). HeLa cells were cultured in minimal essential medium with Earle's salts (MEM, PAA Lab GmbH, E15–888) with 5.6 mM glucose, 2 mM stable glutamine, and sodium bicarbonate, supplemented with 10% FBS (Biochrom AG), 1% MEM nonessential amino acids (Biochrom AG),

and 1% 4–(2–hydroxyethyl)piperazine-1-ethanesulfonic acid (HEPES, PAA Lab GmbH). Immortalized human myoblast MB135 were cultured in mixture of DMEM and 199 medium (4 : 1) supplemented with 15% FBS (HyClone, USA), basic fibroblast growth factor FGF-2 (10 ng/ml PanEco, Russia), and 0.1 μM dexamethasone.

2.3. Microscopy. MRC5-SV40 fibroblasts and EA.hy926 endothelial cells were grown on glass coverslips placed in 6-well cell culture plates at 200,000 cells per well and analyzed using an Axiovert microscope (Carl Zeiss). For analysis of mitochondrial membrane potential, Ea.hy926 cells were incubated with TMRM (100 μM, 30 min) and with MitoTracker Green (250 nM, 30 min). For detection of mitochondrial lipid peroxidation, MitoCLox (200 nM) was added for 2 h. Myoblast MB135 were seeded in 35 mm dishes with glass bottom (SPL) for confocal microscopy at initial density from 0.5 to 6×10^5 cells/dish and cultured for 4 days. Then, MitoCLox (200 nM) was added for 5 h, and cells were analyzed using a Nikon Eclipse Ti (Nikon) confocal microscope with excitation at 488 and 562 nm.

Fluorescence imaging of HeLa cells was carried out with a confocal laser scanning microscope (Leica TCS SP8 SMD) equipped with a 63x water objective (water, HCPL Apo 63x/1.2 W CS2) and two spectral detectors, an Argon and a tunable white light laser. Measurements were performed at 37°C. HeLa cells were incubated with 25 μM menadione or with 100 μM *tert*-butyl hydroperoxide (tBOOH) for 1 h, and 200 nM MitoCLox was added for the indicated time. In the green channel, fluorescence was excited with the 448 nm wavelength of an argon ion laser, and emission was collected in the range of 500–560 nm. In the red channel, fluorescence was excited with the 559 nm laser wavelength of the white light laser, and emission was recorded in the range of 580–630 nm.

2.4. Image Processing. The fluorescence intensity of HeLa cells stained with MitoCLox was analyzed with ImageJ (MacBiophotonics). To exclude the background intensity, the Otsu mask was used as a mask for mitochondria and the background was set to NaN. Ratios were determined from mean grey values for each channel and represent basically the mitochondrial network of a cell.

2.5. Flow Cytometry. MRC5-SV40 cells were incubated with MitoCLox (100-200 nM) for 1 h before addition of H_2O_2 or cumene hydroperoxide. SkQ1 was added for 24 h before stimulation of oxidative stress. To measure the mitochondrial membrane potential (MMP), the cells were stained with 100 nM TMRM for 15 min.

Myoblast MB135 were seeded in 6-well cell culture plates (9.6 cm^2 surface area per well) at initial density 0.5, 1, 2, 4, and 6 ($\times 10^5$ cells/well) and cultured for 4 days. Then, 200 nM MitoCLox was added for 5 h, and cells were analyzed.

Flow cytometry analyses were performed using a Beckman Coulter FC 500, equipped by a single blue (488 nm) laser or BDFACSAria III with 5 lasers (375 nm, 405 nm, 488 nm, 561 nm, and 633 nm). For ratiometric analysis, the Flowing software 2.4 (Cell Imaging Core, Turku Centre for Biotechnology) was used.

2.6. Statistics. Data analysis is presented as the mean ± standard deviation (SD). Comparisons were analyzed by one-way ANOVA. The significance was analyzed with Prism 7.0 software (GraphPad, USA); a p value < 0.05 was considered to be statistically significant. Data analysis of MitoCLox-stained HeLa cells was performed using Origin™ (OriginLab Cooperation, Northampton, MA). The data are presented as means in box-and-whisker plots, with boxes representing the 25th to 75th percentiles. In order to determine differences between treatment groups, analysis of variance (ANOVA) for a single factor (One-way) was performed with the post hoc Scheffe test. Differences were considered to be statistically significant if $p < 0.05$.

3. Results

3.1. Interaction of MitoCLox with Mitochondria of Fibroblasts. To assess the ability of MitoCLox to accumulate in the cell mitochondria of human MRC5-SV40 fibroblasts, we used fluorescence microscopy with the red filter corresponding to the fluorescence of the reduced probe. We observed MitoCLox accumulation in fibroblasts and its colocalization with the mitochondria-specific dye MitoTracker Green (Figure 2(a)). The green fluorescence of MitoCLox was not significant since the dye was reduced and did not affect the colocalization analysis.

The dynamics of dye accumulation and the rate of its release from the cells were evaluated using flow cytometry. Maximal accumulation of MitoCLox in the cells was reached in 45-60 minutes (Figure 2(b)). After removal of MitoCLox from the medium, the fluorescence of the cells slowly decreased and reached 50% of the maximum in approximately 1 h. The addition of a membrane depolarizing agent FCCP during probe removal significantly accelerated the release of MitoCLox from the cells (Figure 2(b)), which indicates the dependence of its accumulation on the mitochondrial membrane potential. When FCCP was added before MitoCLox, the fluorescent dye was diffusively distributed all over the cytosol (not shown).

Oxidation of MitoCLox was analyzed in the same fibroblast cells by minimal flow cytometry setup using a single blue (488 nm) laser and standard bandpass filters 525 ± 40 nm (FL1) to record the emission peak of oxidized MitoCLox versus the peak at 575 ± 40 nm (FL2). Although these settings did not perfectly fit the peaks of BODIPY581/591 fluorescence (Figure 3(a)), the changes in the FL1 signal increased 11-fold after the addition of 500 μM H_2O_2 to living cells. The FL2 signal also raised slightly, which was mostly due to the contribution from the long wavelength shoulder in the fluorescence spectra of the oxidized form (Figure 3). As a result, the oxidation of MitoCLox resulted in a 5-6-fold increase of the FL1/FL2 emission signal ratio. In an attempt to further improve the sensitivity, we applied the flow cytometry setup with two lasers, namely, the blue laser (488 nm) and green laser (561 nm) and bandpass filters of 530 ± 30 nm (FL1) and 582 ± 15 nm (FL2). These settings fit better

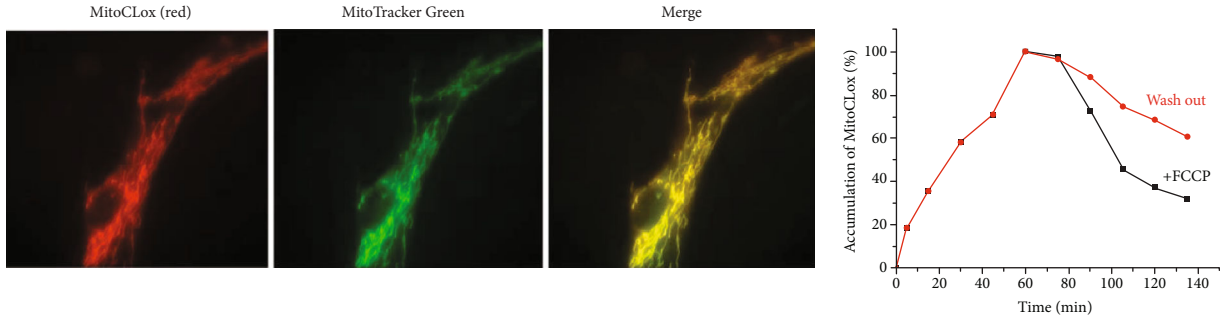

(a) (b)

Figure 2: Accumulation of MitoCLox in MRC5-SV40 cells. (a) Cells were incubated with 200 nM of MitoCLox for 60 min; then, 50 nM MitoTracker Green was added for 15 min. Cells were analyzed with an Axiovert microscope (Carl Zeiss). Bar, 10 μm. (b) Accumulation of MitoCLox (200 nM) as measured by FACS in FL2 channel. After 60 min, the medium was changed to the same but without MitoCLox. FCCP (10 μM) was added after change of the medium where indicated.

the parameters of BODIPY581/591 fluorescence, but the dynamic range of the FL1/FL2 signal for MitoCLox was not significantly better than that in the minimal setup (not shown), so flow cytometry with a single blue laser was used in the further experiments.

The analysis of H_2O_2-induced oxidative stress demonstrated that the MitoCLox oxidation occurred only in a fraction of the cell population at low levels of H_2O_2. At higher doses of H_2O_2, almost normal distribution of oxidized MitoCLox was observed (Figure 3(c)). Kinetics of MitoCLox oxidation induced by 500 μM H_2O_2 reached saturation at approximately 60 min (Figure 3(d)). Cumene hydroperoxide (CumOOH) induced similar responses of MitoCLox but at lower doses (not shown). Mitochondrially targeted antioxidant SkQ1 (10-(6′-plastoquinonyl)decyltriphenyl-phosphonium [27]) inhibited oxidation of MitoCLox induced by H_2O_2 or by CumOOH (Figure 3(e)).

3.2. Measurements of Lipid Peroxidation in Mitochondria of HeLa Cells. HeLa cells were pretreated with such oxidizing compounds as menadione (25 μM) and *tert*-butyl hydroperoxide (tBOOH; 100 μM), respectively, for 1 h. In the cells treated with these oxidants, mitochondria were then stained with MitoCLox (200 nM) for 30 min, and the fluorescence in two channels (λ_{exc1} = 448 nm/λ_{em} = 500-560 nm; λ_{exc2} = 559/λ_{em} = 580-630 nm) was recorded by confocal microscopy (Figure 4(a)). The respective fluorescence images demonstrated significant increase of fluorescence in the green channel and almost no changes in the red channel (Figure 4(a)). Calculations of the green/red fluorescence ratio showed that the increase in the fluorescence ratio (emission ratio λ_{em} = 500-560 nm/λ_{em} = 580-630 nm) after menadione and tBOOH treatment was significant (Figure 4(b)), indicating oxidation of MitoCLox.

3.3. Application of MitoCLox for Tracing Separate Steps in Cell Reaction to Oxidative Stress. Oxidative stress is known to cause both mitochondrial lipid peroxidation and a decrease in the mitochondrial membrane potential (MMP) [9, 24]. To analyze the time pattern of lipid peroxidation and MMP decrease under oxidative stress, we measured MitoCLox oxidation concurrently with the potential-dependent accumulation of tetramethylrhodamine (TMRM) in MRC5-SV40 cells (Figure 5). In cells treated with 0.5 mM hydrogen peroxide, oxidation of MitoCLox started without a delay and was almost complete during the first hour (black squares in Figure 5). A notable drop in MMP could be observed after 40 minutes of incubation (red squares in Figure 5).

3.4. Heterogeneity of MitoCLox Oxidation in a Single Cell. Staining of an endothelial cell culture with MitoCLox revealed a fraction of mitochondria with an increased level of lipid peroxidation (Figure 6(a)). These mitochondria were small, rounded, and located near the nucleus.

In Figure 6(b), we show for comparison a similar example of mitochondrial heterogeneity in endothelial cells that we observed earlier [32, 33]. Using a combination of MitoTracker Green that stained mitochondria independently of MMP and methyl ester of TMRM that accumulated only in mitochondria with high MMP, we revealed a fraction of depolarized mitochondria located near the cell nucleus. These perinuclear mitochondria were smaller and more rounded than the mitochondria with higher potential in the same cell. A comparison of images in Figures 6(a) and 6(b) indicates similarities in heterogeneity patterns for the MitoCLox oxidation and MMP in the mitochondrial population.

3.5. Application of MitoCLox in Myoblast Cell Culture. We have applied MitoCLox to analyze mitochondrial lipid peroxidation in the culture of human myoblast MB135.

Mitochondrial oxidative status is critical for various processes in muscle, including myogenic differentiation (myogenesis)—the process of formation of muscle fibers during embryonic development and muscle regeneration. Myogenesis is accompanied by dramatic reorganization of mitochondrial reticulum through mitophagy and mitochondria biogenesis [34, 35] the processes that critically depend on mitoROS [36]. Thus, analysis of CL peroxidation in myoblast

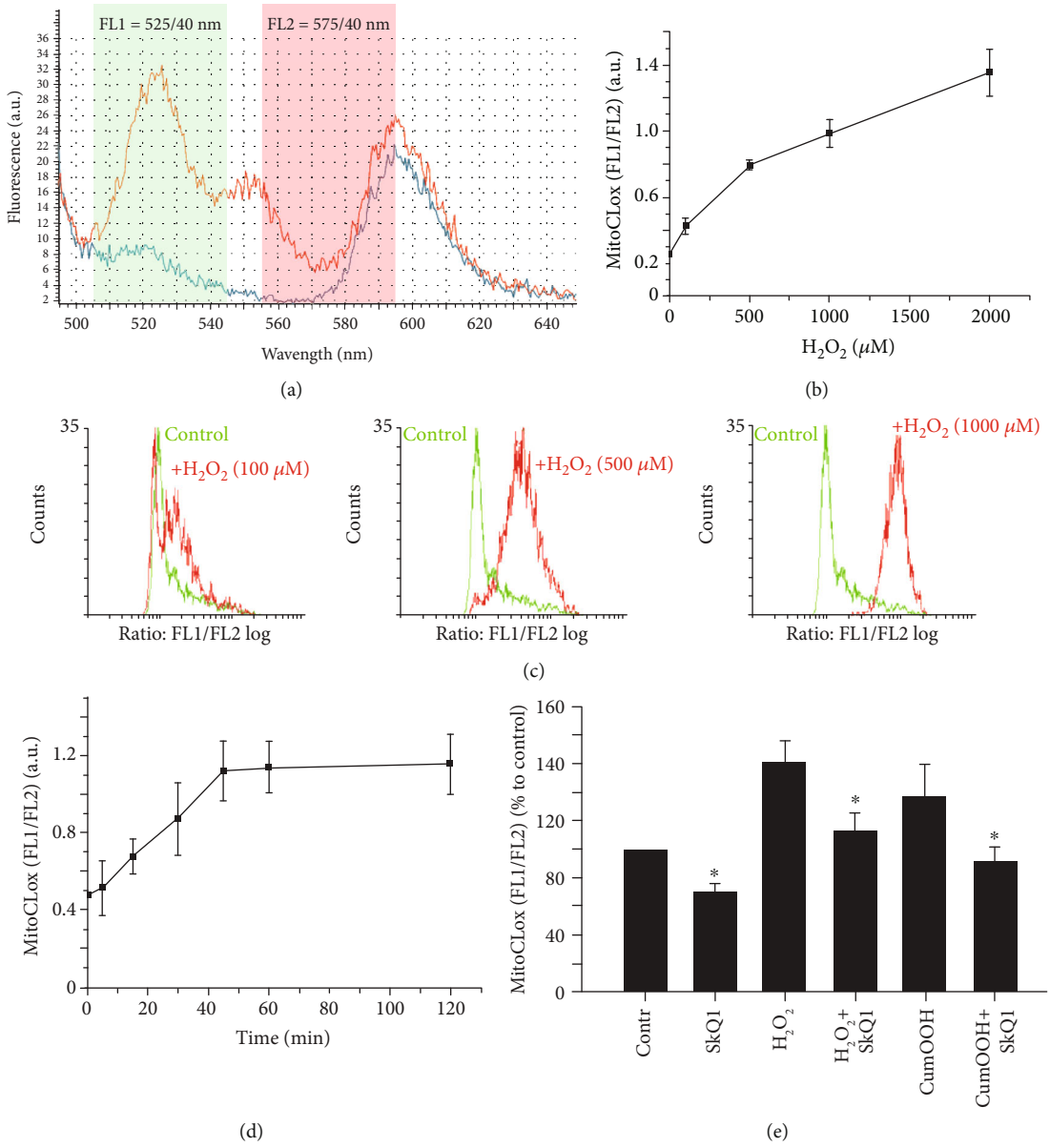

Figure 3: Measurements of MitoCLox oxidation in living cells by flow cytometry. MRC5-SV40 cells were incubated with MitoCLox (200 nM) for 1 h before the addition of peroxides. (a) Fluorescence spectra of reduced MitoCLox (blue line) and MitoCLox oxidized by 500 μM H_2O_2 (red line) at 488 nm excitation. The green area is the part of the spectrum detected by the standard bandpass filter 525/40 nm (FL1); the red area is the part of the spectrum detected by filter 575/40 nm (FL2). (b) The ratiometric measurements (FL1/FL2) of MitoCLox oxidation induced by 1 h incubation with H_2O_2. (c) An example of typical histograms obtained in experiments where the cells were treated with H_2O_2 and MitoCLox oxidation was measured as the FL1/FL2 ratio. (d) The time dependence of the MitoCLox oxidation in response to the addition of H_2O_2 (500 μM). (e) Incubation of the cells with mitochondria-targeted antioxidant SkQ1 (20 nM, 2 h) protects the cells from oxidative stress induced by H_2O_2 (500 μM) or 25 μM cumene hydroperoxide (CumOOH). All experiments were triplicated, and each bar represents the mean ± SD ($^*p < 0.05$ vs. the control or treated cells without SkQ1).

cell cultures could be a valuable tool for studies of myogenesis. We found that a specific fraction of cells exhibited a significant oxidation of MitoCLox in the otherwise homogenous culture of human myoblast MB135. Fluorescence microscopy demonstrated that cells with oxidized MitoCLox formed compact islets in the cell monolayer (Figure 7(a)). The antioxidant Tempol prevented the MitoCLox oxidation. Flow cytometry made it possible to quantify the size of this fraction (Figure 7(b)). The cells with oxidized MitoCLox got accumulated in the cultures that were seeded at an initial density of 1-6 × 10^5 cells/well and reached a high density (80-100% confluence) in 4 days of culturing. If the initial seeding density was too low for the cells to become close to confluency after 4 days (0.5 × 10^5 cells/well), no cells with oxidized MitoCLox were detected. The fraction of the cells with oxidized MitoCLox increased proportionally to the

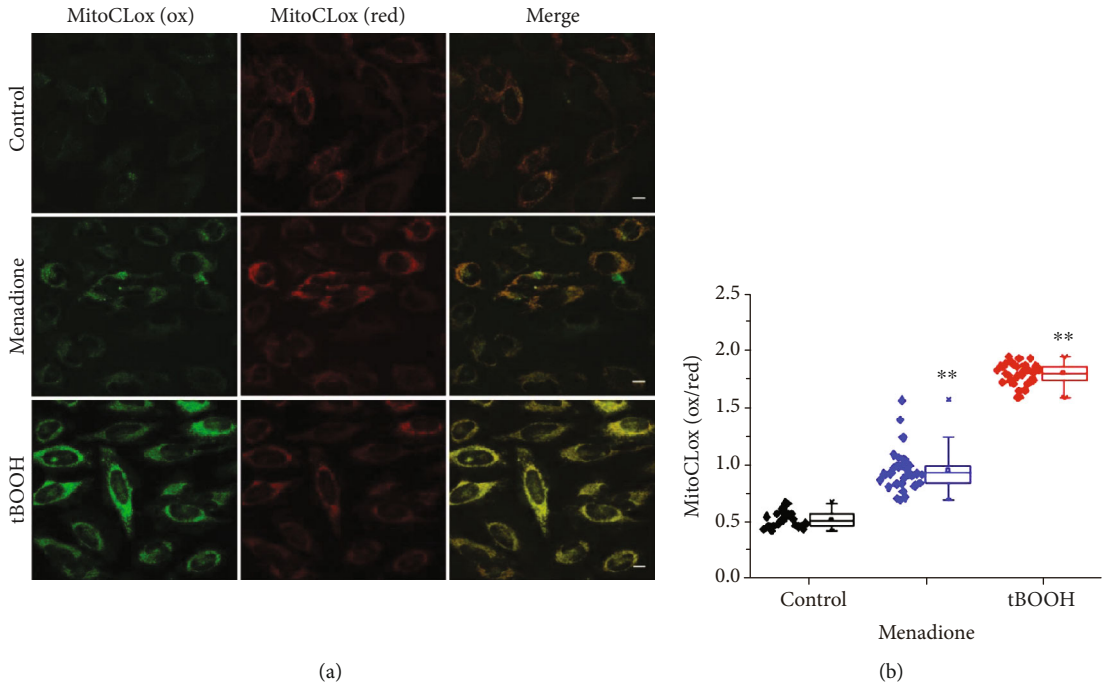

Figure 4: MitoCLox reports CL oxidation in HeLa cells in response to prooxidizing agents. (a) Fluorescence images in the green (λ_{em} = 500-560 nm) and red (λ_{em} = 580-630 nm) emission channels. HeLa cells were incubated with oxidants menadione (25 μM) or *tert*-butyl hydroperoxide (tBOOH, 100 μM) for 1 h, and 200 nM MitoCLox was added for 30 min. Bar, 10 μm. (b) Quantitative ratiometric analysis of MitoCLox response to different prooxidants. SD, $^{**}p < 0.05$ vs. the control.

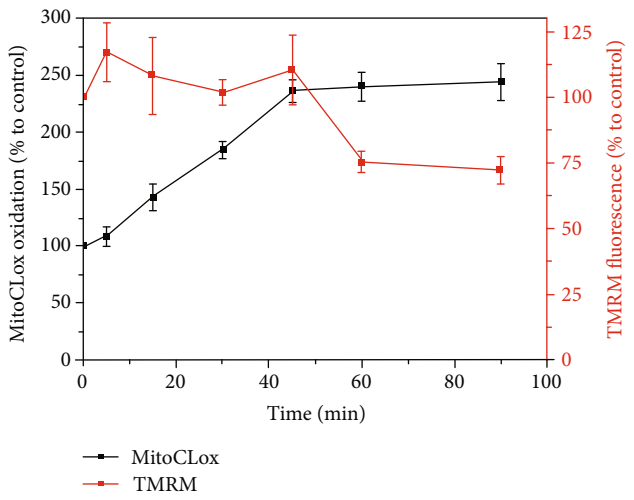

Figure 5: The relationship between lipid peroxidation, as measured by MitoCLox, and decrease in mitochondrial membrane potential under oxidative stress induced by H_2O_2. MRC5-SV40 cells were incubated with MitoCLox (200 nM) for 1 h before addition of H_2O_2 (0.5 mM). TMRM was added for 15 min before measurements to estimate the membrane potential. Flow cytometry analyses were performed using a Beckman Coulter FC 500. All experiments were triplicated, and each bar represents the mean ± SD.

increase of initial seeding density (Figure 7(c)). If the cells were seeded at high density of 6×10^5 cells/well, but cultured only for 24 h instead of 4 days prior to MitoCLox addition, the population of the cells with oxidized MitoCLox was not observed (data not shown). These data allow us to exclude a possible preexistent (either genetic or epigenetic) heterogeneity of the cell culture.

We have observed that mitochondrial fragmentation was significantly more pronounced in the cells with oxidized MitoCLox (Figure 7(a)) in agreement with the key role of mitochondrial ROS in mitochondrial fragmentation [36].

4. Discussion

Here, we tested a new mitochondria-targeted LPO fluorescent probe MitoCLox with different cell cultures and under conditions leading to oxidative stress. In all tested cases, MitoCLox was reliable in reporting LPO. The data obtained are fully consistent with the behavior of MitoCLox in the model liposome system [29].

Specifically, MitoCLox accumulated in the cells in a MMP-dependent way and changed its fluorescence in response to addition of H_2O_2, menadione, and tBOOH (Figures 2–5). The oxidation of MitoCLox could be prevented by a mitochondria-targeted antioxidant SkQ1 (Figure 3), as well as an antioxidant Tempol (Figure 7), which is in a good agreement with high efficiency of these antioxidants in protection of the mitochondrial structure and functions in various cellular models of oxidative stress [27, 37] and their protective action *in vivo* [38, 39].

It is noteworthy that the response of MitoCLox, as measured by flow cytometry (Figure 3), was more pronounced than that in microscopy experiments (Figures 2 and 4–7),

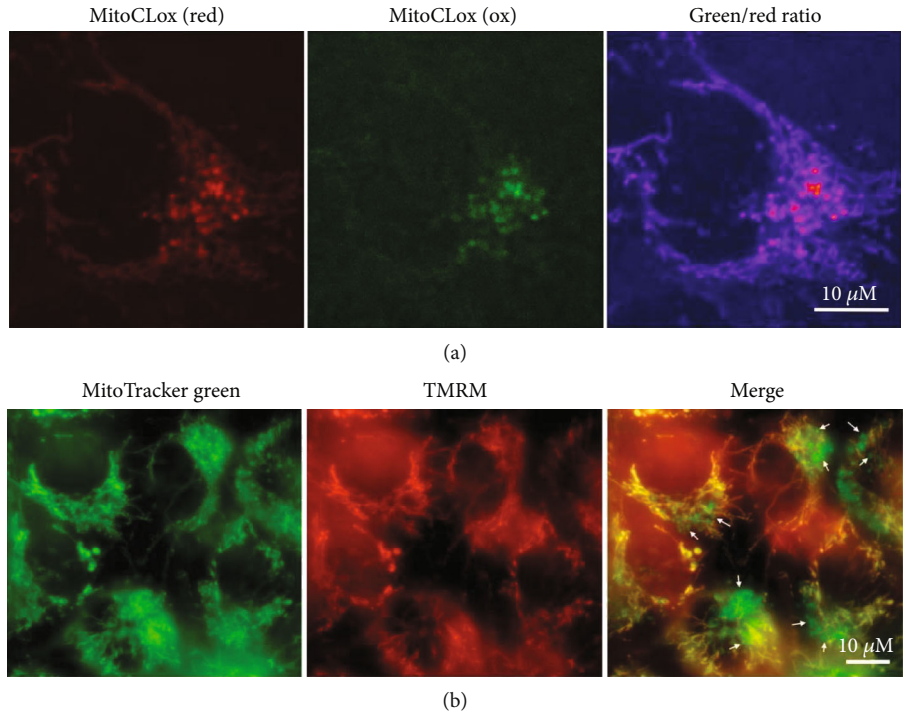

Figure 6: Analysis of mitochondrial heterogeneity in endothelial Ea.hy926 cells. (a) Cells were incubated with MitoCLox (200 nM; 2 h). (b) Cells were incubated with TMRM (100 nM; 30 min) and with MitoTracker Green (250 nM; 30 min). The arrows indicate the area where mitochondria with decreased membrane potential are located.

which renders MitoCLox as a suitable marker of lipid oxidation for flow cytometry measurements.

Oxidation of CL increases the proton leak through the inner mitochondrial membrane and causes a drop in MMP [9, 24]. As suggested by Korshunov and colleagues, the drop in MMP protects cells from oxidative damage by suppressing the generation of ROS [40]. Another mechanism of attenuating oxidative damage is the MMP-dependent fragmentation of the mitochondrial network, which allows to separate damaged mitochondria from integer ones and eliminate the former [9, 41]. Since oxidation of CL is also known to serve as a trigger for assembly of apoptosome [42, 43], it appears that the oxidation of CL triggers both pro- and antiapoptotic reactions. As a result, the fate of the cell appears to be determined by the balance between pro- and antiapoptotic reactions triggered by the same event of CL oxidation [9]. For understanding this interplay, it is needed to follow both the CL oxidation and changes in MMP *in vivo*. Figure 5 shows that the drop in MMP follows the oxidation of MitoCLox with a certain lag. Although the reason of the lag deserves further investigation, it seems tempting to speculate that cells could maintain their MMP for tens of minutes by hydrolyzing their ATP stock. Concentration of ATP should not decrease rapidly in highly glycolytic cells that we used, so the expected increase in membrane proton leakage could be initially counteracted by MMP generation by ATPase (and other proton pumps).

Earlier, it was shown that oxidative stress initially results in an exclusive oxidation of CL molecules [44–46]. Therefore, the fast PLO, as reported by MitoCLox in response to oxidative stress in diverse systems (Figures 2–5), was, most likely, due to the predominant oxidation of CL.

The observation of small perinuclear mitochondria with a low MMP (Figure 6) could be related to the earlier report on mitochondrial heterogeneity in endothelial cells [32, 33]. The data in Figures 6(a) and 6(b) indicates the existence of a specific small subpopulation of mitochondria with a reduced MMP and oxidized CL in endothelial cells. Earlier, similar results were reported by Kuznetsov and Margreiter who observed small round perinuclear mitochondria with decreased MMP in HL-1 cardiac muscle cells [47, 48]. It is tempting to speculate that peroxidation of mitochondrial lipids (primarily CL) could be responsible for the decrease in the MMP in the fraction of the mitochondrial population shown by arrows in Figure 6. Probably, these small mitochondria serve as sensors of cellular homeostasis. It is known that oxidative phosphorylation is not a significant source of ATP in endothelial cells [48] so that a small fraction of depolarized mitochondria would not significantly affect the energy balance of these cells. Our observations indicate that CL peroxidation in a fraction of mitochondrial population could be a reason for functional and structural heterogeneity of mitochondria in a single cell.

Application of MitoCLox allowed us to detect a specific fraction of cells with a high level of mitochondrial lipid peroxidation in the culture of human myoblast MB135. The size of this cell fraction increased with an increase in cell density with increasing culturing time. These specific

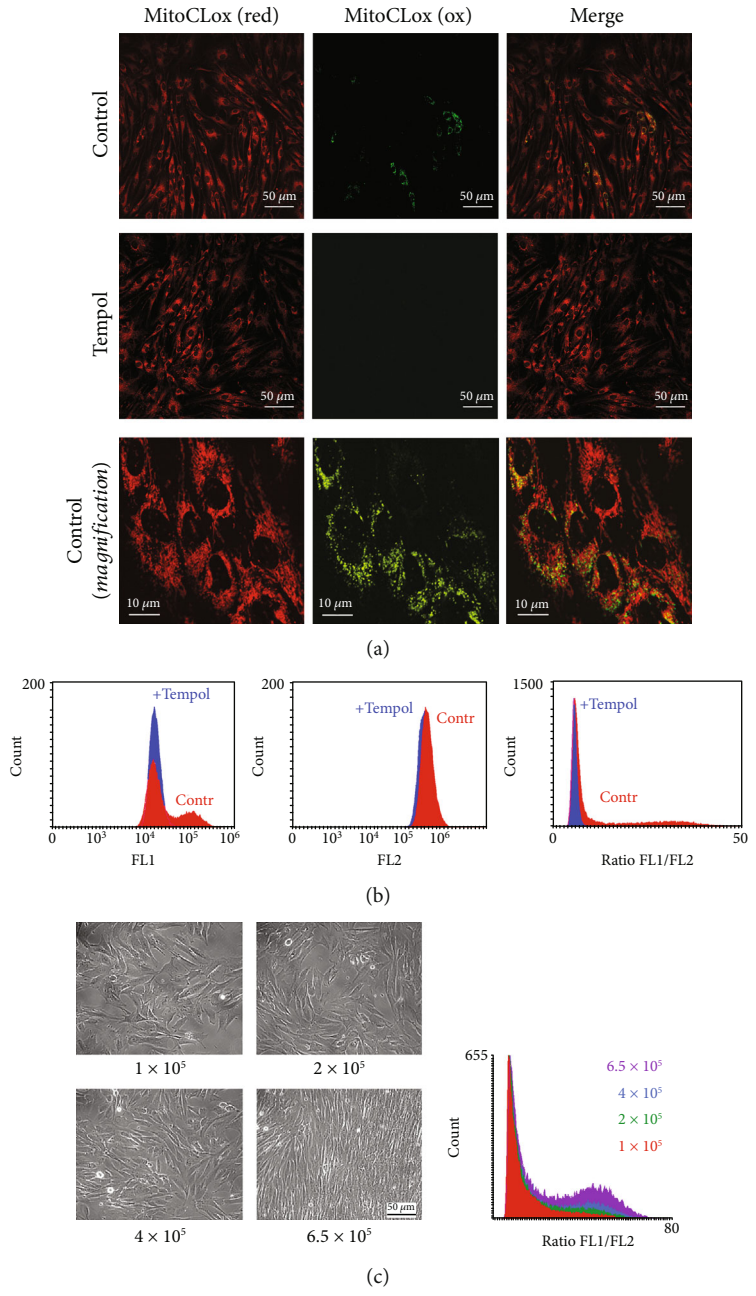

Figure 7: Analysis of MitoCLox oxidation in the culture of myoblast MB135. (a) Myoblasts were seeded in 35 mm dishes at an initial density of 2×10^5 cells/well and cultured for 4 days. Tempol (0.1 mM) was added at the beginning of culturing. Then, 200 nM MitoCLox was added for 5 h, and cells were analyzed using a Nikon Eclipse Ti (Nikon) confocal microscope with excitation at 488 and at 562 nm. Higher magnification was used to reveal mitochondrial morphology. (b) Myoblasts were seeded and cultured as in (a). Then, MitoCLox (200 nM) was added for 5 h, and cells were analyzed using the FC 500 flow cytometer in green (FL1) and red (FL2) channels. (c) Myoblasts were seeded in 6-well cell culture plates (9.6 cm^2 surface area per well) at initial density $1 - 6 \times 10^5$ cells/well and cultured for 4 days. Then, 200 nM MitoCLox was added for 5 h, and cells were analyzed as in (b). The cell fraction with oxidized MitoCLox was measured. Phase-contrast images of the final cultures seeded at different densities are shown.

conditions correlate with increased probability of spontaneous myogenesis *in vitro* [49]. At high cell density, cell-cell contacts initiate contact inhibition of the cell cycle progression, cell fusion, and expression of the key players of myogenesis such as MyoD and myogenin [50]. Moreover, myoblasts were shown to secrete their own extracellular matrix glycoproteins that facilitate myogenic differentiation [51]. It is tempting to speculate that a subpopulation of myoblasts with oxidized mitochondrial CL includes the myoblasts that are committed for differentiation.

Fragmentation of the mitochondrial network and mitophagy are required for mitochondrial biogenesis and

myogenic differentiation [34, 35]. Deregulation of these processes contributes to various types of genetic muscular dystrophy and in age-associated sarcopenia [36]. Cardiolipin is deeply involved in the regulation of mitochondria dynamics since it interacts both with profission (Drp1) [15] and with profusion (Opa1) [13] dynamin-related GTPases. Furthermore, externalization of CL to the outer mitochondrial membrane could act as one of the elimination signal for mitophagy [15]. These data suggest that oxidation of CL (and, perhaps, other lipids) is one of the early events that lead, via mitochondrial fragmentation and mitophagy, to myogenesis. This suggestion is in good agreement with the findings that high doses of mitochondria-targeted antioxidants inhibited myogenesis via inhibition of mitochondrial fragmentation and mitophagy [52–54]. Interestingly, mild depletion of mitochondrial ROS did not block in vitro fusion of primary myoblasts and even stimulated differentiation of myoblasts with some genetic defects [55]. Myogenesis is not the only example of the differentiation program that depends on mitoROS. In mesenchymal stem cells, mitoROS were found not only to initiate differentiation but also to contribute to cell fate determination [56]. Mitochondrial ROS (at least partially via modulation of mitochondrial dynamics and mitophagy) contribute also to keratinocyte differentiation within the epidermis and hair follicle development [57] and differentiation of adipocytes [58] and of immune cells [59]. MitoCLox could be a valuable tool for studies of these differentiation programs.

5. Conclusions

Here, we showed that molecules of a new mitochondria-targeted probe MitoCLox accumulated in mitochondria of living cells and reported the oxidation of mitochondrial lipids under conditions of oxidative stress. Ratiometric measurements of MitoCLox oxidation using flow cytometry revealed a very good dynamic range of the probe. Mitochondria-targeted antioxidant SkQ1 inhibited MitoCLox oxidation that was induced either by hydrogen peroxide or by organic hydroperoxide. The earlier findings demonstrated that CL (a) was selectively oxidized under conditions compatible to those of our experiments and (b) could be protected against oxidation by cationic mitochondria-targeted antioxidants [44–46]. We suggest that MitoCLox most likely preferably reports on the oxidation of CL, in agreement with results of molecular dynamic modeling that predicted a particular affinity of MitoCLox to CL [29]. Specifically, the application of MitoCLox revealed that the oxidation of lipids took place immediately after addition of hydrogen peroxide and preceded the drop in MMP. In the in vitro model of myogenesis, the use of MitoCLox revealed a cell subpopulation with an increased level of lipid oxidation and fragmented mitochondria. These cells were observed only after prolonged culturing of a dense culture of myoblasts, which is a necessary condition for the onset of myogenic differentiation. In sum, the new probe has demonstrated a notable potential for mitochondrial lipid peroxidation studies in living cells.

Data Availability

The data used to support the findings of this study are included within the article.

Conflicts of Interest

There are no conflicts of interest.

Acknowledgments

The work was supported by the grant of the Russian Science Foundation No. 17-14-01314. K.L. would like to thank the German Academic Exchange Service (DAAD) and its Ostpartnerschaften Programm for the support. The authors acknowledge the support from Deutsche Forschungsgemeinschaft (DFG) and the Open Access Publishing Fund of Osnabrück University. K.B. and B.R. were funded by the Deutsche Forschungsgemeinschaft (Bu2288/1-2) and CiM. The studies presented in Figures 6 and 7 were supported in part by the Russian Foundation for Basic Research (Grants No. 17-00-00088 and 1904-01020).

References

[1] N. Ikon and R. O. Ryan, "Cardiolipin and mitochondrial cristae organization," *Biochimica et Biophysica Acta - Biomembranes*, vol. 1859, no. 6, pp. 1156–1163, 2017.

[2] K. Mikel'saar, I. I. Severina, and V. P. Skulachev, "Phospholipids and oxidative phosphorylation," *Uspekhi Sovremennoĭ Biologii*, vol. 78, no. 3, pp. 348–370, 1974.

[3] K. Pfeiffer, V. Gohil, R. A. Stuart et al., "Cardiolipin stabilizes respiratory chain supercomplexes," *The Journal of Biological Chemistry*, vol. 278, no. 52, pp. 52873–52880, 2003.

[4] M. Zhang, E. Mileykovskaya, and W. Dowhan, "Cardiolipin is essential for organization of complexes III and IV into a supercomplex in intact yeast mitochondria," *The Journal of Biological Chemistry*, vol. 280, no. 33, pp. 29403–29408, 2005.

[5] E. Mileykovskaya and W. Dowhan, "Cardiolipin-dependent formation of mitochondrial respiratory supercomplexes," *Chemistry and Physics of Lipids*, vol. 179, pp. 42–48, 2014.

[6] T. H. Haines, "A new look at cardiolipin," *Biochimica et Biophysica Acta (BBA) - Biomembranes*, vol. 1788, no. 10, pp. 1997–2002, 2009.

[7] T. H. Haines and N. A. Dencher, "Cardiolipin: a proton trap for oxidative phosphorylation," *FEBS Letters*, vol. 528, no. 1-3, pp. 35–39, 2002.

[8] T. Wenz, R. Hielscher, P. Hellwig, H. Schagger, S. Richers, and C. Hunte, "Role of phospholipids in respiratory cytochrome bc(1) complex catalysis and supercomplex formation," *Biochimica et Biophysica Acta (BBA) - Bioenergetics*, vol. 1787, no. 6, pp. 609–616, 2009.

[9] A. Y. Mulkidjanian, D. N. Shalaeva, K. G. Lyamzaev, and B. V. Chernyak, "Does oxidation of mitochondrial cardiolipin trigger a chain of antiapoptotic reactions?," *Biochemistry*, vol. 83, no. 10, pp. 1263–1278, 2018.

[10] R. Arias-Cartin, S. Grimaldi, P. Arnoux, B. Guigliarelli, and A. Magalon, "Cardiolipin binding in bacterial respiratory complexes: structural and functional implications," *Biochimica et Biophysica Acta (BBA) - Bioenergetics*, vol. 1817, no. 10, pp. 1937–1949, 2012.

[11] D. V. Dibrova, D. A. Cherepanov, M. Y. Galperin, V. P. Skulachev, and A. Y. Mulkidjanian, "Evolution of cytochrome bc complexes: from membrane-anchored dehydrogenases of ancient bacteria to triggers of apoptosis in vertebrates," *Biochimica et Biophysica Acta (BBA) - Bioenergetics*, vol. 1827, no. 11-12, pp. 1407–1427, 2013.

[12] K. B. Busch, G. Deckers-Hebestreit, G. T. Hanke, and A. Y. Mulkidjanian, "Dynamics of bioenergetic microcompartments," *Biological Chemistry*, vol. 394, no. 2, pp. 163–188, 2013.

[13] V. E. Kagan, J. Jiang, Z. Huang et al., "NDPK-D (NM23-H4)-mediated externalization of cardiolipin enables elimination of depolarized mitochondria by mitophagy," *Cell Death & Differentiation*, vol. 23, no. 7, pp. 1140–1151, 2016.

[14] U. Schlattner, M. Tokarska-Schlattner, R. M. Epand, M. Boissan, M. L. Lacombe, and V. E. Kagan, "NME4/nucleoside diphosphate kinase D in cardiolipin signaling and mitophagy," *Laboratory Investigation*, vol. 98, no. 2, pp. 228–232, 2018.

[15] I. Bustillo-Zabalbeitia, S. Montessuit, E. Raemy, G. Basanez, O. Terrones, and J. C. Martinou, "Specific interaction with cardiolipin triggers functional activation of dynamin-related protein 1," *PLoS One*, vol. 9, no. 7, article e102738, 2014.

[16] T. Ban, T. Ishihara, H. Kohno et al., "Molecular basis of selective mitochondrial fusion by heterotypic action between OPA1 and cardiolipin," *Nature Cell Biology*, vol. 19, no. 7, pp. 856–863, 2017.

[17] C. T. Chu, J. Ji, R. K. Dagda et al., "Cardiolipin externalization to the outer mitochondrial membrane acts as an elimination signal for mitophagy in neuronal cells," *Nature Cell Biology*, vol. 15, no. 10, pp. 1197–1205, 2013.

[18] S. S. Iyer, Q. He, J. R. Janczy et al., "Mitochondrial cardiolipin is required for Nlrp3 inflammasome activation," *Immunity*, vol. 39, no. 2, pp. 311–323, 2013.

[19] E. I. Elliott, A. N. Miller, B. Banoth et al., "Cutting edge: mitochondrial assembly of the NLRP3 inflammasome complex is initiated at priming," *Journal of Immunology*, vol. 200, no. 9, pp. 3047–3052, 2018.

[20] V. E. Kagan, V. A. Tyurin, J. Jiang et al., "Cytochrome c acts as a cardiolipin oxygenase required for release of proapoptotic factors," *Nature Chemical Biology*, vol. 1, no. 4, pp. 223–232, 2005.

[21] N. A. Belikova, Y. A. Vladimirov, A. N. Osipov et al., "Peroxidase activity and structural transitions of cytochrome c bound to cardiolipin-containing membranes," *Biochemistry*, vol. 45, no. 15, pp. 4998–5009, 2006.

[22] A. Tocchi, E. K. Quarles, N. Basisty, L. Gitari, and P. S. Rabinovitch, "Mitochondrial dysfunction in cardiac aging," *Biochimica et Biophysica Acta (BBA) - Bioenergetics*, vol. 1847, no. 11, pp. 1424–1433, 2015.

[23] S. Pope, J. M. Land, and S. J. Heales, "Oxidative stress and mitochondrial dysfunction in neurodegeneration; cardiolipin a critical target?," *Biochimica et Biophysica Acta (BBA) - Bioenergetics*, vol. 1777, no. 7-8, pp. 794–799, 2008.

[24] Z. A. Ma, "The role of peroxidation of mitochondrial membrane phospholipids in pancreatic β -cell failure," *Current Diabetes Reviews*, vol. 8, no. 1, pp. 69–75, 2012.

[25] A. V. Birk, W. M. Chao, S. Liu, Y. Soong, and H. H. Szeto, "Disruption of cytochrome c heme coordination is responsible for mitochondrial injury during ischemia," *Biochimica et Biophysica Acta (BBA) - Bioenergetics*, vol. 1847, no. 10, pp. 1075–1084, 2015.

[26] J. Jiang, A. Bakan, A. A. Kapralov et al., "Designing inhibitors of cytochrome *c*/cardiolipin peroxidase complexes: mitochondria-targeted imidazole-substituted fatty acids," *Free Radical Biology & Medicine*, vol. 71, pp. 221–230, 2014.

[27] V. P. Skulachev, Y. N. Antonenko, D. A. Cherepanov et al., "Prevention of cardiolipin oxidation and fatty acid cycling as two antioxidant mechanisms of cationic derivatives of plastoquinone (SkQs)," *Biochimica et Biophysica Acta (BBA) - Bioenergetics*, vol. 1797, no. 6-7, pp. 878–889, 2010.

[28] A. V. Lokhmatikov, N. Voskoboynikova, D. A. Cherepanov et al., "Impact of antioxidants on cardiolipin oxidation in liposomes: why mitochondrial cardiolipin serves as an apoptotic signal?," *Oxidative Medicine and Cellular Longevity*, vol. 2016, Article ID 8679469, 19 pages, 2016.

[29] K. G. Lyamzaev, N. V. Sumbatyan, A. M. Nesterenko et al., "MitoCLox: a novel mitochondria-targeted fluorescent probe for tracing lipid peroxidation," *Oxidative Medicine and Cellular Longevity*, vol. 2019, Article ID 9710208, 11 pages, 2019.

[30] T. A. Prime, M. Forkink, A. Logan et al., "A ratiometric fluorescent probe for assessing mitochondrial phospholipid peroxidation within living cells," *Free Radical Biology & Medicine*, vol. 53, no. 3, pp. 544–553, 2012.

[31] Y. N. Antonenko, A. V. Avetisyan, L. E. Bakeeva et al., "Mitochondria-targeted plastoquinone derivatives as tools to interrupt execution of the aging program. 1. Cationic plastoquinone derivatives: synthesis and in vitro studies," *Biochemistry*, vol. 73, no. 12, pp. 1273–1287, 2008.

[32] I. I. Galkin, O. Y. Pletjushkina, R. A. Zinovkin et al., "Mitochondria-targeted antioxidants prevent TNFα-induced endothelial cell damage," *Biochemistry*, vol. 79, no. 2, pp. 124–130, 2014.

[33] V. P. Romaschenko, R. A. Zinovkin, I. I. Galkin et al., "Low concentrations of uncouplers of oxidative phosphorylation prevent inflammatory activation of endothelial cells by tumor necrosis factor," *Biochemistry*, vol. 80, no. 5, pp. 610–619, 2015.

[34] J. Sin, A. M. Andres, D. J. Taylor et al., "Mitophagy is required for mitochondrial biogenesis and myogenic differentiation of C2C12 myoblasts," *Autophagy*, vol. 12, no. 2, pp. 369–380, 2016.

[35] P. Fortini, C. Ferretti, E. Iorio et al., "The fine tuning of metabolism, autophagy and differentiation during in vitro myogenesis," *Cell Death & Disease*, vol. 7, no. 3, article e2168, 2016.

[36] P. M. Coen, R. V. Musci, J. M. Hinkley, and B. F. Miller, "Mitochondria as a target for mitigating sarcopenia," *Frontiers in Physiology*, vol. 9, article 1883, 2018.

[37] C. S. Wilcox, "Effects of tempol and redox-cycling nitroxides in models of oxidative stress," *Pharmacology & Therapeutics*, vol. 126, no. 2, pp. 119–145, 2010.

[38] V. P. Skulachev, "Cationic antioxidants as a powerful tool against mitochondrial oxidative stress," *Biochemical and Biophysical Research Communications*, vol. 441, no. 2, pp. 275–279, 2013.

[39] P. K. Chatterjee, S. Cuzzocrea, P. A. Brown et al., "Tempol, a membrane-permeable radical scavenger, reduces oxidant stress-mediated renal dysfunction and injury in the rat," *Kidney International*, vol. 58, no. 2, pp. 658–673, 2000.

[40] S. S. Korshunov, V. P. Skulachev, and A. A. Starkov, "High protonic potential actuates a mechanism of production of reactive oxygen species in mitochondria," *FEBS Letters*, vol. 416, no. 1, pp. 15–18, 1997.

[41] V. P. Skulachev, L. E. Bakeeva, B. V. Chernyak et al., "Thread-grain transition of mitochondrial reticulum as a step of mitoptosis and apoptosis," *Molecular and Cellular Biochemistry*, vol. 256-257, no. 1-2, pp. 341–358, 2004.

[42] V. E. Kagan, H. A. Bayir, N. A. Belikova et al., "Cytochrome *c*/cardiolipin relations in mitochondria: a kiss of death," *Free Radical Biology & Medicine*, vol. 46, no. 11, pp. 1439–1453, 2009.

[43] S. Orrenius and B. Zhivotovsky, "Cardiolipin oxidation sets cytochrome c free," *Nature Chemical Biology*, vol. 1, no. 4, pp. 188-189, 2005.

[44] V. A. Tyurin, Y. Y. Tyurina, W. Feng et al., "Mass-spectrometric characterization of phospholipids and their primary peroxidation products in rat cortical neurons during staurosporine-induced apoptosis," *Journal of Neurochemistry*, vol. 107, no. 6, pp. 1614–1633, 2008.

[45] V. P. Skulachev, V. N. Anisimov, Y. N. Antonenko et al., "An attempt to prevent senescence: a mitochondrial approach," *BBA-Bioenergetics*, vol. 1787, no. 5, pp. 437–461, 2009.

[46] J. Ji, A. E. Kline, A. Amoscato et al., "Lipidomics identifies cardiolipin oxidation as a mitochondrial target for redox therapy of brain injury," *Nature Neuroscience*, vol. 15, no. 10, pp. 1407–1413, 2012.

[47] A. V. Kuznetsov and R. Margreiter, "Heterogeneity of mitochondria and mitochondrial function within cells as another level of mitochondrial complexity," *International Journal of Molecular Sciences*, vol. 10, no. 4, pp. 1911–1929, 2009.

[48] S. M. Davidson and M. R. Duchen, "Endothelial mitochondria: contributing to vascular function and disease," *Circulation Research*, vol. 100, no. 8, pp. 1128–1141, 2007.

[49] S. R. Chowdhury, Y. Muneyuki, Y. Takezawa et al., "Growth and differentiation potentials in confluent state of culture of human skeletal muscle myoblasts," *Journal of Bioscience and Bioengineering*, vol. 109, no. 3, pp. 310–313, 2010.

[50] K. Tanaka, K. Sato, T. Yoshida et al., "Evidence for cell density affecting C2C12 myogenesis: possible regulation of myogenesis by cell-cell communication," *Muscle & Nerve*, vol. 44, no. 6, pp. 968–977, 2011.

[51] V. Chaturvedi, D. E. Dye, B. F. Kinnear, T. H. van Kuppevelt, M. D. Grounds, and D. R. Coombe, "Interactions between skeletal muscle myoblasts and their extracellular matrix revealed by a serum free culture system," *PLoS One*, vol. 10, no. 6, article e0127675, 2015.

[52] S. Lee, E. Tak, J. Lee et al., "Mitochondrial H_2O_2 generated from electron transport chain complex I stimulates muscle differentiation," *Cell Research*, vol. 21, no. 5, pp. 817–834, 2011.

[53] B. Kim, J. S. Kim, Y. Yoon, M. C. Santiago, M. D. Brown, and J. Y. Park, "Inhibition of Drp1-dependent mitochondrial division impairs myogenic differentiation," *American Journal of Physiology-Regulatory, Integrative and Comparative Physiology*, vol. 305, no. 8, pp. R927–R938, 2013.

[54] J. H. Kim, T. G. Choi, S. Park et al., "Mitochondrial ROS-derived PTEN oxidation activates PI3K pathway for mTOR-induced myogenic autophagy," *Cell Death and Differentiation*, vol. 25, no. 11, pp. 1921–1937, 2018.

[55] V. V. Zakharova, C. Dib, Y. B. Saada et al., "Uncoupling of oxidative phosphorylation and antioxidants affect fusion of primary human myoblasts in vitro," *Biopolymers and Cell*, vol. 32, no. 2, pp. 111–117, 2016.

[56] D. Q. Tan and T. Suda, "Reactive oxygen species and mitochondrial homeostasis as regulators of stem cell fate and function," *Antioxidants & Redox Signaling*, vol. 29, no. 2, pp. 149–168, 2018.

[57] R. B. Hamanaka, A. Glasauer, P. Hoover et al., "Mitochondrial reactive oxygen species promote epidermal differentiation and hair follicle development," *Science Signaling*, vol. 6, no. 261, article ra8, 2013.

[58] K. V. Tormos, E. Anso, R. B. Hamanaka et al., "Mitochondrial complex III ROS regulate adipocyte differentiation," *Cell Metabolism*, vol. 14, no. 4, pp. 537–544, 2011.

[59] S. E. Weinberg, L. A. Sena, and N. S. Chandel, "Mitochondria in the regulation of innate and adaptive immunity," *Immunity*, vol. 42, no. 3, pp. 406–417, 2015.

Hindawi
Oxidative Medicine and Cellular Longevity
Volume 2019, Article ID 3218275, 21 pages
https://doi.org/10.1155/2019/3218275

Research Article

Prediabetes Induced by Fructose-Enriched Diet Influences Cardiac Lipidome and Proteome and Leads to Deterioration of Cardiac Function prior to the Development of Excessive Oxidative Stress and Cell Damage

Gergő Szűcs,[1,2] **Andrea Sója**,[1,2] **Mária Péter**,[3] **Márta Sárközy**,[1,2] **Bella Bruszel**,[2,4] **Andrea Siska**,[5] **Imre Földesi**,[5] **Zoltán Szabó**,[2,4] **Tamás Janáky**,[2,4] **László Vígh**,[3] **Gábor Balogh**,[3] **and Tamás Csont**[1,2]

[1]*Metabolic Diseases and Cell Signaling Group, Department of Biochemistry, Faculty of Medicine, University of Szeged, Szeged H-6720, Hungary*
[2]*Interdisciplinary Centre of Excellence, University of Szeged, Szeged H-6720, Hungary*
[3]*Institute of Biochemistry, Biological Research Center of the Hungarian Academy of Sciences, Szeged H-6726, Hungary*
[4]*Institute of Medical Chemistry, Faculty of Medicine, University of Szeged, Szeged H-6720, Hungary*
[5]*Department of Laboratory Medicine, Faculty of Medicine, University of Szeged, Szeged H-6720, Hungary*

Correspondence should be addressed to Gergő Szűcs; szucs.gergo@med.u-szeged.hu
and Tamás Csont; csont.tamas@med.u-szeged.hu

Received 21 June 2019; Revised 3 October 2019; Accepted 16 October 2019; Published 9 December 2019

Guest Editor: Konstantin Lyamzaev

Prediabetes is a condition affecting more than 35% of the population. In some forms, excessive carbohydrate intake (primarily refined sugar) plays a prominent role. Prediabetes is a symptomless, mostly unrecognized disease which increases cardiovascular risk. In our work, we examined the effect of a fructose-enriched diet on cardiac function and lipidome as well as proteome of cardiac muscle. Male Wistar rats were divided into two groups. The control group received a normal diet while the fructose-fed group received 60% fructose-supplemented chow for 24 weeks. Fasting blood glucose measurement and oral glucose tolerance test (OGTT) showed slightly but significantly elevated values due to fructose feeding indicating development of a prediabetic condition. Both echocardiography and isolated working heart perfusion performed at the end of the feeding protocol demonstrated diastolic cardiac dysfunction in the fructose-fed group. Mass spectrometry-based, high-performance lipidomic and proteomic analyses were executed from cardiac tissue. The lipidomic analysis revealed complex rearrangement of the whole lipidome with special emphasis on defects in cardiolipin remodeling. The proteomic analysis showed significant changes in 75 cardiac proteins due to fructose feeding including mitochondria-, apoptosis-, and oxidative stress-related proteins. Nevertheless, just very weak or no signs of apoptosis induction and oxidative stress were detected in the hearts of fructose-fed rats. Our results suggest that fructose feeding induces marked alterations in the cardiac lipidome, especially in cardiolipin remodeling, which leads to mitochondrial dysfunction and impaired cardiac function. However, at the same time, several adaptive responses are induced at the proteome level in order to maintain a homeostatic balance. These findings demonstrate that even very early stages of prediabetes can impair cardiac function and can result in significant changes in the lipidome and proteome of the heart prior to the development of excessive oxidative stress and cell damage.

1. Introduction

Diabetes mellitus is a heterogeneous chronic metabolic disorder characterized by hyperglycemia [1]. The number of people suffering from diabetes increased from 108 million in 1980 to 422 million by 2014, and global prevalence almost doubled since 1980, from 4.7% to 8.5% [2]. According to the International Diabetes Federation, the number of people with diabetes may rise to 629 million by 2045 [3]. Prediabetes—in which glucose levels do not meet the criteria for diabetes but are too high to be considered normal—usually precedes diabetes mellitus and may remain symptomless for several years [4]. Prediabetes affects more than 35% of the population, and it is known that even nondiabetic levels of hyperglycemia and impaired glucose tolerance may be associated with an elevated risk of cardiovascular disease [5]. It has been recently shown that a mild diastolic dysfunction occurs even in prediabetic rats [6].

Type 2 diabetes is associated with myocardial lipotoxicity [7], which can cause impaired mitochondrial function [8]. Impaired mitochondrial function enhances oxidative stress, activates apoptosis, and thus contributes to cardiac dysfunction [7, 9, 10]. Although the role of lipotoxicity, oxidative stress, and apoptosis in diabetes has been well studied, the role of these mechanisms in prediabetes has not yet been well described. Saccharose and high-fructose corn syrup (isoglucose) are often used as sweeteners in the food and drink industry, and the consumption of these fructose-rich foods or beverages has an adverse effect on both animals [11] and humans [12]. A high-fructose diet is often used as a model of prediabetes or impaired glucose tolerance. After absorption, fructose is rapidly and uncontrollably absorbed in the liver, where its metabolism increases de novo lipogenesis (DNL). Induction of DNL has the capacity to alter the circulating nonesterified fatty acid (FA) profile, which, in turn, might affect cardiac lipid composition [13].

Proper cardiac lipid composition is strongly correlated with cardiac function and largely relies on proper cardiolipin (CL) content and species profile [14]. CL is the hallmark phospholipid (PL) of mitochondria that plays a role in many mitochondrial processes, including respiration and energy conversion. The heart is full of mitochondria, and CL accounts for about 10-15 mol% of all membrane lipids. Changes in the CL pool due to either oxidation or pathological remodeling cause mitochondrial dysfunctions and trigger retrograde signaling pathways that are associated with a large number of cardiac diseases including diabetes [15]. It is widely accepted that the symmetric tetralinoleoyl (18:2) CL species, which constitutes up to 80% of mammalian cardiac CL, is required for mitochondria to work optimally in metabolically active tissues [16]. After its initial biosynthesis, premature CL undergoes intensive remodeling processes to produce maturated CL (Supplementary Lipid Figure 1) [14, 15, 17–19]. In the first step of maturation, the removal of a single acyl chain is executed by a calcium-independent phospholipase A_2 to produce monolysocardiolipin (MLCL). Reacylation can be carried out by CoA-dependent acyltransferases or a CoA-independent reversible PL-lysoPL (LPL) transacylase called tafazzin. Tafazzin itself lacks acyl chain preference; still, it is believed to be the major enzyme involved in CL remodeling to produce homo-acylated CL [16]. Mutations in tafazzin cause abnormal molecular species of CL and the clinical phenotype of Barth syndrome, a rare and often fatal x-linked genetic disorder characterized by dilated cardiomyopathy, skeletal myopathy, and neutropenia [20].

Although CL is known to be relatively resistant to dietary manipulations, by "appropriate" interventions, the linoleoyl chain can be replaced [21]. Fructose feeding might represent such an intervention due to its highly lipogenic nature. Therefore, our study is aimed at examining the effects of fructose-enriched diet on the interplay of cardiac function, cardiac lipidome and proteome, and oxidative stress and apoptosis in a rat prediabetes model. To achieve this goal, several methods and techniques were applied including conventional blood tests, detailed serum analysis, enzymatic assays, protein expression analyses, transthoracic echocardiography, and high-performance mass spectrometry- (MS-) based proteomics and lipidomics.

2. Materials and Methods

This investigation conformed to the National Institutes of Health *Guide for the Care and Use of Laboratory Animals* (NIH Publication No. 85-23, Revised 1996) and was approved by the Animal Research Ethics Committee of University of Szeged.

2.1. Experimental Design. Male Wistar rats (310–450 g, $n = 16$ in the entire study) were kept under controlled temperature with 12/12 h light/dark cycles. Animals were divided into two groups and were fed with the following diets for 24 weeks: the control group ($n = 8$) was fed with a standard laboratory chow, while the fructose-fed group ($n = 8$) received a chow containing 60% fructose. Fasting blood glucose was measured every 4 weeks, while at weeks 12, 16, 20, and 24 oral glucose tolerance tests (OGTT) were performed. At week 20 and week 24, blood samples were taken to measure serum parameters. At the end of the feeding protocol, cardiac function was assessed by both in vivo echocardiography and ex vivo working heart perfusions (Figure 1). Following the perfusions, myocardial tissue was harvested for biochemical analysis.

2.2. Transthoracic Echocardiography. Cardiac morphology and function were assessed by transthoracic echocardiography at week 24 as described previously [22–24]. Briefly, rats were anesthetized with sodium pentobarbital (Euthasol, 40 mg/kg body weight i.p.). Then, the chest was shaved, and the rat was placed in a supine position onto a heating pad. Two-dimensional, M-mode, and Doppler echocardiographic examinations were performed by the criteria of the American Society of Echocardiography with a Vivid IQ ultrasound system (General Electric Medical Systems) using a phased array 5.0–11 MHz transducer (GE 12S-RS probe). Data of three consecutive heart cycles were analyzed (EchoPac Dimension software; General Electric Medical Systems) by an experienced investigator in a blinded

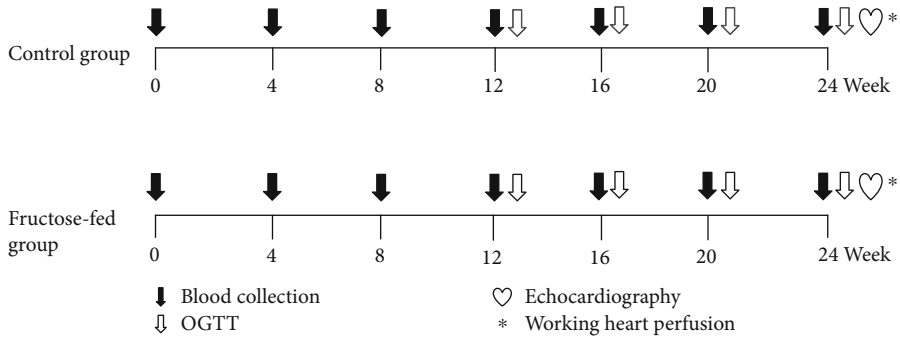

Figure 1: Experimental protocol. Male Wistar rats were divided into control ($n = 8$) and fructose-fed ($n = 8$) groups receiving either a standard chow or a chow supplemented with 60% fructose, respectively, for 24 weeks. Fasting blood glucose measurement or oral glucose tolerance test (OGTT) was performed every four weeks to monitor the development of prediabetic condition. At week 24, transthoracic echocardiography was performed to monitor cardiac function and morphology. Then, the hearts of the animals were isolated and mounted on a working heart perfusion system to measure hemodynamic and pressure parameters. After the perfusions, hearts were frozen for measurement of biochemical parameters.

manner. Systolic and diastolic wall thickness parameters were obtained from parasternal short-axis view at the level of the papillary muscles (anterior and inferior walls) and long-axis view at the level of the mitral valve (septal and posterior walls). The left ventricular diameters were measured by means of M-mode echocardiography from long-axis views between the endocardial borders. Fractional shortening (FS) was used as a measure of cardiac contractility ($\mathrm{FS} = (\mathrm{LVEDD} - \mathrm{LVESD})/\mathrm{LVEDD} \times 100$). Functional parameters including left ventricular end-diastolic volume (LVEDV) and left ventricular end-systolic volume (LVESV) were calculated on four-chamber view images delineating the endocardial borders in diastole and systole. The stroke volume was calculated as the difference of LVEDV and LVESV. The ejection fraction (EF) was calculated according to the formula $(\mathrm{LVEDV} - \mathrm{LVESV})/\mathrm{LVEDV} * 100$. Diastolic function was assessed using pulse-wave Doppler across the mitral valve from the apical four-chamber view. Early (E) and atrial (A) flow velocities provide an indication of diastolic function. Heart rate was also calculated using pulse-wave Doppler images during the measurement of transvalvular flow velocity profiles according to the length of 3 consecutive heart cycles measured between the start points of the E waves. The mean values of three measurements were calculated and used for statistical evaluation.

2.3. Working Heart Perfusion. Immediately after the echocardiography, cardiac performance was assessed in isolated working rat hearts, as described earlier [25–27]. Anesthetized rats were given 500 $\mathrm{U \cdot kg^{-1}}$ heparin intravenously. Hearts were then isolated, and the aorta was cannulated and initially perfused in Langendorff mode (at a constant pressure of 73 mmHg, 37°C) with Krebs-Henseleit buffer containing NaCl 118 mM, $NaHCO_3$ 25 mM, KCl 4.3 mM, $CaCl_2$ 2.4 mM, KH_2PO_4 1.2 mM, $MgSO_4$ 1.2 mM, and glucose 11 mM, gassed with 95% O_2 and 5% CO_2 [22, 28]. Then, the perfusion system was switched to working mode according to Neely with recirculating buffer [28, 29]. Hydrostatic preload and afterload were kept constant at 13 mmHg and 73 mmHg, respectively, throughout the experiments. Hearts were subjected to 10 min equilibration period before measurement ($n = 7 - 8$). Cardiac functional parameters including heart rate, coronary flow, aortic flow, cardiac output, left ventricular developed pressure (LVDP) and its first derivatives (dp/dt max and dp/dt min), and left ventricular end-diastolic pressure (LVEDP) were measured. At the end of the perfusion, the hearts were weighed, and the left and right ventricles were separated. The right and left ventricles were snap frozen in liquid nitrogen and stored at −80°C until they were used for biochemical assays.

2.4. Measurement of Malondialdehyde Levels. In order to measure the level of systemic and cardiac lipid peroxidation, serum malondialdehyde and left ventricular tissue malondialdehyde were assayed spectrophotometrically at 535 nm as described previously [27, 30]. Results are expressed as nmol/mL serum and nmol/mg protein.

2.5. mRNA Expression Profiling by qRT-PCR. Quantitative RT-PCR was performed with gene-specific primers to monitor mRNA expression as described previously [24]. To assess de novo lipid synthesis, expression of sterol regulatory element-binding transcription factor 1 (Srebf1), stearoyl-CoA desaturase 1 (Scd1), stearoyl-CoA desaturase 2 (SCD2), fatty acid synthase (Fasn), acetyl-CoA carboxylase 1 (Acaca), carbohydrate-responsive element-binding protein (Mlxipl), elongation of very-long-chain fatty acids protein 6 (ELOVL6), fatty acid desaturase 1 (Fads1), and fatty acid desaturase 2 (Fads2) were measured from liver samples. To assess cardiac hypertrophy, expression of myosin heavy chain α isoform (MYH6) and myosin heavy chain β isoform (MYH7) was measured. RNA was isolated using Qiagen RNeasy Fibrous Tissue Mini Kit (Qiagen, #74704) from the liver and heart tissues. Briefly, 4 μg and 2.2 μg of total RNA from liver and heart samples, respectively, were reverse transcribed using iScript™ Advanced cDNA Synthesis kit (Bio-Rad, 1725038), and specific primers and SsoAdvanced™ Universal SYBR® Green Supermix (Bio-Rad) were

used according to the manufacturer's instructions. Hypoxanthine phosphoribosyltransferase 1 (Hprt1) was used as control for normalization.

2.6. Lipidomics. Approximately 20 mg of the powdered left ventricle was directly extracted by adding 1 mL of methanol containing 0.001% butylated hydroxytoluene as an antioxidant and 60 μg di20:0 phosphatidylcholine as extraction standard. After a 5 min sonication in a water bath sonicator, the mixture was shaken for 5 min and centrifuged at 10000 × g for 5 min. The supernatant was transferred into a new Eppendorf tube and stored at −20°C until mass spectrometry (MS) analysis.

The solvents used for extraction and MS analyses were of Optima LCMS grade from Thermo Fisher Scientific (Bremen, Germany) and liquid chromatographic grade from Merck (Darmstadt, Germany). Lipid standards were purchased from Avanti Polar Lipids (Alabaster, AL). All other chemicals were from Sigma-Aldrich (Steinheim, Germany) and were of the best available grade.

Mass spectrometric analyses were performed on an LTQ-Orbitrap Elite instrument (Thermo Fisher Scientific, Bremen, Germany) equipped with a robotic nanoflow ion source (TriVersa NanoMate; Advion BioSciences; Ithaca, NY, USA) as described in [31]. Further details of MS measurements and lipid species annotation are given in the Supplementary Methods.

2.7. Proteomics. Approximately 30 mg of powdered left ventricle tissue samples was homogenized in lysate buffer (containing 2% SDS and 0.1 M DTT in 0.1 Tris solution). The homogenized samples were incubated at 98°C for 5 min. Proteins were precipitated by the addition of methanol/chloroform mixture (4 : 1) and were resuspended in 8 M urea. The total protein contents were determined using BCA (Thermo) protocol. 20 μg protein was digested by trypsin (Thermo) using RapiGest (Waters) detergent to enhance the digestion. In-gel fractionation was performed for pooled sample. In-gel fractionated samples were also digested by trypsin.

1D gel samples and pooled samples were measured in DDA (data-dependent acquisition) using a 90 min gradient on a Waters nanoAcquity-Thermo Q Exactive Plus LC-MS system to build a spectrum library of detectable peptides. The individual samples were measured in DIA (Data Independent Acquisition) mode for protein quantification with the same LC gradient using the spectrum library. The acquired data were analyzed with Encyclopedia [32] and statistically evaluated using Perseus [33] software. Enrichment of significantly changing proteins according to subcellular localization was carried out by Gene Ontology analysis (https://www.ebi.ac.uk/QuickGO/). Pathway assignment analysis of significantly altered proteins was performed with Reactome (https://www.reactome.org) after assignment to human genes, for higher annotation coverage. Further details of proteomic analysis are given in the Supplementary Methods.

2.8. Measurement of Serum and Pancreatic Insulin Levels. Serum and pancreatic insulin levels were measured by an enzyme immunoassay (Mercodia, Ultrasensitive Rat Insulin ELISA) in order to verify the development of hyperinsulinemia and decreased pancreatic insulin content as a consequence of beta cell damage in impaired glucose tolerance. Insulin ELISA was carried out according to the instructions of the manufacturer from either sera or homogenized pancreatic tissue samples of fructose-fed and control rats. Sera were centrifuged (2000 g for 10 min at 4°C) and kept at -20°C until further investigation. Pancreata were removed, trimmed free of adipose tissue, and weighed. Pancreata were homogenized in 6 mL cold acidified ethanol (0.7 M HCl : ethanol (1 : 3 *v*/*v*)) with an Ultra Turrax homogenizer and were kept at 4°C for 24 h. Then, pancreas homogenates were centrifuged (900 g for 15 min at 4°C), and the supernatants were stored at 4°C. The pellet was extracted again with 3 mL acidified ethanol for 24 h at 4°C. The supernatant obtained after centrifugation was pooled with the previous one and kept at -20°C until assayed [34, 35].

2.9. HOMA-IR Index. To estimate insulin resistance in fructose-fed or control rats, the widely used HOMA-IR index was calculated [34, 36, 37] by multiplying fasting serum insulin (μU/mL) with fasting serum glucose (mmol/L) then dividing by the constant 22.5, i.e., HOMA-IR = (fasting serum insulin concentration × fasting serum glucose concentration)/22.5.

2.10. Measurement of Serum Lipid Levels. Serum cholesterol, triglyceride, LDL, and HDL levels were measured at week 24 using a test kit supplied by Diagnosticum Zrt. (Budapest, Hungary) as described previously [27].

2.11. 3-NT ELISA. A double-antibody sandwich ELISA kit specific for 3-nitrotyrosine measurement was purchased from Genasiabio (Shanghai, China). Left ventricles were homogenized (Heilscher UP100H Ultrasonic Processor) in Phosphate Buffer Saline (PBS) (pH 7.2–7.4) and then centrifuged at 3000 rpm for 20 min at 4°C. Nitrotyrosine was measured according to the manufacturer's instructions and protocols, and optical densities (OD) were determined at 450 nm. Results were expressed as nmol/mg protein.

2.12. Measurement of Serum Laboratory Parameters. Urea and creatinine levels in serum were quantified by kinetic UV method using urease and glutamate dehydrogenase enzymes and Jaffe method, respectively. The reagents and the platform analyzers were from Roche Diagnostics. Serum sodium, potassium, and chloride levels were determined by indirect potentiometry using ion-selective electrodes at week 24. All reagents and instruments were from Roche Diagnostics. Alanine aminotransferase (ALAT), aspartate aminotransferase (ASAT), creatine kinase (CK), and lactate dehydrogenase (LDH) enzyme activities were measured with Roche UV assays standardized according to the recommendations of IFCC (International Federation of Clinical Chemistry). Creatine kinase MB enzyme activities were determined using an immunological UV assay of Roche.

2.13. Western Blot. To investigate changes of apoptotic proteins, the standard western blot technique was used in case

of Bax, Bcl-2, Bcl-xL, caspase-7, and caspase-3 with actin or tubulin loading background. Left ventricular samples ($n = 8$) were homogenized with an ultrasonicator (UP100H Hielscher, Teltow, Germany) in Radio-Immunoprecipitation Assay (RIPA) buffer (50 mM Tris-HCl (pH 8.0)), 150 mM NaCl, 0.5% sodium deoxycholate, 5 mM ethylenediamine tetra-acetic acid (EDTA), 0.1% sodium dodecyl sulfate, 1% NP-40 (Cell Signaling, Carlsbad, CA, USA) supplemented with phenylmethanesulfonyl fluoride (PMSF). The crude homogenates were centrifuged at 15000 × g for 30 min at 4°C. After quantification of protein concentrations of the supernatants using the BCA Protein Assay Kit (Pierce, Rockford, IL, USA), 25 μg of reduced and denaturized protein was loaded. Then, sodium dodecyl-sulfate polyacrylamide gel electrophoresis (SDS-PAGE) was performed (10% gel, 50 V, 4 h) followed by the transfer of proteins onto a nitrocellulose membrane (20% methanol, 35 V, 1.5 h). The efficacy of transfer was checked using Ponceau staining. The membranes were cut horizontally into parts corresponding to the molecular weights of Bax, Bcl-2, Bcl-xL, caspase-7, caspase-3, actin, and tubulin. Membranes were blocked for 1 h in 5% (w/v) bovine serum albumin (BSA) and were incubated with primary antibodies in the concentrations of 1 : 1000 against Bax (#2772), Bcl-2 (#3498), Bcl-xL (#2764), caspase-7 (#12827), caspase-3 (#14220), α-tubulin (#2144), and β-actin (#4970) overnight at 4°C in 5% BSA. Then, the membranes were incubated with IRDye® 800CW Goat Anti-Rabbit secondary antibody (Li-Cor) for 1 h at room temperature in 5% BSA. Fluorescent signals were detected by Odyssey CLx, and digital images were analyzed and evaluated by Quantity One Software.

2.14. Statistical Analysis. Proteomic data are presented as mean intensities ± CV, fold change, and p value. For proteomic data, the statistical significance was tested using unpaired Welch test. $p < 0.05$ and a fold change > 1.5 were accepted as a statistically significant difference. Lipidomic data are presented as mean ± SEM; statistical significance was determined according to Storey and Tibshirani [38] and was accepted for $p < 0.05$ corresponding to a false discovery rate < 0.05. PCA analyses were performed using MetaboAnalyst [39]. All other parameters are presented as mean ± SEM, and significance between groups was determined with two sample t-test or Mann-Whitney Rank Sum Test.

3. Results and Discussion

3.1. Prediabetes and Characterization of the Animal Model. In the present study, male Wistar rats were fed with 60% fructose-containing chow for 24 weeks to create a model of prediabetes. We have chosen this model in order to examine the effect of a moderate metabolic condition on the heart, rather than looking at the effects of severely disturbed glucose and lipid homeostasis seen for instance in genetically modified diabetes models (e.g., db/db or ob/ob mice) [40, 41]. In order to verify the development of the prediabetic state, fasting blood glucose was measured at every 4th week, and OGTT was performed at weeks 12, 16, 20, and 24. Fasting glucose levels were slightly but significantly higher in fructose-fed rats at weeks 12, 16, 20, and 24 (Figure 2(a)). OGTT area under the curve values were also significantly increased in fructose-fed rats at weeks 16, 20, and 24 (Figure 2(b)). These results demonstrate the development of prediabetes with impaired glucose tolerance in the present model. HOMA-IR, a widely used indicator of insulin resistance, was significantly higher in the fructose-fed rats at week 20, although no significant difference was detected in serum insulin levels (Figure 2(c)). Pancreatic insulin level was significantly higher in the fructose-fed group compared to controls (Figure 2(e)). These data demonstrate the appearance of a mild insulin resistance in our present model.

Although body weight increased in both groups during the course of the study, by the end of 24-week feeding, the weight of the fructose-fed rats was significantly smaller compared to that of the control rats (Figure 3(a)). Weight gain during the study was decreased in fructose-fed rats (Figure 3(b)). Although liver weight was not significantly different in fructose-fed rats, the liver weight to body weight ratio was increased (Table 1). Moreover, during the isolation of organs, we have observed macroscopical signs of fatty degeneration on the liver of fructose-fed animals. These findings may indicate fatty degeneration in the liver due to DNL initiated by fructose feeding. In fact, it has been demonstrated that fructose may activate DNL due to its rapid conversion to pyruvate bypassing the regulatory step of glycolysis catalyzed by the phosphofructokinase-1 enzyme [42]. Compared to the effects of fat-supplemented diet which leads to fat deposits both in the liver and adipose tissue (liver as well as body weight gain), dietary fructose preferably increases lipid accumulation only in the liver [42]. Fructose feeding may affect the metabolism of skeletal muscle through metabolic stress. For instance, Gatineau et al. showed that older rats fed with fructose-containing diet lost significantly more lean body mass and maintained more adipose tissue than control rats [43]. In sucrose-fed rats, significantly lower diet-induced muscle protein synthesis was observed compared to starch-fed rats [43]. Additionally, excessive fructose consumption was shown in the liver to increase production of substances such as methylglyoxal, which leads to oxidative stress in the muscle [44]. Activated DNL leads to endoplasmic reticulum stress [45] and production of hepatokines, such as fetuin-A [46], known to adversely affect muscle energy metabolism and insulin sensitivity [47]. These findings might explain decreased body weight gain in fructose-fed rats in our present study. Despite the macroscopic signs of fatty degeneration in the liver, neither serum lipid parameters (triglycerides, total cholesterol, and LDL and HDL cholesterol) nor liver enzymes (ALAT, ASAT) were increased in fructose-fed rats (Table 2) indicating an early stage of hepatic consequences.

To further characterize metabolic changes in the liver of fructose-fed rats, we performed qRT-PCR. We examined Srebf1 and Mlxipl transcription factors which regulate fatty acid metabolism related genes. No difference was found between control and fructose-fed group. We also examined Acaca and Fasn. Acaca catalyzes the carboxylation of

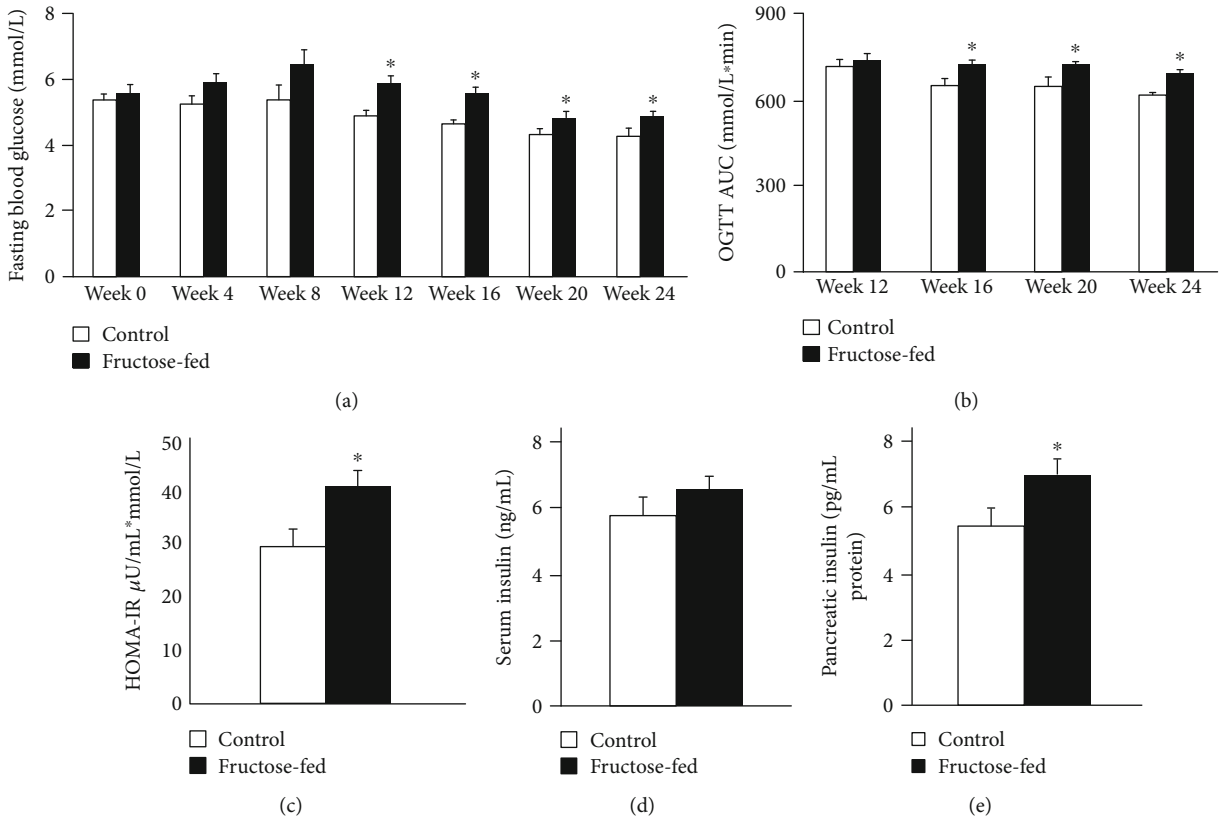

Figure 2: Prediabetic condition: (a) fasting blood glucose levels, (b) area under the curve (AUC) values for OGTT, (c) HOMA-IR index at week 20, (d) serum insulin level at week 20, and (e) pancreatic insulin level at week 24. Values are mean ± SEM (n = 7-8), $^*p < 0.05$.

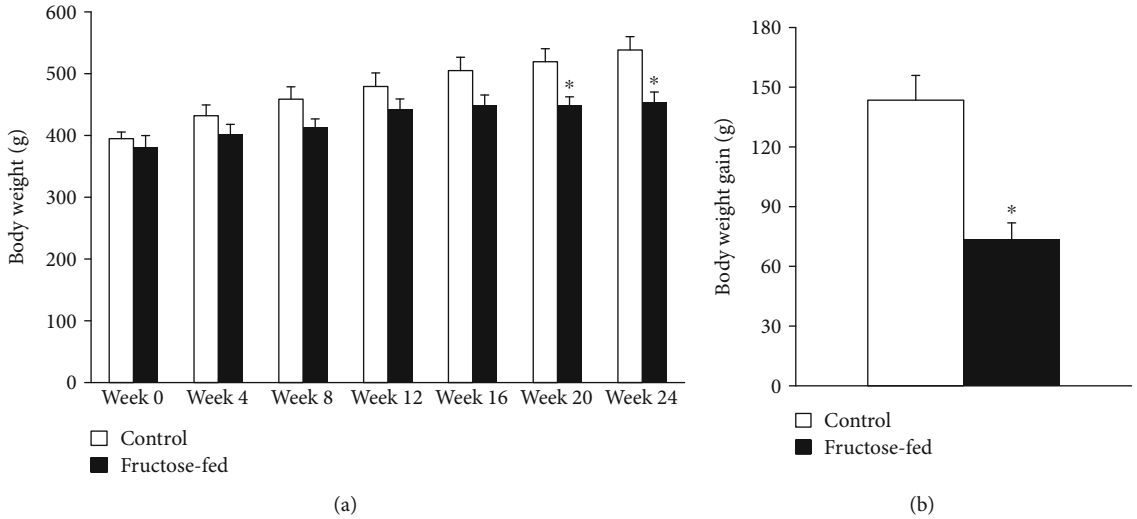

Figure 3: Body weight and weight gain of control and fructose-fed rats. Values are mean ± SEM (n = 8), $^*p < 0.05$.

acetyl-CoA to malonyl-CoA, the rate-limiting step of fatty acid synthesis. Fasn catalyzes the remaining steps of palmitic acid synthesis. Fasn expression showed a tendency of increase, while Acaca expression significantly increased in fructose-fed rats (Figure 4(c)). These findings are consistent with previous results and clearly indicate increased de novo lipid synthesis in fructose-fed rats [48, 49]. ELOVL6 enzyme, which catalyzes the first and rate-limiting reaction of long-chain fatty acid elongation cycle, was also significantly increased in fructose-fed rats. ELOVL6 enzyme is also known to play an important role in nonalcoholic fatty liver disease and steatohepatitis [50, 51] (Figure 4(h)).

Table 1: Isolated organ weights and isolated organ weight to body weight ratios at week 24 in both control and fructose-fed rats. Values are mean ± SEM ($n = 8$), $^*p < 0.05$.

	Control	Fructose-fed	p value
Heart weight (mg)	1726 ± 79	1527 ± 71	0.083
Liver weight (mg)	13292 ± 538	12262 ± 467	0.170
Pancreas weight (mg)	1093 ± 111	1101 ± 467	0.951
Heart (mg)/body weight (g)	3.22 ± 0.14	3.36 ± 0.09	0.422
Liver (mg)/body weight (g)	22.7 ± 0.2	27.0 ± 0.4*	≤0.001
Pancreas (mg)/body weight (g)	2.04 ± 0.19	2.43 ± 0.11	0.095

Table 2: Parameters measured in serum collected at week 24 in both control and fructose-fed rats. Values are mean ± SEM ($n = 8$), $^*p < 0.05$.

	Control	Fructose-fed	p value
Serum triglyceride (mmol/L)	0.96 ± 0.12	0.94 ± 0.20	0.938
Serum cholesterol (mmol/L)	1.78 ± 0.14	1.61 ± 0.11	0.359
LDL (mmol/L)	0.45 ± 0.05	0.43 ± 0.08	0.830
HDL (mmol/L)	0.86 ± 0.08	0.76 ± 0.07	0.335
ALAT (U/L)	38.63 ± 3.35	35.00 ± 4.08	0.500
ASAT (U/L)	77.88 ± 4.05	73.29 ± 5.74	0.517
CK (U/L)	263 ± 46	245 ± 45	0.776
CKMB (U/L)	352 ± 75	256 ± 33	0.264
LDH (U/L)	334.86 ± 63.77	272.50 ± 37.36	0.437
Cl (mmol/L)	102.50 ± 0.78	102.63 ± 0.82	0.914
K (mmol/L)	6.33 ± 0.36	5.95 ± 0.57	0.588
Na (mmol/L)	141.63 ± 0.60	141.38 ± 0.78	0.802

3.2. Heart Function and Morphology. To characterize prediabetes-induced cardiac changes in fructose-fed rats, transthoracic echocardiography was performed at week 24 to investigate cardiac function. Although the weight of the animals was significantly lower in the fructose-fed group, the heart weight and heart weight to body weight ratio were not changed significantly (Table 1).

Echocardiographic parameters of morphology and function are shown in Table 3. To exclude the potential effect of variations in cardiac mass, the morphological data were also given after normalization to heart weight (Table 3). Wall thicknesses and ventricular diameters were not changed significantly due to fructose feeding (except for anterior wall thickness) (Table 3). Although there was no difference in heart rate, ejection fraction, and fractional shortening, the E/A ratio was significantly smaller in fructose-fed rats indicating the impairment of diastolic filling (Table 3). These findings may suggest a very early manifestation of a mild hypertrophy and diastolic dysfunction with preserved systolic function in prediabetic rats.

Following echocardiography, the hearts were isolated to assess cardiac performance on a working heart perfusion system. Left ventricular end-diastolic pressure significantly increased, while cardiac output significantly decreased in fructose-fed rats (Figure 5). However, HR, max and min dp/dt, LVDP, and aortic systolic and diastolic pressures were not changed between groups during working heart perfusion (Table 4). These results demonstrate the appearance of a mild diastolic dysfunction in prediabetic rats. It is well known that left ventricular hypertrophy is more common in diabetic patients and that 40-75% of patients with type 1 or type 2 diabetes have diastolic dysfunction [52, 53]. However, here we show that the deterioration of diastolic function occurs much earlier than the development of overt diabetes. These results are consistent with recent reports showing that the development of diastolic dysfunction can precede complete diabetes [6].

In order to assess cardiac hypertrophy at the molecular level, mRNA expression of myosin heavy chain α isoform (MYH6) and myosin heavy chain β isoform (MYH7) was measured. We have found that cardiac MYH6 mRNA level, consistent with myosin 6 protein level measured by proteomics (Table 5), was increased in fructose-fed rats (Figure 6). However, MYH6/MYH7 ratio did not differ significantly. According to the literature [54–56], these data do not support cardiac hypertrophy in our fructose-fed rats.

It is known that clinical laboratory markers of myocardial injury are increased in diabetic cardiomyopathy [57] and serum ion parameters, especially potassium, can affect heart function. Therefore, we measured serum ions (potassium,

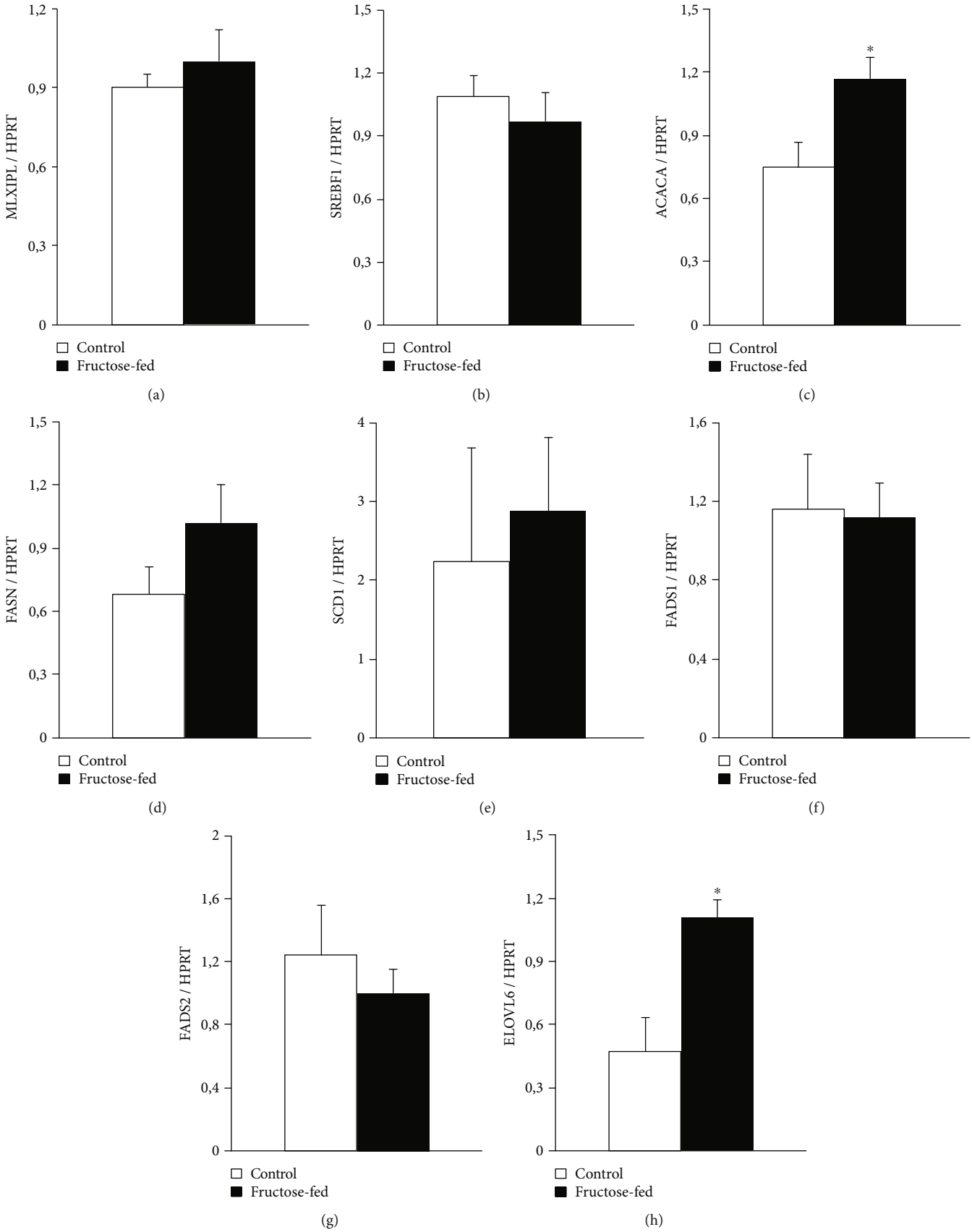

Figure 4: qRT-PCR results at week 24. Liver (a) Mlxipl expression, (b) Srebf1 expression, (c) Acaca expression, (d) Fasn expression, (e) SCD1 expression, (f) Fads1 expression, (g) Fads2 expression, and (h) ELOVL6 expression. Values are mean ± SEM ($n = 6$-7), $^*p < 0.05$.

Table 3: Left ventricular morphological and functional parameters examined by echocardiography at week 24 in both control and fructose-fed rats. Values are mean ± SEM ($n = 8$), $^*p < 0.05$.

Parameter (unit)	View/mode	Control	Fructose-fed	p value
Left ventricle morphology				
Anterior wall thickness in systole (mm)	Short axis/MM	3.59 ± 0.14	3.47 ± 0.12	0.506
Anterior wall thickness in diastole (mm)	Short axis/MM	2.35 ± 0.04	2.00 ± 0.10*	0.012
Inferior wall thickness in systole (mm)	Short axis/MM	3.38 ± 0.18	3.41 ± 0.07	0.871
Inferior wall thickness in diastole (mm)	Short axis/MM	2.20 ± 0.11	2.01 ± 0.08	0.167
Posterior wall thickness in systole (mm)	Long axis/MM	3.33 ± 0.30	3.13 ± 0.19	0.596
Posterior wall thickness in diastole (mm)	Long axis/MM	2.22 ± 0.14	1.96 ± 0.11	0.155
Septal wall thickness in systole (mm)	Long axis/MM	3.88 ± 0.18	3.55 ± 0.20	0.239
Septal wall thickness in diastole (mm)	Long axis/MM	2.33 ± 0.10	2.05 ± 0.17	0.169
Left ventricular end-diastolic diameter (mm)	Long axis/MM	6.85 ± 0.24	6.85 ± 0.21	0.996
Left ventricular end-systolic diameter (mm)	Long axis/MM	3.07 ± 0.16	3.37 ± 0.20	0.270
Left ventricular end-diastolic volume (μL)	4CH	100.3 ± 20.6	90.3 ± 11.7	0.681
Left ventricular end-systolic volume (μL)	4CH	39.23 ± 9.04	36.23 ± 6.03	0.787
Left ventricular morphology/heart weight				
Anterior wall thickness in systole (mm/g)	Short axis/MM	1.96 ± 0.11	2.28 ± 0.06*	0.021
Anterior wall thickness in diastole (mm/g)	Short axis/MM	1.27 ± 0.07	1.32 ± 0.06	0.596
Inferior wall thickness in systole (mm/g)	Short axis/MM	1.96 ± 0.06	2.20 ± 0.11	0.079
Inferior wall thickness in diastole (mm/g)	Short axis/MM	1.38 ± 0.10	1.34 ± 0.10	0.795
Posterior wall thickness in systole (mm/g)	Long axis/MM	1.96 ± 0.20	2.05 ± 0.09	0.665
Posterior wall thickness in diastole (mm/g)	Long axis/MM	1.21 ± 0.12	1.29 ± 0.06	0.559
Septal wall thickness in systole (mm/g)	Long axis/MM	2.28 ± 0.14	2.34 ± 0.11	0.735
Septal wall thickness in diastole (mm/g)	Long axis/MM	1.36 ± 0.06	1.73 ± 0.37	0.348
Left ventricular end-diastolic diameter (mm/g)	Long axis/MM	3.86 ± 0.23	4.56 ± 0.27	0.067
Left ventricular end-systolic diameter (mm/g)	Long axis/MM	1.81 ± 0.10	2.26 ± 0.20	0.082
Left ventricle function				
E/A	4CH	1.21 ± 0.07	1.03 ± 0.02*	0.015
Ejection fraction (%)	4CH	60.96 ± 3.38	62.83 ± 2.32	0.666
Fractional shortening (%)	Short axis/MM	49.57 ± 3.82	54.00 ± 3.60	0.414
MV E velocity (m/s)	4CH	0.81 ± 0.05	0.73 ± 0.06	0.358
MV A velocity (m/s)	4CH	0.71 ± 0.07	0.82 ± 0.06	0.260
Heart rate (1/min)	4CH	346.0 ± 12.9	349.6 ± 6.8	0.819

sodium, and chloride) and enzyme markers of myocardial injury (creatine kinase (CK), creatine kinase-MB (CK-MB), and lactate dehydrogenase (LDH)). Neither serum ion parameters nor markers of myocardial injury were changed significantly in fructose-fed rats compared to controls (Table 2).

3.3. Lipidomics. To characterize and elucidate the metabolic changes in the prediabetic heart induced by chronically applied fructose-rich diet, we performed high-performance, comprehensive shotgun MS-based lipidomic analyses from left ventricular whole membrane extracts. We have identified and quantified approximately 200 lipid molecular species encompassing 20 lipid classes (lipidomic data are summarized in Supplementary Lipid Table expressed either as lipid/protein or as mol% of membrane lipids or mol% of a given lipid class). Because the optimal physical state of the membrane is a prerequisite for proper functioning, in the following, we focus on membrane lipid compositional data. To obtain an overview, mol% of membrane lipid values was subjected to the nonsupervised multivariate statistics principal component analysis (PCA). The clear separation of the sample sets into two nonoverlapping clusters (Figure 7) indicates complex reshaping and metabolic rewiring of the whole lipidome due to fructose feeding. Examining these alterations in more detail and comparing the molecular species patterns for the control and fructose groups revealed 100 statistically significant differences (Supplementary Lipid Table).

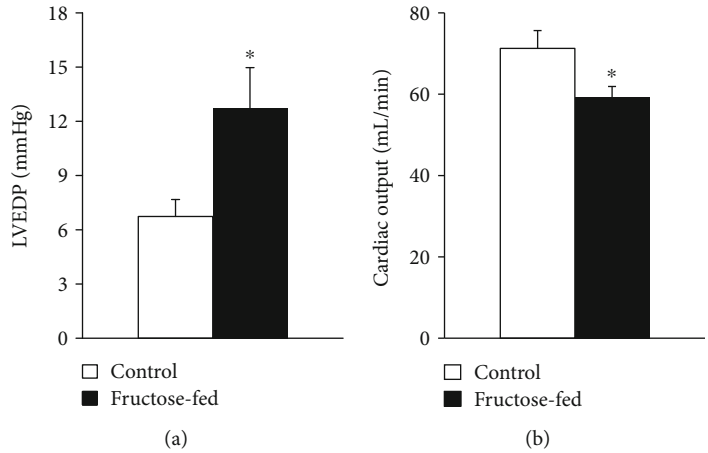

Figure 5: Cardiac function in isolated perfused hearts: (a) left ventricular end-diastolic pressure (LVEDP) and (b) cardiac output. Values are mean ± SEM (n = 7-8), $^*p < 0.05$.

Table 4: Parameters measured by working heart perfusion at week 24 in both control and fructose-fed rats. Values are mean ± SEM (n = 7-8).

	Control	Fructose-fed	p value
Aortic flow (mL)	46.6 ± 3.7	37.4 ± 2.4	0.065
Coronary flow (mL)	24.6 ± 1.1	21.9 ± 1.2	0.121
Max dp/dt (mmHg/s)	5975 ± 330	6063 ± 212	0.832
Min dp/dt (mmHg/s)	−3577 ± 222	−4090 ± 237	0.138
Aortic diastolic pressure (mmHg)	45.7 ± 1.7	42.1 ± 1.3	0.120
Aortic systolic pressure (mmHg)	110.3 ± 2.6	116.2 ± 1.5	0.121
LVDP (mmHg)	137.5 ± 6.0	139.5 ± 4.3	0.803
Heart rate (1/min)	279 ± 14	263 ± 24	0.554

Table 5: Alteration of selected cardiac proteins in fructose-fed rats by proteomic analysis. Values are expressed as fold change and p value.

Protein names	Gene names	Fold change	p value
Alpha B crystallin	Cryab	5.56	0.047
3-ketoacyl-CoA thiolase (mitochondrial)	Acaa2	4.56	0.005
Alpha-aminoadipic semialdehyde dehydrogenase	Aldh7a1	4.34	≤0.001
60 kDa heat shock protein (mitochondrial)	Hspd1	3.37	0.010
Myosin 6	MYH6	3.06	0.003
Peroxiredoxin-6	Prdx6	2.87	0.001
Superoxide dismutase [Mn] (mitochondrial)	Sod2	-1.82	0.033
Protein disulfide-isomerase	P4hb	-3.40	0.001

One of the most noteworthy changes can be connected to the CL remodeling system. It is known that under normal conditions, the levels of LPLs are kept low in general, and CL remodeling requires only trace amounts of MLCL [14]. Therefore, the significantly lowered level of matured CL in parallel with the significantly increased amount of MLCL (Supplementary Lipid Table), and consequently their markedly increased ratio in the membrane (MLCL/CL, Figure 8(a)), obviously report about an aberrant remodeling process in the fructose-fed group as compared to the controls. The ratio of MLCL/CL was found to be a more sensitive indicator than the level changes of CL and MLCL in Barth patients [58]. Furthermore, at the molecular species level, we detected pronounced loss of the most abundant homosymmetric tetra18:2 species CL(72:8) (Figure 8(b)).

This was the most prominent change not only in the context of membrane composition but also when considering absolute values, i.e., the protein-normalized data displayed

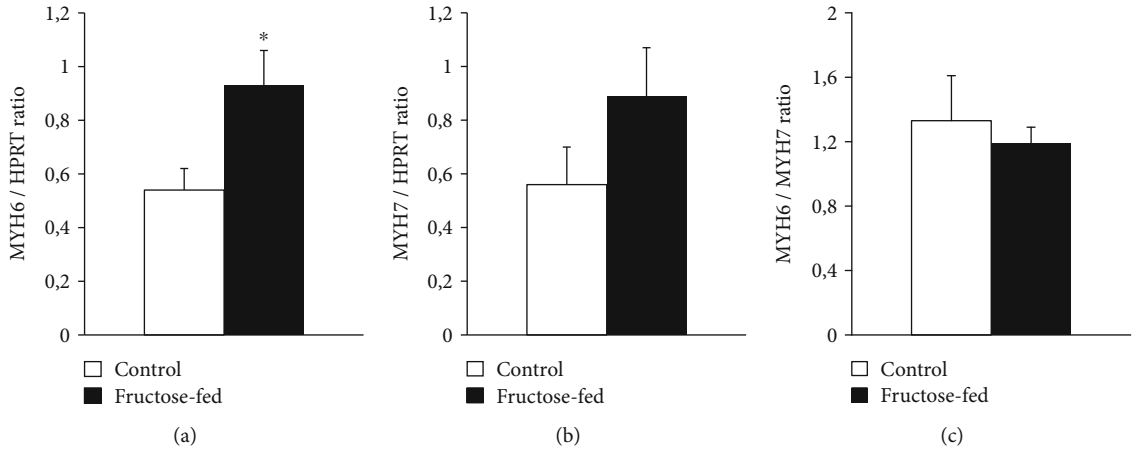

Figure 6: qRT-PCR results at week 24. Heart (a) MYH6 expression, (b) MYH7 expression, and (c) MYH6/MYH7 ratio. Values are means ± SEM (n = 8), $^{*}p < 0.05$.

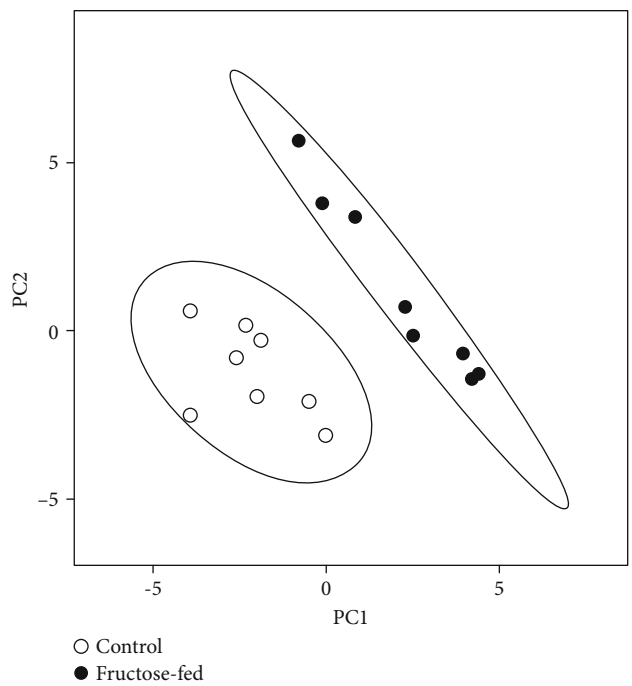

Figure 7: Principal component analysis (PCA) score plot. MS data expressed as mol% of membrane lipids were centered and normalized. Values for 8 independent experiments are shown for control and fructose-fed samples. Dashed lines display 95% confidence regions.

dramatic 45% decrease for CL(72:8) (from 28.5 to 15.7 nmol/protein mg; $p < 0.05$; Supplementary Lipid Table). This observation is in full agreement with other literature data obtained for either more severe diabetic and obesity models [59, 60] or recorded in a more similar early-stage fructose-induced type 2 diabetes study [61]. The loss in CL(72:8) was paralleled by elevations in practically all other asymmetric species independently on chain length and saturation for the fructose-fed animals as opposed to the normal chow diet (sum elevation from 2.82 to 4.35 mol% of membrane lipids, $p < 0.05$) (Figure 8(b)). This altogether resulted in a dramatic drop of the CL "symmetry" factor in the fructose group calculated as the ratio of symmetric/asymmetric species (Figure 8(c)). The major contributions to the increase in asymmetry derived from species which contain one non-18:2 acyl chain, i.e., from the 16:1 FA-containing CL(70:7; 16:1_18:2_18:2_18:2) species, from the CL(74:9) species whose major component is the CL(18:2_18:2_18:2_20:3) isobar, and from the CL(72:7) species corresponding to CL(18:1_18:2_18:2_18:2). This is in correspondence with the result observed in a fructose-induced early type 2 diabetic rat model [61] but differs from more severe mouse models of diabetes and insulin resistance/obesity. In the latter cases, defective cardiac CL remodeling resulted in depletion of 16:1 and enrichment of the highly unsaturated docosahexaenoic acid (DHA, 22:6 n-3) [17, 60], thereby essentially increasing the propensity of CL to peroxidation. In our study, the double bond index (DBI) of CL, a measure of unsaturation, did not change significantly (Supplementary Lipid Table). It can be partially due to the prediabetic nature of the model but also due to the sizeable difference in cardiac CL species composition between mouse and rat. Mouse cardiac CL contains essentially more DHA [61–63]. Therefore, it is more prone to ROS attack and peroxidation than that of the rat CL. Nevertheless, we have to mention that regarding fold increases of the individual CL species in the fructose-fed animals compared to the controls, the highest, ca. 10-fold elevations, was registered for DHA-containing CL species (78:12, 18:0_18:2-20:4_22:6 (major)) and (78:13, 18:1_18:2_20:4_22:6), although their levels barely reached the 0.1 mol% of total CL value even in the fructose group (Supplementary Lipid Table). It is important to note here that we could not detect oxidized lipid species either in CL or in other highly unsaturated and generally oxidation-prone lipid classes, such as plasmalogen phosphatidylethanolamine and phosphatidylserine. However, we could detect "asymmetry" defects already in the MLCL species profile; the major MLCL(54:6, tri18:2) species was found to be significantly reduced whereas the not only 18:2-containing precursors were markedly elevated (Supplementary Lipid Figure 2).

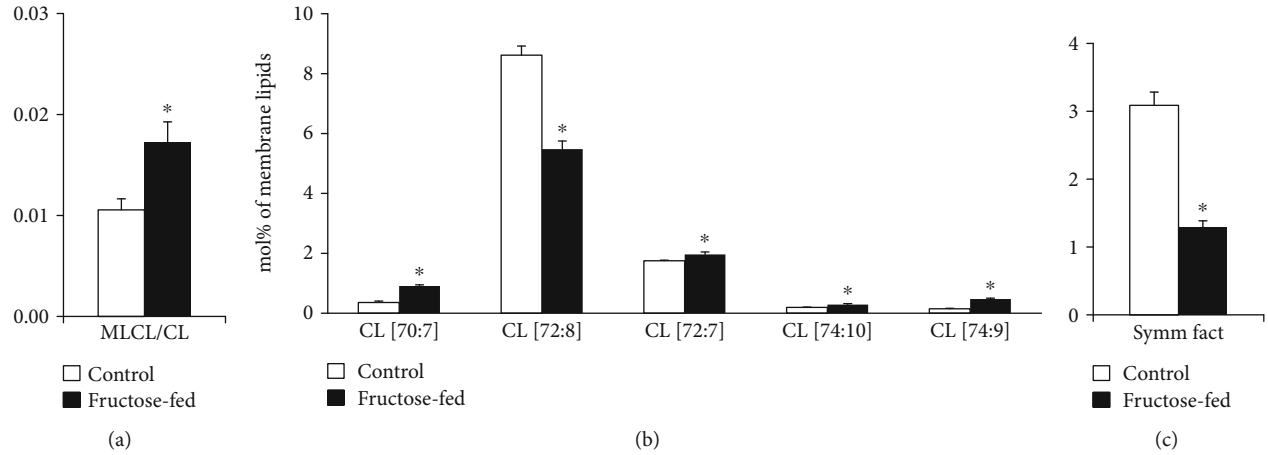

Figure 8: Defects in cardiolipin remodeling. (a) Monolysocardiolipin to cardiolipin ratio (MLCL/CL). (b) Changes in CL species due to fructose feeding. (c) CL symmetry factor calculated as the ratio of symmetric/asymmetric CL species. ESI-MS data are expressed as mol% of membrane lipids or calculated from the corresponding values and presented as means ± SEM ($n = 8$), $^*p < 0.05$.

Another important feature of the lipidome alterations was the general increase in lipid species with sum double bond (db) = 1 that could be detected in all major membrane PL classes in the fructose group as opposed the control animals (sum of db = 1 9.3 vs. 6.9 mol% of membrane lipids, $p < 0.05$; Supplementary Lipid Table). The main contributors, which contain a saturated and a monounsaturated FA leg, were collected in Figure 9(a). PL species with db = 2 predominantly contained a saturated FA in *sn1* and a linoleoyl (18:2) group in *sn2* position of the glycerol backbone; these can serve as potential acyl donors for the formation of tetra18:2 CL for the tafazzin-catalyzed transacylation. In parallel with the elevation of species with db = 1, we detected significant depletion in species with db = 2 in fructose-fed animals (sum of db = 2 7.1 vs. 9.7 mol% of membrane lipids, $p < 0.05$; Supplementary Lipid Table); selected species are demonstrated in Figure 9(b).

Changes in PL molecular species with highly unsaturated acyl chains (db ≥ 4) showed fairly complex picture with several significant alterations including both elevations and decreases (Supplementary Lipid Table). It was reported that the loss of tafazzin enzymatic activity in a Barth syndrome mouse model also resulted in complex alterations of polyunsaturated PL species [64]. Therefore, it is conceivable to suggest that the intricate imbalance in polyunsaturated PL species alters the biophysical and signaling properties of the cardiac membrane.

Since we could not detect the elevation in serum triglyceride levels due to fructose feeding, it is not surprising that neither the total cardiac TG content changed significantly (Supplementary Lipid Table). However, the prominent species profile change of the TG pool is worth mentioning. The robust relative increase in species containing saturated and monounsaturated FAs, such as TG(50:1, 52:2, and 54:3), in parallel with significant reductions in more unsaturated species, e.g., TG(52:4, 54:6, and 56:8) (Figure 9(c)) altogether led to the decrease of the double bond index (DBI), i.e., increase in saturation for cardiac TG (Figure 9(d)). Cardiac TG saturation together with the monoene increase and 18:2 decrease in membrane PLs may indicate the upregulation of DNL leading to a shift in FA profile towards the augmentation of monounsaturated 18:1 (and 16:1) FAs.

A further interesting aspect of the complex lipidome remodeling was the reshaping of the analyzed sphingolipid (SL) pool, ceramide (Cer) and sphingomyelin (SM). Cer has a central role in SL metabolism as well as it is known as a lipid mediator of the eukaryotic stress response. Its role is mostly associated with growth inhibition; the most studied being its function as a proapoptotic molecule [65]. Serum Cers have emerged as potential biomarkers of insulin resistance, diabetes, and heart disease, but also, muscle, liver, or adipose tissue Cers were shown to be associated with insulin resistance [66]. In our study, we measured small but significant elevation in total cardiac Cer at membrane lipid compositional level (approximately 30%; $p < 0.05$, Supplementary Lipid Table), which could be attributed almost exclusively to the increases in very-long-chain Cer-24 species Cer(42:2:2, d18:1/24:1 and 42:3:2, d18:2/24:1) (Figure 10(a)). It was reported that the nature of the acyl chain in Cers influences their contribution to the disease. Long-chain Cer-16 and Cer-18 often showed stronger associations with disease pathologies than very-long-chain Cer-24 [66]. Marchesini et al. reported that in confluent MCF-7 cells cell cycle arrest but not apoptosis was mediated by C24-Cer species [67]. It seems, therefore, that the alterations in Cer in our model might contribute to the observed cardiac dysfunction through changing the membrane biophysical properties rather than inducing sizeable apoptotic signaling. SM is the major structural mammalian SL which accumulates in liquid-ordered microdomains. Its total level showed only an increasing tendency in the membrane ($p = 0.058$), but its species compositions changed completely (Figure 10(b) and Supplementary Lipid Table). This may point to microdomain reorganization and hence, again, to the modulation of the membrane physical state and signaling properties due to fructose-rich diet.

Schlame et al. proposed that the acyl specificity of tafazzin arises from the physical properties of the lipid environment and is born out of a transacylation equilibrium in

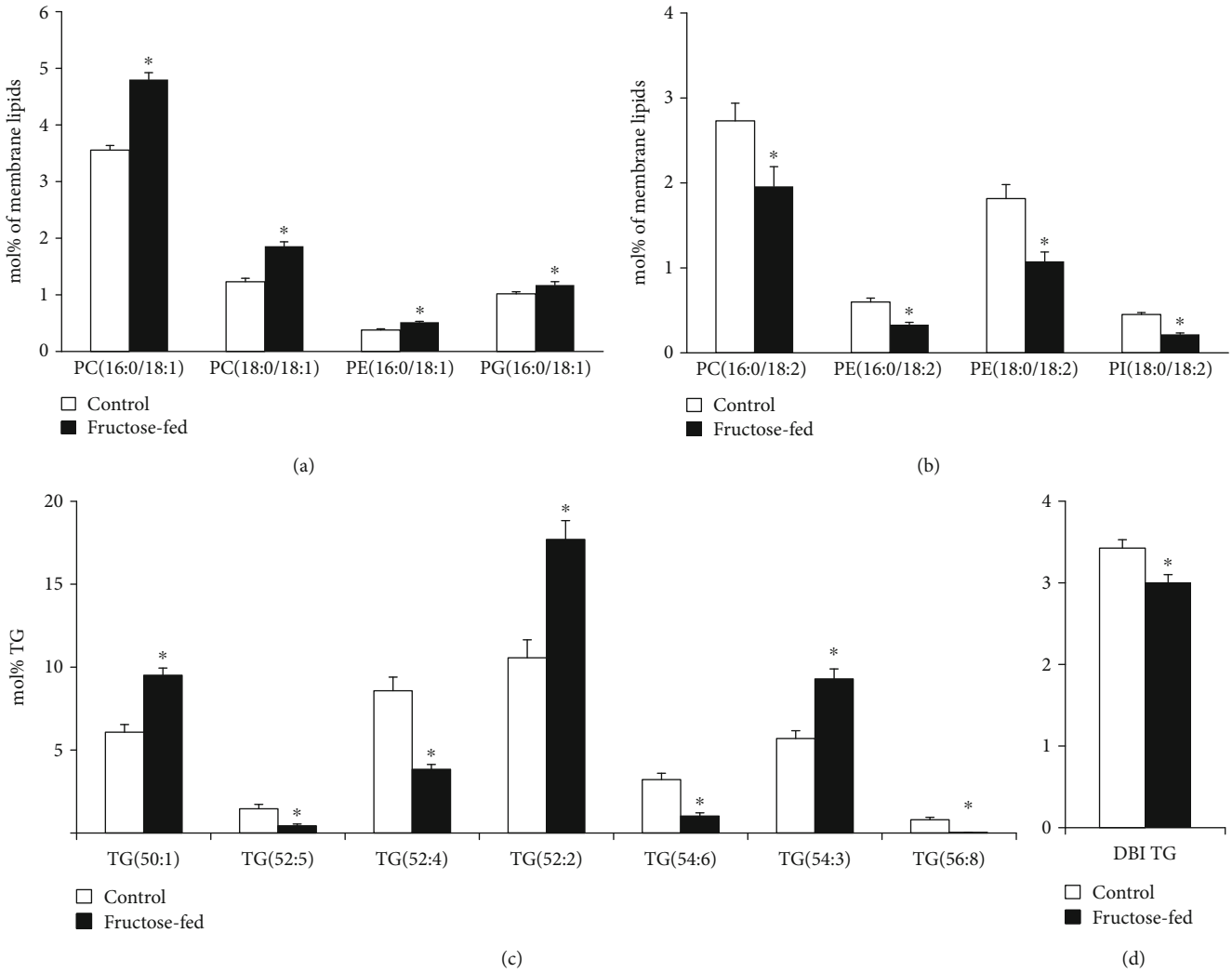

Figure 9: Early signs of de novo lipogenesis induction. (a) Changes in phospholipid species with 1 double bond. (b) Changes in phospholipid species with 2 double bonds. (c) Alterations in cardiac triglyceride (TG) species profile due to fructose feeding. (d) The double bond index calculated for TG. PC: phosphatidylcholine; PE: phosphatidylethanolamine; PG: phosphatidylglycerol; PI: phosphatidylinositol. ESI-MS data are expressed as mol% of membrane lipids or mol% of the specified lipid class and presented as means ± SEM ($n = 8$), $^*p < 0.05$.

which the tissue-specific availability of FAs and the specific packing conditions of lipids are manifested [18]. In line with this proposal, our lipidomic data fully support the disturbance in tafazzin action in the prediabetic state as the very first event leading to defective CL structural uniformity and molecular symmetry. Nevertheless, several other options may contribute to the observed changes. These include the induction of phospholipase A_2, which should increase the level of LPLs. It is known to happen in the diabetic state [68], and the registered increases in the relative levels of cardiac MLCL and LPE (Supplementary Lipid Table) in our prediabetic model might also reflect such an upregulation. In addition, the upregulation of the acyl-CoA:lyso-CL-acyltransferase that lacks preference for the linoleoyl group [69] as well as the downregulation of MLCL acyltransferase that specifically catalyzes the synthesis of tetra18:2 CL [70] also might play a role. However, these possibilities were reported for harsher conditions of later stage diabetes or well-developed oxidative stress induced by hyperthyroidism.

3.4. Proteomics. The complex changes in the heart detected by lipidomics at the metabolite level in the prediabetic state induced by chronic fructose feeding can be further mapped and complemented by alterations that occur at the protein level. Therefore, we performed comprehensive LC-MS-based proteomic analysis from left ventricular extracts.

Altogether, 1406 proteins were identified with at least two validate peptides from 1D-GE bands of pooled left ventricular samples. Using a spectral library built from those identifications, 802 proteins could be repeatedly quantified in individual samples. Seventy-five different proteins were significantly changed ($p \leq 0.05$ and a minimum of 1.5-fold change) in fructose-fed rats compared to control animals. Out of these proteins, 49 were upregulated and 26 were downregulated. Gene ontology analysis based on subcellular localization revealed enrichments of proteins with significant changes in different cell compartments including mitochondria ($n = 27$), cytoplasm ($n = 32$), nucleus ($n = 10$), extracellular space ($n = 8$), lysosome ($n = 3$), and Golgi apparatus

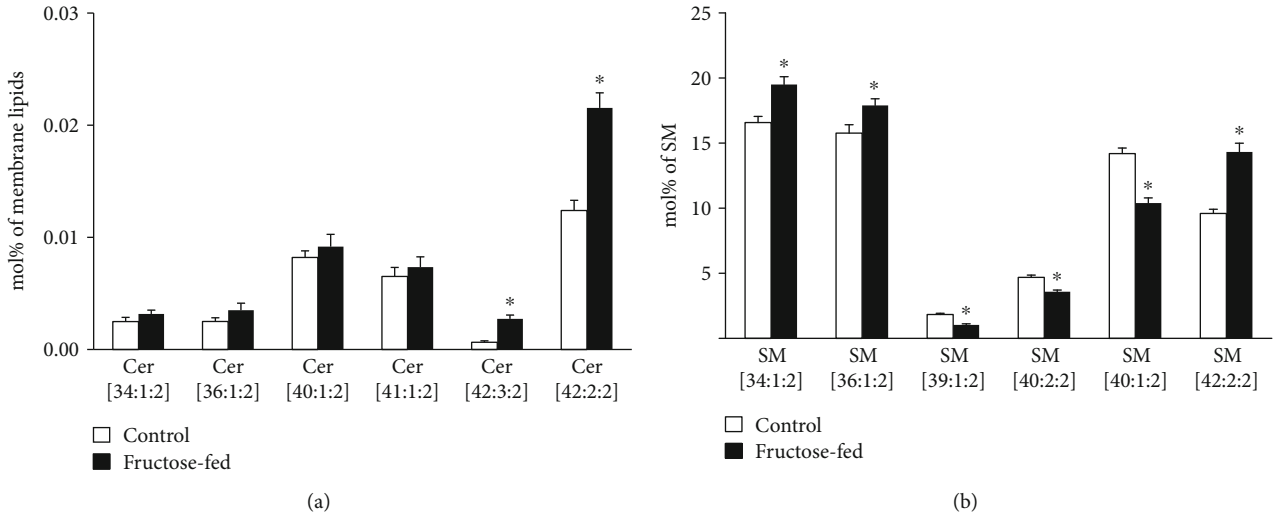

Figure 10: Modulation of the sphingolipid pool. (a) Alterations in ceramide (Cer) species. (b) Changes in the sphingomyelin (SM) species profile. ESI-MS data are expressed as mol% of membrane lipids or mol% of the specified lipid class and presented as means ± SEM ($n = 8$), $^*p < 0.05$.

($n = 3$) (Proteomic Table in the Supplementary Material). The relation of these proteins to different biochemical pathways was further analyzed in Reactome (https://www.reactome.org). The pathway analysis showed that most of the significantly altered proteins are related to metabolism (30 in pathways plus 9 interacting with some pathway proteins). Several metabolic pathways are affected, including the citric acid (TCA) cycle and respiratory electron transport ($n = 10 + 3$), metabolism of proteins ($n = 9 + 11$), lipids ($n = 5 + 3$), amino acids ($n = 8$), and carbohydrates ($n = 6 + 1$) (for a complete list, see the Supplementary Proteomic Table). Significantly altered proteins related to mitochondria, extracellular matrix, histones, oxidative stress, or apoptosis will be discussed in the following chapters.

3.5. Mitochondria. The proteomic analysis revealed changes in several proteins associated to various mitochondrial metabolic pathways due to fructose feeding (Table 6). These altered proteins can be coupled to the pyruvate dehydrogenase complex, electron transport chain, transport processes, and various metabolic pathways, such as the beta oxidation, tricarboxylic acid cycle, or amino acid metabolism. Pyruvate dehydrogenase complex plays a central role in the utilization of glucose as an energy source. Pyruvate dehydrogenase complex-related genes significantly decreased measured by proteomic analysis. In contrast, some beta oxidation-related proteins were increased. The first common point in the breakdown of glucose and fatty acids, citrate synthase, was also increased measured by proteomic analysis. These findings may suggest a shift to fatty acid utilization in cardiac tissue. We have also found both increased and decreased proteins related to the electron transport chain and amino acid metabolism.

3.6. Extracellular Matrix. We have found three extracellular matrix-related proteins to be significantly increased and another one to be decreased in the hearts of fructose-fed rats as assessed by proteomic analysis (Table 7). The increased proteins (prolargin, biglycan, and cathepsin D) may play a role in coping mechanism of the heart to prevent severe impairment. Prolargin was shown to be increased in a porcine model of ischemia/reperfusion injury [71]. Our group had previously shown that biglycan protects cardiomyocytes against hypoxia/reoxygenation injury [72, 73] and increases the expression of several proteins related to cardioprotection [74]. It has been also reported that myocardial cathepsin D upregulation induced by myocardial infarction protects against cardiac remodeling in mice [75]. Interestingly, galectin-1, known to have a protective role in cardiac homeostasis and postinfarction remodeling, is decreased in fructose-fed rats [76]. These results support the activation of adaptive mechanisms in the hearts of prediabetic rats.

3.7. Histones. Interestingly, expression of two histone proteins (core histone macro-H2A.1 and histone H1.5) was significantly increased in the hearts of fructose-fed rats. Histones are involved in packing the DNA in the nucleus, and mis-regulated histone expression is thought to lead to aberrant gene transcription by altering the chromatin structure [77].

3.8. Oxidative Stress and Apoptosis. Oxidative stress has a major role in the development of diabetic cardiomyopathy [7], and oxidative stress has been linked to the development of cardiac dysfunction [27, 78]. Moreover, elevated hydrogen peroxide production, elevated nitrotyrosine formation, and decreased cardiac function were observed in a prediabetes model induced by high-fat chow combined with a single low-dose STZ [6]. In our mild prediabetes model induced by fructose-enriched diet, there was no significant increase in the levels of the peroxidation product malondialdehyde in the serum or left ventricular tissue or in the cardiac level of the nitrooxidative marker 3-nitrotyrosine as compared to control values (Table 8).

Table 6: Alteration of selected mitochondrial proteins in fructose-fed rats by proteomic analysis. Values are expressed as fold change and p value.

Protein names	Gene names	Fold change	p value
Pyruvate dehydrogenase complex			
Dihydrolipoyllysine-residue acetyltransferase component of pyruvate dehydrogenase complex (mitochondrial)	Dlat	-3.47	0.022
Dihydrolipoamide acetyltransferase component of pyruvate dehydrogenase complex	Dbt	-9.53	0.039
Electron transport chain			
ETF-ubiquinone oxidoreductase (mitochondrial)	Etfdh	3.13	0.004
NADH dehydrogenase [ubiquinone] 1 alpha subcomplex subunit 2	Ndufa2	2.06	0.047
NADH-ubiquinone oxidoreductase chain 4	Mt-Nd4	1.59	0.007
Cytochrome c, testis-specific	Cyct	1.56	0.011
Cytochrome b-c1 complex subunit Rieske (mitochondrial)	Uqcrfs1	-1.95	0.001
NADH dehydrogenase [ubiquinone] 1 alpha subcomplex subunit 10 (mitochondrial)	Ndufa10	-3.15	0.038
Amino acid metabolism			
3-Hydroxyisobutyryl-CoA hydrolase (mitochondrial)	Hibch	5.44	0.042
Isovaleryl-CoA dehydrogenase (mitochondrial)	Ivd	-1.90	0.004
Methylcrotonoyl-CoA carboxylase beta chain (mitochondrial)	Mccc2	-2.18	0.046
Transport function			
ADP/ATP translocase 1	Slc25a4	2.47	0.005
Voltage-dependent anion-selective channel protein 3	Vdac3	2.17	0.018
MICOS complex subunit Mic60	Immt	1.58	0.003
Beta oxidation			
Enoyl CoA hydratase domain-containing 2	Echdc2	1.50	0.018
Electron transfer flavoprotein subunit alpha (mitochondrial)	Etfa	-1.94	0.001
Other			
Malic enzyme	Me3	4.27	0.022
Citrate synthase	Cs	3.14	≤0.001
Enoyl-[acyl-carrier-protein] reductase (mitochondrial)	Mecr	-1.61	0.029
Prohibitin-2	Phb2	-1.65	0.001

Table 7: Alteration of selected extracellular matrix proteins in fructose-fed rats by proteomic analysis. Values are expressed as fold change and p value.

Protein names	Gene names	Fold change	p value
Extracellular matrix			
Prolargin	Prelp	5.23	0.001
Biglycan	Bgn	1.91	0.018
Cathepsin D	Ctsd	1.52	0.001
Galectin-1	Lgals1	-3.23	0.005

However, we have detected by proteomics the increase of some oxidative stress-related enzymes from cardiac tissue, which may suggest an initial stage of oxidative stress that seems to be controlled by adaptive responses. We have found that alpha-aminoadipic semialdehyde dehydrogenase was increased in the hearts of fructose-fed rats (Table 5). Alpha-aminoadipic semialdehyde dehydrogenase protects cells from oxidative stress by metabolizing a number of lipid peroxidation-derived aldehydes [79, 80]. We have found that peroxiredoxin-6 was also increased in the fructose-fed group (Table 5). This enzyme catalyzes the reduction of hydrogen peroxide, short chain organic, fatty acid, and phospholipid hydroperoxides. It also has phospholipase activity and can therefore either reduce the oxidized sn2 fatty acyl group of phospholipids (peroxidase activity) or hydrolyze the sn2 ester bond of phospholipids (phospholipase activity). It plays a role in phospholipid homeostasis and in cell protection against oxidative stress by detoxifying peroxides [81]. Mitochondrial superoxide dismutase decreased in fructose-fed rats, and this result is consistent with the findings of Lappalainen et al. showing that SOD2 decreased in the kidney of STZ-induced diabetic rats [82].

Since increased apoptosis often contributes to cardiac dysfunction, in our present study, we also aimed to explore the effect of prediabetes on apoptosis in the heart. We assessed the expression of pro- and antiapoptotic proteins by western blot. Prediabetes did not affect the expression of proapoptotic caspase-7 and Bax in the left ventricles, while the antiapoptotic Bcl-2 was downregulated, and thereby, the Bax/Bcl-2 ratio was significantly increased in the fructose-fed group (Figure 11).

Similar to our results, a modest decrease in Bcl-2 has been shown recently in another model of prediabetes induced by a combination of high-fat diet and low-dose

Table 8: Oxidative stress markers measured in serum and heart tissue in both control and fructose-fed rats. Values are mean ± SEM ($n = 8$).

	Control	Fructose-fed	p value
Serum malondialdehyde (nmol/mg protein)	4.77 ± 0.43	4.03 ± 0.49	0.274
Cardiac malondialdehyde (nmol/mg protein)	1.27 ± 0.16	1.47 ± 0.22	0.482
3-Nitrotyrosine (nmol/mg)	190 ± 6.0	221 ± 20	0.164

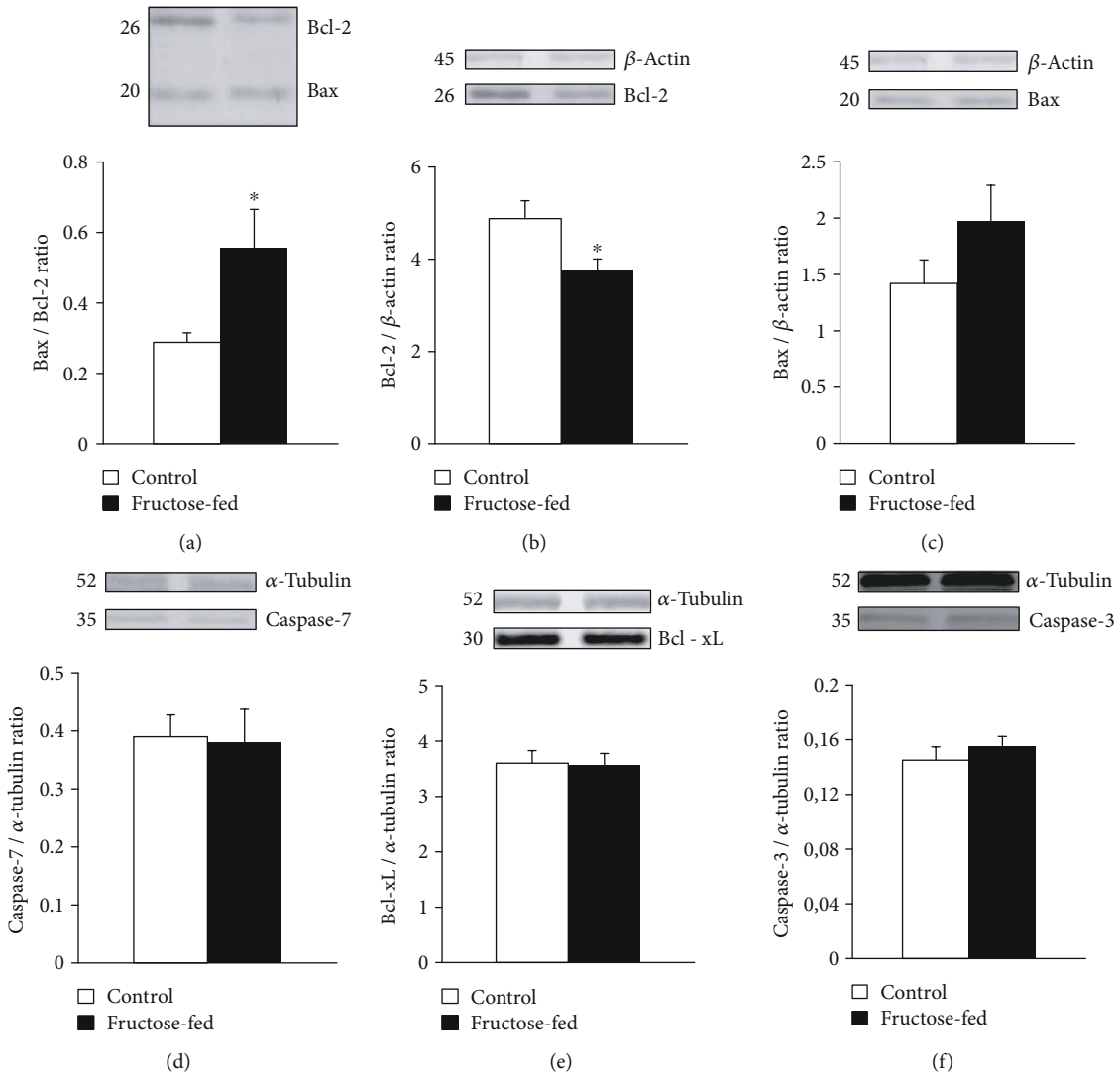

Figure 11: Western blot results at week 24: (a) Bax/Bcl-2 ratio, (b) Bcl-2/β-actin ratio, (c) Bax/β-actin ratio, (d) caspase-7/α-tubulin ratio, (e) Bcl-xL/α-tubulin ratio, and (f) caspase-3/α-tubulin ratio. Values are means ± SEM ($n = 8$), $^*p < 0.05$.

STZ injection [6]. In our present study, we also found in the proteomic results an increase in the antiapoptotic mitochondrial 3-ketoacyl-CoA thiolase in the hearts of fructose-fed rats (Table 5). We think that this alteration is part of the coping mechanism which protects the cardiomyocytes against apoptosis. Indeed, it is known that 3-ketoacyl-CoA thiolase abolishes BNIP3-mediated apoptosis and mitochondrial damage [83]. It was shown that 3-ketoacyl-CoA thiolase increased in the heart of STZ-induced diabetic mice [84]. The -3.4-fold decrease in the disulfide-isomerase protein level may also contribute to the suppression of apoptosis (Table 5) [85]. The upregulation of proapoptotic proteins and the downregulation of antiapoptotic proteins have already been described in a diabetic model in rodents [86, 87]. Our data suggest early dysregulation of pro- and antiapoptotic proteins in prediabetes; however, they do not show high induction of apoptosis. Furthermore, it is generally accepted that in type 1 and type 2 diabetes, the low levels of certain heat stress proteins (e.g., Hsp70 and Hsp27) and their impaired response to stress may contribute to the etiology of the disease [88]. It is important to note that in the prediabetic

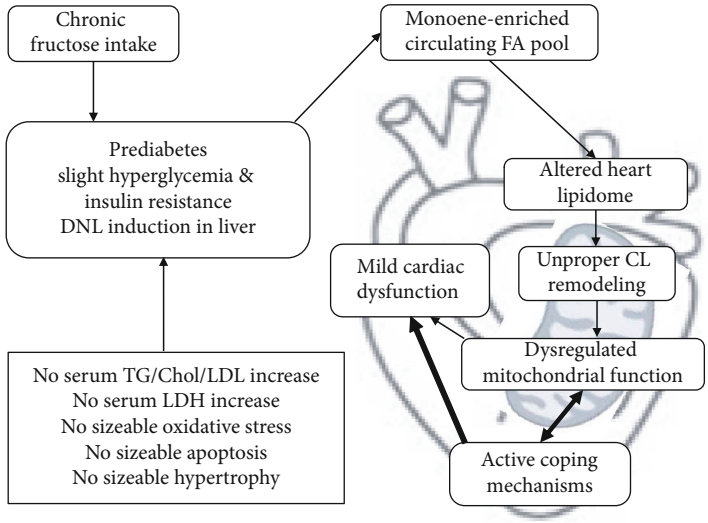

Figure 12: Summary of our findings.

state, we could not detect any disruption of Hsps. Instead, the Hsp60 and alphaB-Crystallin levels were markedly elevated by 3.3- and 5.6-fold, respectively (Table 5).

4. Conclusion

This is the first comprehensive analysis of the effect of prediabetes on the lipidome and proteome of the heart and its relationship to impaired diastolic function in a nongenetic rodent model. In our present study, chronically applied fructose intake led to the development of a prediabetic condition characterized by slight hyperglycemia, glucose intolerance, and insulin resistance (Figure 12).

This prediabetic state likely caused slight DNL induction in the liver. DNL induction has the capacity to alter the circulating accessible fatty acid (FA) pool for lipid biosynthesis in other organs. Consequently, the cardiac lipidome has been altered. The change was found to be comprehensive, deep, and characteristic with main features of monoenoic FA enrichment, decrease in linoleic acid (18:2 FA), complex changes in highly polyunsaturated lipids, and reprofiling of sphingolipid species compositions. Recent large-scale findings highlighted that the lower risk of type 2 diabetes was strongly associated with higher 18:2 FA biomarker levels [89, 90]. Linoleic acid was able to alleviate the STZ-induced diabetic phenotype in mice by normalizing FA metabolism and desaturation and correcting glucose and insulin levels [91].

It is conceivable that the observed lipidomic changes ultimately altered the biophysical properties of membrane lipids, which, together with restricted substrate availability, led to unproper CL remodeling in cardiac mitochondria. Dysregulation of CL remodeling possibly contributed to the impairment of several mitochondrial processes, as it was assessed by proteomic analysis, and finally could result in mild cardiac dysfunction. As mentioned previously, Barth syndrome shares biochemical features, like increased CL molecular species heterogeneity and increased MLCL/CL ratio, with ischemia, hypothyroidism, heart failure, and aging [19, 92, 93]. Moreover, drastic CL remodeling was observed at early stages in type 1 and type 2 diabetic hearts [19]. Evidences from prospective cohort studies and randomized trials have demonstrated that high n-6 polyunsaturated FA (predominantly linoleic acid) intake plays an important role in the dietary prevention of cardiovascular diseases [94]. Altogether, it is well-established that the loss and defective remodeling of CL alone can provoke cardiac dysfunction but it is not sufficient to induce diabetes [95]. However, the deprivation of 18:2 caused by the fructose-induced overproduction of nonessential FAs can be an important contributor to the development of the disease. Moreover, as a consequence of the mitochondrial dysfunction, a vicious cycle can be initiated by ROS-induced damage to mitochondrial components [96] at the transition from the prediabetic to the diabetic stage.

Our data show that at this very early stage of prediabetes there was no sizeable oxidative stress or apoptosis in the heart. Instead, several active coping mechanisms were activated against the harmful consequences of fructose feeding including the upregulation of enzymes responsible for the removal of lipid peroxidation products and upregulation of mitochondrial Hsp60.

Taken together, our study evidences that at the prediabetic stage there are no clinically accessible signs to declare a disease because the generally investigated serum parameters do not report about lipotoxicity, cell damage, or substantial hyperglycemia. Nevertheless, the results presented here clearly demonstrate that the risk for progression of diabetes and cardiovascular disease is silently present in the guise of a complex cardiac lipid metabolic imbalance and altered proteomic pattern. Prediabetes might represent a transient, reversible, "decision-making" state in that process. The nature of our nongenetic model implies that improper food intake must persist chronically; the longer you apply the higher the risk. Therefore, early intervention is important to prevent the transition from prediabetes to more severe disease stages.

Data Availability

All data used to support the findings of this study are included within the article or the supplementary information file.

Conflicts of Interest

The authors declare that there is no conflict of interest regarding the publication of this paper.

Authors' Contributions

Gergő Szűcs, Andrea Sója, and Mária Péter contributed equally. Gábor Balogh and Tamás Csont are equal senior contributors.

Acknowledgments

We acknowledge the outstanding technical support of Flóra Diána Gausz and Alexandra Fejes for blood sampling, oral glucose tolerance test, organ weight measurement, and frozen tissue sample preparation and of Ilona Ungi for anaesthetizing and shaving the animals for echocardiography and of Ferenc Péntek in the sample preparation for proteomics studies. This article was supported by the grants GINOP 2.3.2-15-2016-00006, EFOP 3.6.2-16-2017-00006, OTKA-NKFIH (K115990), and 20391 3/2018/FEKUSTRAT. Márta Sárközy was supported by the János Bolyai Research Scholarship of the Hungarian Academy of Sciences and the New National Excellence Program of the Ministry of Human Capacities (UNKP-18-4-SZTE-63).

Supplementary Materials

Supplementary methods for more detailed descriptions of the methodologies of lipidomics and proteomics. Supplementary Figure 1: cardiolipin (CL) maturation. Supplementary Figure 2: alterations in monolysocardiolipin (MLCL) species composition due to fructose-rich diet. Then, the Supplementary Tables are given to provide detailed data related to lipidomic and proteomic analyses. The Supplementary Tables include the following: lipid compositional data (mol% of membrane lipids), species composition of individual lipid classes (mol% of individual classes), lipid/-protein values (nmol/mg), double bonds (db) and double bond index (DBI), protein quantification, and Reactome pathway analysis. *(Supplementary Materials)*

References

[1] M. Sárközy, G. Szűcs, M. Pipicz et al., "The effect of a preparation of minerals, vitamins and trace elements on the cardiac gene expression pattern in male diabetic rats," *Cardiovascular Diabetology*, vol. 14, no. 1, article 248, 2015.

[2] World Health Organization, *Global Report on Diabetes*, World Health Organization, 2016.

[3] International Diabetes Federation, *IDF Diabetes Atlas*, International Diabetes Federation, Brussels, 8th edition, 2017.

[4] American Diabetes Association, "2. Classification and diagnosis of diabetes: *standards of medical care in diabetes—2019*," *Diabetes Care*, vol. 42, Supplement 1, pp. S13–S28, 2019.

[5] E. L. M. Barr, P. Z. Zimmet, T. A. Welborn et al., "Risk of cardiovascular and all-cause mortality in individuals with diabetes mellitus, impaired fasting glucose, and impaired glucose tolerance: the Australian Diabetes, Obesity, and Lifestyle Study (AusDiab)," *Circulation*, vol. 116, no. 2, pp. 151–157, 2007.

[6] G. Koncsos, Z. V. Varga, T. Baranyai et al., "Diastolic dysfunction in prediabetic male rats: role of mitochondrial oxidative stress," *American Journal of Physiology-Heart and Circulatory Physiology*, vol. 311, no. 4, pp. H927–H943, 2016.

[7] S. Boudina and E. D. Abel, "Diabetic cardiomyopathy, causes and effects," *Reviews in Endocrine & Metabolic Disorders*, vol. 11, no. 1, article 9131, pp. 31–39, 2010.

[8] J. G. Duncan, "Mitochondrial dysfunction in diabetic cardiomyopathy," *Biochimica et Biophysica Acta (BBA) - Molecular Cell Research*, vol. 1813, no. 7, pp. 1351–1359, 2011.

[9] L. Cai and Y. J. Kang, "Cell death and diabetic cardiomyopathy," *Cardiovascular Toxicology*, vol. 3, no. 3, pp. 219–228, 2003.

[10] J. S. Bhatti, G. K. Bhatti, and P. H. Reddy, "Mitochondrial dysfunction and oxidative stress in metabolic disorders – A step towards mitochondria based therapeutic strategies," *Biochimica et Biophysica Acta (BBA) - Molecular Basis of Disease*, vol. 1863, no. 5, pp. 1066–1077, 2017.

[11] G. Kanuri and I. Bergheim, "In vitro and in vivo models of non-alcoholic fatty liver disease (NAFLD)," *International Journal of Molecular Sciences*, vol. 14, no. 6, pp. 11963–11980, 2013.

[12] M. Chung, J. Ma, K. Patel, S. Berger, J. Lau, and A. H. Lichtenstein, "Fructose, high-fructose corn syrup, sucrose, and nonalcoholic fatty liver disease or indexes of liver health: a systematic review and meta-analysis," *The American Journal of Clinical Nutrition*, vol. 100, no. 3, pp. 833–849, 2014.

[13] L. N. Axelsen, J. B. Lademann, J. S. Petersen et al., "Cardiac and metabolic changes in long-term high fructose-fat fed rats with severe obesity and extensive intramyocardial lipid accumulation," *American Journal of Physiology-Regulatory, Integrative and Comparative Physiology*, vol. 298, no. 6, pp. R1560–R1570, 2010.

[14] M. Schlame and M. Ren, "The role of cardiolipin in the structural organization of mitochondrial membranes," *Biochimica et Biophysica Acta (BBA) - Biomembranes*, vol. 1788, no. 10, pp. 2080–2083, 2009.

[15] J. Dudek, "Role of cardiolipin in mitochondrial signaling pathways," *Frontiers in Cell and Development Biology*, vol. 5, p. 90, 2017.

[16] J. J. Maguire, Y. Y. Tyurina, D. Mohammadyani et al., "Known unknowns of cardiolipin signaling: the best is yet to come," *Biochimica et Biophysica Acta (BBA) - Molecular and Cell Biology of Lipids*, vol. 1862, no. 1, pp. 8–24, 2017.

[17] Y. Shi, "Emerging roles of cardiolipin remodeling in mitochondrial dysfunction associated with diabetes, obesity, and cardiovascular diseases," *Journal of Biomedical Research*, vol. 24, no. 1, pp. 6–15, 2010.

[18] M. Schlame, Y. Xu, and M. Ren, "The basis for acyl specificity in the tafazzin reaction," *The Journal of Biological Chemistry*, vol. 292, no. 13, pp. 5499–5506, 2017.

[19] Q. He and X. Han, "Cardiolipin remodeling in diabetic heart," *Chemistry and Physics of Lipids*, vol. 179, pp. 75–81, 2014.

[20] P. G. Barth, F. Valianpour, V. M. Bowen et al., "X-linked cardioskeletal myopathy and neutropenia (Barth syndrome): an update," *American Journal of Medical Genetics. Part A*, vol. 126A, no. 4, pp. 349–354, 2004.

[21] M. Schlame, D. Rua, and M. L. Greenberg, "The biosynthesis and functional role of cardiolipin," *Progress in Lipid Research*, vol. 39, no. 3, pp. 257–288, 2000.

[22] G. F. Kocsis, M. Sárközy, P. Bencsik et al., "Preconditioning protects the heart in a prolonged uremic condition," *American Journal of Physiology—Heart and Circulatory Physiology*, vol. 303, no. 10, pp. H1229–H1236, 2012.

[23] L. Kiscsatári, M. Sárközy, B. Kővári et al., "High-dose radiation induced heart damage in a rat model," *In Vivo*, vol. 30, no. 5, pp. 623–631, 2016.

[24] M. Sárközy, R. Gáspár, Á. Zvara et al., "Chronic kidney disease induces left ventricular overexpression of the pro-hypertrophic microRNA-212," *Scientific Reports*, vol. 9, no. 1, p. 1302, 2019.

[25] T. Csont, S. Viappiania, J. Sawickaa et al., "The involvement of superoxide and iNOS-derived NO in cardiac dysfunction induced by pro-inflammatory cytokines," *Journal of Molecular and Cellular Cardiology*, vol. 39, no. 5, pp. 833–840, 2005.

[26] M. Pipicz, G. Kocsis, L. Sárváry-Arantes et al., "Low-dose endotoxin induces late preconditioning, increases peroxynitrite formation, and activates STAT3 in the rat heart," *Molecules*, vol. 22, no. 3, p. 433, 2017.

[27] T. Csont, E. Bereczki, P. Bencsik et al., "Hypercholesterolemia increases myocardial oxidative and nitrosative stress thereby leading to cardiac dysfunction in apoB-100 transgenic mice," *Cardiovascular Research*, vol. 76, no. 1, pp. 100–109, 2007.

[28] T. Csont, C. Csonka, A. Ónody et al., "Nitrate tolerance does not increase production of peroxynitrite in the heart," *American Journal of Physiology-Heart and Circulatory Physiology*, vol. 283, no. 1, pp. H69–H76, 2002.

[29] T. Csont, C. Csonka, P. Kovács, G. Jancsó, and P. Ferdinandy, "Capsaicin-sensitive sensory neurons regulate myocardial nitric oxide and cGMP signaling," *European Journal of Pharmacology*, vol. 476, no. 1–2, pp. 107–113, 2003.

[30] A. Ónody, C. Csonka, Z. Giricz, and P. Ferdinandy, "Hyperlipidemia induced by a cholesterol-rich diet leads to enhanced peroxynitrite formation in rat hearts," *Cardiovascular Research*, vol. 58, no. 3, pp. 663–670, 2003.

[31] B. Peksel, I. Gombos, M. Péter et al., "Mild heat induces a distinct "eustress" response in Chinese Hamster Ovary cells but does not induce heat shock protein synthesis," *Scientific Reports*, vol. 7, no. 1, article 15643, 2017.

[32] B. C. Searle, L. K. Pino, J. D. Egertson et al., "Chromatogram libraries improve peptide detection and quantification by data independent acquisition mass spectrometry," *Nature Communications*, vol. 9, no. 1, p. 5128, 2018.

[33] S. Tyanova, T. Temu, P. Sinitcyn et al., "The Perseus computational platform for comprehensive analysis of (prote)omics data," *Nature Methods*, vol. 13, no. 9, pp. 731–740, 2016.

[34] M. Sárközy, Á. Zvara, N. Gyémánt et al., "Metabolic syndrome influences cardiac gene expression pattern at the transcript level in male ZDF rats," *Cardiovascular Diabetology*, vol. 12, no. 1, p. 16, 2013.

[35] M. Sárközy, G. Szűcs, V. Fekete et al., "Transcriptomic alterations in the heart of non-obese type 2 diabetic Goto-Kakizaki rats," *Cardiovascular Diabetology*, vol. 15, no. 1, p. 110, 2016.

[36] P. Gayoso-Diz, A. Otero-Gonzalez, M. X. Rodriguez-Alvarez et al., "Insulin resistance index (HOMA-IR) levels in a general adult population: curves percentile by gender and age. The EPIRCE study," *Diabetes Research and Clinical Practice*, vol. 94, no. 1, pp. 146–155, 2011.

[37] E. L. M. Barr, A. J. Cameron, B. Balkau et al., "HOMA insulin sensitivity index and the risk of all-cause mortality and cardiovascular disease events in the general population: the Australian Diabetes, Obesity and Lifestyle Study (AusDiab) study," *Diabetologia*, vol. 53, no. 1, pp. 79–88, 2010.

[38] J. D. Storey and R. Tibshirani, "Statistical significance for genomewide studies," *Proceedings of the National Academy of Sciences of the United States of America*, vol. 100, no. 16, pp. 9440–9445, 2003.

[39] J. Xia and D. S. Wishart, "Web-based inference of biological patterns, functions and pathways from metabolomic data using MetaboAnalyst," *Nature Protocols*, vol. 6, no. 6, pp. 743–760, 2011.

[40] W. Hsueh, E. D. Abel, J. L. Breslow et al., "Recipes for creating animal models of diabetic cardiovascular disease," *Circulation Research*, vol. 100, no. 10, pp. 1415–1427, 2007.

[41] J. C. Russell and S. D. Proctor, "Small animal models of cardiovascular disease: tools for the study of the roles of metabolic syndrome, dyslipidemia, and atherosclerosis," *Cardiovascular Pathology*, vol. 15, no. 6, pp. 318–330, 2006.

[42] N. Fakhoury-Sayegh, V. Trak-Smayra, A. Khazzaka et al., "Characteristics of nonalcoholic fatty liver disease induced in wistar rats following four different diets," *Nutrition Research and Practice*, vol. 9, no. 4, pp. 350–357, 2015.

[43] E. Gatineau, I. Savary-Auzeloux, C. Migné, S. Polakof, D. Dardevet, and L. Mosoni, "Chronic intake of sucrose accelerates sarcopenia in older male rats through alterations in insulin sensitivity and muscle protein synthesis," *The Journal of Nutrition*, vol. 145, no. 5, pp. 923–930, 2015.

[44] I. Dhar, A. Dhar, L. Wu, and K. M. Desai, "Increased methylglyoxal formation with upregulation of renin angiotensin system in fructose fed Sprague Dawley rats," *PLoS One*, vol. 8, no. 9, article e74212, 2013.

[45] H. Malhi and R. J. Kaufman, "Endoplasmic reticulum stress in liver disease," *Journal of Hepatology*, vol. 54, no. 4, pp. 795–809, 2011.

[46] H.-Y. Ou, H.-T. Wu, H.-C. Hung, Y.-C. Yang, J.-S. Wu, and C.-J. Chang, "Multiple mechanisms of GW-9508, a selective G protein-coupled receptor 40 agonist, in the regulation of glucose homeostasis and insulin sensitivity," *American Journal of Physiology-Endocrinology and Metabolism*, vol. 304, no. 6, pp. E668–E676, 2013.

[47] N. Stefan and H. U. Häring, "The role of hepatokines in metabolism," *Nature Reviews Endocrinology*, vol. 9, no. 3, pp. 144–152, 2013.

[48] F. Yang, Y. Dai, C. Min, and X. Li, "Neonatal overfeeding induced glucocorticoid overexposure accelerates hepatic lipogenesis in male rats," *Nutrition & Metabolism*, vol. 15, no. 1, 2018.

[49] M. Baena, G. Sangüesa, N. Hutter et al., "Fructose supplementation impairs rat liver autophagy through mTORC activation without inducing endoplasmic reticulum stress," *Biochimica et Biophysica Acta (BBA) - Molecular and Cell Biology of Lipids*, vol. 1851, no. 2, pp. 107–116, 2015.

[50] S. Softic, D. E. Cohen, and C. R. Kahn, "Role of dietary fructose and hepatic de novo lipogenesis in fatty liver disease," *Digestive Diseases and Sciences*, vol. 61, no. 5, pp. 1282–1293, 2016.

[51] T. Matsuzaka, A. Atsumi, R. Matsumori et al., "Elovl6 promotes nonalcoholic steatohepatitis," *Hepatology*, vol. 56, no. 6, pp. 2199–2208, 2012.

[52] B. A. Brooks, B. Franjic, C. R. Ban et al., "Diastolic dysfunction and abnormalities of the microcirculation in type 2 diabetes," *Diabetes, Obesity and Metabolism*, vol. 10, no. 9, pp. 739–746, 2008.

[53] B. Shivalkar, D. Dhondt, I. Goovaerts et al., "Flow mediated dilatation and cardiac function in type 1 diabetes mellitus," *The American Journal of Cardiology*, vol. 97, no. 1, pp. 77–82, 2006.

[54] K. Pandya, H.-S. Kim, and O. Smithies, "Fibrosis, not cell size, delineates β-myosin heavy chain reexpression during cardiac hypertrophy and normal aging *in vivo*," *Proceedings of the National Academy of Sciences of the United States of America*, vol. 103, no. 45, pp. 16864–16869, 2006.

[55] K. Nakao, W. Minobe, R. Roden, M. R. Bristow, and L. A. Leinwand, "Myosin heavy chain gene expression in human heart failure," *The Journal of Clinical Investigation*, vol. 100, no. 9, pp. 2362–2370, 1997.

[56] K. Pandya and O. Smithies, "β-MyHC and cardiac hypertrophy: size does matter," *Circulation Research*, vol. 109, no. 6, pp. 609-610, 2011.

[57] O. Y. Althunibat, A. M. Al Hroob, M. H. Abukhalil, M. O. Germoush, M. Bin-Jumah, and A. M. Mahmoud, "Fisetin ameliorates oxidative stress, inflammation and apoptosis in diabetic cardiomyopathy," *Life Sciences*, vol. 221, pp. 83–92, 2019.

[58] W. Kulik, H. van Lenthe, F. S. Stet et al., "Bloodspot assay using HPLC-tandem mass spectrometry for detection of Barth syndrome," *Clinical Chemistry*, vol. 54, no. 2, pp. 371–378, 2008.

[59] X. Han, J. Yang, H. Cheng, K. Yang, D. R. Abendschein, and R. W. Gross, "Shotgun lipidomics identifies cardiolipin depletion in diabetic myocardium linking altered substrate utilization with mitochondrial dysfunction," *Biochemistry*, vol. 44, no. 50, pp. 16684–16694, 2005.

[60] X. Han, J. Yang, K. Yang, Z. Zhao, D. R. Abendschein, and R. W. Gross, "Alterations in myocardial cardiolipin content and composition occur at the very earliest stages of diabetes: a shotgun lipidomics study," *Biochemistry*, vol. 46, no. 21, pp. 6417–6428, 2007.

[61] P. H. Lou, E. Lucchinetti, K. Y. Scott et al., "Alterations in fatty acid metabolism and sirtuin signaling characterize early type-2 diabetic hearts of fructose-fed rats," *Physiological Reports*, vol. 5, no. 16, article e13388, 2017.

[62] X. Han, K. Yang, J. Yang, H. Cheng, and R. W. Gross, "Shotgun lipidomics of cardiolipin molecular species in lipid extracts of biological samples," *Journal of Lipid Research*, vol. 47, no. 4, pp. 864–879, 2006.

[63] F. Novák, E. Tvrzická, B. Hamplová, F. Kolář, and O. Nováková, "Postnatal development of phospholipids and their fatty acid profile in rat heart," *Molecular and Cellular Biochemistry*, vol. 293, no. 1–2, pp. 23–33, 2006.

[64] M. A. Kiebish, K. Yang, X. Liu et al., "Dysfunctional cardiac mitochondrial bioenergetic, lipidomic, and signaling in a murine model of Barth syndrome," *Journal of Lipid Research*, vol. 54, no. 5, pp. 1312–1325, 2013.

[65] T. A. Taha, T. D. Mullen, and L. M. Obeid, "A house divided: ceramide, sphingosine, and sphingosine-1-phosphate in programmed cell death," *Biochimica et Biophysica Acta (BBA) - Biomembranes*, vol. 1758, no. 12, pp. 2027–2036, 2006.

[66] W. L. Holland and S. A. Summers, "Strong heart, low ceramides," *Diabetes*, vol. 67, no. 8, pp. 1457–1460, 2018.

[67] N. Marchesini, W. Osta, J. Bielawski, C. Luberto, L. M. Obeid, and Y. A. Hannun, "Role for mammalian neutral sphingomyelinase 2 in confluence-induced growth arrest of MCF7 cells," *The Journal of Biological Chemistry*, vol. 279, no. 24, pp. 25101–25111, 2004.

[68] X. Su, X. Han, D. J. Mancuso, D. R. Abendschein, and R. W. Gross, "Accumulation of long-chain acylcarnitine and 3-hydroxy acylcarnitine molecular species in diabetic myocardium: identification of alterations in mitochondrial fatty acid processing in diabetic myocardium by shotgun lipidomics," *Biochemistry*, vol. 44, no. 13, pp. 5234–5245, 2005.

[69] J. Cao, W. Shen, Z. Chang, and Y. Shi, "ALCAT1 is a polyglycerophospholipid acyltransferase potently regulated by adenine nucleotide and thyroid status," *American Journal of Physiology-Endocrinology and Metabolism*, vol. 296, no. 4, pp. E647–E653, 2009.

[70] T. Mutter, V. W. Dolinsky, B. J. Ma, W. A. Taylor, and G. M. Hatch, "Thyroxine regulation of monolysocardiolipin acyltransferase activity in rat heart," *The Biochemical Journal*, vol. 346, no. 2, Part 2, pp. 403–406, 2000.

[71] T. Martin-Rojas, L. Mourino-Alvarez, S. Alonso-Orgaz et al., "iTRAQ proteomic analysis of extracellular matrix remodeling in aortic valve disease," *Scientific Reports*, vol. 5, article 17290, 2015.

[72] T. Csont, A. Görbe, E. Bereczki et al., "Biglycan protects cardiomyocytes against hypoxia/reoxygenation injury: role of nitric oxide," *Journal of Molecular and Cellular Cardiology*, vol. 48, no. 4, pp. 649–652, 2010.

[73] R. Gáspár, M. Pipicz, F. Hawchar et al., "The cytoprotective effect of biglycan core protein involves Toll-like receptor 4 signaling in cardiomyocytes," *Journal of Molecular and Cellular Cardiology*, vol. 99, pp. 138–150, 2016.

[74] E. Bereczki, S. Gonda, T. Csont et al., "Overexpression of biglycan in the heart of transgenic mice: an antibody microarray study," *Journal of Proteome Research*, vol. 6, no. 2, pp. 854–861, 2007.

[75] P. Wu, X. Yuan, F. Li et al., "Myocardial upregulation of cathepsin D by ischemic heart disease promotes autophagic flux and protects against cardiac remodeling and heart failure," *Circulation. Heart Failure*, vol. 10, no. 7, 2017.

[76] I. M. Seropian, J. P. Cerliani, S. Toldo et al., "Galectin-1 controls cardiac inflammation and ventricular remodeling during acute myocardial infarction," *The American Journal of Pathology*, vol. 182, no. 1, pp. 29–40, 2013.

[77] Q. Mei, J. Huang, W. Chen et al., "Regulation of DNA replication-coupled histone gene expression," *Oncotarget*, vol. 8, no. 55, pp. 95005–95022, 2017.

[78] Z. V. Varga, K. Kupai, G. Szűcs et al., "MicroRNA-25-dependent up-regulation of NADPH oxidase 4 (NOX4) mediates hypercholesterolemia-induced oxidative/nitrative stress and subsequent dysfunction in the heart," *Journal of Molecular and Cellular Cardiology*, vol. 62, pp. 111–121, 2013.

[79] T. Xu, L. Zheng, L. Xu et al., "Protective effects of dioscin against alcohol-induced liver injury," *Archives of Toxicology*, vol. 88, no. 3, pp. 739–753, 2014.

[80] C. Brocker, N. Lassen, T. Estey et al., "Aldehyde dehydrogenase 7A1 (ALDH7A1) is a novel enzyme involved in cellular defense against hyperosmotic stress," *The Journal of Biological Chemistry*, vol. 285, no. 24, pp. 18452–18463, 2010.

[81] E. V. Karaduleva, E. K. Mubarakshina, M. G. Sharapov et al., "Cardioprotective effect of modified peroxiredoxins in retrograde perfusion of isolated rat heart under conditions of oxidative stress," *Bulletin of Experimental Biology and Medicine*, vol. 160, no. 5, pp. 639–642, 2016.

[82] J. Lappalainen, N. K. J. Oksala, D. E. Laaksonen et al., "Suppressed heat shock protein response in the kidney of exercise-trained diabetic rats," *Scandinavian Journal of Medicine & Science in Sports*, vol. 28, no. 7, pp. 1808–1817, 2018.

[83] W. Cao, N. Liu, S. Tang et al., "Acetyl-coenzyme A acyltransferase 2 attenuates the apoptotic effects of BNIP3 in two human cell lines," *Biochimica et Biophysica Acta (BBA) - General Subjects*, vol. 1780, no. 6, pp. 873–880, 2008.

[84] W. Li, M. Yao, R. Wang et al., "Profile of cardiac lipid metabolism in STZ-induced diabetic mice," *Lipids in Health and Disease*, vol. 17, no. 1, p. 231, 2018.

[85] B. G. Hoffstrom, A. Kaplan, R. Letso et al., "Inhibitors of protein disulfide isomerase suppress apoptosis induced by misfolded proteins," *Nature Chemical Biology*, vol. 6, no. 12, pp. 900–906, 2010.

[86] A. H. Amin, M. A. El-Missiry, and A. I. Othman, "Melatonin ameliorates metabolic risk factors, modulates apoptotic proteins, and protects the rat heart against diabetes-induced apoptosis," *European Journal of Pharmacology*, vol. 747, pp. 166–173, 2015.

[87] W. Yu, W. Zha, S. Guo, H. Cheng, J. Wu, and C. Liu, "Flos puerariae extract prevents myocardial apoptosis via attenuation oxidative stress in streptozotocin-induced diabetic mice," *PLoS One*, vol. 9, no. 5, article e98044, 2014.

[88] P. L. Hooper, G. Balogh, E. Rivas, K. Kavanagh, and L. Vigh, "The importance of the cellular stress response in the pathogenesis and treatment of type 2 diabetes," *Cell Stress & Chaperones*, vol. 19, no. 4, pp. 447–464, 2014.

[89] J. H. Y. Wu, M. Marklund, F. Imamura et al., "Omega-6 fatty acid biomarkers and incident type 2 diabetes: pooled analysis of individual-level data for 39 740 adults from 20 prospective cohort studies," *The Lancet Diabetes and Endocrinology*, vol. 5, no. 12, pp. 965–974, 2017.

[90] N. G. Forouhi, F. Imamura, S. J. Sharp et al., "Association of plasma phospholipid n-3 and n-6 polyunsaturated fatty acids with type 2 diabetes: the EPIC-InterAct case-cohort study," *PLoS Medicine*, vol. 13, no. 7, article e1002094, 2016.

[91] L. Canetti, H. Werner, and A. Leikin-Frenkel, "Linoleic and alpha linolenic acids ameliorate streptozotocin-induced diabetes in mice," *Archives of Physiology and Biochemistry*, vol. 120, no. 1, pp. 34–39, 2014.

[92] N. Ikon and R. O. Ryan, "Barth syndrome: connecting cardiolipin to cardiomyopathy," *Lipids*, vol. 52, no. 2, pp. 99–108, 2017.

[93] A. J. Chicco and G. C. Sparagna, "Role of cardiolipin alterations in mitochondrial dysfunction and disease," *American Journal of Physiology-Cell Physiology*, vol. 292, no. 1, pp. C33–C44, 2007.

[94] D. D. Wang, "Dietary n-6 polyunsaturated fatty acids and cardiovascular disease: epidemiologic evidence," *Prostaglandins, Leukotrienes, and Essential Fatty Acids*, vol. 135, pp. 5–9, 2018.

[95] W. T. Cade, C. T. Spencer, D. N. Reeds et al., "Substrate metabolism during basal and hyperinsulinemic conditions in adolescents and young-adults with Barth syndrome," *Journal of Inherited Metabolic Disease*, vol. 36, no. 1, pp. 91–101, 2013.

[96] T. K. Silzer and N. R. Phillips, "Etiology of type 2 diabetes and Alzheimer's disease: Exploring the mitochondria," *Mitochondrion*, vol. 43, pp. 16–24, 2018.

Hindawi
Oxidative Medicine and Cellular Longevity
Volume 2019, Article ID 9186469, 12 pages
https://doi.org/10.1155/2019/9186469

Research Article

ALCAT1 Overexpression Affects Supercomplex Formation and Increases ROS in Respiring Mitochondria

Bettina Rieger,[1] **Adéla Krajčová**,[1,2] **Patrick Duwe**,[1] **and Karin B. Busch**[1]

[1]*Institute of Molecular Cell Biology, Department of Biology, University of Muenster, Muenster, Germany*
[2]*Department of Biochemistry, Cell and Molecular Biology, Third Faculty of Medicine, Charles University in Prague, Czech Republic*

Correspondence should be addressed to Bettina Rieger; berieger@uni-muenster.de and Karin B. Busch; buschkar@uni-muenster.de

Received 30 June 2019; Revised 5 September 2019; Accepted 24 September 2019; Published 6 December 2019

Guest Editor: Eugenia Mileykovskaya

Cardiolipin (CL) is a multifunctional dimeric phospholipid that physically interacts with electron transport chain complexes I, III, and IV, and ATP synthase (complex V). The enzyme ALCAT1 catalyzes the conversion of cardiolipin by incorporating polyunsaturated fatty acids into cardiolipin. The resulting CL species are said to be more susceptible to oxidative damage. This is thought to negatively affect the interaction of cardiolipin and electron transport chain complexes, leading to increased ROS production and mitochondrial dysfunction. Furthermore, it is discussed that ALCAT1 itself is upregulated due to oxidative stress. Here, we investigated the effects of overexpression of ALCAT1 under different metabolic conditions. ALCAT1 is located at the ER and mitochondria, probably at contact sites. We found that respiration stimulated by galactose supply promoted supercomplex assembly but also led to increased mitochondrial ROS levels. Endogeneous ALCAT1 protein expression levels showed a fairly high variability. Artificially induced ALCAT1 overexpression reduced supercomplex formation, further promoted ROS production, and prevented upregulation of coupled respiration. Taken together, our data suggest that the amount of the CL conversion enzyme ALCAT1 is critical for coupling mitochondrial respiration and metabolic plasticity.

1. Introduction

Cardiolipin (CL) is a unique phospholipid that was first identified in 1947 in beef heart [1]. It is also known as the mitochondrial signature lipid [2–4]. Approximately 75% of the CL content in mitochondria is present in the inner mitochondrial membrane (IM), where its biosynthesis takes place [5, 6]. CL is important for mitochondrial function and activity and influences amongst others the electron transport chain (ETC). Therefore, it is not surprising that CL alterations or CL depletion are part of many pathologies. For instance, mutations in the TAZ1 gene, a protein that is important for the final acyl chain composition of CL, lead to an X-linked disease, called Barth syndrome. The disease is characterized by skeletal and cardiac myopathies and cyclic neutropenia, whereas heart deficiency and opportunistic infections are the main reasons of mortality [2, 7]. CL is a negatively charged phospholipid dimer that consists of two phosphatidic acid molecules connected through glycerol. The fact that each CL molecule has four acyl chains differentiate it from all other phospholipids [8, 9].

CL is a multifunctional phospholipid that, under nonpathological conditions, is suggested to participate in different mitochondrial mechanisms such as apoptotic cell death signaling, oxidative phosphorylation (OXPHOS), and fusion and fission events [10, 11]. It interacts with intermembrane space (IMS) or membrane bound proteins such as the electron transport chain (ETC) complexes as well as with soluble proteins, e.g., the phosphotransferase of the IMS, NDPK-D (nucleoside-diphosphate kinase-D), and MtCK (mitochondrial creatine kinase) [11, 12]. The interaction of CL with complex I (CI), III (CIII), and IV (CIV) of the ETC is suggested to support their assembly to respiratory supercomplexes (SCs), which are discussed to favor lower ROS production [13, 14]. The lipid composition of the IM may be important for SC assembly [13]. Studies of SC arrangement propose binding sites of loosely and tightly bound CL [15]. CL was shown to be tightly bound to CI and be

necessary for electron transport by this complex [16, 17]. Oxidation of CL and a decreased CL level resulted in less SC formation [15, 18]. Deregulated ETC is seen as the major source of ROS [19–21]. CL also interacts with complex V, the ATP synthase. CL is suggested to promote ATP synthase dimerization, which is relevant for the cristae architecture [22, 23]. Deficiency of CL resulted in an increased level of monomeric ATP synthase in Drosophila [22].

The definite acyl chain composition of one CL molecule is generated in a postsynthetic modification step, called remodeling [9]. Remodeling increases the amount of unsaturated acyl chains in CL [9, 24] and is part of the CL maturation process [25] involving three enzymes: tafazzin (TAZ), monolysocardiolipin acyltransferase 1 (MLCLAT1), and acyl-CoA:lysocardiolipin acyltransferase 1 (ALCAT1) [8, 26]. It is suggested that the remodeling of CL by TAZ is important for sustaining the normal acyl chain composition. ALCAT1 is an Acyl-CoA:lyso-CL acyltransferase and an isoform of MLCLAT1 [8]. CL species in cells overexpressing ALCAT1 had an increased level of polyunsaturated fatty acids, especially DHA (C22:6n3), and a significantly reduced amount of C16-C18 fatty acids [27].

Here, we set out to investigate whether ALCAT1 levels are variable under different metabolic conditions. Moreover, we wanted to determine the effect of artificially overexpressed ALCAT1 under glycolytic and respiratory galactose conditions. We found no significant differences in ALCAT levels under different respiratory conditions due to the high variation in endogenous ALCAT1 levels. ALCAT1 was localized at the ER and mitochondria, probably contact sites. Artificially elevated ALCAT1 levels hampered supercomplex formation and promoted ROS production.

2. Materials and Methods

2.1. Cell Culture. HeLa WT cells were cultivated in Minimal Essential Medium Earle's Salt (5.6 mM glucose+L-glutamine) supplemented with 10% FCS (fetal calf serum), 1% HEPES, 1% NEAA (nonessential amino acids), and 1% penicillin/-streptomycin at 37°C and 5% CO_2. The cells were split when they were 80-100% confluent using trypsin/EDTA for cell detachment. For cell respiration assays, cells were cultivated in XF Base Medium Minimal DMEM containing 10 mM D-galactose (Seahorse Bioscience, wo D-Glc, wo L-glutamine, phenol red, wo $NaHCO_3$) supplemented with 10% FCS, 1% HEPES, 1% NEAA (nonessential amino acids), 1% penicillin/streptomycin, 2% alanyl-L-glutamine, and 2,875% mL $NaHCO_3$. HeLa cells were purchased from the Leibniz Institute DSMZ-German Collection of Microorganisms and Cell Cultures and transiently transfected by the calcium transfection method if required. The transfected cells were used 48-72 h after transfection.

The following plasmids were used for transfection: pSems-ALCAT1-2A-GFP-NLS, pSems-ALCAT1-HA, and pSems-ALCAT1-mCherry. Sequences of the according plasmids are shown in the supplementary material. pSems-ALCAT1-2A-GFP-NLS results in the expression of untagged ALCAT1 in parallel with a nuclear-targeted GFP as reporter for successful transfection. Moreover, we used the plasmids CoxVIIIa-sEcGFP and CoxIV-sEcGFP [28].

2.2. Seahorse XF Cell Mito Stress Test Kit. The Seahorse XF Cell Mito Stress Test Kit enables metabolic profiling of mitochondria measuring the oxygen consumption rate (OCR) and extracellular acidification rate (ECAR). Sequential injection of inhibitors and uncouplers of the OXPHOS (oligomycin, FCCP, and rotenone/antimycin A) is used to determine basal respiration, proton leak, ATP production, and nonmitochondrial respiration (Supplementary Fig. S1). On the day prior to the measurement, ~30,000 cells per well were seeded in the Seahorse XF Cell Culture Microplate and incubated at 37°C and 5% CO_2. 180 μL XF Calibrant was added to each well of the calibration hydrate sensor cartridge and incubated at 37°C and 0% CO_2. Next day, the cells were washed with PBS and incubated in an assay medium for 1 h at 37°C and 0% CO_2. The inhibitor stock solutions were prepared and mixed with an XF Base medium (5.6 mM glucose or 10 mM galactose, 4 mM glutamine, pH 7.4) to get the constant compound concentrations: 1 μM oligomycin, 1 μM FCCP, and 0.5 μM rotenone/antimycin A. The inhibitor solutions were loaded into the ports of the hydrate sensor cartridge (A: Oligomycin, B: FCCP, and C: rotenone/antimycin A). After calibration of the Seahorse with the hydrate sensor cartridge, basal and ATP synthesis-linked respiration, proton leak, maximal respiration, and nonmitochondrial respiration were measured for 18 min each. The results were analyzed with the Seahorse XF Stress Test Report Generator (XF Cell Mito Stress Test Kit User Guide).

2.3. Immunoblotting. Cells, grown in a glucose or galactose medium for 48 h, were harvested from T25-flask dishes in SDS sample buffer by using a cell scraper and transferred to a 1.5 mL reaction tube. After vortexing, the cell lysate was incubated on ice for 10 min and then boiled at 95°C for 5 min. The SDS samples were stored at -20°C. The SDS-PAGE run was performed at 60 V. When the samples reached the separation gel, the voltage was increased to 100-150 V. PageRuler Prestained Protein Ladder (product #26619, ThermoFisher Scientific) was used as a marker. The proteins were transferred to a PVDF membrane, and the blotting was performed in a semidry manner at 100 mA for 2 h. After blotting, the membrane was incubated with Ponceau S for 10 min to control the protein transfer. Ponceau S was washed away with MilliQ, and the membrane was blocked with 10 mL of 10% skimmed milk/TBST (20 mM Tris; 0.137 M NaCl, 0.1% Tween 20) for 1 h to prevent unspecific binding of the primary antibody. The primary antibody was diluted in 1% skimmed milk/TBST and was added to the membrane overnight at 4°C. Then, the membrane was washed three times with TBST for 15 min and incubated for 1 h with the secondary antibody, also diluted in 1% skimmed milk in TBST. Again, the membrane was washed three times with TBST for 15 min. Finally, SuperSignal West Pico Chemiluminescent Substrate 1 : 1 (ThermoFisher Scientific) were added to the membrane and the fluorescent signal was detected with the ChemiDoc MP Imaging System (BIO-RAD). The primary antibodies that were used for the protein

expression analysis are listed in Supplementary Table 1. The peroxidase-conjugated AffiniPure Goat Anti-Rabbit IgG (H+L) (Jackson ImmunoResearch, Dianova) was used as a secondary antibody at a final dilution of 1 : 2000.

Images of Western Blot results were processed with Adobe Photoshop, and quantitative analysis of protein levels was executed with ImageJ™ (MacBiophotonics). The mean and integrated density grey values of the protein of interest were normalized with VDAC (voltage-dependent anion channel), a mitochondrial membrane protein that is correlated with mitochondrial mass. For two-sample, two-sided *t*-test statistical analysis, Origin (OriginPro 2016, OriginLab) was used.

2.4. Microscopy. For microscopy, the cells were seeded on coverslips in 3 cm dishes (70% confluency) in a medium with glucose or galactose as sugar source for 48 h. For imaging, the coverslips were mounted in a cell chamber supplied with 1 mL medium. The cells were imaged using an inverted confocal microscope (TCS SP8 SMD, Leica) equipped with a 63x water objective (N.A. 1.2) and a Time-Correlated Single Photon Counting (TCSPC) device. Living cells were imaged at 37°C supplied with 5% CO_2. Recording of the fluorescence lifetime of excited CoxVIIIa-sEcGFP and CoxIV-sEcGFP was performed by TCSPC. HyD's with GaASP photocathodes were used as detectors for dual color recording and FLIM (fluorescence lifetime imaging microscopy). For FLIM, emission was restricted to 525/50 nm (ex. 488 nm, 20 MHz). The acquisition was performed until at least 1,000 photons in the brightest pixel were reached. Data analysis was performed with SymphoTime software (64 bit) and biexponential fitting of the fluorescence decay curves (substracting the IRF) from ROIs of the whole mitochondrial network of a cell. From biexponential fits, the average lifetime τ_{amp} was calculated. For standard microscopy, HeLa WT cells were transiently transfected with ALCAT1-2A-GFP-NLS plasmid DNA, except for localization of ALCAT1. For FLIM, HeLa WT cells were transiently transfected with ALCAT1-mCherry and either CoxVIIIa-sEcGFP or CoxIV-sEcGFP.

2.5. Mitochondrial Membrane Potential, Mitochondrial Footprint, and ROS Determination. To determine the morphology under different nutrition conditions, HeLa WT and ALCAT1-2A-GFP-NLS expressing cells were cultivated in a glucose and galactose medium for 48 h and stained with 100 nM MitoTracker Red under normal growth conditions (37°C, 5% CO_2) for 30 min. Then, the cells were washed two times with PBS and one-time with a medium to remove the dye. The fluorescence of ~45 cells was examined with the fluorescence microscope (TCS SP8, Leica) with a 63x water-immersion objective. The excitation source was a pulsed supercontinuum white light laser (Leica Microsystems, at 80 MHz). The emission of nuclear-targeted GFP was set to 510-540 nm (ex. 488 nm), and the emission of MitoTracker Red was colleced between 600-700 nm (ex. 561 nm), recorded by hybrid detectors. Finally, the mitochondrial morphology (mean branch length and mitochondrial footprint) was analyzed with the ImageJ™ plugin "MiNA" (Valente et al., 2017). For determination of ROS, MitoTracker Red was used. MitoTracker Red is a reduced, nonfluorescent version of MitoTracker Red (M-7512, ThermoFisher) that fluoresces upon oxidation. Z-stacks of 7 slices (step size of 360 nm) of the MitoTracker Red stained cells were recorded with the same settings as described above. The fluorescence intensity was analyzed with ImageJ (MacBiophotonics). To exclude the background intensity, the Otsu mask was used for thresholding. A higher grey value corresponds to a higher ROS level, respectively mitochondrial membrane potential. For determination of the mitochondrial membrane potential, the cells were stained with 7 nM TMRE instead of 100 nM MitoTracker Red CM-H2XRos.

2.6. Localization of ALCAT1. HeLa WT cells were cotransfected with ALCAT1-mCherry plasmid and CoxIV-sEcGFP plasmid DNA. The antibody anti-KDEL from Santa Cruz Biotechnology (10C3; 1 : 50) served as a marker of the ER. As secondary antibody, Goat anti-mouse IgG H&L (Alexa Fluor® 647; 1 : 500) was used. Briefly, antibody staining was performed after cell fixation with 4% paraformaldehyde, permeabilization with 0.1% Triton-X, blocking with 2% BSA, and washing with 0.01% Tween-20, all in PBS. The cells were examined with the fluorescent microscope (TCS SP8, Leica mCherry: ex. 561 nm, em. 585-605 nm; mEGFP: ex. 488 nm, em. 510-530 nm; Alexa 647: ex. 633 nm, em. 720-800 nm). Alternatively, HeLa WT cells were cotransfected with ALCAT1-mCherry plasmid and CoxIV-sEcGFP and stained with LysoTracker blue™ (LysoTracker blue™: ex. 405 nm, em. 420-460 nm; mCherry: ex. 580 nm, em. 610-630 nm; mEGFP: ex. 488 nm, em. 500-535 nm). Scatterplots with linear regression as well as Pearson's and Manders' coefficients were determined with the ImageJ™ plugin "colocalization threshold."

2.7. Statistics. For the comparison of samples with the same sample size, we used ANOVA with post hoc Tukey test; for the comparison of samples with unequal sample size, we used ANOVA with post hoc Scheffe or Fisher LSD for statistics analysis. The box and whisker plots show the 25th to 75th % percentile in the box. The square is the mean; the horizontal line in the box is the respective median of the cohort. Manders and Pearson coefficients were calculated to characterize the degree of overlap of ALCAT1 signal with mitochondria and lysosomes, respectively.

3. Results

3.1. ALCAT1 Is Localized at the ER and Mitochondria. It was reported that FLAG-tagged ALCAT1 is localized at the ER [8], while another study reported that ALCAT1 is predominantly localized in the mitochondrial-associated membrane [27]. To test for colocalization between ALCAT1, ER, and mitochondria, HeLa cells were transfected with CoxIV-sEcGFP for mitochondrial staining and ALCAT1-mCherry. To visualize the ER, we performed immune-staining against KDEL, an ER-localized protein, in addition. Alexa Fluor® 647 was used as secondary antibody. We performed triple color analysis in cells with moderate (Figure 1(a)) and high (Figure 1(b)) ALCAT1 expression. Interestingly, we did not only find high overlap between ALCAT1 and KDEL but also

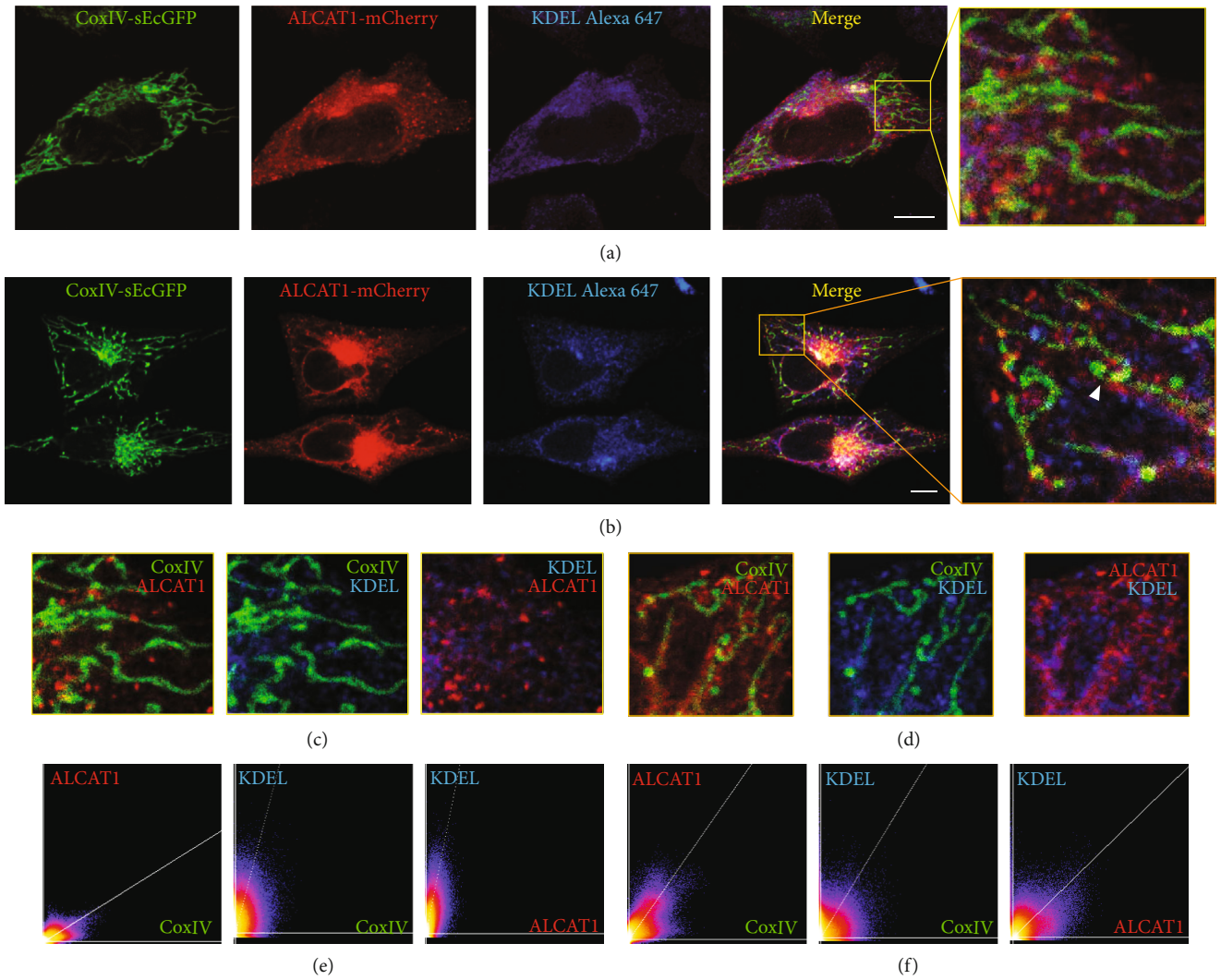

Figure 1: Overexpressed ALCAT1 is localized in the ER and mitochondria. Fluorescence microscopic analysis of transiently transfected cells expressing CoxIV-sEcGFP, ALCAT1-mCherry stained with an antibody against ER marker KDEL. (a) Low ALCAT1-mCherry expression. (b) High ALCAT1-mCherry expression. Arrowheads in zoom image are pointing to ALCAT1-mCherry localized between ER and mitochondria, in other words MAMs. (c) Merged two-color images of ROIs shown in (a). (d) Merged two-color zoom images of ROI shown in (b). (e, f) Colocalization analysis showing scatterplots after setting thresholds in both color channels. (e) Colocalization analysis of the region shown in (a+c), (f) Colocalization analysis of the area shown in (b+d). Upper left quadrant = Ch2 above threshold; Ch1 below threshold; lower left quadrant = Ch1 below threshold; Ch2 below threshold; lower right quadrant = Ch1 above threshold; Ch2 below threshold; upper right quadrant = Ch1 above threshold; Ch2 above threshold; with linear regression; channel 1 (Ch1) = x-axis, channel 2 (Ch2) = y-axis. Thresholds for scatterplots were automatically determined for each channel (ImageJ plugin "colocalization threshold"), while presented images were manually processed with ImageJ to enhance the contrast. Scale bars: 10 μM (a, b).

quite high overlap between ALCAT1 and CoxIV-sEcGFP, demonstrated by the 2D histograms (scatterplots), where the two intensity values for each pixel (voxel) are plotted against each other. Correlation is visualized by the presence of a cloud of information in the middle of the scatterplot, fitted with a linear regression. The brighter the color, the higher the correlation of intensity values for the two channels (Figures 1(c) and 1(d)). This data clearly shows here that ALCAT1 is not only localized in the ER (colocalization can be seen in Figure 1(f)) but also in mitochondria. However, in order to reveal whether this overlap indeed indicates ER-mitochondria contact sites, further studies using superresolution microscopy are required.

A significant proportion of the overexpressed ALCAT1-mCherry in transfected HeLa cells was found in point-like structures near the nucleus resembling lysosomes (Figure 1). Lysosomal localization of overexpressed proteins is not unusual. To check whether part of ALCAT1 was localized in lysosomes, we conducted three-color fluorescence colocalization microscopy with genetically coded fluorescent and lysosomal markers in cells under glucose conditions. Images were taken of cells expressing ALCAT1-mCherry and CoxIV-sEcGFP and stained with LysoTracker blue™ (Supplementary Fig. 1A). Indeed, a significant amount of ALCAT1 is found in lysosomes. The quantitative colocalization analysis showed that the fraction of ALCAT1

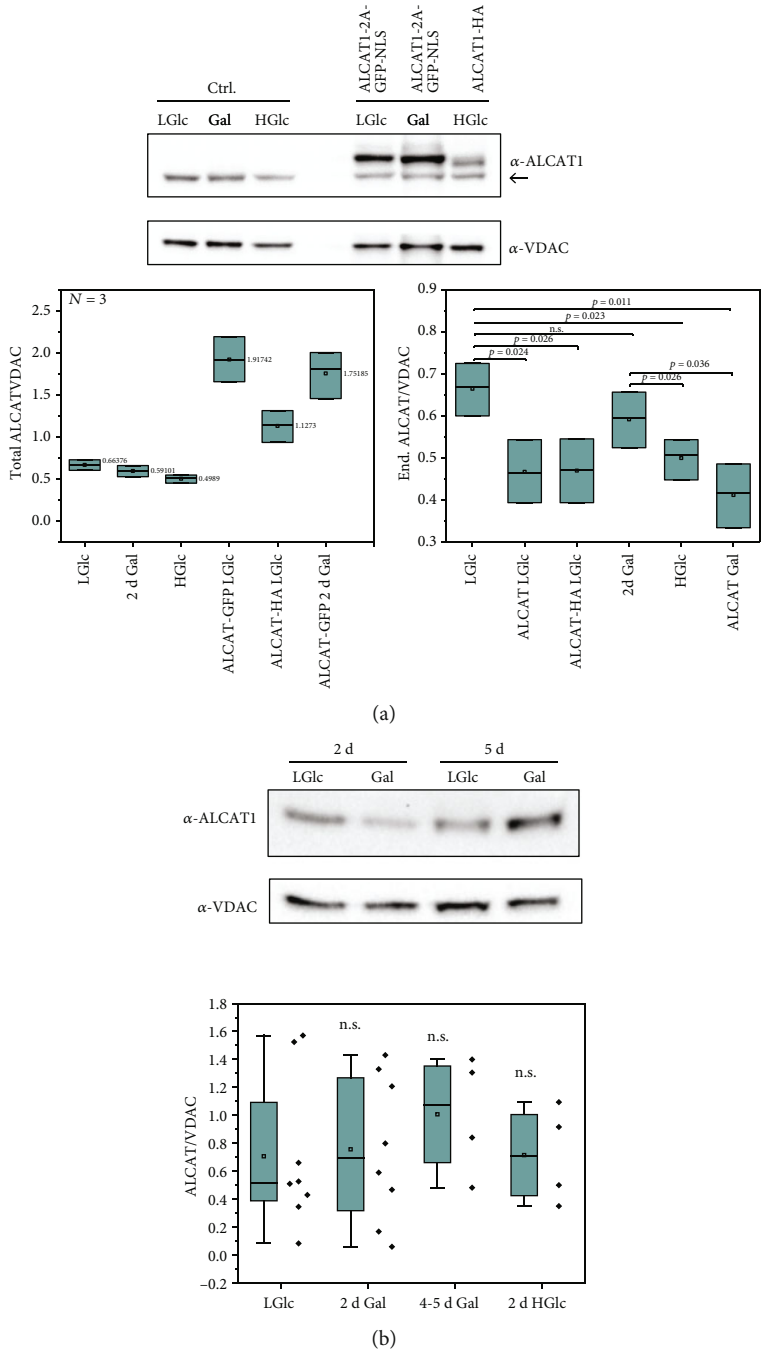

Figure 2: Artificially induced and endogenous ALCAT1 levels. (a) Determination of relative ALCAT1 levels in HeLa cells supplied with different sugars and in cells transiently transfected with ALCAT1-EGFP and ALCAT1-HA-tag, respectively, 48 h after transfection. The transfection efficiency usually was ~60%; the data shown is not corrected for this. The upper band shows the tagged ALCAT1 version, the lower band the endogenous ALCAT1. VDAC, a mitochondrial protein, was used as loading control. For the quantification, ALCAT1 was normalized on the VDAC level. Total ALCAT1 and endogenous ALCAT levels were determined. A-GFP: ALCAT1-2A-GFP-NSL, A-HA: ALCAT1-HA-tag. $N = 3$ biological replicates. Left graph: total ALCAT levels, mean values are indicated. Right graph: only endogenous ALCAT levels are shown. Box and whisker plots. Statistics: ANOVA with post hoc Tukey. (b) Influence of metabolic conditions on endogenous ALCAT1 levels. The quantification includes values from (a). $N = 8$ technical replicates from $n > 2$ biological preparation for ALCAT in low glucose (LGlc; 5.6 mM), $N = 8/n = 3$ for galactose (Gal) 2 d; $N = 4/n = 3$ for galactose 4-5 d; $N = /n = 2$ for high glucose (HGlc, 25 mM). VDAC was used as a loading control. Statistics: SD are shown, ANOVA with post hoc Fisher LSD test. n.s.: no significant differences of the mean values.

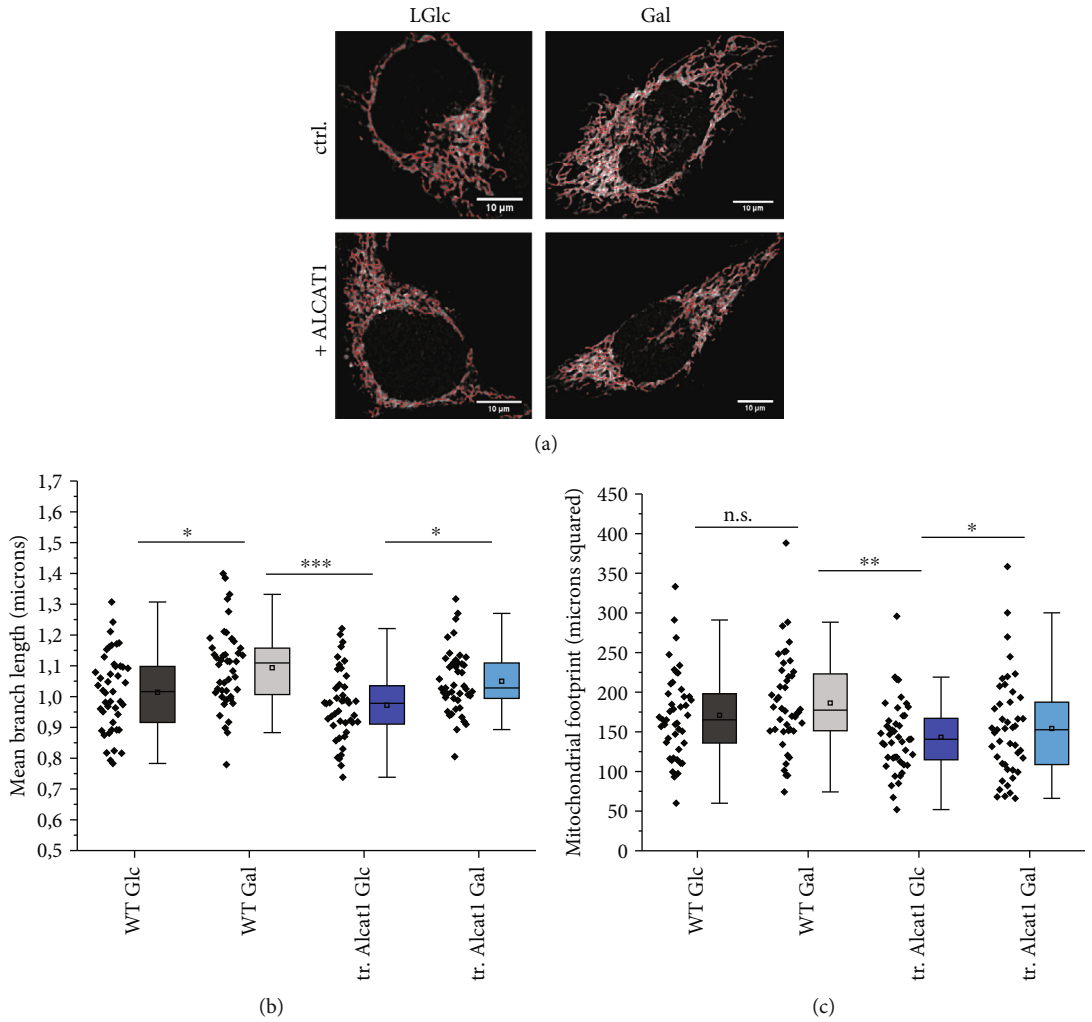

Figure 3: Analysis of mitochondrial morphology in ALCAT1 overexpressing cells. Transiently transfected ALCAT1-2A-GFP-NLS (tr. ALCAT1) and HeLa WT cells were supplied with 5.6 mM glucose and 10 mM galactose, respectively, for 48 h. Quantitative analysis of mitochondrial network morphology by the ImageJ™ plugin MiNA. MitoTracker Red stained mitochondria were analyzed. Morphological data are extracted from the MiNA-processed (= contrast enhanced) images. (a) MiNa-processed images (mitochondrial skeleton in red) of HeLa cells after MitoTracker Red staining of HeLa WT and ALCAT1 overexpressing cells in Glc and Gal (scale bars: 10 μm). (b) Quantitative MiNA analysis of mean branch length of mitochondria. (c) Quantitative MiNA analysis of mitochondrial footprint. The footprint is simply the sum of positive pixels per cell and represents the mitochondrial area. $N = 2$ biological replicates. Each data point represents data from one cell. Statistics: data was analyzed by One-Way ANOVA with post hoc Fisher LSD ($^{***}p < 0{,}001$; $^{**}p < 0.01$; and $^{*}p < 0.05$), SD are shown.

colocalizing with lysosomes was higher than the colocalization of ALCAT1 and mitochondria (Supplementary Fig. 1b-c). Together, these data suggest that artificially induced ALCAT1 is associated with different cell organelles including lysosomes. Whether this reflects the natural distribution of ALCAT1 has to be revealed in future studies when suitable ALCAT1 antibodies for immune-staining are available.

3.2. Artificially Induced ALCAT1 Is Moderately Overexpressed and Represses Endogenous ALCAT1. Cells transiently expressing tagged ALCAT1 had in average a 2-3~threefold higher level of total ALCAT1 than the control (Figure 2(a)). This in accordance to what was observed earlier in a different cell line, where the mRNA levels increased threefold [29]. Interestingly, artificially induced ALCAT1 overexpression resulted in a significant decrease of the endogenous ALCAT1 levels (Figure 3(a)). At this stage, we cannot rule out a feedback mechanism that suppresses the transcription of endogenous ALCAT1. The same had already been shown for ALCAT1 overexpressing COS7 cells, but not commented on [8].

3.3. Natural ALCAT1 Levels Vary. Natural ALCAT1 levels increase under pathological conditions as in diabetes, obesity, and cardiomyopathy [8, 27]. We asked whether ALCAT1 levels also would change under nonpathological conditions. The activity of mitochondria changes under different metabolic conditions [30], including a remodeling of the OXPHOS system. It can be assumed that this also

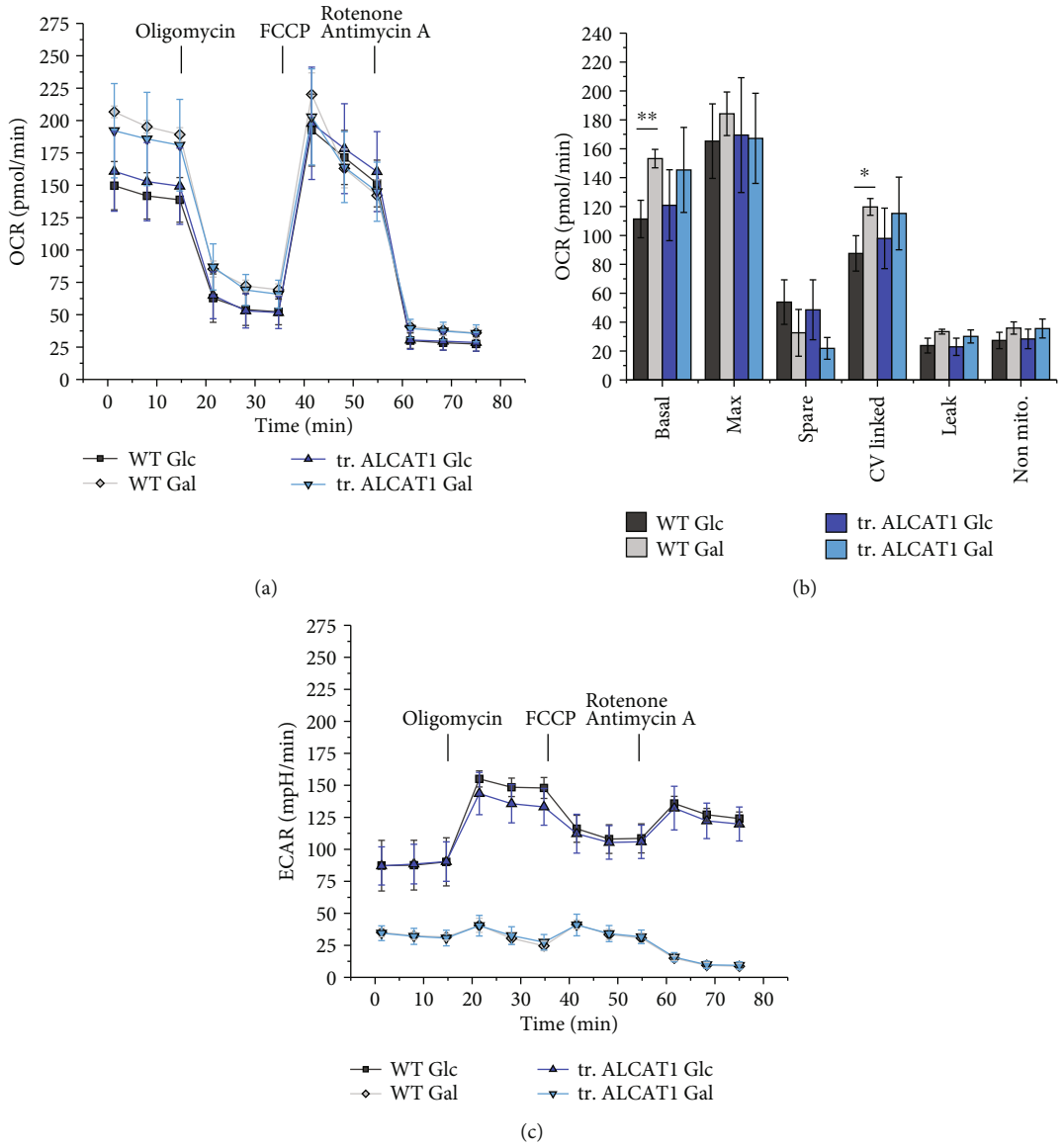

Figure 4: Effects of elevated ALCAT1 levels on mitochondrial bioenergetics. Automatic flux analysis of oxygen consumption rate (OCR) and extracellular acidification rate (ECAR) of HeLa WT supplied with glucose and galactose for 48 h and ALCAT1 overexpressing cells under the same conditions. (a) Oxygen consumption rate (OCR) of HeLa WT and transiently transfected ALCAT1 overexpressing cells. OCRs (and ECAR) were analyzed with the Seahorse XF Cell Mito Stress Test Kit by sequential injection of oligomycin (2 μM), FCCP (1 μM), and rotenone/antimycin A (0.5 μM). The cells were supplied with 5.6 mM glucose or 10 mM galactose for 48 h before measurement. $N = 5$ replicates with 30 wells for each condition. (b) Basal and maximal respiration, spare respiratory capacity, CV-linked respiration, proton leak, and nonmitochondrial respiration determined from OCRs shown in (a). One Way ANOVA with post hoc Scheffe ($^{***}p < 0{,}001$; $^{**}p < 0.01$; and $^{*}p < 0.05$). (c) Corresponding extracellular acidification rates (ECAR).

concerns cardiolipin and its remodeling. Here, we examined whether metabolic changes induced by a change of the sugar source had an effect on ALCAT1 levels. We found no significant changes in ALCAT1 levels when the cells were supplied with galactose or high glucose levels instead of glucose as sugar intake (Figure 2(b)). However, we found a high variation of the endogenous ALCAT1 content under all conditions.

3.4. Effects of ALCAT1 on Mitochondrial Morphology. To analyze whether different ALCAT1 levels would affect mitochondrial morphology, we transiently transfected HeLa WT cells with ALCAT1-2A-GFP-NLS and stained the cells with MitoTracker Red™ (Figure 3(a)). The mitochondrial area per cell was determined using an automatic analysis tool (ImageJ™ plugin MiNA). Morphological data were extracted from the binary image that was generated by applying an automatic threshold. A copy of the binary image was overlaid to the original image. From the morphological skeleton, the mean and standard deviation of the branch lengths in each network were determined. The footprint was calculated as the sum of positive pixels (of the binary image) per cell and represents the mitochondrial area. Cells supplied with galactose showed a higher branch

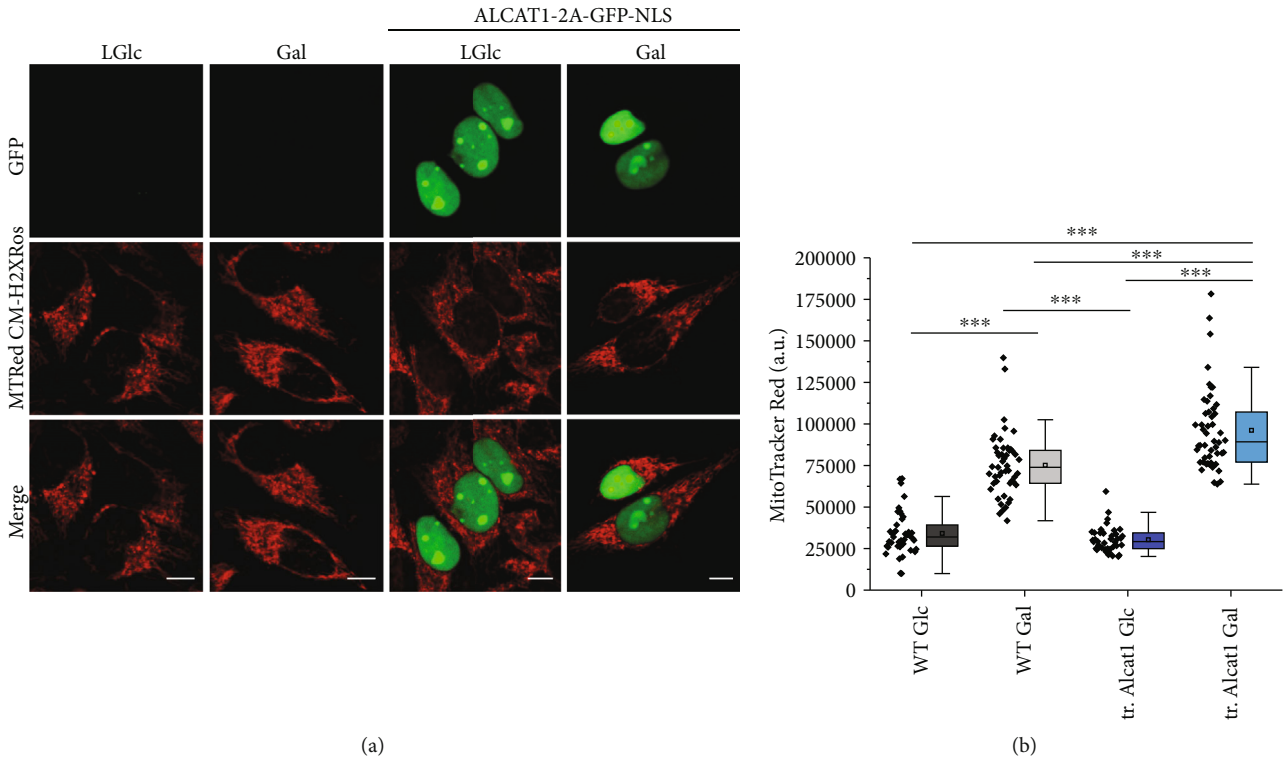

Figure 5: Mitochondrial ROS levels in ALCAT1 overexpressing cells under different nutrition conditions. (a) Dual color images showing ROS formation in cells with normal ALCAT1 levels and cells with artificially elevated ALCAT1 levels (tr. ALCAT1: transiently transfected cells expressing ALCAT1-2A-GFP-NLS). The transfected cells were identified by their green nuclei (GFP::NLS). Cells were supplied with different sugars as indicated before for 48 h. After staining with MitoTracker Red, cells were analyzed with a fluorescence microscope (MitoTracker Red: $\lambda_{ex.}$ 561 nm, $\lambda_{em.}$ 600-700 nm, GFP: $\lambda_{ex.}$ 488 nm, $\lambda_{em.}$ 510-540 nm). (b) Quantitative analysis of ROS formation as MitoTracker Red fluorescence intensity signal (arbitrary units, a.u.). Results are presented as box plots with the measured fluorescence intensities of ~45 measured cells. Data was analyzed by One-Way ANOVA with post hoc Scheffe ($^{***}p < 0.001$; $^{**}p < 0.01$; and $^{*}p < 0.05$), SD are shown.

length compared to glucose-fed cells ($p \leq 0.05$). Cells transiently expressing ALCAT1 also had a higher branch length in galactose than in glucose ($p \leq 0.05$) as seen in Figure 3(b). In glucose, ALCAT1 overexpressing cells did not display a significant change in mitochondrial branch length compared to control cells. No difference in mitochondrial area (footprint) was found between galactose and glucose supplied cells. However, cells that were artificially overexpressing ALCAT1 had a significant reduced mitochondrial area (in μm^2) compared to control cells ($p \leq 0.01$) in glucose and ALCAT1 overexpressing cells ($p \leq 0.05$) in galactose (Figure 3(c)). In sum, we found no relation between ALCAT1 overexpression and mitochondrial morphology under the same metabolic conditions.

3.5. Effects of ALCAT1 on Mitochondrial Bioenergetics. To analyze possible changes in mitochondrial respiration and ATP synthesis (oxidative phosphorylation, OXPHOS) with respect to ALCAT1 overexpression, we determined the mitochondrial oxygen consumption rate (OCR) and in parallel the extracellular acidification rate (ECAR) with an automatic flux analyzer (Seahorse/Agilent XF 96). We used the stress test as described in Materials and Methods with subsequent addition of the ATP synthase inhibitor oligomycin, the uncoupler carbonylcyanid-p-trifluoromethoxyphenylhydrazone (FCCP), and complex I and III inhibitors rotenone/antimycin A (Supplementary Figure S2). In addition, we compared the OCR and ECAR of cells cultured in glucose or galactose for 48 h. HeLa wild-type (WT) cells showed increased basal and ATP synthesis- (CV-) linked OCR in galactose (Figures 4(a) and 4(b)). With galactose as sugar supply, cells are forced to rely on ATP synthesis by oxidative phosphorylation (OXPHOS) as described earlier [30], shown here as a significant increase in basal- and CV-linked respiration. ALCAT1 overexpression prevented the galactose-induced increase in respiration.

Next, the effects of ALCAT1 overexpression on glycolysis are presented. Both HeLa control and ALCAT1 overexpressing cells showed a higher extracellular acidification rate (ECAR) in glucose supply than in galactose, which is a measure of increased glycolysis (Figure 5(c)). This in turn means that the stimulation of respiration evoked by galactose is at the expense of glycolysis. ALCAT1 overexpression had no significant effect on the galactose-induced decrease of glycolysis. Together, these data suggest that high ALCAT1 levels interfere with the OXPHOS stimulation caused by a switch from glucose to galactose, but have no effect on glycolysis rates.

3.6. Mitochondrial ROS Levels increase under Elevated ALCAT1 Levels. In isolated mitochondria, the reactive

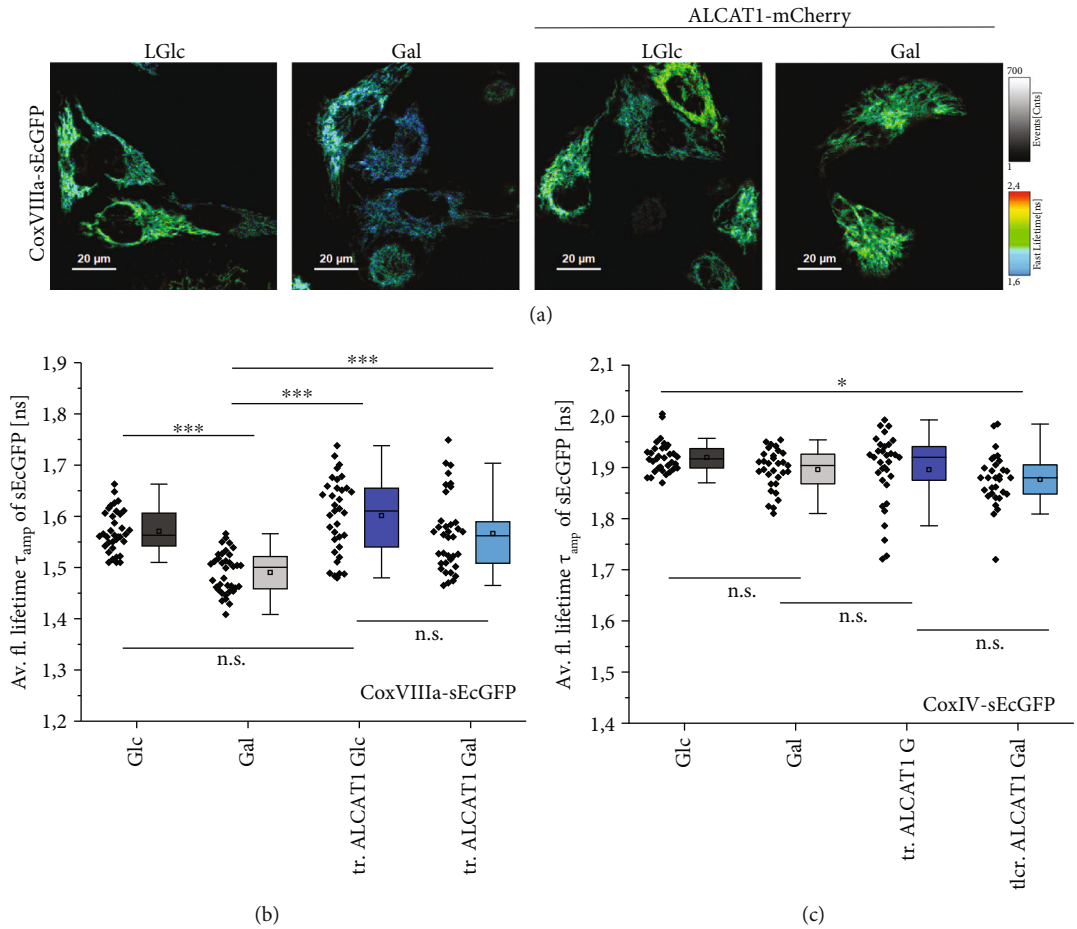

Figure 6: ALCAT1 hampers SC formation under stimulated OXPHOS conditions. (a) Fluorescence lifetime images of sEcGFP at subunit CoxVIIIa. This construct is buried in an existing respiratory supercomplex and has a reduced fluorescence lifetime τ. As a control, subunit CoxIV was labeled with sEcGFP, which does not respond to SC formation by decreased lifetime [28]. Cells were transfected with ALCAT1-mCherry (tr. ALCAT1) and grown in a glucose (5.6 mM) or galactose (10 mM) medium for 48 h. (b) Average fluorescence lifetimes τ_{amp} of CoxVIIIa-sEcGFP under different respiratory conditions +/- ALCAT1-mCherry overexpression. (c) Average fluorescence lifetimes τ_{amp} of CoxIV-sEcGFP under different respiratory conditions±ALCAT1-mCherry overexpression. $N = 2$ replicates. Data was analyzed by One-Way ANOVA with post hoc Scheffe test. Scale bars: 20 μM (a).

oxygen species (ROS) H_2O_2 increased in ALCAT1 overexpressing cells [29]. However, isolated mitochondria tend to lose their ROS detoxifying system which might result in higher ROS levels [31]. We here determined what effects the increased respiration would have on reactive oxygen species (ROS) levels in intact cells with normal and elevated ALCAT1 levels. Glucose and galactose supplied HeLa control and ALCAT1 overexpressing cells were stained with MitoTracker Red, a ROS indicator, to study the effect of ALCAT1 on ROS production under different nutrition conditions. The ROS level was significantly increased in both wild-type and ALCAT1 overexpressing cells supplied with galactose (respiratory conditions) (Figure 5). Only in galactose, ALCAT1 overexpressing cells showed higher ROS formation than cells with normal ALCAT1 levels. The mitochondrial membrane potential was slightly increased in ALCAT1 overexpressing cells under both nutrition conditions compared to HeLa control in glucose (Supplementary Fig. S3). Together, these data show that elevated ALCAT1 levels under respiratory conditions are correlated with increased ROS levels also *in cellulo*.

3.7. Effects of ALCAT1 on Respiratory Supercomplex Formation. The interaction of CL with complex I (CI), complex III (CIII), and complex IV (CIV) of the ETC is suggested to support their assembly into respiratory supercomplexes (SCs). Oxidation of CL, increased unmature CL, and a decreased overall CL level resulted in reduced SC formation, a phenomenon described in association with the Barth syndrome [32]. We wondered what effects ALCAT1 overexpression has on SC formation. To test this, we used a life cell compatible sensor for SC formation, sEcGFP fused to subunit CoxVIIIa of CIV. When SCs are formed, CoxVIIIa-sEcGFP is buried in a dense molecular environment at the interface of CI, CIII, and CIV which decreases the fluorescence lifetime τ of the sensor sEcGFP [28]. As a control, another subunit of CIV, CoxIV, was fused to sEcGFP. Even in a SC, the sensor

sEcGFP at CoxIV is not exposed to a different environment and the fluorescence lifetime does not change. τ was determined by time correlated single photon counting. As depicted in Figure 6, τ decreased under conditions of higher respiration (Galactose conditions), indicating more SCs. In ALCAT1 overexpressing cells, this effect was not observed; the mean τ was the same in glucose and galactose and similar to the low glucose conditions of HeLa cells. Apparently, ALCAT1 levels above a certain threshold hampered SC formation, probably mediated by CL.

4. Discussion

Here, we describe the effects of elevated ALCAT1 levels on mitochondrial bioenergetics, ROS formation, and respiratory supercomplex formation. Elevated ALCAT1 levels were obtained by the expression of an exogenous plasmid. We could show that ALCAT1, when artificially overexpressed, is localized at the ER but also at mitochondrial membranes as described before [8, 27]. The colocalization of the ALCAT1-mCherry signal with the ER marker KDEL together with the findings of [27], who showed that ALCAT1 enzyme activity is higher in subcellular fractions of MAMs than of mitochondria, point to a preferential localization in the MAMs. However, this localization is not exclusively as mitochondria themselves still exhibit ALCAT1 activity [27] and in the liver of mice, a mass spectrometry-based proteomic analysis of the MAMs did not identify ALCAT1 at all [33]. A plausible, but still to be tested hypothesis is that critical high ALCAT1 levels such as induced by artificial overexpression result in ALCAT1 accumulation in MAMs. In contrast, localization in lysosomes is probably a general overexpression artifact.

We wondered whether ALCAT1 levels would naturally change under different metabolic conditions. Different metabolic conditions were induced by the change of sugars in the medium. A switch from glucose to galactose is known to upregulate OXPHOS [30] by changing the activity and/or expression of proteins involved in aerobic energy metabolism [34]. The determination of endogenous ALCAT1 protein levels by immunoblotting showed a high variability, though. For this reason, our data on endogenous ALCAT1 levels in cells do not allow a conclusive statement as to whether ALCAT1 levels change under different metabolic conditions. When glucose was replaced by galactose, mitochondrial respiration was stimulated and ATP was preferably produced by aerobic phosphorylation. Accordingly, we found that in galactose ROS production was enhanced, in particular in ALCAT1 overexpressing cells. In this context, it is an important observation that artificially enhanced ALCAT1 negatively affected respiratory supercomplex (SC) assembly. CL binds to the ETC complexes I, III, and IV and the ADP/ATP carriers. To maintain full enzymatic function, CIV requires two associated CL molecules, while CIII also needs CL to maintain its quaternary structure and function [35]. It was reported that membrane-embedded transmembrane helices form a cavity in the transmembrane region of CIII [36]. The cavity, which is located at the CIII/CIV interface, is filled with CL and phosphatidylethanolamine. Since CL's bound to ETC complexes promote SC assembly [15, 37], CLs can be seen as a glue for supercomplexes [38]. For these reasons, it does not seem unlikely that reduced supercomplex formation in ALCAT1 overexpressing cells is the result of altered cardiolipin levels or specifically modified CLs that do not provide the glue for supercompex formation anymore. Further studies should directly address how and to to which extend cardiolipin species or cardiolipin levels are affected under enhanced ALCAT1 conditions. These studies specifically should focus on the peroxidation of CL.

Data Availability

Data will be made available upon request.

Conflicts of Interest

The authors do not declare any competing financial interests.

Authors' Contributions

K.B.B. and B.R. contributed in the conception and design. B.R., A.K., and P.D. helped in acquiring data. K.B.B., B.R., A.K., and P.D. analyzed and interpreted the data. K.B.B. and B.R. wrote the article.

Acknowledgments

We thank Wladislaw Kohl for technical assistance in cloning and Franziska Speer for valuable preliminary data. We kindly acknowledge the support of B.R. by the GRF-funded CRC944, grant INST-190/167-2.

Supplementary Materials

Suppl. Figure 1: Seahorse XF Cell Mito Stress Test Profile. The serial injection of ETC complex inhibitors enables the measurement of basal respiration, proton leak, maximal respiration, and nonmitochondrial respiration (XF Cell Mito Stress Test Kit User Guide). Suppl. Figure S3: Western Blot analysis of tr. ALCAT1-2A-GFP-NLS. (A) Western Blot result of VDAC and ALCAT1 in HeLa wt and tr. ALCAT-2A-GFP-NLS cells in glucose 48 h after transfection. (B) Quantitative analysis of ALCAT1 protein expression after normalization with VDAC. The bands in the middle are not included as they belong to another experiment. Table 1: primary antibodies used for Western Blot analysis. *(Supplementary Materials)*

References

[1] C. Pangborn, "Isolation and purification of a serologically active phospholipid from beef heart," *Journal of Biological Chemistry*, vol. 143, pp. 247–256, 1942.

[2] S. M. Claypool and C. M. Koehler, "The complexity of cardiolipin in health and disease," *Trends in Biochemical Sciences*, vol. 37, no. 1, pp. 32–41, 2012.

[3] G. Daum, "Lipids of mitochondria," *Biochimica et Biophysica Acta (BBA) - Reviews on Biomembranes*, vol. 822, no. 1, pp. 1–42, 1985.

[4] N. Gebert, A. S. Joshi, S. Kutik et al., "Mitochondrial cardiolipin involved in outer-membrane protein biogenesis: implications for Barth syndrome," *Current Biology: CB*, vol. 19, no. 24, pp. 2133–2139, 2009.

[5] A. L. Boscia, B. W. Treece, D. Mohammadyani et al., "X-ray structure, thermodynamics, elastic properties and MD simulations of cardiolipin/dimyristoylphosphatidylcholine mixed membranes," *Chemistry and Physics of Lipids*, vol. 178, pp. 1–10, 2014.

[6] M. Schlame and D. Haldar, "Cardiolipin is synthesized on the matrix side of the inner membrane in rat liver mitochondria," *Journal of Biological Chemistry*, vol. 268, no. 1, pp. 74–79, 1993.

[7] M. Schlame and M. Ren, "Barth syndrome, a human disorder of cardiolipin metabolism," *FEBS Letters*, vol. 580, no. 23, pp. 5450–5455, 2006.

[8] J. Cao, Y. Liu, J. Lockwood, P. Burn, and Y. Shi, "A novel cardiolipin-remodeling pathway revealed by a gene encoding an endoplasmic reticulum-associated acyl-CoA:lysocardiolipin acyltransferase (ALCAT1) in mouse," *Journal of Biological Chemistry*, vol. 279, no. 30, pp. 31727–31734, 2004.

[9] M. Schlame, "Cardiolipin synthesis for the assembly of bacterial and mitochondrial membranes," *Journal of Lipid Research*, vol. 49, no. 8, pp. 1607–1620, 2008.

[10] Y. W. Lu and S. M. Claypool, "Disorders of phospholipid metabolism: an emerging class of mitochondrial disease due to defects in nuclear genes," *Frontiers in Genetics*, vol. 6, pp. 1–27, 2015.

[11] G. Paradies, V. Paradies, V. De Benedictis, F. M. Ruggiero, and G. Petrosillo, "Functional role of cardiolipin in mitochondrial bioenergetics," *Biochimica et Biophysica Acta - Bioenergetics*, vol. 1837, no. 4, pp. 408–417, 2014.

[12] T. Tatsuta, M. Scharwey, and T. Langer, "Mitochondrial lipid trafficking," *Trends in Cell Biology*, vol. 24, no. 1, pp. 44–52, 2014.

[13] E. Maranzana, G. Barbero, A. I. Falasca, G. Lenaz, and M. L. Genova, "Mitochondrial respiratory supercomplex association limits production of reactive oxygen species from complex I," *Antioxidants & Redox Signaling*, vol. 19, no. 13, pp. 1469–1480, 2013.

[14] E. A. Shoubridge, "Supersizing the mitochondrial respiratory chain," *Cell Metabolism*, vol. 15, no. 3, pp. 271-272, 2012.

[15] E. Mileykovskaya and W. Dowhan, "Cardiolipin-dependent formation of mitochondrial respiratory supercomplexes," *Chemistry and Physics of Lipids*, vol. 179, pp. 42–48, 2014.

[16] M. Fry and D. E. Green, "Cardiolipin requirement for electron transfer in complex I and III of the mitochondrial respiratory chain," *Journal of Biological Chemistry*, vol. 256, no. 4, pp. 1874–1880, 1981.

[17] G. Paradies, G. Petrosillo, M. Pistolese, and F. M. Ruggiero, "Reactive oxygen species affect mitochondrial electron transport complex I activity through oxidative cardiolipin damage," *Gene*, vol. 286, no. 1, pp. 135–141, 2002.

[18] M. Zhang, E. Mileykovskaya, and W. Dowhan, "Cardiolipin is essential for organization of complexes III and IV into a supercomplex in intact yeast mitochondria," *Journal of Biological Chemistry*, vol. 280, no. 33, pp. 29403–29408, 2005.

[19] N. Apostolova and V. M. Victor, "Molecular strategies for targeting antioxidants to mitochondria: therapeutic implications," *Antioxidants & Redox Signaling*, vol. 22, no. 8, pp. 686–729, 2015.

[20] M. P. Murphy, "How mitochondria produce reactive oxygen species," *The Biochemical Journal*, vol. 417, no. 1, pp. 1–13, 2009.

[21] G. Paradies, V. Paradies, F. M. Ruggiero, and G. Petrosillo, "Oxidative stress, cardiolipin and mitochondrial dysfunction in nonalcoholic fatty liver disease," *World Journal of Gastroenterology*, vol. 20, no. 39, pp. 14205–14218, 2014.

[22] D. Acehan, A. Malhotra, Y. Xu, M. Ren, D. L. Stokes, and M. Schlame, "Cardiolipin affects the supramolecular organization of ATP synthase in mitochondria," *Biophysical Journal*, vol. 100, no. 9, pp. 2184–2192, 2011.

[23] J. Habersetzer, W. Ziani, I. Larrieu et al., "ATP synthase oligomerization: from the enzyme models to the mitochondrial morphology," *International Journal of Biochemistry and Cell Biology*, vol. 45, no. 1, pp. 99–105, 2013.

[24] M. Schlame, M. Ren, Y. Xu, M. L. Greenberg, and I. Haller, "Molecular symmetry in mitochondrial cardiolipins," *Chemistry and Physics of Lipids*, vol. 138, no. 1-2, pp. 38–49, 2005.

[25] M. Schlame and B. Rüstow, "Lysocardiolipin formation and reacylation in isolated rat liver mitochondria," *The Biochemical Journal*, vol. 272, no. 3, pp. 589–595, 1990.

[26] W. A. Taylor and G. M. Hatch, "Identification of the human mitochondrial linoleoyl-coenzyme A monolysocardiolipin acyltransferase (MLCL AT-1)," *The Journal of Biological Chemistry*, vol. 284, no. 44, pp. 30360–30371, 2009.

[27] J. Li, C. Romestaing, X. Han et al., "Cardiolipin remodeling by ALCAT1 links oxidative stress and mitochondrial dysfunction to obesity," *Cell Metabolism*, vol. 12, no. 2, pp. 154–165, 2010.

[28] B. Rieger, D. N. Shalaeva, A. C. Sohnel et al., "Lifetime imaging of GFP at CoxVIIIa reports respiratory supercomplex assembly *in live cells*," *Scientific Reports*, vol. 7, no. 1, 2017.

[29] J. Li, X. Liu, H. Wang, W. Zhang, D. C. Chan, and Y. Shi, "Lysocardiolipin acyltransferase 1 (ALCAT1) controls mitochondrial DNA fidelity and biogenesis through modulation of MFN2 expression," *Proceedings of the National Academy of Sciences of the United States of America*, vol. 109, no. 18, pp. 6975–6980, 2012.

[30] R. Rossignol, R. Gilkerson, R. Aggeler, K. Yamagata, S. J. Remington, and R. A. Capaldi, "Energy substrate modulates mitochondrial structure and oxidative capacity in cancer cells," *Cancer Research*, vol. 64, no. 3, pp. 985–993, 2004.

[31] M. Picard, T. Taivassalo, D. Ritchie et al., "Mitochondrial structure and function are disrupted by standard isolation methods," *PLoS One*, vol. 6, no. 3, article e18317, 2011.

[32] I. A. Chatzispyrou, S. Guerrero-Castillo, N. M. Held et al., "Barth syndrome cells display widespread remodeling of mitochondrial complexes without affecting metabolic flux distribution," *Biochimica et Biophysica Acta - Molecular Basis of Disease*, vol. 1864, no. 11, pp. 3650–3658, 2018.

[33] A. Sala-Vila, I. Navarro-Lerida, M. Sanchez-Alvarez et al., "Interplay between hepatic mitochondria-associated membranes, lipid metabolism and caveolin-1 in mice," *Scientific Reports*, vol. 6, no. 1, 2016.

[34] C. Aguer, D. Gambarotta, R. J. Mailloux et al., "Galactose enhances oxidative metabolism and reveals mitochondrial dysfunction in human primary muscle cells," *PLoS ONE*, vol. 6, no. 12, p. e28536, 2011.

[35] B. Gomez Jr. and N. C. Robinson, "Quantitative determination of cardiolipin in mitochondrial electron transferring complexes by silicic acid high-performance liquid

chromatography," *Analytical Biochemistry*, vol. 267, no. 1, pp. 212–216, 1999.

[36] C. Hunte, J. Koepke, C. Lange, T. Rossmanith, and H. Michel, "Structure at 2.3 Å resolution of the cytochrome bc_1 complex from the yeast *Saccharomyces cerevisiae* co-crystallized with an antibody Fv fragment," *Structure*, vol. 8, no. 6, pp. 669–684, 2000.

[37] R. Vartak, C. A. M. Porras, and Y. Bai, "Respiratory supercomplexes: structure, function and assembly," *Protein & Cell*, vol. 4, no. 8, article 3032, pp. 582–590, 2013.

[38] M. Zhang, E. Mileykovskaya, and W. Dowhan, "Gluing the respiratory chain together - cardiolipin is required for supercomplex formation in the inner mitochondrial membrane," *Journal of Biological Chemistry*, vol. 277, no. 46, pp. 43553–43556, 2002.

Hindawi
Oxidative Medicine and Cellular Longevity
Volume 2019, Article ID 3836186, 13 pages
https://doi.org/10.1155/2019/3836186

Review Article

The Role of Cardiolipin and Mitochondrial Damage in Kidney Transplant

Alejandra Guillermina Miranda-Díaz,[1] **Ernesto Germán Cardona-Muñoz**,[1] **and Fermín Paul Pacheco-Moisés**[2]

[1]*Instituto de Terapéutica Experimental y Clínica del Centro Universitario de Ciencias de la Salud de la Universidad de Guadalajara, Guadalajara, Jalisco, Mexico*
[2]*Departamento de Química del Centro Universitario de Ciencias Exactas e Ingenierías, Universidad de Guadalajara, Guadalajara, Jalisco, Mexico*

Correspondence should be addressed to Alejandra Guillermina Miranda-Díaz; kindalex1@outlook.com

Received 18 April 2019; Revised 27 August 2019; Accepted 11 September 2019; Published 25 November 2019

Guest Editor: Konstantin Lyamzaev

Chronic kidney disease (CKD) is highly incident and prevalent in the world. The death of patients with CKD is primarily due to cardiovascular disease. Renal transplantation (RT) emerges as the best management alternative for patients with CKD. However, the incidence of acute renal graft dysfunction is 11.8% of the related living donor and 17.4% of the cadaveric donor. Anticardiolipin antibodies (ACAs) or antiphospholipid antibodies (APAs) are important risk factors for acute renal graft dysfunction. The determination of ACA or APA to candidates for RT could serve as prognostic markers of early graft failure and would indicate which patients could benefit from anticoagulant therapy. Cardiolipin is a fundamental molecule that plays an important role in the adequate conformation of the mitochondrial cristae and the correct assembly of the mitochondrial respiratory supercomplexes and other proteins essential for proper mitochondrial function. Cardiolipin undergoes a nonrandom oxidation process by having pronounced specificity unrelated to the polyunsaturation pattern of its acyl groups. Accumulation of hydroxyl derivatives and cardiolipin hydroperoxides has been observed in the affected tissues, and recent studies showed that oxidation of cardiolipin is carried out by a cardiolipin-specific peroxidase activity of cardiolipin-bound cytochrome c. Cardiolipin could be responsible for the proapoptotic production of death signals. Cardiolipin modulates the production of energy and participates in inflammation, mitophagy, and cellular apoptosis. The determination of cardiolipin or its antibodies is an attractive therapeutic, diagnostic target in RT and kidney diseases.

1. Introduction

Chronic kidney disease (CKD) is a serious public health problem in México and in the world [1]. The reports of the CKD registry in Jalisco (México) estimate the annual incidence rate of 411 per million inhabitants and the prevailing rate of 1556 per million inhabitants [2]. CKD has the capacity to progress to end-stage renal disease (ESRD) and to trigger serious complications that condition the death of patients. Cardiovascular disease (CVD) is the leading cause of death in patients with ESRD [3]. Hemodialysis (HD), peritoneal dialysis (PD), and renal transplantation (RT) constitute renal replacement therapy in ESDR [4, 5]. RT is the treatment of choice for patients with ESRD; however, the capacity of health systems worldwide is insufficient to meet the current needs [6]. It has been reported that the incidence of acute transplanted renal graft dysfunction ranges from 11.8% of related living donors to 17.4% of cadaveric donors [7, 8]. The existence of anticardiolipin antibodies (ACAs) may be a risk factor for renal thrombotic microangiopathy after RT. Asymptomatic ACA may be associated with acute graft dysfunction, even if thrombotic episodes are not observed [9]. Possibly, the early oxidation of cardiolipin can initiate the oxidation of low-density cholesterol (oxLDL), which could generate other inflammatory phospholipids [10]. OxLDL is abundantly found in atherosclerotic lesions and

favors proinflammatory properties by activating T cells, endothelial cells, and monocytes/macrophages [11]. As reported, anticardiolipin antibodies (ACAs) are not associated with an increased risk of death among patients with HD or CVD [12]. Determining ACA and antiphospholipid antibody (APA) in candidates for RT can warn of possible early graft failure and indicate which patients can benefit from anticoagulant therapy [13]. In the present review, the cardiolipin in mitochondria and its effect on inflammation, oxidative stress, and mitophagy in CKD and RT are addressed. In addition, the role of ACA and APA in CKD and RT was reviewed.

1.1. The Nephron. The nephron is the functional unit of the kidney, whose main objective is to regulate the composition of body fluids through the processes of filtering, reabsorption, and secretion [14]. The active and passive solute reabsorption is carried out by the renal tubules in a process that consumes high levels of adenosine triphosphate (ATP) [15]. The production of ATP is mainly generated by aerobic metabolism [15]. Normal renal function involves numerous types of cells, including tubular epithelial cells, endothelial cells, and podocytes that work in coordination to form a delicate balance that involves many enzymatic processes and activities that require intensive energy use; among them was the transport of sodium that requires close coordination between supply and demand [16]. Renal tubular cells are rich in mitochondria and depend on the oxidative phosphorylation process for the generation of ATP for proper functioning. In case of mitochondrial injury or failure, renal cell functions are severely affected [17]. Even at rest, the metabolic rate of the kidney is high; a large number of functional mitochondria are required to provide enough energy to regulate fluid and electrolyte balance, maintain acid-base homeostasis, regulate blood pressure, eliminate waste from the bloodstream, and reabsorb the nutrients. Glomerular filtration is a passive process that depends on the maintenance of hydrostatic pressure in the glomeruli [18]. In contrast, the reabsorption of glucose, ions, and nutrients is driven by ionic gradients and occurs through ATP-dependent channels and transporters [19, 20]. The mitochondria are the main source of generation of reactive oxygen species (ROS) and the internal mitochondrial membrane respiratory complex. Complexes III and I are the main sites for the generation of the superoxide radical anion ($O_2^{\cdot-}$) [21]. Cytochrome c (cyt c) catalyzes the oxidation of cardiolipin in the presence of ROS, which contributes to permeabilization of the mitochondrial membrane [22]. In addition, it has been reported that oxidation of ROS-induced cardiolipin affects the activity of respiratory chain complex I [23].

1.2. Cardiolipin. Cardiolipin (1,3-bis(sn-3′-phosphatidyl)-sn-glycerol) plays an important biological role by associating with subcellular particles of mitochondria [24]. Cardiolipin is a tetra-acyl anionic phospholipid highly conserved in bacteria and mitochondria, it is a dimeric phosphatidic acid with glycerol, and characteristically it contains a central prochiral carbon, two phosphates, and four acyl chains. Cardiolipin shows asymmetry in relation to the chains of acyl groups and their distribution in the internal mitochondrial membrane [25]. Cardiolipin phosphate groups were originally described as strong acids due to their pK values. Phosphates are ionized at a physiological pH, which makes cardiolipin an amphiphilic lipid with a negative net charge [26]. It was previously described that cardiolipin could have a pK1 close to 3 and a pK2 > 7.5. However, recently by calorimetric and pH titrations using cardiolipin with uniform saturation and fatty acid length chains, a pK1 = 2.15 and a pK2 = 3.15 were detected [27]. This is very important because the ionization state of cardiolipin influences (1) its interaction with other molecules in the mitochondrial inner membrane, (2) the membrane structure, and (3) the transport of molecules and ions [28]. Structurally, the four-acyl chains of the cardiolipin together with its negatively charged polar part give the cardiolipin a conical shape, the polar region being the top of the cone and the flexible and variable acyl chains the base of the cone. Cardiolipin spontaneously forms inverse laminar or hexagonal structures depending on the saturation of the acyl chains and the pH of the solution. Cardiolipin is crucial to maintain the curvature of the mitochondrial ridges and the potential of the inner membrane. The length, saturation, and oxidation of acyl groups provide differential influences on the shape, binding, function, and stability of cardiolipin [29]. Cardiolipin participates in the maintenance of the structural integrity of the mitochondrial membrane. The highest concentration of cardiolipin is concentrated in the inner monolayer of the inner mitochondrial membrane, and a significant portion binds to proteins. The enzymatic respiratory complexes of the mitochondrial respiratory chain, the adenine nucleotide transporter, the F_0F_1-ATP synthase, and decoupling protein 1 bind with high affinity to the cardiolipin for the correct assembly and stability of its quaternary structure and its correct functioning [30]. Each species of cardiolipin has subtle structural differences, and polyunsaturated acyl chains are candidates for lipid peroxidation. Like their unsaturated phospholipid equivalents, many cardiolipin oxidation products have the potential to transmit information to lipoperoxidation product receptors. Acyl fragments of the oxidized cardiolipin chains are capable of transmitting information upon dissociation [31]. The interactions of cardiolipin with proteins are essential to understand many of its functions. It has been documented that many proteins interact structurally and functionally with cardiolipin and their presence is essential for many of them [32]. Cardiolipins bound to respiratory complexes III and IV are crucial for electron transport. The cytochrome bc1 cardiolipin binding sites are located on the surface exposed to the membrane of respiratory chain complex III [33]. To maintain the integrity of the structure of complex III, the cardiolipin spontaneously diffuses at the interface of the cytochrome bc1 dimer that postulates the separate reduction of the quinone and the oxidation of the quinol site by completing a catalytic cycle, a site that receives a quinone molecule, two heme b electrons, and two protons from the negative membrane site, which also suggests that cardiolipins have an important role in the proton transport [34]. Cardiolipin molecules are strongly linked to cytochrome c oxidase (cyt c oxidase), a terminal complex of the respiratory chain essential for their function [35]. In

fact, the sequential elimination of 3-4 cardiolipin molecules strongly bound to each cyt c oxidase monomer leads to the loss of electron transport activity and favors the dissociation of the VIa and VIb subunits of the enzyme complex [36]. Two cardiolipin binding sites in cyt c oxidase are involved in the pathways that bind cardiolipins to the entrance of proton D and H channels, highlighting the importance of cardiolipins in proton delivery to complex IV [37]. Other peripheral membrane proteins and soluble proteins interact with cardiolipin. For example, light chain 3 of the 1A/1B proteins associated with microtubules is involved in the mitochondrial degradation process (mitophagy) by recognizing the externalization of cardiolipin by damaged mitochondria [38]. In addition, cardiolipin participates in the maintenance of the nonspheroidal membrane structure [39]. Cardiolipin and its oxidation products should be recognized as cellular signals that regulate various metabolic pathways [40]. Polyunsaturated acyl chains of cardiolipin after oxidation produce countless lipid mediators of cell signaling [41]. The initially synthesized mitochondrial cardiolipin may include a variety of acyl chains. However, in various tissues, including the kidney, the nascent cardiolipin undergoes further transformations by a remodeling process to form cardiolipins with identical acyl chains. It is believed that excessive production of $O_2^{\cdot-}$ radicals by the mitochondrial electron chain and by dehydrogenases of the Krebs cycle can produce random reactions of chemical oxidation in different biomolecules, including phospholipids that generate highly diversified molecular speciation of cardiolipins [42].

1.3. Mitochondria and Cardiolipin. Mitochondria are very varied complex and dynamic subcellular compartments; in a specific tissue, mitochondria can exist as small individual organelles or form a large tubular network attached to an interconnected membrane depending on environmental factors. The fundamental functions of mitochondria are cellular respiration, calcium homeostasis, phospholipid synthesis, fatty acid oxidation, apoptosis, ROS generation, and detoxification, among others [43]. Mitochondria contain four compartments: the outer membrane, the inner membrane, the intramembrane space, and the matrix. The outer membrane surrounds the organelle, is relatively permeable, and houses protein complexes that regulate the importation of proteins. The inner membrane is impermeable to ions and molecules, which is critical to maintain the electrochemical gradient that drives oxidative phosphorylation, is aligned adjacent to the outer membrane, and is characterized by the presence of numerous ridges that are divided into two distinct regions: the inner boundary membrane (IBM) and the ridges. The surface area of the inner membrane (IBM plus ridges) is >4 times larger than that of the outer membrane [44]. The expansion and contraction of ridges are physiologically relevant processes that occur in response to metabolic disturbances [45]. *In vitro* studies show that in giant unilamellar vesicles (GUV), cardiolipin induces the formation of narrow and dynamic tubular extensions or invaginations similar to mitochondrial ridges that can change shape according to the pH of the medium. Therefore, cardiolipin plays a crucial role in the formation of GUV-like invaginations; this effect may be relevant for the biogenesis of mitochondrial ridges [46]. For survival and interaction with the environment, cells require continuous production of ATP. The oxidative phosphorylation system produces 90-95% of ATP for tissues and organs that require high energy demand such as the brain, heart, and kidney. ATP is generated through the gradual oxidation of carbohydrates, amino acids, and fatty acids. For that reason, mitochondrial dysfunction is strongly associated with aging and many complex diseases [47]. Cardiolipin is crucial for the normal bioenergetic processes of mitochondria. It seems that peroxidation and cardiolipin depletion contribute to age-related mitochondrial dysfunction [48]. The structure of cardiolipin contributes to the formation of mitochondrial ridges, and it has been proposed that cardiolipin phosphate groups located in the outer monolayer of mitochondrial ridges trap protons [49]. Cardiolipin participates in the transformation of the proton gradient into an essential transmembrane electrochemical potential to maintain the synthesis of ATP by F_0F_1-ATP synthase [49]. Cardiolipin also acts as a scaffold for the correct assembly of respiratory complexes and supercomplexes, which facilitates the optimal transfer of electrons in the mitochondrial inner membrane [50]. Cardiolipin plays an important role in anchoring cyt c to the inner mitochondrial membrane and facilitating the transfer of electrons from complex III to complex IV [51]. Coenzyme Q within the internal mitochondrial membrane facilitates the transfer of electrons from complex I to complex III, while cyt c mediates the transfer of electrons through its heme that changes between the reduced ferrous state (Fe^{2+}) and the oxidized ferric iron (Fe^{3+}) [52]. Met 80 and His 17 are axial ligands of heme iron in cyt c, and they are also essential to stabilize the native conformation and electron transfer [53]. To support the transfer of electrons from complex III to complex IV, cyt c must be very close to these complexes. Therefore, the cardiolipin provides an anionic platform for electrostatic interaction with highly cationic cyt c (9+ net charge), which makes cyt c slightly attached to the electron transport chain. The electrostatic interaction of cyt c with cardiolipin is physiologically compatible with high levels of ATP synthesis [54]. When the concentration of ATP decreases in pathological conditions such as CKD, cyt c is closely associated with cardiolipin through hydrophobic interactions. The interaction of cardiolipin with cyt c leads to the disruption of the Fe-Met 80 bond, so the cyt c/cardiolipin complex acquires peroxidase/oxygenase activity [55]. The peroxidase activity of the cyt c/cardiolipin complex is favored in the presence of ROS and contributes to the oxidation of cardiolipin by facilitating the opening of the transition pore of mitochondrial permeability (mPTP) and the release of cyt c to the cytosol and triggering apoptosis. Therefore, cyt c has two contrasting functions, and its predominant activity is determined by oxidative stress and its interaction with cardiolipin [56]. In mitochondria, lipid peroxidation particularly affects cardiolipin that is expressed exclusively in the inner mitochondrial membrane and that plays a central role in preserving mitochondrial structure and function. Mitochondrial fission factor (Mff) deficiency reduces cytoplasm leakage in the cytoplasm relieving cardiolipin oxidation resulting from damage to electron transport

chain complexes and overproduction of mitochondrial reactive oxygen species [57]. Under physiological conditions, cardiolipin strongly traps cyt c within the inner mitochondrial membrane. However, selective peroxidation of cardiolipin facilitates the release of cyt c from the outer surface of the inner mitochondrial membrane by opening the mPTP and its subsequent release to the cytoplasm by blocking oligomerization of the dependent anion of channel 1 voltage and the subsequent separation of hexokinase 2 from the mitochondria. It is not clear whether the fission associated with Mff triggers the opening of mPTP and the leakage of the cytoplasm by regulating the dissociation of hexokinase 2 and the oxidation of cardiolipin. If that happens, it is important to know which molecule links fission to changes in the release of hexokinase 2 and the peroxidation of cardiolipin. For example, during an acute traumatic brain injury, a significant number of mitochondria are released in the systemic circulation. These particles are highly procoagulant through the cardiolipin exposed to the surface [58]. A similar event could happen in the process of ischemia/reperfusion in RT. Oxidative stress is an event that arises from the reperfusion of an organ after a long period of ischemia and that leads to tissue damage. Reperfusion injury is a major problem in organ transplantation. In RT, the increase in reactive oxygen species (ROS) causes a delay in graft function by affecting the energy metabolism of renal cells. ROS-induced ischemia/reperfusion injury has a common substrate: the transition of mitochondrial permeability that causes permeability of the internal mitochondrial membrane after massive accumulation of Ca^{2+}. The increase in nonspecific permeability occurs after the opening of a nonspecific pore with a diameter of approximately 2-3 nm that allows the release of the matrix content with a molecular weight of up to 1500 Da [59].

1.4. Cardiolipin and ATP Synthesis. Cardiolipin binds with high affinity to three sites in the mitochondrial carrier ADP/ATP. The conservation of amino acid residues at cardiolipin binding sites to other members of the mitochondrial transporter superfamily suggests that cardiolipin binding could be important for the function of all mitochondrial carriers [60]. Cardiolipin modulates mitochondrial functions, including the synthesis of ATP; however, the biophysical mechanisms by which cardiolipin generates nonlamellar structures and the degree to which these structures contribute to the synthesis of ATP are still unclear [61]. ATP synthase is a key enzyme for the conversion of mitochondrial energy, and the alteration of its activities is associated with several acute and chronic pathologies such as CKD [62]. Mitochondria provide energy to the Na^+/K^+-ATPase enzyme to generate ion gradients across the cell membrane. Because proximal renal tubules contain more mitochondria than any other kidney structure, more active transport mechanisms than other types of renal cells are required to reabsorb 80% of the filtrate that passes through the glomerulus, including glucose, ions, and the nutrients. The proximal tubule, the loop of Henle, the distal tubule, and the collecting duct require active transport to reabsorb the ions. Proximal tubular epithelial cells are rich in mitochondria and depend on oxidative phosphorylation for the generation of ATP [63]. The ability of mitochondria to detect and respond to energy demand and changes in nutrient availability through the maintenance of mitochondrial homeostasis is essential for the proper functioning of the proximal renal tubules [64]. In the late 1990s, Xie and Askari published studies that indicated that the enzyme Na^+/K^+-ATPase not only acts as an ion pump but also interacts as a signal transducer with several signaling pathways. Since then, numerous studies have shown that Na^+/K^+-ATPase participates in the mediation of long-term physiological adaptation processes that Neal Bricker originally proposed in the 1970s. It has been shown that Na^+/K ligand$^+$-ATPase, like cardiotonic steroids, emits signals through Na^+/K^+-ATPase and is involved in mediating adaptive and nonadaptive responses to volume overload, fibrosis, and oxidative stress [65]. Long-term hyperuricemia has the ability to induce hypertension, renal vasoconstriction, tubular damage, oxidative stress of the renal cortex, mitochondrial dysfunction, and decreased ATP levels [66].

1.5. Mitochondrial Dysfunction in CKD. The so-called "unifying hypothesis" is based mainly on the notion that mitochondrial dysfunction mediated by ROS overproduction is a common pathway in the pathogenesis of microvascular complications of diabetes mellitus that include diabetic nephropathy and progression to CKD [67]. The hypothesis does not explain all related phenomena, including ischemia as a common factor in CKD capable of producing mitochondrial inflammation and loss of membrane ridges in proximal podocytes and tubules [68]. The persistent accumulation of damaged mitochondria conditions deterioration of mitochondrial quality control [69]. Many mitochondria show evidence of proteolytic degradation that affects the mitophagy and favors the elimination of proteins damaged by mitochondrial proteases [70]. In experimental studies of CKD, fatty acid oxidation defects have been reported. Apparently, the high-fat diet causes the accumulation of lipids in the tubular cells and downregulates cathepsin-1 [71]. Defective fatty acid oxidation is frequently observed in patients with diabetic nephropathy. In a previous report, an increase in lipid deposition was reported and intracellular lipid drops in renal biopsies [72]. Lipid deposition is associated with negative regulation of several key genes involved in the oxidation of fatty acids. Transcriptome analysis of the entire genome of a large cohort of fibrotic kidney biopsies revealed low expression of cathepsin-1, cathepsin-2, and other genes involved in the metabolic pathways of fatty acid and glucose oxidation [73]. *In vitro* inhibition of fatty acid oxidation in tubular epithelial cells decreases the synthesis of ATP and produces metabolic alterations similar to those observed in CKD [73].

1.6. Oxidative Stress and Cardiolipin. Peroxidation of phospholipid fatty acids is presented as the main cause of oxidative signaling; therefore, deregulation of these pathways can lead to the accumulation of excessive amounts of lipid oxidation products at specific sites [74]. Several enzymes of the Krebs cycle, such as 2-oxoglutarate dehydrogenase (OGDH), branched chain complex-2-oxoacid dehydrogenase (BCKDH), and pyruvate dehydrogenase (PDH), are

capable of producing considerable production of $O_2^{\cdot-}$ and H_2O_2. BCKDH can produce $O_2^{\cdot-}$ and H_2O_2 at higher rates compared to mitochondrial complexes I and III, which represents an additional source of ROS [75, 76]. Enzymatically catalyzed oxidation reactions can affect specific phospholipid molecules capable of leading to activation of the intrinsic mitochondrial apoptotic pathway. It has been reported that phospholipid-specific oxidation is one of the characteristic features of oxidation reactions triggered by different stimuli in different tissues [77]. The oxidation process of cardiolipin is not random; it has pronounced specificity not related to the polyunsaturation pattern of cardiolipin. The accumulation of hydroxyl derivatives and cardiolipin hydroperoxide in the tissues of affected animals has been observed. The above suggests that there are specific enzymatic mechanisms, such as the peroxidase activity of the cyt c/cardiolipin complex, which could be primarily responsible for the proapoptotic production of death signals [78]. The peroxidation of cardiolipin causes its translocation to the external mitochondrial membrane, where it has been proposed that it serves as a coupling site for the assembly of the inflammasome, while mitochondrial ROS activate the inflammasome to produce caspase-1 [79].

1.7. Cardiolipin, Inflammation, and Innate Immunity. The innate immune system is implicated in acute and chronic kidney injury [80]. Necrotic cells release damage-molecular patterns (DAMP) which can trigger an inflammatory form of cell death mediated by Nod-like receptors (NLRs) [81]. Several NLRs form a multimeric protein complex called the inflammasome, of which NLRP3 is best understood for its involvement in acute and CKD [82]. The NLRP3 inflammasome activates caspase-1 that causes the secretion of IL-1β and IL-18 proinflammatory cytokines and is considered a final common pathway that supports the cycle of inflammation and fibrosis in CKD. IL-1β and IL-18 represent possible therapeutic targets for CKD [83]. The inflammasome is activated in response to various stimuli that seem to converge on mitochondrial ROS generation [61]. NLRP3 binds directly to cardiolipin, suggesting that mitochondrial damage and translocation of cardiolipin to the outer mitochondrial membrane may provide the coupling signal for the assembly and activation of the inflammasome [84]. The continued presence of externalized cardiolipin in mitochondria damaged by the failure of its effective elimination by the innate immune system or by constant production because of cell death activates antigen-presenting cells (dendritic cells and macrophages) through interactions with T and B cells. They have the ability to stimulate the adaptive immune response that results in the production of ACA [85]. The effects of cardiolipin can be increased with beta-2-glycoprotein 1 (β2GPI). β2GPI is a glycoprotein present in high concentrations in plasma with the ability to bind effectively to anionic phospholipids (including cardiolipins). Excessive formation and accumulation of APA, particularly ACA, may condition the development of a systemic autoimmune disease [86]. Cardiolipin complexes with cyt c that produce proapoptotic signals catalyze the oxidation of the polyunsaturated acyl chains of cardiolipin. Countless cardiolipin species exert messaging functions and oxidation products with important intra- and extracellular signals for innate and adaptive immunity systems [87]. Correlation between mitochondrial DNA (mDNA) levels in donor plasma and early allograft dysfunction in liver transplant recipients has been demonstrated, suggesting the potential role of circulating mtDAMP in allograft results. The current advisable approach to prolonging allograft survival in addition to immune suppression in the transplant recipient may be to attack inflammatory factors in donors (deceased) before obtaining as a potential strategy to improve transplant results [88]. Several primary and systemic kidney diseases are associated with the activation of the NLRP3 inflammasome/IL-1β/IL-18 axis. The spectrum of the disease includes ureteral obstruction, ischemia/reperfusion injury, glomerulonephritis, sepsis, hypoxia, glycerol-induced renal failure, and crystalline nephropathy. In addition, the IL-1/IL-18 axis may be responsible for the development of CKD and its related complications [83].

1.8. Mitophagy and Cardiolipin. The collapse of asymmetry in the distribution of lipids in the mitochondrial inner membrane represents a promitophagy mechanism by which externalized cardiolipin acts as a signal to initiate mitophagy [46]. The autophagic machinery releases damaged mitochondria in double-membrane vesicles (autophagosomes), which fuse with late endosomes or lysosomes so that lysosomal enzymes degrade the autophagosome content, including the internal autophagosome membrane [89]. Receptors or selective autophagic loading adapters (p62 and optineurin) unify their mitochondrial load attached to the autophagosome membrane by interacting with the lipid protein (phosphatidylethanolamine ATG8, microtubule-1-associated protein (LC3))/protein associated with the amino acid gamma butyric receptor (GABARAP) intimately associated with autophagosome membrane charge receptors [90]. Autophagy LC3 protein mediates autophagosome formation and load recognition because it contains important cardiolipin binding sites to facilitate thickening of mitochondria [91]. In normally functioning mitochondria, cardiolipin is limited to the internal mitochondrial membrane (predominantly oriented to the matrix near the site of its synthesis). Recognition by cytosolic LC3 requires the presence of cardiolipin on the mitochondrial surface, suggesting that transmembrane redistribution of cardiolipin should be performed in damaged mitochondria that undergo mitophagy. In mitochondria that maintain their electrochemical membrane potential, cardiolipin binds directly to many membrane proteins and respiratory complexes and supercomplexes. Negligible amounts of cardiolipin bind to soluble proteins [92]. Previously, the general dependence of mitophagy and the externalization of cardiolipin on the total cardiolipin content have been established. The mechanisms of translocation of cardiolipins within mitochondrial membranes have not yet been completely deciphered. It is suspected that decoupling proteins, anionic transporters of the internal mitochondrial membrane and phospholipid scramblase-3, may participate in this phenomenon [30]. Association of autophagy with the pathogenesis of various diseases has been reported: neurodegeneration, cancer, infections,

and kidney diseases. Proximal tubules potentially require a lot of energy to degrade. Apparently, autophagy plays an important role in the physiology of the proximal tubules. Autophagy has been reported to have a protective role against damage to the proximal contoured tubules by the ischemia/reperfusion and nephrotoxic processes, including cisplatin and cyclosporine [93].

1.9. Anticardiolipin Antibodies. High prevalence of ACA (19%) is reported in CKD patient candidates for RT compared to the general population due to the association of ACA with autoimmune diseases. Patients with CKD are more likely to suffer from comorbid conditions (infections, aging, and the use of nephrotoxic medications) [94]. Patients without a history of coagulation disorders have no transplant thrombosis compared to those with APA-positive diagnosis [95]. ACAs can also be detected after bacterial or viral infections. Among patients receiving dialysis, having a positive antibody concentration was not associated with age or having received RT. The presence of ACA was more common among patients with chronic glomerulonephritis than among those with other diagnoses [89].

The incidence of acute rejection leading to graft failure in patients with ACA but not APA is considerably high (27%) in contrast to the group of patients without ACA and with APA (14%) ($p < 0.05$) vs. healthy controls [96]. ACA-positive patients may have a better immune response. Patients with APA syndrome who do not receive anticoagulation before RT have an incidence of 100% of graft thrombosis with graft insufficiency [97]. Anticoagulation before or at the time of RT in patients with APA significantly reduces the incidence of posttransplant thrombosis and graft failure [70]. None of the ACA isotypes is specific for the development of thrombosis in patients with APA syndrome and ESRD. Several authors have noted that APA thrombosis is associated with ACA of the IgG, IgM, and IgA isotypes [98]. The nature of the target molecules for ACA is unclear. It has been reported that there may be more than one candidate molecule (β2 glycoprotein and/or phosphatidylserine) [73]. The mechanisms underlying vascular thrombosis remains uncertain; however, it has been postulated that the surgical procedure and endothelial cell damage can act synergistically in patients with APA to induce the thrombotic process in allografts [99]. Several authors have shown that alloantibodies against endothelial and/or epidermal antigens can cause acute accelerated loss of the graft [100] (Table 1).

1.10. Antiphospholipid Antibodies. APAs are a heterogeneous group of autoantibodies present in a wide range of diseases. Among the APAs, those directed against cardiolipin and its cofactor (β2-GP1) are best characterized and used in clinical practice. APA produces the antiphospholipid syndrome [101]. APAs are autoantibodies associated with venous and arterial thrombosis [102]. The presence of antithrombus and/or anticardiolipin antibodies indicates a worse long-term renal prognosis. ACA positivity is a strong predictor of venous and arterial systemic vascular thrombotic complications [103]. APAs are a heterogeneous group of immunoglobulins directed against negatively charged phospholipids, protein-phospholipid complexes, or plasma β2-GPI [104]. APAs include ACAs and lupus anticoagulant (LAC). ACAs are recognized for their high ability to bind to anionic phospholipids in solid-phase immunoassays with the ability to lengthen phospholipid-dependent coagulation tests [19]. APAs can interfere with the atherogenic process and cross-react with low-density lipoprotein (LDL) antioxidant antibodies (Table 1).

1.11. Cardiolipin Inhibition of Platelet-Activating Factor Could Lead to Thrombosis. Platelet-activating factor (PAF) (1-0-alkyl-2-acetyl-sn-glycero-3-phosphocholine) is a natural lipid mediator with a wide range of *in vivo* and *in vitro* effects including pathological responses in inflammation and allergy. PAF has the ability to stimulate platelets, neutrophils, macrophages, and endothelial cells that induces platelet aggregation and activation of the coagulation system [105]. Cardiolipin is a specific inhibitor of PAF [106]. It is possible that the vascular thrombosis observed in HD patients, as well as in ACA or APA syndrome, is the result of the inactivation of circulating ACA that leads to increased PAF activity. Thrombosis in patients undergoing HD could be the result of the action of PAF in platelets and the activation of the coagulation cascade [107]. This topic is interesting as a diagnostic target.

1.12. Cardiolipin and Nephropathy. Cardiolipin is essential for the formation of the crystalline membrane and organizes the components of the electron transport chain, preserving the integrity and mitochondrial structure. The metabolic syndrome increases more saturated species such as C18:1, C18:0, and hydrolysis products of renal cardiolipin (lysocardiolipin), which implies the oxidation of cardiolipin [108]. Renal adiposity, lipid peroxidation, and elevated levels of isoprostanes seen in mitochondrial syndrome probably contribute to renal mitochondrial injury by mitochondrial cardiolipin peroxidation [109]. Patients with uremia have a high incidence of infectious, cardiovascular, and thrombotic events caused by ACA. In dialyzed patients, ACA levels are higher than those in healthy subjects without association who have received a previous RT. It is more common to find ACA in patients with glomerulonephritis than in patients undergoing RT [110]. ACAs are clinically associated with hypercoagulability. Vascular access thrombosis and systemic thrombosis in HD coexist with immunoregulation abnormalities in ESRD [86]. IgG-ACA is strongly associated with the presence of venous and arterial thrombosis in patients with normal renal function. High titers of IgG-ACA have also been reported in HD patients [111].

1.13. Cardiolipin and Kidney Transplant. It is well known that CVD is more common among RT recipients than in the general population and is the leading cause of death [112, 113]. One of the characteristics of APA syndrome is the presence of ACA in association with thrombotic disorders or thrombocytopenia of the arterial and/or venous systems [114]. Since the 1990s, increased serum levels of ACA have been reported in HD patients and in RT recipients, with a prevalence of 4.8 to 46.4%. The clinical importance of ACA

Table 1: Features of ACA and APA antibodies in the kidney.

ACA	APA
	Venous thrombophilic and arterial autoimmune condition [1]
Antibodies associated with hypercoagulability	Primary; absence of another related disease. The initial presentation may be with vasculitis [2]. The kidney can be the initial target [3]
In hemodialysis, systemic thrombosis and vascular access thrombosis coexist [86]	Secondary to another concurrent autoimmune disease
High incidence of infectious, cardiovascular, and thrombotic events	The presentation may vary; it mimics many other medical conditions
Antibodies more frequent in those with glomerulonephritis than in those undergoing kidney transplantation	Kidney clinical manifestations [4]
Thrombotic disorders/thrombocytopenia of the arterial and/or venous systems [86]	Hypertension, microscopic hematuria, proteinuria (from mild to nephritic levels), renal insufficiency, thrombosis or stenosis of the renal artery, thrombosis of the renal vein, graft loss due to thrombosis after kidney transplantation, injury of the renal microvasculature (renal nephropathy) APA
Disproportionately high rates of arteriosclerosis [91]	Kidney biopsy [5]
High risk of developing renal thrombosis in 1 week after transplant, thrombosis can be limited to the graft [46]	Acute lesions of thrombotic microangiopathy, chronic intrarenal vascular lesions, intimal fibrous interlobular hyperplasia, recanalizing arterial and arteriolar thrombosis, fibrous arterial occlusion, and focal cortical atrophy
Thrombosis can occur in the second week after transplantation and represents 12.2% of failed primary transplants and 19.2% of failed repeated transplants [89]	

positivity in these patients was uncertain. Serum IgG and IgM-ACA levels of 61 patients were measured in HD. 14 were RT recipients and 38 were healthy controls. The authors reported increased levels of ACA-IgG in four HD patients, in two RT (14%) and two healthy controls. After one year of follow-up, serum ACA-IgM levels were normal in all patients without observing events [115]. Acquired thrombophilia is specifically considered for the presence of APA with the ability to predispose to adverse outcomes after transplantation, although this association is not clear [96]. ACAs are by far the most common prevalence in ESRD which are considerably higher than those in healthy controls. Primary and secondary APA positivity is associated with specific intrarenal changes characterized by fibrous intimal hyperplasia, focal cortical atrophy, and thrombotic microangiopathy [116]. Several published series have reported ACA in 10-30% of dialysis patients in contrast to 1-8% of the general population [117]. Similar findings have been reported of the presence of APA in patients with RT [118].

Inflammatory phenomena secondary to episodes of acute RT rejection may be responsible for *de novo* production of APA by contributing to the development and progression of CVD [119]. In this context, cell death occurs due to necrosis or apoptosis for the exposure of the immune system to autoantigens towards which there is no tolerance [119]. Patients with ESRD with APA are at high risk of developing renal thrombosis within a period as short as 1 week after transplantation. When the thrombosis process begins, no treatment protocol that destroys the clot to save the RT is available [120]. Therefore, prevention of thrombosis is of the utmost importance; it is required that potential transplant recipients be diagnosed with APA or ACA before transplantation so that anticoagulant therapy can be initiated before transplantation. Thrombosis that occurs in renal grafts shortly after kidney transplantation in the absence of prior systemic coagulopathy is considered a result of acute rejection or immunologically induced coagulopathy [121]. Previous fibrin deposition has been reported in failed grafts without evidence of systemic coagulopathy, indicating that thrombosis is limited to the graft [122]. Thrombosis can occur up to the second week after transplantation and represents 12.2% of failed primary transplants and 19.2% of failed repeat transplants [123]. The effects of APA include interference with the atherogenic process by crossreacting with antibodies against oxidized low-density lipoprotein, improved uptake of oxidized LDL macrophages, and promotion of thrombosis [124]. It is well known that stable RT recipients have disproportionately high rates of atherosclerosis, where APA may apparently be involved [125]. Moreover, the presence of APA is considered an independent cardiovascular risk factor in RT recipients [113]. The evaluation of APA at the time the patient appears as a candidate for RT facilitates the identification of patients at high risk of early graft dysfunction. In addition, predisposition to thrombotic complications after RT has been identified in patients with a history of deep venous thrombosis before transplantation. RT candidates with a history of one or more thrombotic events may have increased risk of APA systemic vascular thrombosis [126]. The pretransplant determination of each patient's APA *status* can predict which patients may benefit from prophylactic anticoagulant therapy to prevent graft thrombosis [127]. Previous reports indicate that most APA may be acquired in the pretransplant period [128]. More than half of patients with APA before transplantation lost these antibodies after transplantation [129]. However, the persistence of APA identified before transplantation in the posttransplant period is associated with excessive risk of atherosclerotic events [113]. In fact, patients who never had APA and those who lost APA before transplantation during the posttransplant period seem to have a lower risk of atherosclerotic events. This result is important for the search of APA and the management of patients in the transplant period [116]. Prophylactic measures are not likely to be indicated in all APA-positive patients during the initial period after RT. These measures should be analyzed if the APA positivity persists during the months after the transplant [130]. APA syndrome is one of the differential diagnoses for thrombotic microangiopathy that can cause acute loss of graft

function or fatal thrombotic complications. A patient with polycythemia was previously reported after RT incompatible ABO and negative APA screening tests before transplantation. The patient was treated with desensitization therapy (plasmapheresis and rituximab); however, he developed acute graft dysfunction on day 112 postoperatively. Graft biopsy revealed microvascular inflammation of the glomerular capillaries without immunoglobulin deposition. The ACA was positive repeatedly without previous thrombotic episodes. The treatment was based on intensive steroid pulse, plasmapheresis, and induction with rituximab. The ACA disappeared, and the graft function recovered and stabilized for 52 months. The authors suggest that asymptomatic ACA may be associated with acute graft dysfunction [9].

1.14. Cardiolipin in RT-Related Diseases. Bone mineral disorders frequently occur in RT recipients and are associated with a high risk of fractures, morbidity, and mortality. The pathophysiology underlying bone disorders after RT results from a complex interaction of factors, including preexisting renal osteodystrophy and bone loss related to immunosuppression and alterations in the growth factor of fibroblast 23-parathyroid hormone-vitamin D [131]. The neurological complications observed in solid organ transplants are reported in almost 9 of 10 recipients. The intensity, severity, and type of anomalies may vary. More often, complications appear to be associated with the direct or indirect effect of immunosuppressants because of their direct effect on cells and blood vessels and susceptibility to infections [132]. However, we found no information in the available literature on the complications of RT related to cardiolipin and its antibodies. We believe that this could be an interesting topic to investigate in RT recipients.

1.15. Elamipretide and Cardiolipin. Antioxidants are considered protective molecules against oxidative stress by acting predominantly through mechanisms of elimination of free radicals [133]. Alternative ideas related to enzymatically regulated oxidative reactions have been presented, including phospholipid peroxidation reactions as the main cause of oxidative signaling. Deregulation of these reactions can lead to the accumulation of excessive amounts of lipid oxidation products capable of exacerbating oxidative damage in specific molecular targets [56]. Apparently, phospholipids are oxidized in a manner dependent on the amount of double bonds in their acyl groups, rather than the nature of their polar group [134]. Elamipretide (SS-31) is a cationic synthetic tetrapeptide (D-Arg-2′6′-dimethyl Tyr-Lys-Phe-NH2) that specifically binds with high affinity to cardiolipin in the inner mitochondrial membrane. SS-31 favors electron transfer of cyt c to cyt c oxidase and minimizes ROS production. Another proposed mechanism of the SS-31 is based on the protection of the highly curved structure of the mitochondrial ridges facilitating the transport of electrons and minimizing the production of ROS [109]. This tetrapeptide has antioxidant properties and inhibits the peroxidase activity of the cyt c-cardiolipin complex, which inhibits the opening of the mPTP [109]. In a recent experimental study, it was reported that treatment with elamipretide restored renal function in swine reno-vascular disease [135]. A recent study showed that elamipretide prevents glomerulopathy induced by a high-fat diet and a proximal tubular lesion in mice [136]. In 2017, a study was reported in which SS-31 was administered in experimental animals. Administration began 1 month after producing ischemia and was maintained for 6 weeks. The authors observed protection of mitochondrial integrity, and the progression of glomerulosclerosis and tubular interstitial fibrosis was avoided. Protection by SS-31 was maintained for 6 months after the end of treatment [136]. In addition, there was positive regulation of IL-1β and IL-18 nine months after ischemia, suggesting that SS-31 reduced CKD by protecting mitochondria and preventing the activation of the inflammasome [51]. Cardiolipin promotes mitochondrial ridge formation, promotes normal assembly of respiratory complexes to form supercomplexes, facilitates efficient electron transfer, promotes ATP synthesis, and reduces electron leakage [136]. Dysfunctional mitochondria generate ROS, and cardiolipin is particularly susceptible to lipid peroxidation. In the presence of ROS, cyt c acts as peroxidase and produces peroxidation of cardiolipin, which causes degradation of mitochondrial ridges [43]. Previously, it has been reported in experimental models of renal and cardiac insufficiency that SS-31 restores cardiolipin content and mitochondrial ridge structure and improves mitochondrial energy [137]. The release of mitochondrial DNA, ROS, and cardiolipin from damaged mitochondria can activate the NLRP3 inflammasome. The administration of SS-31 promotes bioenergetic recovery and the structure of the podocytes allowing the repair of the actin cytoskeleton [138]. In addition, SS-31 prevents positive regulation of IL-1β and IL-18 after acute renal ischemia as previously mentioned [139].

In conclusion, cardiolipin is a fundamental component of the total phospholipids of body tissues. Cardiolipin is characteristically associated with the internal mitochondrial membrane, where it plays an important biological role in favoring the high rate of ATP synthesis. The ionization state of cardiolipin influences the interaction with other molecules of the internal mitochondrial membrane. In addition, *in vitro* studies suggest that cardiolipin induces the formation of dynamic narrow tubular extensions or invaginations similar to mitochondrial ridges capable of changing shape depending on the pH of the medium. Therefore, by keeping cardiolipin the highly curved structure of mitochondrial ridges, it modulates essential mitochondrial enzymatic activities such as those of F_0F_1-ATP synthase, ATP/ADP transporter, and decoupling protein and electron chain transport, among others. APA and ACA are heterogeneous groups of autoantibodies involved in various pathologies. In patients with CKD, candidates for RT, there is a high prevalence of ACA (19%) and the incidence of acute rejection of RT in patients positive for ACA but negative for APA is 27%. The above suggests that ACA-positive patients have an intensified immune response, which could condition renal graft loss. Patients with ESRD and ACA or APA positivity have a high risk of developing venous or artery renal thrombosis shortly after RT. The management of the thrombosis process in these patients is very difficult and jeopardizes the viability of the

transplanted graft. It is convenient to determine the presence of ACA or APA in RT candidates; in the positive case, the appropriate antithrombotic treatment was provided to prevent graft loss. The determination of cardiolipin or its antibodies is an attractive therapeutic, diagnostic target in RT and kidney diseases.

Conflicts of Interest

The authors declare that they have no conflicts of interest.

References

[1] G. Garcia-Garcia and J. S. Chavez-Iñiguez, "The tragedy of having ESRD in Mexico," *Kidney International Reports*, vol. 3, no. 5, pp. 1027–1029, 2018.

[2] United States Renal Data System 2017 USRDS annual data report: international comparisons, *Epidemiology of kidney disease in the United States*, National Institutes of Health, National Institute of Diabetes and Digestive and Kidney Diseases, Bethesda, MD, 2017, https://www.usrds.org/2017/view/v2_11.aspx.

[3] M. Liu, X. C. Li, L. Lu et al., "Cardiovascular disease and its relationship with chronic kidney disease," *European Review for Medical and Pharmacological Sciences*, vol. 18, no. 19, pp. 2918–2926, 2014.

[4] R. Saran, Y. Li, B. Robinson et al., "US Renal Data System 2015 Annual Data Report: epidemiology of kidney disease in the United States," *American Journal of Kidney Diseases*, vol. 67, no. 3, Suppl 1, p. A4, 2016.

[5] A. Eirin, A. Lerman, and L. O. Lerman, "The emerging role of mitochondrial targeting in kidney disease," *Handbook of Experimental Pharmacology*, vol. 240, pp. 229–250, 2017.

[6] USRDS United States Renal Data System, "2012 Annual Data Report: epidemiology of kidney disease in the United States," National Institutes of Health, National Institute of Diabetes and Digestive and Kidney Diseases, Bethesda, MD, 2012.

[7] J. Alberú-Gómez, E. A. Hernández-Méndez, I. Oropeza-Barrera et al., "Incidence of acute rejection in patients with renal graft dysfunction," *Revista de Investigación Clínica*, vol. 65, no. 5, pp. 412–419, 2013.

[8] S. Carrillo-Ibarra, J. I. Cerrillos-Gutiérrez, A. Escalante-Núñez et al., "The oxidative and inflammatory state in patients with acute renal graft dysfunction treated with tacrolimus," *Oxidative Medicine and Cellular Longevity*, vol. 2016, Article ID 5405847, 8 pages, 2016.

[9] A. Tsuchimoto, Y. Matsukuma, U. Kenji et al., "Thrombotic microangiopathy associated with anticardiolipin antibody in a kidney transplant recipient with polycythemia," *CEN Case Reports*, vol. 8, no. 1, article 354, pp. 1–7, 2019.

[10] Y. H. Huang, L. Schäfer-Elinder, R. Wu, H. E. Claesson, and J. Frostegård, "Lysophosphatidylcholine (LPC) induces pro-inflammatory cytokines by a platelet-activating factor (PAF) receptor-dependent mechanism," *Clinical and Experimental Immunology*, vol. 116, no. 2, pp. 326–331, 1999.

[11] J. A. Berliner, M. C. Territo, A. Sevanian et al., "Minimally modified low density lipoprotein stimulates monocyte endothelial interactions," *The Journal of Clinical Investigation*, vol. 85, no. 4, pp. 1260–1266, 1990.

[12] J. Frostegård, "Atherosclerosis in patients with autoimmune disorders," *Arteriosclerosis, Thrombosis, and Vascular Biology*, vol. 25, no. 9, pp. 1776–1785, 2005.

[13] D. R. Wagenknecht, D. G. Becker, W. M. LeFor, and J. A. McIntyre, "Antiphospholipid antibodies are a risk factor for early renal allograft failure," *Transplantation*, vol. 68, no. 2, pp. 241–246, 1999.

[14] X. Wang and M. R. Garrett, "Nephron number, hypertension, and CKD: physiological and genetic insight from humans and animal models," *Physiological Genomics*, vol. 49, no. 3, pp. 180–192, 2017.

[15] J. Bastin, N. Cambon, M. Thompson, O. H. Lowry, and H. B. Burch, "Change in energy reserves in different segments of the nephron during brief ischemia," *Kidney International*, vol. 31, no. 6, pp. 1239–1247, 1987.

[16] P. F. Mount and D. A. Power, "Balancing the energy equation for healthy kidneys," *The Journal of Pathology*, vol. 237, no. 4, pp. 407–410, 2015.

[17] J. F. O'Toole, "Renal manifestations of genetic mitochondrial disease," *International Journal of Nephrology and Renovascular Disease*, vol. 7, pp. 57–67, 2014.

[18] M. J. Holechek, "Glomerular filtration: an overview," *Nephrology Nursing Journal*, vol. 30, no. 3, pp. 285–290, 2003.

[19] P. M. O'Connor, "Renal oxygen delivery: matching delivery to metabolic demand," *Clinical and Experimental Pharmacology & Physiology*, vol. 33, no. 10, pp. 961–967, 2006.

[20] Z. Wang, Z. Ying, A. Bosy-Westphal et al., "Specific metabolic rates of major organs and tissues across adulthood: evaluation by mechanistic model of resting energy expenditure," *The American Journal of Clinical Nutrition*, vol. 92, no. 6, pp. 1369–1377, 2010.

[21] J. Lu, K. Cheng, B. Zhang et al., "Novel mechanisms for superoxide-scavenging activity of human manganese superoxide dismutase determined by the K68 key acetylation site," *Free Radical Biology & Medicine*, vol. 85, pp. 114–126, 2015.

[22] J. Hanske, J. R. Toffey, A. M. Morenz, A. J. Bonilla, K. H. Schiavoni, and E. V. Pletneva, "Conformational properties of cardiolipin-bound cytochrome c," *Proceedings of the National Academy of Sciences of the United States of America*, vol. 109, no. 1, pp. 125–130, 2012.

[23] G. Paradies, G. Petrosillo, M. Pistolese, N. Di Venosa, A. Federici, and F. M. Ruggiero, "Decrease in mitochondrial complex I activity in ischemic/reperfused rat heart: involvement of reactive oxygen species and cardiolipin," *Circulation Research*, vol. 94, no. 1, pp. 53–59, 2004.

[24] P. V. Ioannou and B. T. Golding, "Cardiolipins: their chemistry and biochemistry," *Progress in Lipid Research*, vol. 17, no. 3, pp. 279–318, 1979.

[25] J. Lecocq and C. E. Ballou, "On the structure of cardiolipin," *Biochemistry*, vol. 3, no. 7, pp. 976–980, 1964.

[26] A. V. Few, A. R. Gilby, and G. V. F. Seaman, "An electrophoretic study of structural components of Micrococcus lysodeikticus," *Biochimica et Biophysica Acta*, vol. 38, pp. 130–136, 1960.

[27] G. Olofsson and E. Sparr, "Ionization constants pKa of Cardiolipin," *PLoS One*, vol. 8, no. 9, article e73040, 2013.

[28] M. Kates, J. Y. Syz, D. Gosser, and T. H. Haines, "pH-dissociation characteristics of cardiolipin and its 2′-deoxy analogue," *Lipids*, vol. 28, no. 10, pp. 877–882, 1993.

[29] A. Saric, K. Andreau, A. S. Armand, I. M. Moller, and P. X. Petit, "Barth syndrome: from mitochondrial dysfunctions

associated with aberrant production of reactive oxygen species to pluripotent stem cell studies," *Frontiers in Genetics*, vol. 6, p. 359, 2015.

[30] S. M. Claypool, Y. Oktay, P. Boontheung, J. A. Loo, and C. M. Koehler, "Cardiolipin defines the interactome of the major ADP/ATP carrier protein of the mitochondrial inner membrane," *The Journal of Cell Biology*, vol. 182, no. 5, pp. 937–950, 2008.

[31] E. Mileykovskaya, P. A. Penczek, J. Fang, V. K. Mallampalli, G. C. Sparagna, and W. Dowhan, "Arrangement of the respiratory chain complexes in Saccharomyces cerevisiae supercomplex III2IV2 revealed by single particle cryo-electron microscopy," *The Journal of Biological Chemistry*, vol. 287, no. 27, pp. 23095–23103, 2012.

[32] J. Planas-Iglesias, H. Dwarakanath, D. Mohammadyani, N. Yanamala, V. E. Kagan, and J. Klein-Seetharaman, "Cardiolipin interactions with proteins," *Biophysical Journal*, vol. 109, no. 6, pp. 1282–1294, 2015.

[33] C. Arnarez, J. P. Mazat, J. Elezgaray, S. J. Marrink, and X. Periole, "Evidence for cardiolipin binding sites on the membrane-exposed surface of the cytochrome bc1," *Journal of the American Chemical Society*, vol. 135, no. 8, pp. 3112–3120, 2013.

[34] S. Poyry, O. Cramariuc, P. A. Postila et al., "Atomistic simulations indicate cardiolipin to have an integral role in the structure of the cytochrome bc $_1$ complex," *Biochimica et Biophysica Acta (BBA) - Bioenergetics*, vol. 1827, no. 6, pp. 769–778, 2013.

[35] G. Paradies, G. Petrosillo, M. Pistolese, and F. M. Ruggiero, "The effect of reactive oxygen species generated from the mitochondrial electron transport chain on the cytochrome c oxidase activity and on the cardiolipin content in bovine heart submitochondrial particles," *FEBS Letters*, vol. 466, no. 2-3, pp. 323–326, 2000.

[36] E. Sedlák and C. N. Robinson, "Phospholipase A(2) digestion of cardiolipin bound to bovine cytochrome c oxidase alters both activity and quaternary structure," *Biochemistry*, vol. 38, no. 45, pp. 14966–14972, 1999.

[37] C. Arnarez, S. J. Marrink, and X. Periole, "Identification of cardiolipin binding sites on cytochrome _c_ oxidase at the entrance of proton channels," *Scientific Reports*, vol. 3, no. 1, p. 1263, 2013.

[38] C. T. Chu, J. Ji, R. K. Dagda et al., "Cardiolipin externalization to the outer mitochondrial membrane acts as an elimination signal for mitophagy in neuronal cells," *Nature Cell Biology*, vol. 15, no. 10, pp. 1197–1205, 2013.

[39] K. Balasubramanian, A. Maeda, J. S. Lee et al., "Dichotomous roles for externalized cardiolipin in extracellular signaling: promotion of phagocytosis and attenuation of innate immunity," *Science Signaling*, vol. 8, no. 395, p. ra95, 2015.

[40] V. E. Kagan, Y. Y. Tyurina, V. A. Tyurin et al., "Cardiolipin signaling mechanisms: collapse of asymmetry and oxidation," *Antioxidants & Redox Signaling*, vol. 22, no. 18, pp. 1667–1680, 2015.

[41] Y. Y. Tyurina, R. M. Domingues, V. A. Tyurin et al., "Characterization of cardiolipins and their oxidation products by LC-MS analysis," *Chemistry and Physics of Lipids*, vol. 179, pp. 3–10, 2014.

[42] C. Ye, Z. Shen, and M. L. Greenberg, "Cardiolipin remodeling: a regulatory hub for modulating cardiolipin metabolism and function," *Journal of Bioenergetics and Biomembranes*, vol. 48, no. 2, pp. 113–123, 2016.

[43] K. Labbé, A. Murley, and J. Nunnari, "Determinants and functions of mitochondrial behavior," *Annual Review of Cell and Developmental Biology*, vol. 30, pp. 357–391, 2014.

[44] D. C. Logan, "The mitochondrial compartment," *Journal of Experimental Botany*, vol. 57, no. 6, pp. 1225–1243, 2006.

[45] D. A. Patten, J. Wong, M. Khacho et al., "OPA1-dependent cristae modulation is essential for cellular adaptation to metabolic demand," *The EMBO Journal*, vol. 33, no. 22, pp. 2676–2691, 2014.

[46] N. Ikon and R. O. Ryan, "Cardiolipin and mitochondrial cristae organization," *Biochimica et Biophysica Acta - Biomembranes*, vol. 1859, no. 6, pp. 1156–1163, 2017.

[47] D. C. Wallace, "Bioenergetics in human evolution and disease: implications for the origins of biological complexity and the missing genetic variation of common diseases," *Philosophical Transactions of the Royal Society of London Series B, Biological Sciences*, vol. 368, no. 1622, article 20120267, 2013.

[48] E. J. Lesnefsky, Q. Chen, and C. L. Hoppel, "Mitochondrial metabolism in aging heart.," *Circulation Research*, vol. 118, no. 10, pp. 1593–1611, 2016.

[49] Y. Huang, C. Powers, S. K. Madala et al., "Cardiac metabolic pathways affected in the mouse model of Barth syndrome," *PLoS One*, vol. 10, no. 6, article e0128561, 2015.

[50] M. Schlame and M. Ren, "The role of cardiolipin in the structural organization of mitochondrial membranes," *Biochimica et Biophysica Acta*, vol. 1788, no. 10, pp. 2080–2083, 2009.

[51] M. Rytömaa and P. K. Kinnunen, "Reversibility of the binding of cytochrome c to liposomes. Implications for lipid-protein interactions," *The Journal of Biological Chemistry*, vol. 270, no. 7, pp. 3197–3202, 1995.

[52] M. G. Mason, P. Nicholls, M. T. Wilson, and C. E. Cooper, "Nitric oxide inhibition of respiration involves both competitive (heme) and noncompetitive (copper) binding to cytochrome c oxidase," *Proceedings of the National Academy of Sciences of the United States of America*, vol. 103, no. 3, pp. 708–713, 2006.

[53] W. R. Fisher, H. Taniuchi, and C. B. Anfinsen, "On the role of heme in the formation of the structure of cytochrome c," *The Journal of Biological Chemistry*, vol. 248, no. 9, pp. 3188–3195, 1973.

[54] E. J. Snider, J. Muenzner, J. R. Toffey, Y. Hong, and E. V. Pletneva, "Multifaceted effects of ATP on cardiolipin-bound cytochrome c," *Biochemistry*, vol. 52, no. 6, pp. 993–995, 2013.

[55] V. E. Kagan, G. G. Borisenko, Y. Y. Tyurina et al., "Oxidative lipidomics of apoptosis: redox catalytic interactions of cytochrome _c_ with cardiolipin and phosphatidylserine," *Free Radical Biology & Medicine*, vol. 37, no. 12, pp. 1963–1985, 2004.

[56] A. V. Birk, W. M. Chao, C. Bracken, J. D. Warren, and H. H. Szeto, "Targeting mitochondrial cardiolipin and the cytochrome c/cardiolipin complex to promote electron transport and optimize mitochondrial ATP synthesis," *British Journal of Pharmacology*, vol. 171, no. 8, pp. 2017–2028, 2014.

[57] H. Zhou, S. Hu, Q. Jin et al., "Mff-dependent mitochondrial fission contributes to the pathogenesis of cardiac microvasculature ischemia/reperfusion injury via induction of mROS-mediated cardiolipin oxidation and HK2/VDAC1 disassociation-involved mPTP opening," *Journal of the*

American Heart Association, vol. 6, no. 3, article e005328, 2017.

[58] Z. Zhao, M. Wang, Y. Tian et al., "Cardiolipin-mediated procoagulant activity of mitochondria contributes to traumatic brain injury–associated coagulopathy in mice," *Blood*, vol. 127, no. 22, pp. 2763–2772, 2016.

[59] C. Zazueta, M. Franco, and F. Correa, "Hypothyroidism provides resistance to kidney mitochondria against the injury induced by renal ischemia-reperfusion," *Life Sciences*, vol. 80, no. 14, pp. 1252–1258, 2007.

[60] A. L. Duncan, J. J. Ruprecht, E. R. S. Kunji, and A. J. Robinson, "Cardiolipin dynamics and binding to conserved residues in the mitochondrial ADP/ATP carrier," *Biochimica et Biophysica Acta (BBA) – Biomembranes*, vol. 1860, no. 5, pp. 1035–1045, 2018.

[61] S. E. Gasanov, A. A. Kim, L. S. Yaguzhinsky, and R. K. Dagda, "Non-bilayer structures in mitochondrial membranes regulate ATP synthase activity," *Biochimica et Biophysica Acta (BBA) - Biomembranes*, vol. 1860, no. 2, pp. 586–599, 2018.

[62] S. Wen, K. Niedzwiecka, W. Zhao et al., "Identification of G8969>A in mitochondrial *ATP6* gene that severely compromises ATP synthase function in a patient with IgA nephropathy," *Scientific Reports*, vol. 6, no. 1, article 36313, 2016.

[63] A. Aperia, E. E. Akkuratov, J. M. Fontana, and H. Brismar, "Na^+-K^+-ATPase, a new class of plasma membrane receptors," *American Journal of Physiology Cell Physiology*, vol. 310, no. 7, pp. C491–C495, 2016.

[64] S. P. Soltoff, "ATP and the regulation of renal cell function," *Annual Review of Physiology*, vol. 48, pp. 9–31, 1986.

[65] F. K. Khalaf, P. Dube, A. Mohamed et al., "Cardiotonic steroids and the sodium trade balance: new insights into trade-off mechanisms mediated by the Na^+/K^+-ATPase," *International Journal of Molecular Sciences*, vol. 19, no. 9, article E2576, p. 2576, 2018.

[66] M. Cristóbal-García, F. E. García-Arroyo, E. Tapia et al., "Renal oxidative stress induced by long-term hyperuricemia alters mitochondrial function and maintains systemic hypertension," *Oxidative Medicine and Cellular Longevity*, vol. 2015, Article ID 535686, 8 pages, 2015.

[67] D. L. Galvan, N. H. Green, and F. R. Danesh, "The hallmarks of mitochondrial dysfunction in chronic kidney disease," *Kidney International*, vol. 92, no. 5, pp. 1051–1057, 2017.

[68] S. Liu, Y. Soong, S. V. Seshan, and H. H. Szeto, "Novel cardiolipin therapeutic protects endothelial mitochondria during renal ischemia and mitigates microvascular rarefaction, inflammation, and fibrosis," *American Journal of Physiology Renal Physiology*, vol. 306, no. 9, pp. F970–F980, 2014.

[69] H. H. Szeto, S. Liu, Y. Soong et al., "Mitochondria protection after acute ischemia prevents prolonged upregulation of IL-1β and IL-18 and arrests CKD," *Journal of the American Society of Nephrology*, vol. 28, no. 5, pp. 1437–1449, 2017.

[70] M. T. Sweetwyne, J. W. Pippin, D. G. Eng et al., "The mitochondrial-targeted peptide, SS-31, improves glomerular architecture in mice of advanced age," *Kidney International*, vol. 91, no. 5, pp. 1126–1145, 2017.

[71] S. Kume, T. Uzu, S. Araki et al., "Role of altered renal lipid metabolism in the development of renal injury induced by a high-fat diet," *Journal of the American Society of Nephrology*, vol. 18, no. 10, pp. 2715–2723, 2007.

[72] M. Herman-Edelstein, P. Scherzer, A. Tobar, M. Levi, and U. Gafter, "Altered renal lipid metabolism and renal lipid accumulation in human diabetic nephropathy," *Journal of Lipid Research*, vol. 55, no. 3, pp. 561–572, 2014.

[73] H. M. Kang, S. H. Ahn, P. Choi et al., "Defective fatty acid oxidation in renal tubular epithelial cells has a key role in kidney fibrosis development," *Nature Medicine*, vol. 21, no. 1, pp. 37–46, 2015.

[74] E. Niki, Y. Yoshida, Y. Saito, and N. Noguchi, "Lipid peroxidation: mechanisms, inhibition, and biological effects," *Biochemical and Biophysical Research Communications*, vol. 338, no. 1, pp. 668–676, 2005.

[75] C. L. Quinlan, R. L. Goncalves, M. Hey-Mogensen, N. Yadava, V. I. Bunik, and M. D. Brand, "The 2-oxoacid dehydrogenase complexes in mitochondria can produce superoxide/hydrogen peroxide at much higher rates than complex I," *The Journal of Biological Chemistry*, vol. 289, no. 12, pp. 8312–8325, 2014.

[76] V. I. Bunik, A. Artiukhov, A. Kazantsev et al., "Specific inhibition by synthetic analogs of pyruvate reveals that the pyruvate dehydrogenase reaction is essential for metabolism and viability of glioblastoma cells," *Oncotarget*, vol. 6, no. 37, pp. 40036–40052, 2015.

[77] V. E. Kagan, A. A. Kapralov, C. M. St. Croix et al., "Lung macrophages "digest" carbon nanotubes using a superoxide/peroxynitrite oxidative pathway," *ACS Nano*, vol. 8, no. 6, pp. 5610–5621, 2014.

[78] Y. Y. Tyurina, S. M. Poloyac, V. A. Tyurin et al., "A mitochondrial pathway for biosynthesis of lipid mediators," *Nature Chemistry*, vol. 6, no. 6, pp. 542–552, 2014.

[79] J. Tschopp and K. Schroder, "NLRP3 inflammasome activation: the convergence of multiple signalling pathways on ROS production?," *Nature Reviews Immunology*, vol. 10, no. 3, pp. 210–215, 2010.

[80] H. J. Anders and L. Schaefer, "Beyond tissue injury-damage-associated molecular patterns, toll-like receptors, and inflammasomes also drive regeneration and fibrosis," *Journal of the American Society of Nephrology*, vol. 25, no. 7, pp. 1387–1400, 2014.

[81] S. S. Iyer, W. P. Pulskens, J. J. Sadler et al., "Necrotic cells trigger a sterile inflammatory response through the Nlrp3 inflammasome," *Proceedings of the National Academy of Sciences of the United States of America*, vol. 106, no. 48, pp. 20388–20393, 2009.

[82] C. Kurts, U. Panzer, H. J. Anders, and A. J. Rees, "The immune system and kidney disease: basic concepts and clinical implications," *Nature Reviews Immunology*, vol. 13, no. 10, pp. 738–753, 2013.

[83] C. M. Turner, N. Arulkumaran, M. Singer, R. J. Unwin, and F. W. Tam, "Is the inflammasome a potential therapeutic target in renal disease?," *BMC Nephrology*, vol. 15, no. 1, p. 21, 2014.

[84] S. S. Iyer, Q. He, J. R. Janczy et al., "Mitochondrial cardiolipin is required for Nlrp3 inflammasome activation," *Immunity*, vol. 39, no. 2, pp. 311–323, 2013.

[85] A. Broder, J. J. Chan, and C. Putterman, "Dendritic cells: an important link between antiphospholipid antibodies, endothelial dysfunction, and atherosclerosis in autoimmune and non-autoimmune diseases," *Clinical Immunology*, vol. 146, no. 3, pp. 197–206, 2013.

[86] L. L. van den Hoogen, J. A. van Roon, T. R. Radstake, R. D. Fritsch-Stork, and R. H. Derksen, "Delineating the deranged immune system in the antiphospholipid syndrome," *Autoimmunity Reviews*, vol. 15, no. 1, pp. 50–60, 2016.

[87] J. J. Maguire, Y. Y. Tyurina, D. Mohammadyani et al., "Known unknowns of cardiolipin signaling: the best is yet to come," *Biochimica et Biophysica Acta (BBA) - Molecular and Cell Biology of Lipids*, vol. 1862, no. 1, pp. 8–24, 2017.

[88] J. Pollara, R. W. Edwards, L. Lin, V. A. Bendersky, and T. V. Brennan, "Circulating mitochondria in deceased organ donors are associated with immune activation and early allograft dysfunction," *JCI Insight*, vol. 3, no. 15, article 121622, 2018.

[89] S. I. Yamashita and T. Kanki, "How autophagy eats large mitochondria: autophagosome formation coupled with mitochondrial fragmentation," *Autophagy*, vol. 13, no. 5, pp. 980-981, 2017.

[90] J. D. Mancias and A. C. Kimmelman, "Mechanisms of selective autophagy in normal physiology and cancer," *Journal of Molecular Biology*, vol. 428, no. 9 Part A, pp. 1659–1680, 2016.

[91] C. T. Chu, H. Bayır, and V. E. Kagan, "LC3 binds externalized cardiolipin on injured mitochondria to signal mitophagy in neurons: implications for Parkinson disease," *Autophagy*, vol. 10, no. 2, pp. 376–378, 2014.

[92] M. A. Sani, O. Keech, P. Gardestrom, E. J. Dufourc, and G. Grobner, "Magic-angle phosphorus NMR of functional mitochondria: in situ monitoring of lipid response under apoptotic-like stress," *The FASEB Journal*, vol. 23, no. 9, pp. 2872–2878, 2009.

[93] N. Pallet, N. Bouvier, C. Legendre et al., "Autophagy protects renal tubular cells against cyclosporine toxicity," *Autophagy*, vol. 4, no. 6, pp. 783–791, 2008.

[94] R. L. Bick, "The antiphospholipid-thrombosis Syndromes:-Fact, fiction, Confusion, and controversy," *American Journal of Clinical Pathology*, vol. 100, no. 5, pp. 477–480, 1993.

[95] J. Y. Choi, J. H. Jung, S. Shin, Y. H. Kim, and D. J. Han, "Living donor renal transplantation in patients with antiphospholipid syndrome: a case report," *Medicine*, vol. 95, no. 46, article e541, 2016.

[96] J. P. Forman, J. Lin, M. Pascual, M. D. Denton, and N. Tolkoff-Rubin, "Significance of anticardiolipin antibodies on short and long term allograft survival and function following kidney transplantation," *American Journal of Transplantation*, vol. 4, no. 11, pp. 1786–1791, 2004.

[97] A. B. F. L. Cosimi and R. B. Colvin, "Renal thrombotic microangiopathy associated with anticardiolipin antibodies in hepatitis C-positive renal allograft recipients," *Journal of the American Society of Nephrology*, vol. 10, no. 1, pp. 146–153, 1999.

[98] P. Brunet, M. F. Aillaud, M. S. Marco et al., "Antiphospholipids in hemodialysis patients: relationship between lupus anticoagulant and thrombosis," *Kidney International*, vol. 48, no. 3, pp. 794–800, 1995.

[99] D. R. J. Arachchillage and M. Laffan, "Pathogenesis and management of antiphospholipid syndrome," *British Journal of Haematology*, vol. 178, no. 2, pp. 181–195, 2017.

[100] S. Sumitran-Karuppan, G. Tyden, F. Reinholt, U. Berg, and E. Moller, "Hyperacute rejections of two consecutive renal allografts and early loss of the third transplant caused by non-HLA antibodies specific for endothelial cells," *Transplantation Immunology*, vol. 5, no. 4, pp. 321–327, 1997.

[101] W. A. Wilson, A. E. Gharavi, T. Koike et al., "International consensus statement on preliminary classification criteria for definite antiphospholipid syndrome. Report of an international workshop," *Arthritis & Rheumatism*, vol. 42, no. 7, article 1309, 1311 pages, 1999.

[102] D. A. Triplett, "Antiphospholipid-protein antibodies: laboratory detection and clinical relevance," *Thrombosis Research*, vol. 78, no. 1, pp. 1–31, 1995.

[103] S. Bhandari, P. Harnden, A. M. Brownjohn, and J. H. Turney, "Association of anticardiolipin antibodies with intraglomerular thrombi and renal dysfunction in lupus nephritis," *QJM*, vol. 91, no. 6, pp. 401–409, 1998.

[104] M. Greaves, "Antiphospholipid antibodies and thrombosis," *The New England Journal of Medicine*, vol. 353, pp. 1348–1353, 1999.

[105] A. Tselepis, D. Tsoukatos, C. A. Demopoulos, and V. M. Kapoulas, "Effects of AGEPC on the intracellular levels of ions in Tetrahymena pyriformis," *Biochemistry International*, vol. 13, no. 6, pp. 999–1008, 1986.

[106] L. Silvestro, C. Ruikun, F. Sommer et al., "Platelet-Activating Factor-Induced endothelial cell expression of adhesion molecules and modulation of surface Glycocalyx, Evaluated by electron spectroscopy for chemical analysis," *Seminars in Thrombosis and Hemostasis*, vol. 20, no. 02, pp. 214–222, 1995.

[107] F. Garcia-Martin, A. De Arriba, and T. Carrascosa, "Anticardiolipin antibodies and lupus anticoagulant in end-stage renal disease," *Nephrology Dialysis Transplantation*, vol. 6, no. 8, pp. 543–547, 1991.

[108] M. Schlame, "Cardiolipin synthesis for the assembly of bacterial and mitochondrial membranes," *Journal of Lipid Research*, vol. 49, no. 8, pp. 1607–1620, 2008.

[109] A. V. Birk, S. Liu, Y. Soong et al., "The mitochondrial-targeted compound SS-31 re-energizes ischemic mitochondria by interacting with cardiolipin," *Journal of the American Society of Nephrology*, vol. 24, no. 8, pp. 1250–1261, 2013.

[110] C. Grönhagen-Riska, A. M. Teppo, A. Helanterä, E. Honkanen, and H. Julkunen, "Raised concentrations of antibodies to cardiolipin in patients receiving dialysis," *BMJ*, vol. 300, no. 6741, pp. 1696-1697, 1990.

[111] T. Sitter and H. Schiffl, "Anticardiolipin antibodies in patients on regular hemodialysis: an epiphenomenon?," *Nephron*, vol. 64, no. 4, pp. 655-656, 1993.

[112] B. L. Kasiske, C. Guijarro, Z. A. Massy, M. R. Wiederkehr, and J. Z. Ma, "Cardiovascular disease after renal transplantation," *Journal of the American Society of Nephrology*, vol. 7, p. 158, 1996.

[113] D. Ducloux, E. Bourrinet, G. Motte, and J. M. Chalopin, "Antiphospholipid antibodies as a risk factor for atherosclerotic events in renal transplant recipients," *Kidney International*, vol. 64, no. 3, pp. 1065–1070, 2003.

[114] D. A. Triplett, "Clinical significance of antiphospholipid antibodies," *Hemostasis Thrombosis Check Sample*, vol. 10, p. 1, 1988.

[115] B. Ferlazzo, A. Barrile, D. Bonanno et al., "Anticardiolipin antibodies in hemodialysis patients and in renal transplant recipients: prevalence and significance," *Recenti Progressi in Medicina*, vol. 89, no. 9, pp. 434–437, 1998.

[116] D. Nochy, E. Daugas, and D. Droz, "The intrarenal vascular lesions associated with primary antiphospholipid syndrome," *Journal of the American Society of Nephrology*, vol. 10, no. 3, pp. 507–518, 1999.

[117] C. M. Nzerue, K. Hewan-Lowe, S. Pierangeli, and E. N. Harris, ""Black swan in the kidney": renal involvement in

the antiphospholipid antibody syndrome," *Kidney International*, vol. 62, no. 3, pp. 733–744, 2002.

[118] G. Canaud, F. Bienaimé, L. H. Noël et al., "Severe vascular lesions and poor functional outcome in kidney transplant recipients with lupus anticoagulant antibodies," *American Journal of Transplantation*, vol. 10, no. 9, pp. 2051–2060, 2010.

[119] H. Lopez-Escribano, E. Miñambres, M. Labrador, M. J. Bartolomé, and M. López-Hoyos, "Induction of cell death by sera from patients with acute brain injury as a mechanism of production of autoantibodies," *Arthritis and Rheumatism*, vol. 46, no. 12, pp. 3290–3300, 2002.

[120] S. Vaidya, C. C. Wang, K. Gugliuzza, and J. C. Fish, "Relative risk of post transplant renal thrombosis in patients with antiphospholipid antibodies," *Clinical Transplantation*, vol. 12, p. 439, 1998.

[121] T. E. Starzl, H. J. Boehmig, H. Amemiya et al., "Clotting changes, including disseminated intravascular coagulation, during rapid renal-homograft rejection," *The New England Journal of Medicine*, vol. 283, no. 8, pp. 383–390, 1970.

[122] F. Rodriguez-Erdmann and R. D. Guttmann, "Coagulation in renal-allograft rejection," *The New England Journal of Medicine*, vol. 281, no. 25, p. 1428, 1969.

[123] A. Singh, D. Stablein, and A. Tejani, "Risk factors for vascular thrombosis in pediatric renal transplantation," *Transplantation*, vol. 63, no. 9, pp. 1263–1267, 1997.

[124] Y. Hasunuma, E. Matsuura, and Z. Makita, "Involvement of beta2-glycoprotein I and anticardiolipin antibodies in oxidatively modified low-density lipoprotein uptake by macrophages," *Clinical and Experimental Immunology*, vol. 107, no. 3, pp. 569–573, 1997.

[125] B. L. Kasiske, H. A. Chakkera, and J. Roel, "Explained and unexplained ischemic heart disease risk after renal transplantation," *Journal of the American Society of Nephrology*, vol. 11, pp. 1735–1740, 2000.

[126] K. El Zorkany, J. M. Bridson, A. Sharma, and A. Halawa, "Transplant renal vein thrombosis," *Experimental and Clinical Transplantation*, vol. 15, no. 2, pp. 123–129, 2017.

[127] A. Siedlecki, W. Irish, and D. C. Brennan, "Delayed graft function in the kidney transplant," *American Journal of Transplantation*, vol. 11, no. 11, pp. 2279–2296, 2011.

[128] A. Turrent-Carriles, J. P. Herrera-Félix, and M. C. Amigo, "Renal involvement in antiphospholipid syndrome," *Frontiers in Immunology*, vol. 9, p. 1008, 2018.

[129] C. Morath, J. Beimler, G. Opelz et al., "Living donor kidney transplantation in crossmatch-positive patients enabled by peritransplant immunoadsorption and anti-CD20 therapy," *Transplant International*, vol. 25, no. 5, pp. 506–517, 2012.

[130] A. Humar, E. M. Hohnson, K. J. Gillingham et al., "Venous thromboembolic complications after kidney and kidney-pancreas transplantation: a multivariate analysis," *Transplantation*, vol. 65, p. 229, 1998.

[131] A. Bouquegneau, S. Salam, P. Delanaye, R. Eastell, and A. Khwaja, "Bone disease after kidney transplantation," *Clinical Journal of the American Society of Nephrology*, vol. 11, no. 7, pp. 1282–1296, 2016.

[132] P. C. Piotrowski, A. Lutkowska, A. TsibulskA, M. Karczewski, and P. P. Jagodziński, "Neurologic complications in kidney transplant recipients," *Folia Neuropathologica*, vol. 2, no. 2, pp. 86–109, 2017.

[133] V. E. Kagan, P. Wipf, D. Stoyanovsky et al., "Mitochondrial targeting of electron scavenging antioxidants: regulation of selective oxidation vs random chain reactions," *Advanced Drug Delivery Reviews*, vol. 61, no. 14, pp. 1375–1385, 2009.

[134] B. Halliwell and S. Chirico, "Lipid peroxidation: its mechanism, measurement, and significance," *The American Journal of Clinical Nutrition*, vol. 57, no. 5, pp. 715S–725S, 1993, discussion 724S- 725S.

[135] A. Eirin, B. Ebrahimi, X. Zhang et al., "Mitochondrial protection restores renal function in swine atherosclerotic renovascular disease," *Cardiovascular Research*, vol. 103, no. 4, pp. 461–472, 2014.

[136] H. H. Szeto, S. Liu, Y. Soong, N. Alam, G. T. Prusky, and S. V. Seshan, "Protection of mitochondria prevents high-fat diet-induced glomerulopathy and proximal tubular injury," *Kidney International*, vol. 90, no. 5, pp. 997–1011, 2016.

[137] A. Eirin, B. Ebrahimi, S. H. Kwon et al., "Restoration of mitochondrial cardiolipin attenuates cardiac damage in swine renovascular hypertension," *Journal of the American Heart Association*, vol. 5, no. 6, article e003118, 2016.

[138] K. Nakahira, J. A. Haspel, V. A. Rathinam et al., "Autophagy proteins regulate innate immune responses by inhibiting the release of mitochondrial DNA mediated by the NALP3 inflammasome," *Nature Immunology*, vol. 12, no. 3, pp. 222–230, 2011.

[139] A. Vilaysane, J. Chun, M. E. Seamone et al., "The NLRP3 inflammasome promotes renal inflammation and contributes to CKD," *Journal of the American Society of Nephrology*, vol. 21, no. 10, pp. 1732–1744, 2010.

Hindawi
Oxidative Medicine and Cellular Longevity
Volume 2019, Article ID 9710208, 11 pages
https://doi.org/10.1155/2019/9710208

Research Article

MitoCLox: A Novel Mitochondria-Targeted Fluorescent Probe for Tracing Lipid Peroxidation

Konstantin G. Lyamzaev,[1] **Natalia V. Sumbatyan**,[2] **Alexey M. Nesterenko**,[1,3] **Ekaterina G. Kholina**,[4] **Natalia Voskoboynikova**,[5] **Heinz-Jürgen Steinhoff**,[5] **Armen Y. Mulkidjanian**,[1,5,6] **and Boris V. Chernyak**[1]

[1]*Belozersky Institute of Physico-Chemical Biology, Lomonosov Moscow State University, Moscow, Russia*
[2]*Department of Chemistry, Lomonosov Moscow State University, Moscow, Russia*
[3]*M.M. Shemyakin and Yu.A. Ovchinnikov Institute of Bioorganic Chemistry Russian Academy of Sciences, Moscow, Russia*
[4]*Department of Biology, Lomonosov Moscow State University, Moscow, Russia*
[5]*Department of Physics, University of Osnabrueck, D-49069 Osnabrueck, Germany*
[6]*Department of Bioengineering and Bioinformatics, Lomonosov Moscow State University, Moscow, Russia*

Correspondence should be addressed to Armen Y. Mulkidjanian; amulkid@uni-osnabrueck.de
and Boris V. Chernyak; bchernyak1@gmail.com

Received 30 June 2019; Accepted 12 September 2019; Published 13 November 2019

Academic Editor: Maria Isaguliants

Peroxidation of cardiolipin (CL) in the inner mitochondrial membrane plays a key role in the development of various pathologies and, probably, aging. The four fatty acid tails of CL are usually polyunsaturated, which makes CL particularly sensitive to peroxidation. Peroxidation of CL is involved in the initiation of apoptosis, as well as in some other important cellular signaling chains. However, the studies of CL peroxidation are strongly limited by the lack of methods for its tracing in living cells. We have synthesized a new mitochondria-targeted fluorescent probe sensitive to lipid peroxidation (dubbed MitoCLox), where the BODIPY fluorophore, carrying a diene-containing moiety (as in the C11-BODIPY (581/591) probe), is conjugated with a triphenylphosphonium cation (TPP^+) via a long flexible linker that contains two amide bonds. The oxidation of MitoCLox could be measured either as a decrease of absorbance at 588 nm or as an increase of fluorescence in the ratiometric mode at 520/590 nm (emission). In CL-containing liposomes, MitoCLox oxidation was induced by cytochrome c and developed in parallel with cardiolipin oxidation. TPP^+-based mitochondria-targeted antioxidant SkQ1, in its reduced form, inhibited oxidation of MitoCLox concurrently with the peroxidation of cardiolipin. Molecular dynamic simulations of MitoCLox in a cardiolipin-containing membrane showed affinity of positively charged MitoCLox to negatively charged CL molecules; the oxidizable diene moiety of MitoCLox resided on the same depth as the cardiolipin lipid peroxides. We suggest that MitoCLox could be used for monitoring CL oxidation in vivo and, owing to its flexible linker, also serve as a platform for producing peroxidation sensors with affinity to particular lipids.

1. Introduction

Mitochondria, as sources of reactive oxygen species (ROS), are major targets of oxidative damage. The inner mitochondrial membrane (IMM) is particularly sensitive to lipid peroxidation (LPO) since it harbors both ROS-producing respiratory enzymes and easily oxidizable lipids such as cardiolipin. The specific peroxidation of cardiolipin, which is exclusively located in the inner mitochondrial membrane, could play an important role in the regulation of some intracellular signaling pathways and in apoptosis [1–3]. The excessive LPO in the inner mitochondrial membrane could significantly contribute to various pathologies and to aging. Therefore, the prevention of LPO by mitochondria-targeted, membranophilic antioxidants has high therapeutic and anti-aging potency [4–6].

Studies of cardiolipin peroxidation are hindered by the absence of means to trace it in real time. Currently, such an analysis requires chromatographic and mass spectrometric techniques [7]. Our goal is to obtain a cardiolipin-specific fluorescent LPO probe(s). Such probes should be able to accumulate in mitochondria and have a specific affinity to CL. Earlier, Prime and colleagues developed a mitochondria-targeted fluorescent LPO probe, MitoPerOx [8]. In this probe, the BODIPY(581/591) moiety was conjugated with the membrane-penetrating triphenylphosphonium (TPP) cation by propionyl aminoethyl linker [8]. Generally, TPP-carrying compounds selectively accumulate in mitochondria being driven by the mitochondrial membrane potential (160–180 mV, negative inside) [9]. During the last decades, TPP^+ moieties were applied to deliver diverse antioxidants and fluorescent probes into mitochondria [5, 10, 11]. MitoPerOx was shown to accumulate in mitochondria and to report lipid peroxidation [8].

We also relayed on the widely used fluorescent LPO probe C11-BODIPY (581/591) that consists of a BODIPY fluorophore bearing a conjugated diene moiety sensitive to peroxidation and a C11-hydrocarbon tail as a membrane anchor [12]. The oxidation of the diene results in a strong increase in the fluorescence emission at 520 nm whereas the initial fluorescence at 590 nm decreases. These properties allow the application of C11-BODIPY (581/591) as a ratiometric dye. In addition, we were encouraged by data of Birk and colleagues who have shown that the SS-20 peptide (Phe-*D*-Arg-Phe-Lys-NH_2) could enter mitochondria and selectively target CL [13]. Because CL is the major negatively charged phospholipid in the mitochondrial membrane, a chimera of MitoPerOx and SS20 with several positive charges could show a specific affinity to cardiolipin and report its oxidation. Indeed, it was shown that TPP-containing compounds effectively displaced molecules of N-nonyl acridine orange (NAO), a specific cardiolipin probe, from mitochondrial membranes [14]. The affinity to cardiolipin might contribute to the effective prevention of cardiolipin oxidation by TPP-containing quinolic antioxidants and presumably underlay the high efficiency of TPP-based mitochondria-targeted antioxidants in various physiological models [2].

Here, we describe the synthesis and characterization of a new mitochondria-targeted lipid peroxidation probe MitoCLox where a BODIPY (581/591) fluorophore was conjugated with TPP residue using a long flexible linker that contained two peptide bonds to imitate the SS-20 peptide. This linker is currently used by us as a scaffold for inserting additional positive charges. MitoCLox reported the cytochrome c-dependent oxidation of CL in liposomes and did not interfere with the TPP-based mitochondria-targeted antioxidant SkQ1. Molecular dynamic simulations showed that the diene residue of MitoCLox was localized within the lipid bilayer next to the cardiolipin lipid peroxides and therefore should be efficiently oxidized by lipid radicals. The *in vivo* application of MitoCLox for the analysis of mitochondrial LPO in living cells is presented in a separate article (Lyamzaev et al. "The Novel Fluorescent Mitochondria-Targeted Probe MitoCLox Reports Lipid-Mediated Response to Oxidative Stress." *Oxid Med Cell Longev*, 2019, this issue).

2. Materials and Methods

2.1. Chemical Synthesis of MitoCLox. MitoCLox was synthesized from 4-difluoro-5-(4-phenyl-1,3-butadienyl)-4-bora-3a,4a-diaza-s-indacene-3-propionic acid succinimidyl ester (BODIPY581/591 SE) (Invitrogen Life Technologies) and {5-[(4-aminobutyl)amino]-5-oxopentyl}(triphenyl)phosphonium bromide (5) (Figure 1).

Initially, triphenylphosphine (TPP, 1) (1.0 g, 3.8 mmol) was condensed with 5-bromovaleric acid (2) (688 mg, 3.8 mmol) for 12 h at 85°C. The product (4-carboxybutyl)(triphenyl)phosphonium bromide (3) was purified on silica gel 60 using the chloroform-methanol mixture (4 : 1 (*v*/*v*)) as eluent to give the pure product with 90% yield (1.51 g). TLC: R_f (chloroform-MeOH, 4 : 1) 0.30; LC-MS: τ(HPLC) = 0.78 min(ACQUITY BEH C18 (2.1 × 50 mm, 1.7 μm) column (Waters); 0.5 ml/min, 20 mM formic acid, gradient 5-100% MeCN for 3 min); *m*/*z* calculated for $C_{23}H_{24}O_2P^+$, 363.2, found 363.2.

The product 3 was introduced (108 mg, 0.25 mmol) into the reaction with *tert*-butyl (4-aminobutyl)carbamate (4) (47 mg, 0.25 mmol) in the presence of 1.5 equivalents of N,N-dicyclohexylcarbodiimide (DCC, 78 mg, 0.375 mmol) and 2 equivalents of diisopropylethylamine (DIPEA, 0.085 ml, 0.5 mmol) in dichloromethane (1 ml, a small amount of DMF was added until completely dissolved) for 2 h under cooling and 12 h at room temperature. The reaction mixture was diluted with 20 ml of dichloromethane and 10 ml of 0.1 M aqueous HCl. Aqueous layer was extracted with dichloromethane (2 × 10 ml); combined organic layers were washed with water (2 × 5 ml), 5% solution of $NaHCO_3$ (1 × 5 ml), water (2 × 5 ml), and saturated NaCl (1 × 3 ml) and dried over anhydrous Na_2SO_4; and the volatiles were evaporated *in vacuo*. The residue was crystalized from the MeOH-diethyl ether mixture, and the product (tert-butyloxycarbonyl derivative of compound 5) was isolated from the precipitate on silica gel column eluting with solvent system dichloromethane: MeOH, 7 : 1. Yield: 100 mg (65%) TLC: R_f (chloroform – MeOH, 4 : 1) 0.70; R_f (chloroform-MeOH-water, 65 : 25 : 4) 0.65; LC-MS: τ(HPLC) = 1.06 min (ACQUITY BEH C18 (2.1 × 50 mm, 1.7 μm) column (Waters); 0.5 ml/min, 20 mM formic acid, gradient 5-100% MeCN for 3 min);*m*/*z*calculated for $C_{32}H_{42}N_2O_3P^+$, 533.29, found 533.2. To 27 mg (0.044 mmol) of the product 0.5 ml of 98% formic acid was added. The mixture was stirred for 6 h at room temperature and then evaporated *in vacuo*. The residue was dissolved in a minimal amount of methanol and treated with ether. The resulted precipitate was centrifuged and dried *in vacuo* to give the pure compound 5 as a thick colorless oil with 88% yield (20 mg). TLC: R_f (chloroform-MeOH-25% aqueous NH_3, 65 : 25 : 4) 0.10, R_f (chloroform-MeOH-water-ethyl acetate-25% aqueous NH_3, 336 : 130 : 17 : 5 : 10) 0.17; R_f (chloroform-MeOH-water, 65 : 25 : 4) 0.30; LC-MS: τ(HPLC) = 0.91 min (ACQUITY BEH C18 (2.1 × 50 mm, 1.7 μm) column; 0.5 ml/min, 20 mM formic acid, gradient 5-100% MeCN for 3 min); *m*/*z* calculated for $C_{27}H_{34}N_2OP+$, 433.2, found 433.4.

For the synthesis of MitoCLox, a solution of of compound 5 (3.2 mg, 6.15 μmol) in sodium bicarbonate buffer (0.1 N, pH 9.2,

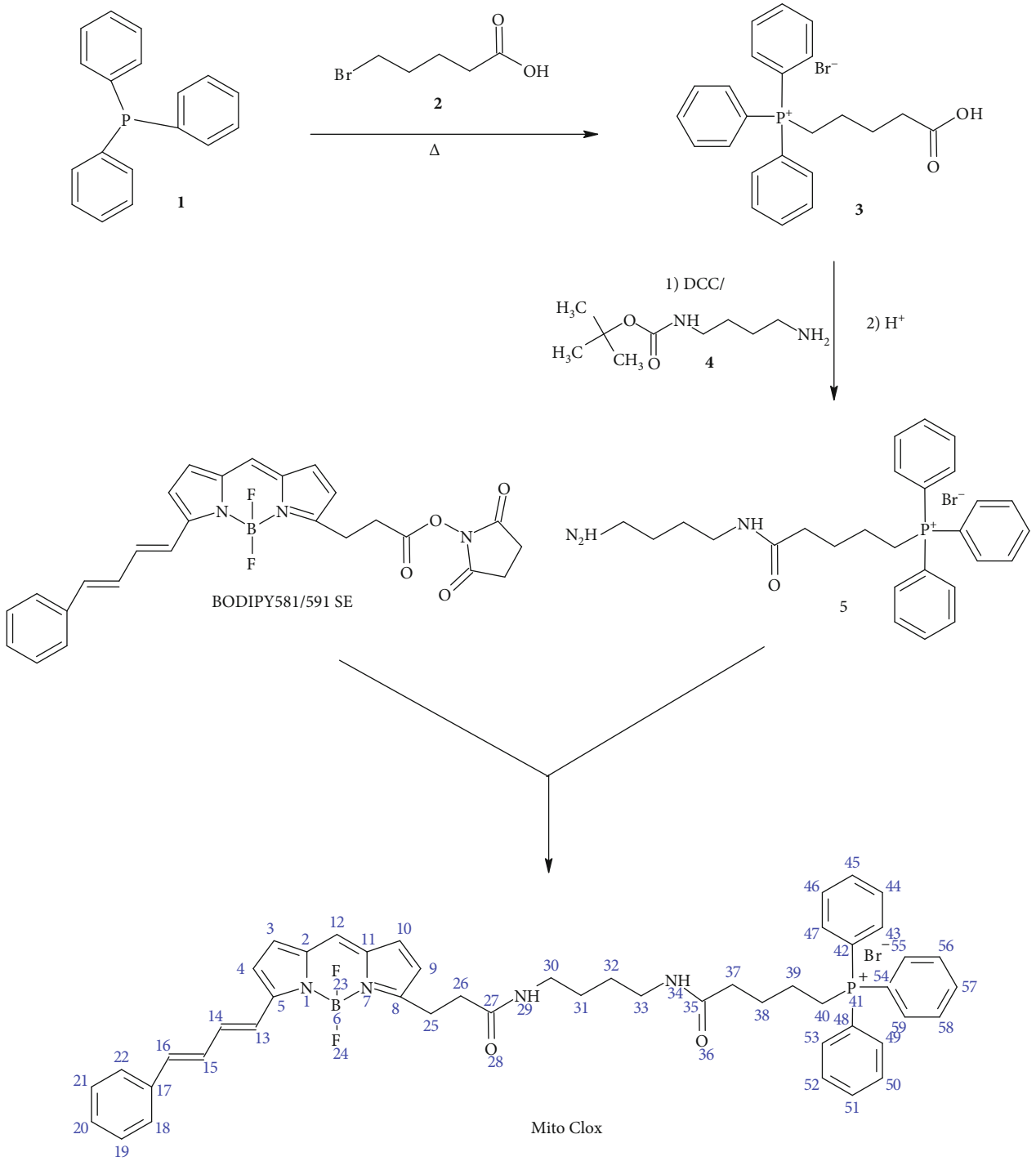

Figure 1: Scheme of chemical synthesis of MitoCLox.

0.2 ml) was added to the solution of BODIPY581/591 SE (2.0 mg, 4.1 μmol) in N-methylpyrrolidone (0.2 ml). The mixture was kept for 2 h at room temperature in the dark, and 0.1 M HCl was added to adjust pH 7.0. The product was extracted with dichloromethane (2 × 3 ml), washed with water (2 × 1 ml), dried, evaporated in vacuo, and separated on a silica gel by using a chloroform-methanol mixture (7 : 1 (v/v)) as an eluent. The pure product triphenyl(5-{[4-(4,4-difluoro-5-(4-phenyl-1,3-butadienyl)-4-bora-3a,4a-diaza-s-indacene-3-(propionylamino)butyl]amino}-5-oxopentyl) phosphonium chloride (MitoCLox) was obtained as a blue solid with 80% yield (2.8 mg). In some cases, additional purification was performed using a C18 column (10 × 250 mm, 5 μm bead size) at a 5 ml/min flow rate in 20-80% gradient of acetonitrile in 0.01% aqueous TFA for 20 min (τ = 16.5 min). TLC: R_f (chloroform-MeOH, 4 : 1) 0.65; R_f (chloroform-MeOH, 7 : 1) 0.29; UV (MeOH):λ_{max} = 585 nm, 347 nm, 334 nm; fluorescence (EtOH): λ_{ex} = 585 nm, λ_{em} =

595 nm; LC-MS: τ(HPLC) = 2.27 min (ACQUITY BEH C18 (2.1 × 50 mm, 1.7 μm) column; 0.5 ml/min, 20 mM formic acid, gradient 5-100% MeCN for 3 min); *m/z* calculated for $C_{49}H_{51}BF_2N_4O_2P^+$, 807.38, found 807.59; ^{1}H NMR (500.13 MHz, $CDCl_3$) δ ppm 0.91 (m, 8H, 31, 32, 38, 39), 1.11-1.79 (m, 8H, 25, 22, 29, 34, 37), 3.19-3.79 (m, 6H, 30, 33, 40), 6.41-7.23 (m, 9H, 13-16, 14, 15, 19, 21, 22), 7.41 (m, 5H, 18-22), 7.78 (m, 15H, 43-47, 49-53, 55-59). ^{13}C{^{1}H}-JMOD NMR (125.76 MHz, $CDCl_3$) δ ppm 29.51 (d, 1C, J = 165 Hz, 40), 29.71 (s, 4C, 31, 32, 38, 39), 31.94 (s, 1C, 25), 38.16 (s, 2C, 26, 37), 59.54 (s, 2C, 30, 33), 118.22 (d, 3C, J = 325 Hz, 42, 48, 54), 124.81 (s, 2C, 5, 8), 125.46-130.02 (m, 9C, 3, 4, 9, 10, 12, 13-16), 126.15 (s, 1C, 17), 128.20 (s, 2C, 2, 11), 130.79 (m, 6C, 43, 47, 49, 53, 55, 59), 134.30 (m, 3C, 45, 51, 57), 135.27 (m, 6C, 44, 46, 50, 52, 56, 58), 173.93 (bs, 2C, 27, 35).

2.2. Preparation of Cardiolipin Liposomes. The liposomes were produced by extrusion, based on the method of Hope and coworkers [15, 16], similar to our previous study [17]. Liposomes were prepared by suspending the CL from a bovine heart (Avanti Polar Lipids Inc., Alabaster, USA) as a powder at 3 mg/ml by 5 minutes of vortexing in a 50 mM sodium phosphate buffer (pH 7.4) containing 0.1 mM diethylenetriaminepentaacetic acid (buffer A) to bind possible traces of metals. Liposomes were obtained with a miniextruder equipped with two syringes (Avanti), each of 1 ml volume; a membrane with a pore diameter of 100 nm (Avanti) was used. The homogeneous lipid suspension was passed through the membrane 19 times. The liposome samples were stored on ice until use within the same day.

2.3. CL Oxidation in Liposomes. CL oxidation was initiated by cytochrome c (CytC) from an equine heart (Sigma-Aldrich, Cat. No. C2506). Liposomes in buffer A at a final CL concentration of 0.1 mM were incubated with CytC (1 μM) at 37°C in a 3 mL quartz cuvette inside the UV-2450 spectrophotometer (Shimadzu, Tokyo, Japan) equipped with a Peltier thermoelement. Oxidation of CL was monitored by changes in absorbance at 234 nm which correspond to the formation of conjugated dienes [18, 19]. The value of the molar absorptivity of conjugated dienes was taken as 27400 M^{-1} cm^{-1}. SkQ1 also absorbed in the UV range (with a maximum at 267 nm), and this absorbance decreased with reduction to $SkQ1H_2$; however, the "oxidized minus reduced" spectra had an isosbestic point close to 234 nm and therefore did not contribute to the absorbance changes at 234 nm. Spectra were recorded every 5 minutes at the wavelengths of 210–600 nm and against a reference cuvette containing the same components, except for CytC. SkQ1, MitoCLox, and the other additions were done to both chambers either initially or 30 minutes after the start of the experiment.

To reduce SkQ1 to the corresponding quinol ($SkQ1H_2$), 2-3 mg of dry sodium borohydride was added to 1-2 mM SkQ1 solution in ethanol. The excess of reductant was removed by a small volume of fuming HCl followed by at least two centrifugations at 15800 g (5 minutes each) to remove the sodium borate pellet. The reduced $SkQ1H_2$ was stored at −80°C until use.

2.4. Molecular Dynamic Modeling. For molecular dynamic modeling of the membrane bilayer, we used phospholipid composition close to that of the inner mitochondrial membrane [20]: 1-palmitoyl-2-linoleoyl-phosphatidylcholine(PLPC), 1-stearoyl-2-linoleoyl-phosphatidylcholine (SLPE), 1-palmitoyl-2-oleoyl-phosphatidylcholine (POPC), and tetralinoleoyl cardiolipin-cardiolipin (TLCL) mixed in the ratio of 7 : 21 : 7 : 8. The initial structure was prepared with a CHARMM-GUI server [21]. We used the CHARMM36 force field for simulation [22]. The force field of the dye was obtained from the *ab initio* density functional theory (DFT) calculations that were carried out with the Firefly package [23] using the 6-31G∗ basis set and the B3LYP5 functional. The package performed energy minimization in delocalized coordinates built as linear combinations of internal coordinates, with the rotating angle constrained, whereby the decision on which vectors do form the optimization subspace could affect the calculated energies. Thus, we deposited the protocol as well as the resulting rotating movie over calculated coordinates at each step (see the XYZ movie file) in the Github archive (https://git.io/JevG6).

The partial charges derived from quantum chemical calculations were implemented into the force field. Additionally, we parametrized dihedral angles around the bonds between diene carbons (C13-C14, C14-C15, and C15-C16 in Figure 1) of the phenyldiene tail. We calculated the potential energy surface and fit dihedral parameters to reproduce it in molecular dynamic (MD) simulations. Production MD simulations with 2-fs step in an NPT ensemble were of about 1000 ns; the preceding equilibration MD simulations were of about 100 ns.

To simulate CL mono-hydroperoxides, we modeled 8 variants of the oxidized molecule. There are four variants of hydroperoxides of linoleic acid [24]:

(1) 13-Hydroperoxy-(*E*,*E*)-octadeca-9,11-dienoic acid ("13EE")

(2) 13-Hydroperoxy-(*Z*,*E*)-octadeca-9,11-dienoic acid ("13ZE")

(3) 9-Hydroperoxy-(*E*,*E*)-octadeca-10,12-dienoic acid ("9EE")

(4) 9-Hydroperoxy-(*E*,*Z*)-octadeca-10,12-dienoic acid ("9EZ")

CL can carry oxidized glycero-1-acid or glycero-2-acid making the total amount of mono-peroxidized CL variants equal to eight.

To supplement the CHARMM force field, we performed *ab initio* calculations of the following small molecules:

(1) 7-Peroxy-(*E*,*E*)-nona-3,5-diene

(2) 7-Peroxy-(*Z*,*E*)-nona-3,5-diene

In both molecules, we calculated partial charges and the potential energy profile around the dihedral angle C3-C4-C5-C6.

Using the derived molecules, we constructed two model membranes: with four variants of CL with the peroxide at

the 9th position and with four variants with the peroxide at the 13th position.

The archives with MD simulation results are deposited at GitHub: https://github.com/comcon1/MitoMDMembranes.

3. Results and Discussion

3.1. Synthesis. MitoCLox was synthesized from 4-difluoro-5-(4-phenyl-1,3-butadienyl)-4-bora-3a,4a-diaza-s-indacene-3-propionic acid succinimidyl ester (BODIPY581/591 SE, Invitrogen Life Technologies) and {5-[(4-aminobutyl)amino]-5-ekoxopentyl}(triphenyl)phosphonium bromide (Figure 1). MitoCLox was synthesized in water-organic mixture (N-methylpyrrolidone/0.1 N sodium bicarbonate, pH 9.2) for 2 h at room temperature with the 80% yield after purification on silica gel. The structure was confirmed with 1H and 13C NMR spectra.

The fluorescence spectra of MitoCLox (reduced and oxidized forms) were measured in the liposomes (Figure 2) and did not differ from that of C11-BODIPY581/591 [8].

3.2. MitoCLox Oxidation in Cardiolipin Liposomes. CL oxidation in liposomes was initiated by cytochrome c (CytC) and monitored via changes in absorbance at 234 nm which correspond to the formation of conjugated dienes [17, 25]. The oxidation of MitoCLox was registered either by a decrease of absorbance at 581 nm (Figure 3) or by changes in MitoCLox fluorescence (Figures 2 and 4). The absorbance measurements were instrumental because they allowed us to concurrently follow the oxidation of the dye and the accumulation of conjugated dienes. Changes in fluorescence spectra of MitoCLox did not differ from those of C11-BODIPY581/591 indicating that the products of the probe oxidation by lipid radicals are similar. Kinetics of MitoCLox absorbance changes, and kinetics of conjugated diene formation measured in the same assay were linear during at least 50 min after the addition of CytC (Figures 3(c) and 3(d)). In these experiments, approximately 20% of CL was oxidized. These data indicate that MitoCLox oxidation is proportional to CL oxidation in a wide range of oxidized CL/reduced CL ratios. These observations also indicate that the generation of reactive CL radicals in reaction with CytC is much slower than the formation of CL diene conjugates and oxidation of MitoCLox.

We applied MitoCLox for the analysis of various antioxidants in CL-containing liposomes. It was found that tert-butylhydroquinone (TBHQ) efficiently prevented the MitoCLox oxidation induced by CytC (Figures 3(a)–3(d)). After the addition of TBHQ, conjugated dienes did not form anymore (Figures 3(a) and 3(c)) and the absorbance of MitoCLox at 581 nm did not change (Figures 3(b) and 3(d)).

It is important that the addition of MitoCLox did not affect the oxidation of CL as was confirmed by monitoring the formation of conjugated dienes (Figures 3(e) and 3(f)). These data demonstrate that MitoCLox neither interfered with interaction of CytC with CL nor scavenged linoleic peroxy radicals in CL to a notable extent.

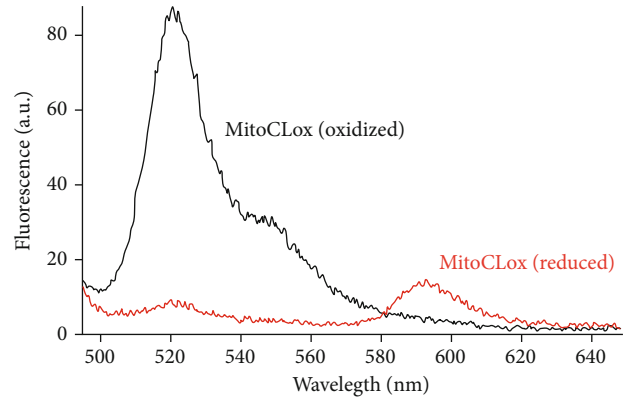

Figure 2: Fluorescence spectra of the oxidized (dark line) and reduced (red line) MitoCLox in CL-containing liposomes at 488 nm excitation. Oxidation of MitoCLox was induced by cytochrome c (for details, see Figure 3).

Figure 4 shows changes in the fluorescence of MitoCLox in a suspension of CL liposomes where peroxidation was induced by addition of CytC. Mitochondria-targeted antioxidant SkQ1 efficiently prevented the further MitoCLox oxidation induced by CytC (cf. Figures 4(a) and 4(b)). In the control experiments, the oxidized quinone form of SkQ1 did not affect the MitoCLox oxidation (Figure 4(c)). These data indicate that the cationic TPP residue of SkQ1 does not affect the interaction of MitoCLox with CL.

3.3. Molecular Dynamic Modeling. Dienes in phenyl-butadienyl residue of BODIPY581/591 are oxidized by chain-propagating species, especially derivatives of polyunsaturated fatty acids (PUFA) including $LO^{\cdot}$ and $LOO^{\cdot}$ [26]. Therefore, we studied the distribution of the dye in the model mitochondrial membrane by all-atom molecular dynamic simulation.

Ab initio potential energy surface (PES) scans of the MitoCLox molecule were performed using relaxed scan methodology implemented in Firefly v. 8+ as described in Materials and Methods. It is assumed that a relaxed surface scan gives lower energy values than a simple surface scan, and the resulting values are more close to the experimental ones.

To create the mechanical model including new dihedral angles, we first calculated charges by the RESP procedure. We calculated the charges for the PDT-BODIPY part (a) and TPP part (b) of the molecule separately (Figure 5). Then, we fit the dihedral parameters to bring the MD potential energy profile close to the *ab initio* profile. The MD profile was verified by rotational script that is deposited at Github (https://git.io/JevGX). This script performs a relaxed scan in MD by the following steps: (1) fixing the angle of interest at some value, (2) performing energy minimization with the angle fixed, (3) performing the mechanical energy calculation by one-step dynamic run, and (4) repeating from step (1) with a new angle value.

The only flexible part of the hydrophobic fragment is the butadienyl spacer between the BODIPY core and the phenyl group. Our *ab initio* calculations showed that some single

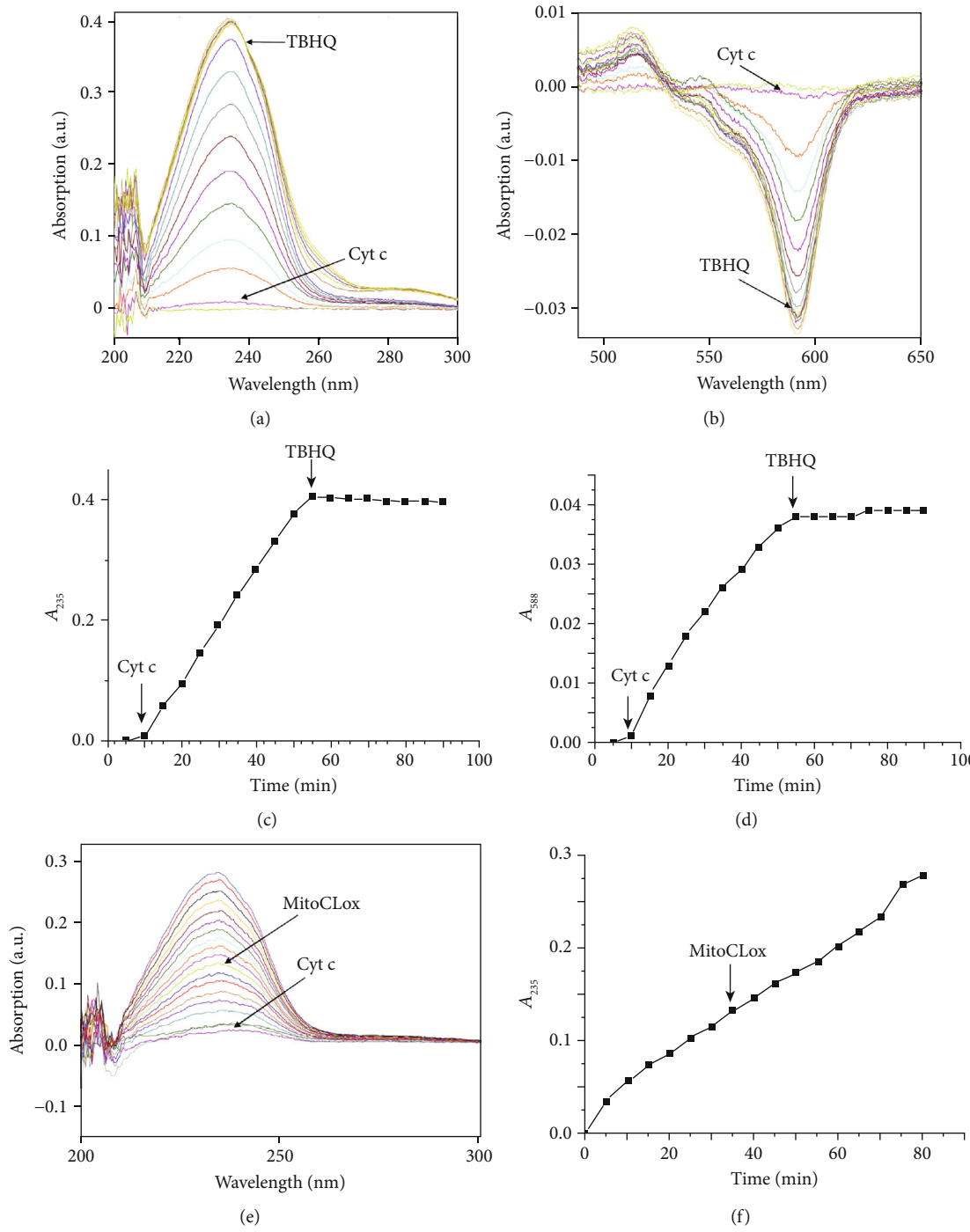

Figure 3: Cardiolipin oxidation in liposomes (100 μM) as induced by the addition of 1 μM cytochrome c. Additions are shown by arrows. (a, b) Absorbance spectra of liposomes around 235 nm (a, accumulation of diene conjugates) and around 595 nm (b, oxidation of MitoCLox); the arrow indicates the time of addition of the antioxidant tert-butylhydroquinone (TBHQ, 10 μM). (c, d) Kinetics of accumulation of diene conjugates (c) and of the oxidized form of MitoCLox (d); the arrow indicates the time of addition of the antioxidant tert-butylhydroquinone (TBHQ, 10 μM). (e, f) Effect of MitoCLox (300 nM, the addition is indicated by an arrow) on the rate of accumulation of dienes in cardiolipin liposomes upon stimulation of oxidation by cytochrome c (CytC, 1 μM).

bonds are relatively flexible (Figure 6) and that the dihedral angle around these bonds can change in the range of 50 degrees within the 2kT energy range. These *ab initio* results underlay our MD model of the dye; thus, the behavior of the classical model corresponded well to quantum estimations.

To analyze the mutual arrangement of MitoCLox and the surrounding lipids (especially CL), we simulated this dye in a bilayer of complex composition that resembled the inner mitochondrial membrane [20]. The model bilayer was composed of tetra-linoleoyl-cardiolipin (TLCL) and

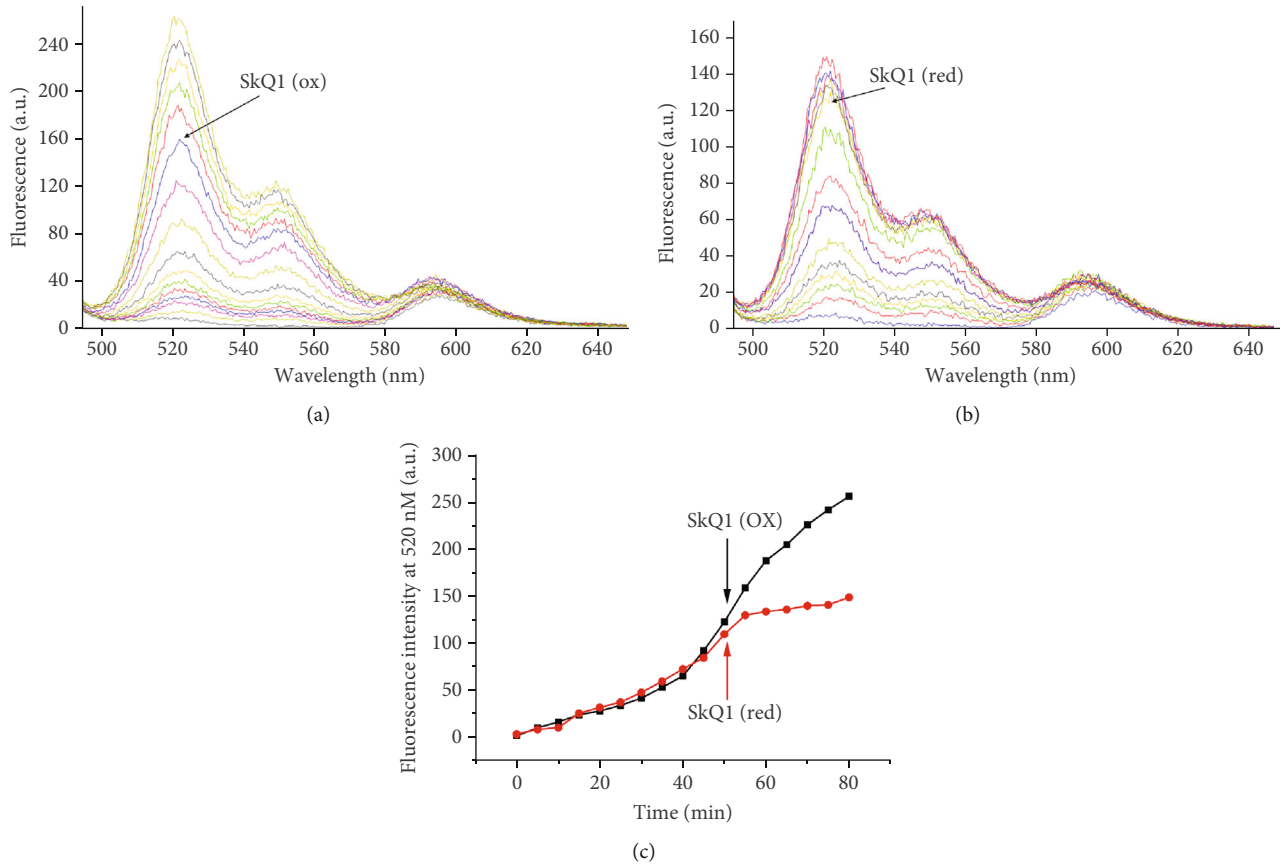

Figure 4: The effect of SkQ1 (1 μM) in its oxidized (a) or reduced (b) form on the peroxidation rate of cardiolipin liposomes (100 μM) as detected by MitoCLox (300 nM). (c) Kinetics of MitoCLox oxidation. The fluorescence of MitoCLox was measured with the excitation wavelength of 488 nm.

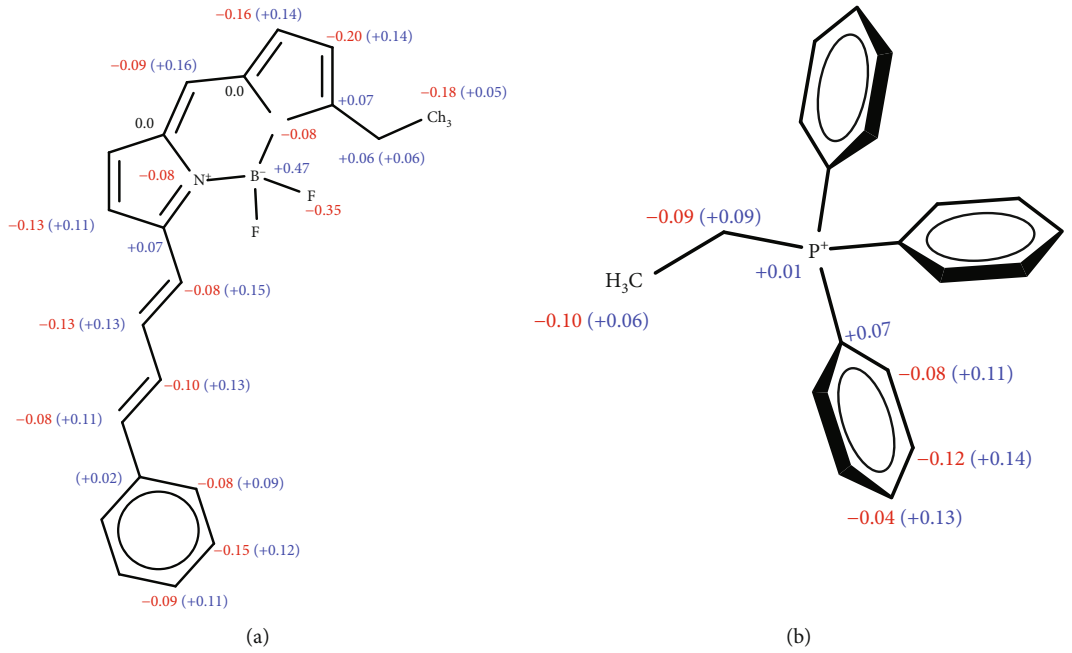

Figure 5: Partial charges of the molecular fragments calculated in order to develop the force field for the MitoCLox dye.

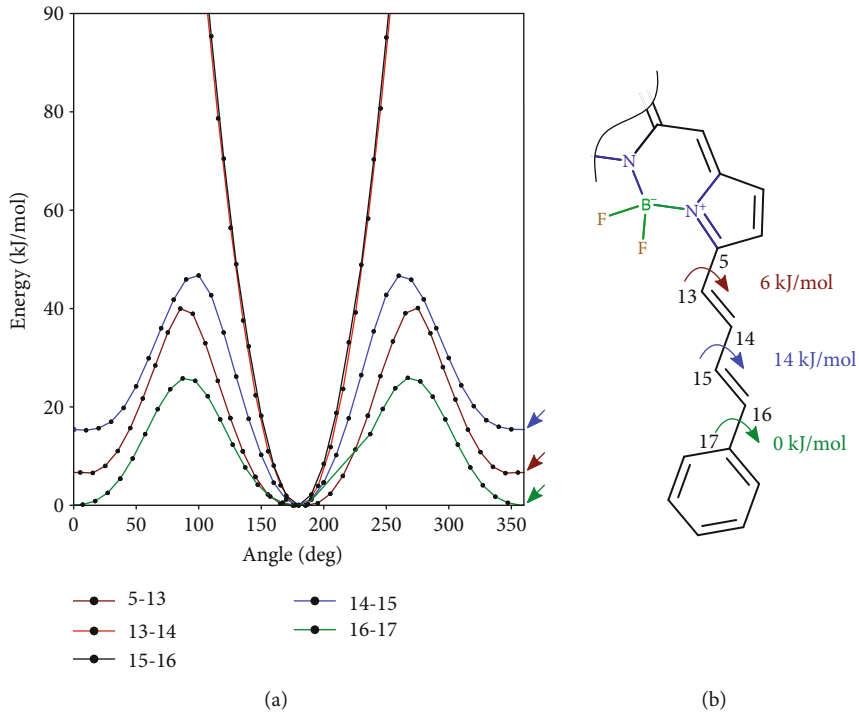

Figure 6: Potential energy surfaces (a) along the selected dihedral angles calculated as a relaxed scan with DFT (B3LYP5) using the 6-31G* basis set. The bond of rotation is indicated in the legend. The atom numbering is shown in (b) as well as cis-trans energy differences for single bonds (marked with arrows in (a)).

major zwitterionic phospholipids with choline and ethanolamine head groups (see Materials and Methods for details). Figure 7 illustrates the density distribution of some system components along the normal to the bilayer plane. The hydrophobic phenyl-butadienyl side chain (green dashed curve) is located in the region of acyl lipid residues whereas the BODIPY core, the linker, and TPP^+ (red dash-dotted curve) occupy the polar lipid head group region at the lipid/-water interface. The depth density distribution of the diene carbons of MitoCLox (blue dashed curve) significantly overlapped with the distribution of TLCL double bonds (gray dashed line), which are the targets of peroxide radicals. The analysis of the density distribution of MitoCLox parts along the normal to the bilayer plane demonstrates that the dye is L-shaped. The phenyl-butadienyl side chain is oriented approximately along the normal to the bilayer plane while the linker dwells in the plane of the membrane. In agreement with this conclusion, the molecular dynamic modeling revealed the similar density distribution for MitoPerOx (with a shorter linker, see [8]) in the same membrane (not shown).

Additionally, we checked the depth distribution of hydroperoxide moieties in the model of the oxidized membrane, where one linoleic acid in each CL molecule carried a hydroperoxide. We simulated separately the membranes containing CL with a hydroperoxide either at the 9th or at the 13th position (Figure 8). The depth distribution of the C9-hydroperoxide showed more overlap with the distribution of oxidizable diene in MitoCLox than that of the C13-hydroperoxide, which indicates that the hydroperoxide in the 9th position should be more efficient in oxidation of MitoCLox.

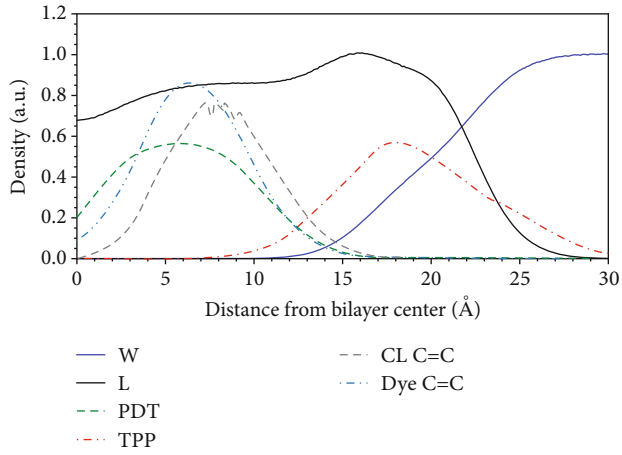

Figure 7: The density distributions of the following components at the bilayer-water interface: L: lipids; W: water; PDT: phenyl-butadienyl tail of the dye; TPP: TPP^+; CL C=C: double bonded carbons of CL; dye C=C: diene carbons of the dye. The density is averaged over 700 ns part of the MD simulation trajectory of the MitoCLox-containing system. The density values are given in different units to be visually comparable: in g/cm^3 (L, W), in $10\ g/cm^3$ (CL C=C), and in $10\ mol/cm^3$ (PDT, TPP, and dye C=C).

To study the interaction of the dye with different lipids, we analyzed the lateral distribution of CL and the most common phospholipid 1-stearoyl-2-linoleoyl-phosphatidylethanolamine (SLPE) in relation to the dye (Figure 9). Near the

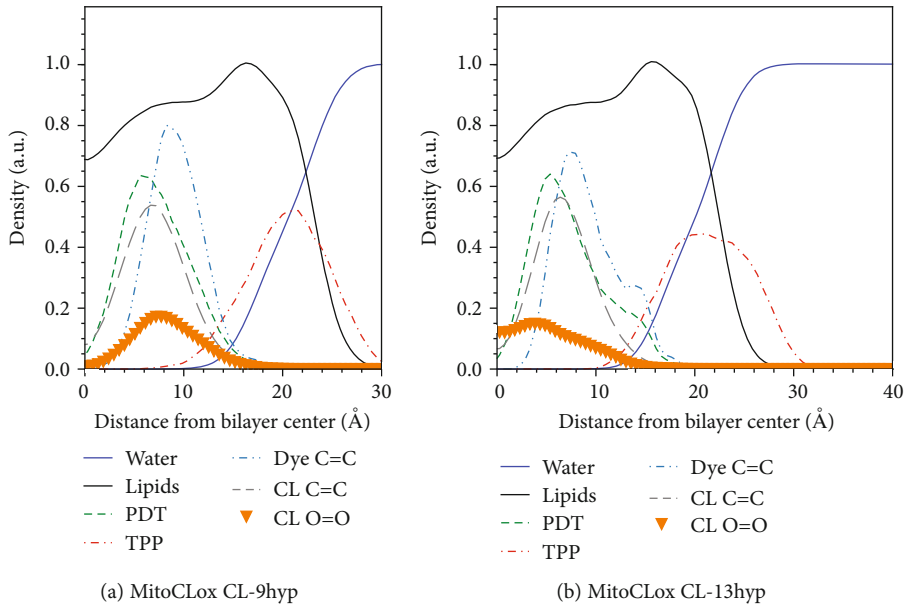

(a) MitoCLox CL-9hyp (b) MitoCLox CL-13hyp

Figure 8: The density distribution of parts of the MitoCLox and CL peroxide groups in two oxidized bilayer models, namely, with the mono-9-hydroperoxy-CL (a) and mono-13-hydroperoxy-CL (b). Only the monolayer containing the dye is shown. The distributions of the same groups of MitoCLox as in Figure 6 are shown. The distributions of the peroxide group of oxidized CL (CL O-O) and double bonded carbons of CL (CL C=C) are also depicted. The density is averaged as in Figure 6.

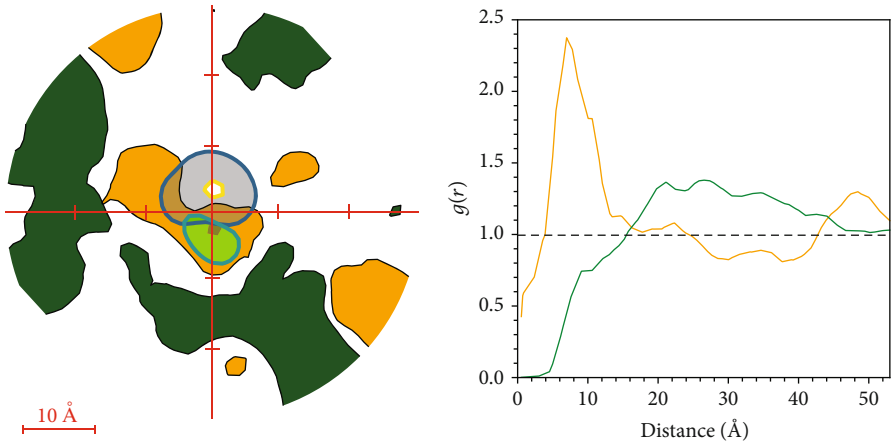

(a) (b)

Figure 9: Distribution of TLCL and SLPE lipids in MitoCLox-containing monolayer. (a) All frames are aligned according to the plane projection of phenyldiene→TPP^+ vector, which corresponds to the OY axis in the used coordinate system. For TLCL (orange) and SLPE (green), the areas with average concentration higher than 50% of the lipid concentration in the bilayer are plotted. Distributions of the phenyldiene tail (light green) and TPP (gray) are seen near the zero point. (b) Radial distribution function for dye-lipid distance measured between the phosphorus atom of TPP and C2 glycerol atom of TLCL (orange curve) or SLPE (green curve). This function was calculated over the trajectory of the MitoCLox simulation.

center of the top diagram, the distributions of the phenyl-butadienyl side chain (light green spot) and TPP (gray spot) are shown. We observed a highly populated area of CL (orange) near MitoCLox indicating a certain affinity of this dye to CL. For comparison, the areas highly populated with SLPE (dark green spots) are mostly located distantly from the dye indicating the absence of a specific affinity between SLPE and the dye. The same effect is clearly visible in plots of the radial distribution function of phosphorus atoms of TPP and the C_2 glycerol atom of CL. This plot for MitoCLox shows a peak at ~25 Å for SLPE and a peak at ~7 Å for TLCL (Figure 9(b)). A very similar lateral distribution of MitoCLox in relation to CL and SLPE was also observed in the model of an oxidized bilayer (not shown).

Being relatively rigid in the BODIPY-butadienyl part, the structure of MitoCLox is much more flexible in the linker

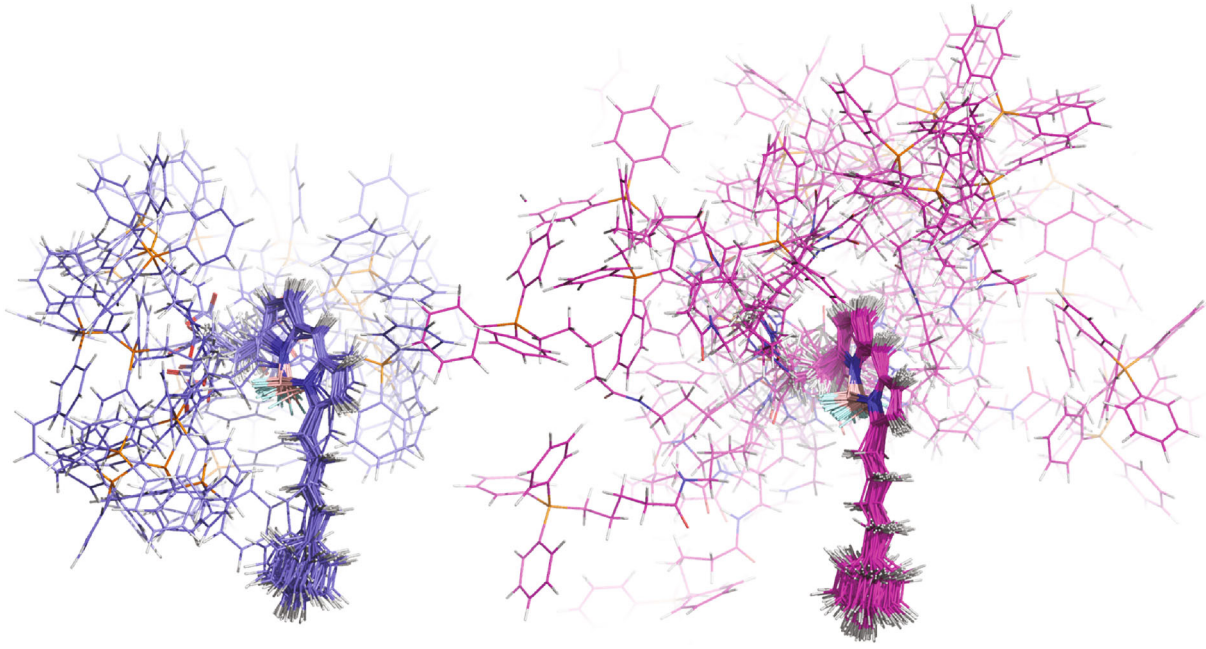

(a) (b)

Figure 10: Flexibility of MitoPerOx (a) and MitoCLox (b) during the simulation in the model membrane. Frames are fitted by the BODIPY core and phenyldiene tail. Centroids of all clusters built with RMSD cutoff 0.3 are presented simultaneously.

region in comparison with that of MitoPerOx (Figure 10). Such a high flexibility of the linker in the lipid bilayer might be important for interaction with CL molecules that are occluded within respiratory supercomplexes of the inner mitochondrial membrane [27].

4. Conclusions

Here, we show that MitoCLox reliably reports oxidation of CL in the membrane and, at the same time, does not quench the propagation of lipid radicals. The oxidation of MitoCLox could be prevented by mitochondria-targeted antioxidants concomitantly with the oxidation of CL. The observation that oxidized SkQ1 did not affect the oxidation of MitoCLox indicates that MitoCLox, in the *in vivo* experiments, could be combined with other TPP^+-carrying fluorescent probes without danger of interference of these probes with the interaction between MitoCLox and CL.

The results of the MD modeling demonstrate that the TPP^+ group of MitoCLox is located in the close proximity with the areas of CL high density in the bilayer. The results of MD simulations suggest that MitoCLox could reliably and, most likely, specifically react with CL radicals during membrane peroxidation. Higher flexibility of MitoCLox in comparison with MitoPerOx could enable its interaction even with those CL molecules that are occluded within respiratory supercomplexes [3, 25, 28–30].

Data Availability

The web archives references for the data used to support the findings of this study are included within the article.

Conflicts of Interest

There are no conflicts of interest.

Acknowledgments

Very useful discussions with Prof. V.P. Skulachev are greatly appreciated. The work was supported by the grant from the Russian Science Foundation (No. 17-14-01314), as well as by the Russian Presidential Scholarship (No. 5511.2018.4) (to AMN). K.L. would like to thank the German Academic Exchange Service (DAAD) and its Ostpartnerschaften Programm for the support. The molecular dynamic modeling was partly supported by the Russian Foundation for Basic Research (Grant No. 17-00-00088). Experiments with CL liposomes were supported by the German Research Foundation (DFG) (Project #STE640/15 to H.-J.S.). We acknowledge the support from Deutsche Forschungsgemeinschaft (DFG) and the Open Access Publishing Fund of Osnabrück University. The simulations were performed on the SMP computers of the Division of Biophysics and Computer Science of Complex Systems at the Department of Biophysics (School of Biology, Lomonosov Moscow State University).

References

[1] J. J. Maguire, Y. Y. Tyurina, D. Mohammadyani et al., "Known unknowns of cardiolipin signaling: the best is yet to come," *Biochimica et Biophysica Acta (BBA) - Molecular and Cell Biology of Lipids*, vol. 1862, no. 1, pp. 8–24, 2017.

[2] V. P. Skulachev, Y. N. Antonenko, D. A. Cherepanov et al., "Prevention of cardiolipin oxidation and fatty acid cycling as two antioxidant mechanisms of cationic derivatives of

plastoquinone (SkQs)," *Biochimica et Biophysica Acta (BBA) - Bioenergetics*, vol. 1797, no. 6-7, pp. 878–889, 2010.

[3] A. Y. Mulkidjanian, D. N. Shalaeva, K. G. Lyamzaev, and B. V. Chernyak, "Does oxidation of mitochondrial cardiolipin trigger a chain of antiapoptotic reactions?," *Biochemistry*, vol. 83, no. 10, pp. 1263–1278, 2018.

[4] R. A. J. Smith, C. M. Porteous, C. V. Coulter, and M. P. Murphy, "Selective targeting of an antioxidant to mitochondria," *European Journal of Biochemistry*, vol. 263, no. 3, pp. 709–716, 1999.

[5] V. P. Skulachev, "Cationic antioxidants as a powerful tool against mitochondrial oxidative stress," *Biochemical and Biophysical Research Communications*, vol. 441, no. 2, pp. 275–279, 2013.

[6] M. V. Skulachev and V. P. Skulachev, "Programmed aging of mammals: proof of concept and prospects of biochemical approaches for anti-aging therapy," *Biochemistry*, vol. 82, no. 12, pp. 1403–1422, 2017.

[7] Y. Y. Tyurina, V. A. Tyurin, T. Anthonymuthu et al., "Redox lipidomics technology: looking for a needle in a haystack," *Chemistry and Physics of Lipids*, vol. 221, pp. 93–107, 2019.

[8] T. A. Prime, M. Forkink, A. Logan et al., "A ratiometric fluorescent probe for assessing mitochondrial phospholipid peroxidation within living cells," *Free Radical Biology and Medicine*, vol. 53, no. 3, pp. 544–553, 2012.

[9] E. A. Liberman, V. P. Topaly, L. M. Tsofina, A. A. Jasaitis, and V. P. Skulachev, "Mechanism of coupling of oxidative phosphorylation and the membrane potential of mitochondria," *Nature*, vol. 222, no. 5198, pp. 1076–1078, 1969.

[10] V. P. Skulachev, V. N. Anisimov, Y. N. Antonenko et al., "An attempt to prevent senescence: a mitochondrial approach," *Biochimica et Biophysica Acta (BBA) - Bioenergetics*, vol. 1787, no. 5, pp. 437–461, 2009.

[11] A. T. Hoye, J. E. Davoren, P. Wipf, M. P. Fink, and V. E. Kagan, "Targeting mitochondria," *Accounts of Chemical Research*, vol. 41, no. 1, pp. 87–97, 2008.

[12] E. H. W. Pap, G. P. C. Drummen, V. J. Winter et al., "Ratio-fluorescence microscopy of lipid oxidation in living cells using C11-BODIPY$^{581/591}$," *FEBS Letters*, vol. 453, no. 3, pp. 278–282, 1999.

[13] A. V. Birk, W. M. Chao, S. Liu, Y. Soong, and H. H. Szeto, "Disruption of cytochrome c heme coordination is responsible for mitochondrial injury during ischemia," *Biochimica et Biophysica Acta (BBA) - Bioenergetics*, vol. 1847, no. 10, pp. 1075–1084, 2015.

[14] Y. N. Antonenko, A. V. Avetisyan, L. E. Bakeeva et al., "Mitochondria-targeted plastoquinone derivatives as tools to interrupt execution of the aging program. 1. Cationic plastoquinone derivatives: synthesis and *in vitro* studies," *Biochemistry*, vol. 73, no. 12, pp. 1273–1287, 2008.

[15] M. J. Hope, M. B. Bally, G. Webb, and P. R. Cullis, "Production of large unilamellar vesicles by a rapid extrusion procedure. Characterization of size distribution, trapped volume and ability to maintain a membrane potential," *Biochimica et Biophysica Acta (BBA) - Biomembranes*, vol. 812, no. 1, pp. 55–65, 1985.

[16] L. D. Mayer, M. J. Hope, and P. R. Cullis, "Vesicles of variable sizes produced by a rapid extrusion procedure," *Biochimica et Biophysica Acta (BBA) - Biomembranes*, vol. 858, no. 1, pp. 161–168, 1986.

[17] A. V. Lokhmatikov, N. E. Voskoboynikova, D. A. Cherepanov et al., "Prevention of peroxidation of cardiolipin liposomes by quinol-based antioxidants," *Biochemistry*, vol. 79, no. 10, pp. 1081–1100, 2014.

[18] R. C. R. M. Vossen, M. C. E. Vandammieras, G. Hornstra, and R. F. A. Zwaal, "Continuous monitoring of lipid peroxidation by measuring conjugated diene formation in an aqueous liposome suspension," *Lipids*, vol. 28, no. 9, pp. 857–861, 1993.

[19] N. Noguchi, H. Yamashita, N. Gotoh, Y. Yamamoto, R. Numano, and E. Niki, "2,2′-Azobis (4-methoxy-2,4-dimethylvaleronitrile), a new lipid-soluble azo initiator: application to oxidations of lipids and low-density lipoprotein in solution and in aqueous dispersions," *Free Radical Biology and Medicine*, vol. 24, no. 2, pp. 259–268, 1998.

[20] J. Comte, B. Maisterrena, and D. C. Gautheron, "Lipid composition and protein profiles of outer and inner membranes from pig heart mitochondria. Comparison with microsomes," *Biochimica et Biophysica Acta (BBA) - Biomembranes*, vol. 419, no. 2, pp. 271–284, 1976.

[21] E. L. Wu, X. Cheng, S. Jo et al., "CHARMM-GUI membrane builder toward realistic biological membrane simulations," *Journal of Computational Chemistry*, vol. 35, no. 27, pp. 1997–2004, 2014.

[22] J. B. Klauda, R. M. Venable, J. A. Freites et al., "Update of the CHARMM all-atom additive force field for lipids: validation on six lipid types," *The Journal of Physical Chemistry B*, vol. 114, no. 23, pp. 7830–7843, 2010.

[23] A. A. Granovsky, "Firefly version 8," http://classic.chem.msu.su/gran/firefly/index.html.

[24] H. Iwahashi, T. Hirai, and K. Kumamoto, "High performance liquid chromatography/electron spin resonance/mass spectrometry analyses of radicals formed in an anaerobic reaction of 9- (or 13-) hydroperoxide octadecadienoic acids with ferrous ions," *Journal of Chromatography A*, vol. 1132, no. 1-2, pp. 67–75, 2006.

[25] A. V. Lokhmatikov, N. Voskoboynikova, D. A. Cherepanov et al., "Impact of antioxidants on cardiolipin oxidation in liposomes: why mitochondrial cardiolipin serves as an apoptotic signal?," *Oxidative Medicine and Cellular Longevity*, vol. 2016, Article ID 8679469, 19 pages, 2016.

[26] G. P. Drummen, L. C. van Liebergen, J. A. Op den Kamp, and J. A. Post, "C11-BODIPY$^{581/591}$, an oxidation-sensitive fluorescent lipid peroxidation probe: (micro)spectroscopic characterization and validation of methodology," *Free Radical Biology and Medicine*, vol. 33, no. 4, pp. 473–490, 2002.

[27] T. Althoff, D. J. Mills, J. L. Popot, and W. Kuhlbrandt, "Arrangement of electron transport chain components in bovine mitochondrial supercomplex $I_1III_2IV_1$," *The EMBO Journal*, vol. 30, no. 22, pp. 4652–4664, 2011.

[28] K. Pfeiffer, V. Gohil, R. A. Stuart et al., "Cardiolipin stabilizes respiratory chain supercomplexes," *Journal of Biological Chemistry*, vol. 278, no. 52, pp. 52873–52880, 2003.

[29] S. Bazan, E. Mileykovskaya, V. K. Mallampalli, P. Heacock, G. C. Sparagna, and W. Dowhan, "Cardiolipin-dependent reconstitution of respiratory supercomplexes from purified *Saccharomyces cerevisiae* complexes III and IV," *The Journal of Biological Chemistry*, vol. 288, no. 1, pp. 401–411, 2013.

[30] E. Mileykovskaya and W. Dowhan, "Cardiolipin-dependent formation of mitochondrial respiratory supercomplexes," *Chemistry and Physics of Lipids*, vol. 179, pp. 42–48, 2014.

Hindawi
Oxidative Medicine and Cellular Longevity
Volume 2019, Article ID 3849692, 14 pages
https://doi.org/10.1155/2019/3849692

Review Article

Astaxanthin: A Potential Mitochondrial-Targeted Antioxidant Treatment in Diseases and with Aging

Mónika Sztretye,[1] Beatrix Dienes,[1] Mónika Gönczi,[1] Tamás Czirják,[1] László Csernoch,[1] László Dux,[2] Péter Szentesi,[1] and Anikó Keller-Pintér[2]

[1]*Department of Physiology, Faculty of Medicine, University of Debrecen, Debrecen H-4002, Hungary*
[2]*Department of Biochemistry, Faculty of Medicine, University of Szeged, Szeged H-6720, Hungary*

Correspondence should be addressed to Péter Szentesi; szentesi.peter@med.unideb.hu
and Anikó Keller-Pintér; keller.aniko@med.u-szeged.hu

Received 19 April 2019; Accepted 30 August 2019; Published 11 November 2019

Guest Editor: Konstantin Lyamzaev

Oxidative stress is characterized by an imbalance between prooxidant and antioxidant species, leading to macromolecular damage and disruption of redox signaling and cellular control. It is a hallmark of various diseases including metabolic syndrome, chronic fatigue syndrome, neurodegenerative, cardiovascular, inflammatory, and age-related diseases. Several mitochondrial defects have been considered to contribute to the development of oxidative stress and known as the major mediators of the aging process and subsequent age-associated diseases. Thus, mitochondrial-targeted antioxidants should prevent or slow down these processes and prolong longevity. This is the reason why antioxidant treatments are extensively studied and newer and newer compounds with such an effect appear. Astaxanthin, a xanthophyll carotenoid, is the most abundant carotenoid in marine organisms and is one of the most powerful natural compounds with remarkable antioxidant activity. Here, we summarize its antioxidant targets, effects, and benefits in diseases and with aging.

1. Introduction

The extended human life span over the past decades is causing the world's population to age. Accordingly, the prevalence of chronic diseases, cognitive decline, and disability increases in the aged population [1]. The first theory to explain the cellular and molecular background of aging was the Free Radical Theory of Aging (FRTA), proposed in the 1950's [2], and has become one of the most studied theories. The basic idea of this theory is that reactive oxygen species and free radicals generated during physiological metabolism and arising from reactions to exogenous factors initiate degradation of biomolecules and the progressive accumulation of these cellular damages ultimately results in aging and age-related diseases. Because of increasing inconsistent evidence, it is now accepted that this theory in its original form or its variants cannot alone explain the aging process [3, 4]. Nevertheless, FRTA cannot be rejected in its entirety, since an impressive amount of data indicates that reactive oxygen species- (ROS-) mediated aging phenotypes and age-related disorders (aside from spontaneous errors in signaling pathways and reactions of metabolites, e.g., reactive aldehydes and sugars) [5–10] exist.

In normal metabolic cells, the production of reactive oxygen and nitrogen species (ROS/RNS) from several sources and their removal by antioxidant systems, including endogenous or exogenous antioxidant molecules, are very precisely balanced. Mitochondria play a major role in supporting the redox balance, so maintaining the structural and functional integrity of these organelles is essential for normal cellular function. At physiological concentrations, ROS/RNS are crucial in signaling processes. These ROS/RNS are produced at very low levels, and the damage caused is almost instantly repaired. The antioxidant enzymes within the cells like catalase, superoxide dismutase (SOD), lactoperoxidases, and glutathione peroxidase inhibit the production

of such free radicals and thus present a protecting effect on cells maintaining the balance.

Oxidative stress is defined as an imbalance between prooxidants and antioxidants, resulting in macromolecular damage and disruption of redox signaling and cellular control [11]. Prooxidants are factors that help to generate ROS, which in turn destroy cellular macromolecules, i.e., induce protein oxidation, lipid peroxidation, and DNA damage [12]. mtDNA due to its proximity to the site of ROS production was thought to be intrinsically vulnerable [13]. By contrast, antioxidants reduce oxidative stress, since they act to counter or reduce the effects of ROS [14].

Mitochondrial defects have been proposed to contribute to the development of oxidative stress-related diseases [15, 16]. Impaired mitochondrial function has been involved in various human diseases; particularly, it is considered as the main mediator of the aging process and subsequent age-related diseases [17, 18]. If the reactions of free radicals and other oxygen species contribute to accumulation of molecular damages giving rise to aging and age-related diseases, antioxidants should prevent or slow down these processes and prolong longevity. Based on this assumption, a huge amount of studies were established and aimed at estimating the effect of the level of endogenous antioxidants and/or of the administration of exogenous antioxidants on aging and age-related processes and diseases.

The antioxidant's positive effects are verified by the experimental biological observations which have found that long-term administration of vitamin C decreased the isoprostane levels in rats [19]. Vitamin C was shown to decrease the α-tocopheroxyl level in membranes or low-density lipoprotein (LDL) and inhibits α-tocopheroxyl radical-mediated propagation [20]. The protective effect of vitamin E against oxidative damage was also demonstrated. It is explained by its direct action on a variety of oxygen radicals. The mechanism of action of antioxidants seems to be widespread: they might directly neutralize free radicals, they quench iron which subsequently decrease ROS production, and they decrease the concentration of peroxide and restore oxidized membranes [21]. Antioxidants are considered as a chemical to be able to induce antioxidant gene expression, to prevent LDL cholesterol from oxidation and provide the brain, the heart, and the liver with antiapoptotic protection [22].

Carotenoids have gained special interest during the last decades, due to their strong antioxidant, repairing, antiproliferative, anti-inflammatory, and potential antiaging effects. They can be used to prevent oxidative stress-related diseases and chronic inflammation. Astaxanthin is one of the most powerful carotenoid on the market. In this review, special focus is oriented towards these compounds.

2. The Mode of Action of Retinoids

Vitamin A (retinol) and its derivatives with or without biological activity, collectively referred to as retinoids, are crucial for normal development and homeostasis of vertebrates. The only source of retinoids is through diet (milk, liver, and eggs), because these compounds cannot be synthesized *de novo*

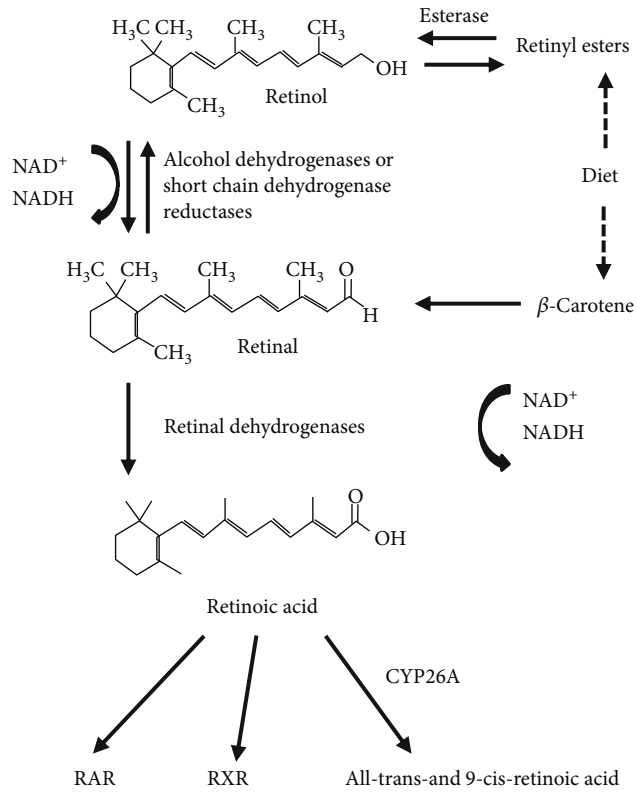

Figure 1: The retinoid conversion cascade.

[23]. Retinoids have long been appreciated as essential factors for controlling the differentiation program of certain epithelial cells and for their benefic effects on vision, growth, reproduction, and resistance to infection [24]. The predominant natural retinoid in circulation is retinol that is transported at high concentrations (micromolar levels) via the serum bound to retinol-binding protein (RBP), and from there, it can be taken up by any cell for storage or potential conversion into retinoic acid (RA). Once inside, the cell retinol is converted into retinal via a reversible reaction catalyzed by short-chain dehydrogenase/reductases (SDRs). In this reaction, the first step is the conversion to retinaldehyde with the concomitant generation of NADH, and lastly, the formation of retinoic acid by cytosolic aldehyde dehydrogenases (Figure 1). Retinoic acid can bind to and activate nuclear hormone receptors (retinoic acid receptor (RAR) and retinoid X receptor (RXR)). Three different RXR isotypes (RXR α, β, and γ) have been reported so far [25, 26]. RXRγ has limited tissue expression including high levels in the brain, anterior pituitary, and skeletal muscle [27].

Retinoic acid, the active metabolite of vitamin A, has notable effects on lipid and energy metabolism by modulating the phosphorylation state of AMPK and Akt [28] and the rate of glucose uptake in L6 myotubes [29]. Treatment of mice with all-trans retinoic acid (atRA) was described to reduce body weight and adiposity independently of changes in food intake, improved insulin sensitivity, and glucose tolerance in lean and obese mice [30, 31] and was found to promote skeletal muscle fatty acid oxidation [32] and irisin production in skeletal muscles [32].

SDRs are ubiquitary expressed and constitute a large protein family involved in the reduction of a variety of substrates. SRP-35 (Sarcoplasmic Reticulum Protein of 35 kDa) was identified using a proteomic approach by Treves et al. [33], and it belongs to the DHRS7C subfamily [34]. In muscle cells, using retinol as its substrate, SRP-35 was proposed as a target to affect glucose metabolism in human patients with metabolic disorders [35]. The biochemical characterization of SRP-35 firmly support that it is a membrane-bound protein with its catalytic site facing the cytoplasm; as a consequence, both its products (retinaldehyde) and NAD(P)H are released into the myoplasm. The generation of NADH in the myoplasm may possess functional signaling relevance; lactate dehydrogenase requires NADH as reducing power to generate lactate from pyruvate, and NADH is available in the mitochondria where it is used to generate ATP. Nevertheless, cytosolic NADH has been shown to regulate the activity of the RyRs, especially in the heart [36, 37].

3. Astaxanthin: A Special Carotenoid

Carotenoids, the precursors of vitamin A, are natural pigments supplied with regular highly conjugated π-bond systems, providing the natural yellow, orange, or red colors of many vegetables and fruits [38]. Since the structural elucidation of β-carotene by the two scientists Kuhn and Karrer in 1930, more than 750 naturally occurring carotenoids have been reported to date [39]. Based on their structure, carotenoids can be compiled into two main groups: (i) the carotenes, also called carotenoid hydrocarbons, which only contain carbon and hydrogen and (ii) the xanthophylls or oxygenated carotenoids that may contain different functional groups (epoxy, methoxy, hydroxy, carbonyl, and carboxyl acid groups) [40, 41].

Besides the most notable carotenoid, β-carotene, another carotenoid has been receiving great attention lately: astaxanthin, a marine xanthophyll carotenoid first isolated from a lobster by Kuhn and Soerensen [42]. Astaxanthin is extensively produced by algal species such as *Haematococcus pluvialis* (where it accumulates up to 3.8% on the dry weight basis), *Chlorella zofingiensis*, and *Chlorococcum* and also by the yeast *Phaffia rhodozyma* [43, 44]. Astaxanthin confers the rich pink color observed in various aquatic species including the salmonids and crustaceans and even some non-aquatic species such as the flamingo. Sea creatures cannot produce astaxanthin themselves and must obtain it from their diets, which include zooplankton and krill. Krill oil contains appreciable content of astaxanthin at 0.1 to 1.5 mg/mL depending on processing methods [45]. Krill oil is a superior source of EPA (eicosapentaenoic acid) and DHA (docosahexaenoic acid) which are both long-chain omega-3 fatty acids because the polyunsaturated fats are packaged as phospholipids, which ultimately can be used instantly by our body.

Astaxanthin is a fat-soluble nutrient (it incorporates into cell membranes) with increased absorption when consumed with omega-3-rich seed oil; however, it cannot be converted to vitamin A and therefore cannot support retinol-specific processes such as vision. With its unique molecular structure [46], astaxanthin stretches through the bilayer membrane, providing resilient protection against oxidative stress. It can scavenge and quench ROS and free radicals (superoxide anion, hydrogen peroxide, singlet oxygen, etc.) in both the inner and outer layers of the cellular membrane [46] unlike most antioxidants, which work either in the inner (e.g., vitamin E and β-carotene) or the outer side of the membrane (e.g., vitamin C). Astaxanthin derived from the microalgae *H. pluvialis* has been approved as a color additive agent in salmon feeds and as a dietary supplement for human consumption for more than 20 years in dosages up to 12 mg per day and up to 24 mg per day for no more than 30 days in Europe, Japan, and USA [47].

Recent human studies elaborate on the safety perspectives of natural astaxanthin, and so far, no documented negative effects have been found over its 20 years of consumption as a dietary [48]. Clinical studies have found that natural astaxanthin supplementation improved blood flow in humans [49] and enhanced blood rheology by increasing the flexibility of erythrocyte membranes [50].

Astaxanthin emerged in the spotlight because of its potential pharmacological effects, including anticancer [44, 51, 52], antidiabetic [53, 54], anti-inflammatory [55], immune-stimulating effects [44, 52], and antioxidant activities [55–59] as well as neuro-, cardiovascular, ocular-, and skin-protective effects [60–64]. Studies found that astaxanthin reduces the oxidative stress caused by hyperglycemia in pancreatic β-cells and improves glucose and serum insulin levels in diabetes [65]. Furthermore, it has been suggested that astaxanthin is a potential therapeutic agent against atherosclerotic cardiovascular disease [66]. In an elegant work, Barros et al. showed that "astaxanthin can directly cross the blood-brain barrier to reach different mammalian brain regions" [64, 67, 68]. Here, we summarize the effects of astaxanthin on metabolism, insulin resistance, and type-2 diabetes mellitus; furthermore, its advantages on muscle performance, recovery, and atrophy, and effects in the central nervous system and the skin will also be discussed.

4. The Metabolic Effects of Astaxanthin

4.1. Insulin-Mediated Glucose Uptake. Skeletal muscle accounts for 30-40% of body mass. As the major metabolic tissue of the body, it plays an important role in the whole-body metabolism and homeostasis. In the postprandial state, skeletal muscle tissue is responsible for over 80% of insulin-induced glucose uptake. The molecular mechanisms of insulin-mediated glucose transport are intensively studied. GLUT4 (glucose transporter type 4) is a glucose transporter responsible for glucose uptake into adipocytes and muscle tissue. The GLUT4 vesicles are mainly found perinuclearly at a basal state which are translocated to the plasma membrane by insulin-regulated vesicular traffic leading to glucose transport into the cells and a simultaneous decrease of blood glucose. Importantly, in case of insulin resistance and type-2 diabetes mellitus, the amount of GLUT4 is decreased [69] and its translocation is impaired [70]. The insulin receptor signaling involves the insulin receptor substrate- (IRS-) 1-mediated activation of PI3K (phosphatidylinositol-3-kinase),

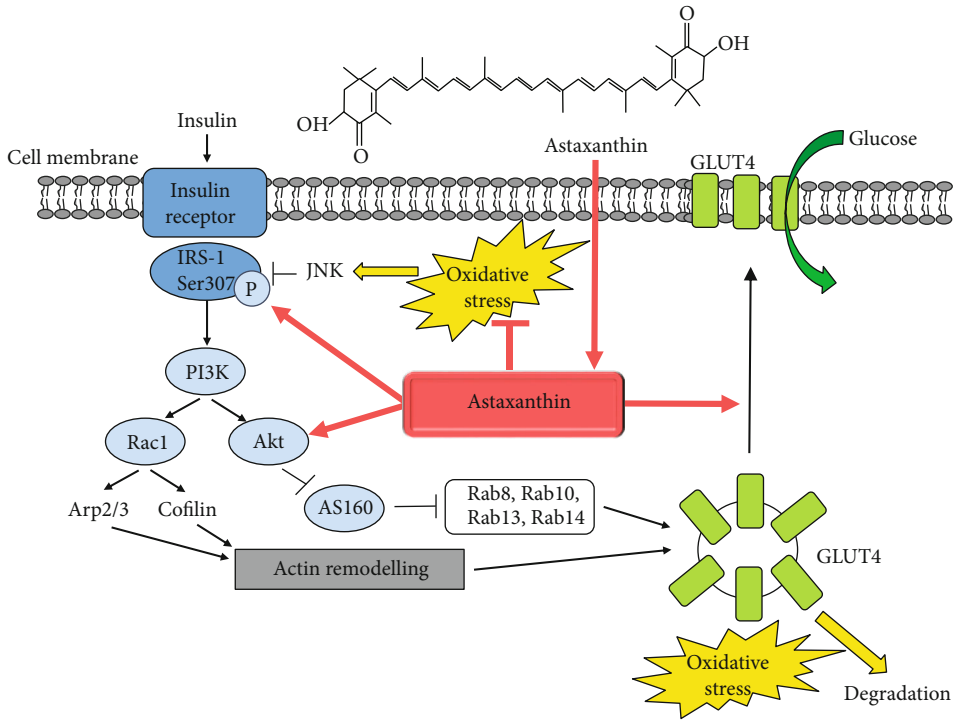

Figure 2: Astaxanthin improves insulin sensitivity and glucose uptake. Schematic representation of the insulin-mediated signaling pathway resulting in the translocation of GLUT4 glucose transporter and glucose uptake. The oxidative stress can lead to insulin resistance by activating various kinases such as JNK, which catalyze the phosphorylation of serine residues in IRS-1 inhibiting its activity and preventing its interaction with the insulin receptor. Furthermore, oxidative stress switches the GLUT4 sorting to the degradation of GLUT4 vesicles. The dietary astaxanthin administration improves insulin sensitivity, IRS-1 activation, Akt phosphorylation, and GLUT4 translocation in skeletal muscle leading to increased insulin sensitivity and a decrease in blood glucose level.

resulting in Akt2 activation, inhibition of the Akt2 substrate AS160 (Akt substrate 160, a GTPase-activating protein for Rabs), and consequently, the activation of Rab8a and Rab14 GTPases in muscle cells [71]. The PI3K can also activate the Rho-family GTPase Rac1 that is involved in the remodeling of a cortical actin network by regulating the Arp2/3 complex and cofilin influencing GLUT4 translocation [72]. The joint activation of the PI3K-mediated Akt2/AS160 and Rac1 signaling pathways is necessary for the translocation of GLUT4 (Figure 2).

4.2. Oxidative Stress and Insulin Resistance. Insulin resistance is a definition for insufficient response of tissues to the effect of insulin, resulting decreased insulin-mediated glucose uptake into the skeletal muscle, increased hepatic glucose production in the liver, and impaired suppression of lipolysis in adipose tissue. The development of insulin resistance is an intensively studied, complex, and not fully known process. Numerous papers have reported that the mitochondrial dysfunction is linked to insulin resistance and type-2 diabetes mellitus [73–75]; however, it remains unclear whether perturbations in mitochondrial functional capacity are causes, consequences, or key contributors to insulin resistance [74, 76]. Mitochondria are the major sources of reactive oxygen species. Insulin resistance is characterized by inefficient mitochondrial coupling, low level of ATP, and the formation of excess amount of ROS despite the normal to high oxygen consumption [73, 75]. Mitochondrial dysfunction was first described in glucose intolerance in 1975 [77]. Several studies suggested that the loss in mitochondrial content and/or function and consequently the decreased mitochondrial oxidative capacity lead to insufficient lipid oxidation, accumulation of lipid excess resulting in the development of insulin resistance [74]. The accumulation of ROS can activate various kinases such as PKCs (protein kinases C), IKK β (inhibitor κB kinase-β), JNK (c-Jun N-terminal kinase), and p38 MAPK (mitogen-activated protein kinase), which induce the phosphorylation of serine residues in IRS-1 leading to the inhibition of its activity and directing it to proteasomal degradation [74, 78–81]. JNK1 has a crucial role in the development of insulin resistance by inhibiting IRS activity via phosphorylation of Ser307 residue preventing its interaction with the insulin receptor [82, 83]. Furthermore, oxidative stress inhibits the retromer function in a casein kinase-2- (CK2-) dependent manner leading to the sorting of GLUT4 vesicles to lysosomes for degradation [84] (Figure 2).

4.3. Astaxanthin Treatment, Insulin Sensitivity, and Muscle Metabolism. Astaxanthin accumulated in skeletal muscle and was shown to reduce hyperglycemia and ameliorate insulin secretion and sensitivity by improvement of glucose metabolism and β-cell dysfunction by GLUT4 regulation. Astaxanthin administration increased the translocation of

GLUT4 transporter and also insulin-dependent glucose uptake in line with increased phosphorylation of IRS-1 tyrosine and Akt and a decrease in JNK and IRS-1 Ser307 phosphorylation in L6 muscle cells [85]. Inflammatory cytokines (e.g., TNFα, tumor necrosis factor α) and fatty acids are released from adipose tissue and serve as the major contributors to induce insulin resistance [85, 86]. Palmitate generate ceramide which triggers mitochondrial oxidative stress and insulin resistance [87], and the role of TNFα in the generation of insulin resistance was also shown [86]. Importantly, astaxanthin treatment restored TNFα- and palmitate-induced insulin resistance and decreased ROS generation of L6 muscle cells [85].

Astaxanthin treatment (8 mg/day, 8 weeks) was effective in patients with type-2 diabetes mellitus: reduced visceral fat mass, serum triglyceride, very-low-density lipoprotein cholesterol concentration, and decreased systolic blood pressure. Furthermore, astaxanthin significantly reduced the fructosamine and plasma glucose concentration [54]. In a metabolic syndrome model SHR/NDmcr-cp (cp/cp) rats where spontaneous hypertension, obesity, hyperinsulinemia, and mild hyperlipidemia evolved, the astaxanthin treatment (22 weeks) ameliorated features of metabolic syndrome: improved insulin resistance; decreased fasting blood glucose, homeostasis of insulin resistance (HOMA-IR), triglyceride, and fatty acid levels; and induced a significant reduction of arterial blood pressure and the size of fat cells in white adipose tissue [88]. Astaxanthin ameliorated high-fat, cholesterol and cholate diet-induced glucose intolerance and reversed hepatic inflammation and fibrosis in C57BL/6J mice [89]. Moreover, astaxanthin administration in a type-2 diabetic db/db (leptin receptor mutated) mice improved the intraperitoneal glucose tolerance test and protected pancreatic β-cells against glucose toxicity by reducing blood glucose concentration and hyperglycemia-induced oxidative stress [65]. Insulin resistance can also be detected in another animal model (high fat and high fructose diet-fed mice), where the astaxanthin treatment improved their insulin sensitivity parameters [53]: lowered insulin and glucose levels in the plasma, ameliorated insulin signaling, and enhanced Akt phosphorylation and GLUT4 translocation in skeletal muscle [53].

The number and function of mitochondria influence the fatty acid utilization of the skeletal muscle. The peroxisome proliferator-activated receptor-γ coactivator-1a (PGC-1α) is a key transcriptional coactivator playing a role in the biogenesis of mitochondria in the muscle. PGC-1α was significantly elevated in skeletal muscle samples following astaxanthin intake, and cytochrome C levels were also increased in mice [90]. Moreover, the levels of plasma fatty acids were decreased after exercise in the astaxanthin-fed mice [90], and the fat utilization of skeletal muscle was improved during exercise in a treadmill running model by activation of carnitine palmitoyltransferase I [91]. Interestingly, PGC-1α increases the level of GLUT4 and has multiple roles in the pathogenesis of type-2 diabetes mellitus [92], but the effects of astaxanthin on the PGC-1α/GLUT4 pathway have not been studied. It has also been demonstrated that peroxisome proliferator-activated receptor (PPAR), which has a major role in the carbohydrate metabolism, is a novel target for astaxanthin. The antioxidant molecule can bind dose-dependently to PPARγ and act as an antagonist or an agonist depending on the cell context [93].

4.4. Protective Effect of Astaxanthin on Diabetes Mellitus Complications. Diabetes mellitus increases ROS production and also decreases antioxidant defense capacity. Reactive radicals are produced in several ways, one source is the activated macrophages and neutrophils. Release of large amounts of ROS leads to oxidative stress of all cell components and induces chronic inflammatory responses [81, 94]. It has also been suggested that carotenoids are capable of protecting the different tissues from the long-term consequences of diabetes including nephropathy, infectious diseases, and abnormalities in the neuronal system and eye. Several reports try to examine and discuss the mechanisms behind the biological effects of carotenoids for the prevention of the complications of diabetes mellitus.

Astaxanthin supplementation markedly reduced the level of inflammation-related proteins COX-2 (cyclooxygenase-2), iNOS (inducible nitric oxide synthase), MCP-1 (monocyte chemoattractant protein 1), NF-β (nuclear factor beta) in the liver, and the ROS-induced lipid peroxidation in streptozotocin-induced diabetic rats [95]. In human mesangial cells, astaxanthin prevented the high-glucose exposure-induced elevated ROS production in the mitochondria, so it can have a protective effect against diabetic neuropathy [96]. In human neutrophil cells, astaxanthin prevented the high-glucose-induced ROS/RNS production and improved the phagocytic capacity of the cells [97]. The redox balance in the lymphocytes was ameliorated by astaxanthin application via lowering the activities of catalase, restoring ratio between glutathione peroxidase and glutathione reductase activities and lowering the scores of lipid oxidation in an alloxan-induced diabetic rat model [98]. Inflammation-related neuronal apoptosis leads to learning and memory deficits. Astaxanthin decreased the activity of apoptosis-related molecules (TNF, IL-1, and IL-6) and caspases 3 and 9 in the cortex and hippocampus of diabetic rats improving cognitive deficits [99]. High-glucose concentration-induced superoxide, nitric oxide, and peroxynitrite generation was also reduced by astaxanthin treatment in proximal tubular epithelial cell, which inhibited the nuclear translocation of NF-κB p65 subunit [100]. Oxidative stress is the major cause of renal fibrosis during the progression of diabetic nephropathy. In diabetic (db/db) mice, astaxanthin administration improved the development and acceleration of diabetic nephropathy [101]; it improved experimental diabetes-induced renal oxidative stress and prevented renal fibrosis by upregulating connexin43 and activating the antioxidant Nrf2- (NF-E2-related factor 2-) ARE (antioxidant responsive element) pathway in glomerular mesangial cells [102]. In streptozotocin-induced diabetic rats, 12 weeks of astaxanthin treatment ameliorated morphological changes in the kidney via decreasing the protein expression of fibronectin and collagen IV and through the activation of Nrf2-ARE signaling [103]. The therapeutic effect of astaxanthin and other carotenoids regarding long-term complications of

diabetes mellitus has been demonstrated in a review of Roohbakhsh et al. [104].

5. Effects of Astaxanthin on Muscle Performance, Recovery, and Atrophy

5.1. Effects of Antioxidants and Their Targets in Skeletal Muscle Work. During skeletal muscle work, ROS are generated from either mitochondrial or nonmitochondrial sources. These include NADPH, xanthine oxidases, phospholipase A2, and nitric oxide that originates from NO synthase. During moderate exercise, oxidative balance is kept within physiological limits to minimize the effects of oxidative damage [105]. It contains a complicated antioxidant defense system: antioxidant enzymes like glutathione peroxidases, superoxide dismutase (SOD), thioredoxins, peroxiredoxins, and catalase. They are capable of reducing ROS, while endogenous antioxidant substrates such as glutathione can scavenge ROS/RNS [105]. Physical exercise *per se* has antioxidant effects by enhancing these endogenous antioxidant defenses [106], and in pathological conditions, like diabetes or cancer, this endogenous antioxidant effect is probably the most efficient health-promoting mechanism. Despite this, antioxidant treatment is very popular and widely used in medical treatment and also among individuals doing recreational or professional sports to enhance activity. These treatments can modify skeletal muscle signaling like force production, glucose uptake, insulin sensitivity, ion pump functions, and mitochondrial biogenesis [105]. However, the frequently supplemented antioxidants are usually vitamin C and E which generalized nontarget scavengers of all ROS. This leads to the fact that in some cases, these antioxidant supplementations does not decrease, or may even increase, the incidence of human diseases [107] explaining the urgent need of new, more specifically working antioxidant compounds.

Mitochondria have an essential role in skeletal muscle contraction. This is the place of ATP synthesis, modulates redox status, controls pH, and contributes in physiological calcium ho-homeostasis. Since without ATP and calcium muscle fibers do not contract, any alteration on mitochondrial status could lead to myopathy or muscle-related disease like diabetes. It was shown that chronic exercise increased mitochondrial size and density and its cardiolipin content in type-2 diabetes [108]. In Barth syndrome, which is an X-linked recessive disorder manifesting in muscle weakness and cardiomyopathy, dysfunction of tafazzin (a mitochondrial acyltransferase) reduces cardiolipin content and alters mitochondrial function. Treatment with mito-Tempo (a mitochondria-specific antioxidant) in cardiac myocytes lacking tafazzin normalized its level, decreased mitochondrial ROS production, and increased cellular ATP content [109]. Unfortunately, not all the mitochondrial-targeted treatment have beneficial effects. Recent study shows in Barth Syndrome again that a targeted overexpression of catalase in mitochondria did not prevent the development of myopathy in mice [110]. Next to the pathological conditions, aging also decreases mitochondrial functions. In a special animal model of aging, mtDNA mutator mice (they accumulate errors in their mitochondrial DNA and present subsequent changes in the respiratory chain composition) were treated with the antioxidant SkQ1 (10-(6′-plastoquinonyl)decyltri-phenylphosphonium cation) and the phosphorylation capacity of mitochondria in skeletal muscle was improved [111]. This positive effect of SkQ1 was partly because the treatment restored the cardiolipin amount in the mtDNA mutator mice to a wild-type level.

5.2. Effects of Astaxanthin during Physical Exercise and Muscle Injury. During heavy exercise, training and competition elevation of reactive oxygen and nitrogen species evolve causing damage in lipid, protein, and nucleic acid molecules. That is why, special nutritional strategy, like supplementation with antioxidant compounds, is now essential for active individuals and athletes. Based upon mouse exercise experiments, supplementation with astaxanthin can effectively improve the side effects of exercise metabolism and the individual's performance and recovery.

Four weeks of astaxanthin treatment in mice prolonged the running to exhaustion. During exercise, astaxanthin administration facilitated lipid metabolism instead of glucose utilization, which improved the endurance and reduced adipose tissue [91]. The same group showed the effect of astaxanthin on ROS-targeted proteins involved in skeletal muscle metabolism during exercise. They found that the oxidative stress-induced modification of lipid peroxidase carnitine palmitoyltransferase I (CPT I) was reduced with the application of antioxidant astaxanthin [112]. Liu and coworkers [90] also suggested that astaxanthin intake increases the PGC-1α level in skeletal muscle leading to the acceleration of lipid utilization by the activation of mitochondrial aerobic metabolism during exercise. In oxidative-type soleus muscle, 45 days of astaxanthin supplementation resulted mitochondrial-targeted action, as the treatment increased glutathione content in the mitochondria during exercise, limited oxidative stress, and delayed exhaustion in Wistar rats [113].

Unlike in exercising mouse model, where astaxanthin supplementation enhanced mainly the utilization of fat and depleted muscle glycogen stores during endurance exercise [114], 4 weeks of treatment did not influence significantly the carbohydrate and fat oxidation rate in exercising humans [115]. In this study, Res et al. also reported that there is no significant effect of astaxanthin supplementation on performance during endurance training not even on longer training time periods or in a higher dose (20 mg/day, 4 weeks) in young, trained individuals [115]. Moreover, a high carotene-containing diet also proved to be effective to moderate some of the negative outcomes of sarcopenia on a low physical performance by reducing DNA damage in aged humans [116]. It has been proved that astaxanthin-containing diet modified the expression level of PGC-1α, thereby inducing the mitochondrial biogenesis *in vivo* [90]. It was shown also that the prolonged supplementation has not modified the lipid oxidation in order to spare glycogen stores during training, as it already proved in animal studies, which can be due to the increased fitness levels of the

inspected subjects [91]. Krill oil treatment also activated the mTORC1 signaling pathway as it was shown in C2C12 myoblasts; however, in young, untrained, healthy individuals, 3 g of krill oil (0.5 g astaxanthin content) administration during 8 weeks did not elevate significantly the muscle force in resistance exercise [117]. In elder subjects (between 65 and 85 years), astaxanthin-containing (12 mg) diet with additional antioxidative properties (10 mg tocotrienol, 6 mg zinc) significantly improved the performance in endurance training and additionally enhanced the force and muscle mass compared to the control group with placebo and training alone [118]. However, authors did not provide information about which signaling pathways were involved and there was also a lack of data about the chronic effects of the astaxanthin treatment.

A fresh study showed that astaxanthin treatment helps to preserve mitochondrial integrity and function in heat-induced skeletal muscle injury examined in cultured C2C12 cells and isolated rat skeletal muscle fibers. The supplementation prevented mitochondrial fragmentation and depolarization, reduced apoptotic cell death, and increased PGC-1α and mitochondrial transcription factor A expression following heat stress [119]. Human investigations have also been carried out to show the effect of astaxanthin application on exercise-induced muscle injury. Eccentric loading was applied for 3 weeks in resistance-trained men, and different markers of muscle injury (muscle soreness, creatine kinase level, and muscle performance) were tested. According to the results, the antioxidant supplementation did not favorably affect the aforementioned markers [120]. In another study, cardiac troponin release was examined after endurance-type exercise in cyclists. In this experiment, astaxanthin treatment had no effect on antioxidant capacity (uric acid, malondialdehyde) and inflammation (high-sensitivity C-reactive protein) markers and did not change creatine kinase release induced by exercise [121]. However, a positive effect of antioxidant astaxanthin was suggested in untrained healthy men, where the supplementation significantly increased carbohydrate oxidation and oxygen consumption during exercise and decreased the plasma insulin level. These results indicate that astaxanthin-rich foods can positively affect aerobic metabolism of carbohydrate and fat during rest and exercise [122].

However, several studies using a variety of animal model of myocardial ischemia and reperfusion demonstrated efficiency of astaxanthin supplementation by reducing markers of oxidative stress and inflammation [123]; one has to consider several aspects with regard the use of antioxidant nutritional supplementation for attenuating muscle injury. These supplements seem to attenuate a certain sign of muscle injury during exercise; however, it is not clear what is the optimal dose and treatment period and whether the effectiveness is specific to nonresistance-trained individuals [124]. It is also urgent to find the best markers of skeletal muscle injury and more suitable analytical methods so that more reliable conclusion can be generated regarding the effect of antioxidant agents like astaxanthin in exercise-induced muscle damage. All the questioned aspects of astaxanthin supplementation on exercise performance and recovery have been collected and discussed in a recent review [125].

5.3. Muscle Atrophy Is Ameliorated by Astaxanthin Treatment. Skeletal muscle atrophy can occur in case of physiological and several pathological conditions such as immobilization, aging, chronic diseases (e.g., heart failure and renal failure), or cancer. A correlation between oxidative stress and muscle mass has already been observed, the increased production of reactive oxygen species has important roles in disuse muscle atrophy by increasing protease activation [126, 127], and the activation of oxidative stress pathways in atrophying muscles has been suggested to cause apoptosis. Oxidative stress participates in the activation of lysosomal proteases (e.g., cathepsin L), calcium-activated proteases (calpain), and also the ubiquitin-proteasome pathway during disuse muscle atrophy leading to the activation of proteolysis [126–128]. The effects of antioxidants in disuse muscular atrophy have been investigated [129], and the antioxidant astaxanthin comes to the front as an effective molecule to prevent inactivity-induced muscle atrophy. Astaxanthin supplementation prior and/or during hind limb unloading prevented muscle atrophy in different animal models. Dietary astaxanthin intake for 14 days before and during hind limb immobilization attenuated muscle atrophy in rats and interfere with the increased expression of CuZn-SOD (CuZn-superoxide dismutase), cathepsin L, calpain, and ubiquitin caused by immobilization [130]. In another rat model, the dietary astaxanthin supplementation for 2 weeks prior to unloading and during 7-day long immobilization attenuated soleus muscle atrophy and suppressed myonuclear apoptosis measured by the number of TUNEL-positive nuclei [131]. The capillary number is related to the loading and activity of skeletal muscle [132]; the unloading results in capillary regression. Administration of astaxanthin decreased the ROS production, decreased the level of SOD-1, and increased the expression of VEGF (vascular endothelial growth factor) in the soleus of hind limb unloaded rats [133, 134]; furthermore, the 7-day long astaxanthin administration reduced the capillary regression during unloading [133], while the 2-week long treatment maintained the capillary network near control levels [134]. Interestingly, the 2-week astaxanthin diet had a little effect on soleus muscle mass during unloading; other muscles were not examined in this study [134]. Further study showed that the combinatory treatment with dietary astaxanthin supplementation and heat stress prevented disuse muscle atrophy in the soleus muscle, and this protective effect may be partially due to the higher number of satellite cells (stem cells of the skeletal muscle) [135]. Increased ROS production within immobilization-induced skeletal muscle mediates TGF-β1-induced fibrosis via promoting the differentiation of fibroblasts and increasing collagen synthesis, where astaxanthin application attenuated skeletal muscle fibrosis [136]. Based on a recent paper by Liu et al., astaxanthin formulation in combination with a functional training program increased the tibialis anterior muscle size determined from magnetic resonance imaging in the elderly [118].

6. Effects of Astaxanthin in the Central Nervous System and the Skin

Oxidative stress is thought to be involved in the pathogenesis and progression of age-related cognitive impairments [137] as well. The high lipid content and metabolic rate make the neuronal system particularly vulnerable to oxidative stress. Mitochondrial damage and dysfunction due to oxidative stress are reflected in age-related neurodegenerative diseases such as Alzheimer's disease, Parkinson's disease, Huntington's disease, and amyotrophic lateral sclerosis [138]. In addition to metabolic failure, the membrane of the damaged mitochondria is impaired, their membrane potentials are lost, and they become permeable resulting in the release of cytochrome c. These processes lead to the activation of caspases that induce apoptosis of neuronal cells.

Dietary supplementation with antioxidant vitamins has shown preventive action against oxidative stress and protected or even reversed the age-related changes in antioxidant activity in the central nervous system [139]. In a recent review, Vina and colleagues [140] demonstrated that the systemic oxidative stress and the cognitive function in Alzheimer's disease patients are inversely proportional. The administration of antioxidants, such as vitamin C or E, has been shown to be effective in reducing the symptoms of oxidative stress and cognitive loss [141]. Astaxanthin has recently gained a lot of interest, because among its variety of health-promoting effects mainly through the modulation of parameters related to oxidative stress but also to inflammation, it is able to penetrate the blood-brain barrier accumulating in the brain and has evidenced positive effects on neurodegeneration as well. The neuroprotective effect of astaxanthin was also published using in vitro and in vivo models. The 1-methyl-4-phenylpyridinium (MPP+) toxin was examined which induces neuronal cytotoxicity. The oxidative stress evoked by this neurotoxin opens the mitochondrial permeability transition pore and subsequently triggers the release of cytochrome c. Astaxanthin increases the activity of SOD and catalase, leading to the inhibition of MPP+-induced ROS generation [142]. Astaxanthin seems to restore brain-derived neurotrophic factor (BDNF) levels in both the brains and the hippocampus in rats, thereby slowing brain aging [143]. Astaxanthin's antineurotoxic effect was also demonstrated in an in vivo mouse model of Parkinson's disease [144]. A recent review summarizes further information on the potential neuroprotective role of astaxanthin [145].

Age-related changes of the skin are thought to be driven by two basic mechanisms: biological aging and exposure to ultraviolet rays (photoaging). Photoaging leads to the degradation of components of the extracellular matrix (collagen, elastin), resulting in wrinkles, pigmentation, and deterioration of the skin texture [146]. UV light initiates production of ROS in the skin. Oxidation of C8 guanine base by ROS, 8-hydroxy-2deoxyguanosine (8-OHdG) is produced, which is a marker of DNA damage [147]. In keratinocytes and fibroblasts, ROS activate cytokine receptors and growth factors that will induce the mitogen-activated protein kinase (MAP kinase) and subsequently activate transcription factors of activator protein-1 (AP-1) [148]. AP-1 potentiates the expression of the matrix degrading enzymes, the matrix metalloproteinases (MMPs), which impair collagen in the skin [146]. Continuous carotenoid administration demonstrated protection against UV light [149], and in particular, astaxanthin supplementation had a positive impact on aging skin status, the skin elasticity was restored, the wrinkle formation was attenuated, and epidermal barrier integrity was preserved [150–153]. A comprehensive review of Davinelli et al. summarizes the role of astaxanthin in skin physiology [154].

7. Conclusions

To summarize, the antioxidant astaxanthin has attracted increasing attention as an effective molecule to prevent oxidative stress-mediated and age-related diseases. Astaxanthin has been reported to lower plasma glucose and insulin levels and to improve whole body insulin sensitivity and insulin-stimulated glucose uptake. Based on the reviewed studies, it can act as an insulin sensitizer. Astaxanthin also improved disuse muscle atrophy, and it has a neuroprotective role and can prevent the photoaging of the skin. Several papers showed that the excess amount of ROS is involved in the development and progression of chronic diseases, including the pathogenesis of insulin resistance and type-2 diabetes. Pinpointing the further details of the antioxidant astaxanthin effect can yield translational benefits for people with metabolic disease. However, results of studies on the supplementation of model organisms with antioxidants, vitamins, and other antioxidants are divergent; many studies show no effect or even negative life-prolonging effect. Despite these contradictory conclusions, the beneficial effects of antioxidants are undoubted in pathological cases (e.g., antioxidant deficiency); additional studies are needed to demonstrate a positive correlation between antioxidant administration and longevity/or slowing aging for healthy people.

Conflicts of Interest

The authors declare that there is no conflict of interest regarding the publication of this paper.

Authors' Contributions

Péter Szentesi and Anikó Keller-Pintér contributed equally to this work.

Acknowledgments

This work was supported by NKFIH NK-115461, PD-128370, GINOP-2.3.2-15-2016-00040, and EFOP-3.6.2-16-2017-00006 grants of the Hungarian National Research, Development and Innovation Office (Hungary) and was financed by the Higher Education Institutional Excellence Programme of the Ministry of Human Capacities in Hungary, within the framework of the 20428-3/2018/FEKUTSTRAT

thematic programme of the University of Debrecen. Additional fundings are János Bolyai Research Scholarship of the Hungarian Academy of Sciences (to A. K.-P. and M. Sz.) and New National Excellence Program of the Ministry for Innovation and Technology Sciences (UNKP-18-4-DE-157 to M. Sz. and UNKP-19-4-SZTE-23 to A. K.-P.).

References

[1] J. Campisi, "Aging, cellular senescence, and cancer," *Annual Review of Physiology*, vol. 75, no. 1, pp. 685–705, 2013.

[2] D. Harman, "Aging: a theory based on free radical and radiation chemistry," *Journal of Gerontology*, vol. 11, no. 3, pp. 298–300, 1956.

[3] A. D. Romano, G. Serviddio, A. de Matthaeis, F. Bellanti, and G. Vendemiale, "Oxidative stress and aging," *Journal of Nephrology*, vol. 23, pp. S29–S36, 2010.

[4] J. Vina, C. Borras, K. M. Abdelaziz, R. Garcia-Valles, and M. C. Gomez-Cabrera, "The free radical theory of aging revisited: the cell signaling disruption theory of aging," *Antioxidants & Redox Signaling*, vol. 19, no. 8, pp. 779–787, 2013.

[5] F. L. Muller, M. S. Lustgarten, Y. Jang, A. Richardson, and H. Van Remmen, "Trends in oxidative aging theories," *Free Radical Biology & Medicine*, vol. 43, no. 4, pp. 477–503, 2007.

[6] A. B. Salmon, A. Richardson, and V. I. Perez, "Update on the oxidative stress theory of aging: does oxidative stress play a role in aging or healthy aging?," *Free Radical Biology & Medicine*, vol. 48, no. 5, pp. 642–655, 2010.

[7] G. J. Brewer, "Epigenetic oxidative redox shift (EORS) theory of aging unifies the free radical and insulin signaling theories," *Experimental Gerontology*, vol. 45, no. 3, pp. 173–179, 2010.

[8] C. A. Cefalu, "Theories and mechanisms of aging," *Clinics in Geriatric Medicine*, vol. 27, no. 4, pp. 491–506, 2011.

[9] P. Zimniak, "Relationship of electrophilic stress to aging," *Free Radical Biology & Medicine*, vol. 51, no. 6, pp. 1087–1105, 2011.

[10] S. I. Rattan, "Theories of biological aging: genes, proteins, and free radicals," *Free Radical Research*, vol. 40, no. 12, pp. 1230–1238, 2009.

[11] H. Sies, C. Berndt, and D. P. Jones, "Oxidative stress," *Annual Review of Biochemistry*, vol. 86, no. 1, pp. 715–748, 2017.

[12] D. Wu and A. I. Cederbaum, "Alcohol, oxidative stress, and free radical damage," *Alcohol Research & Health*, vol. 27, no. 4, pp. 277–284, 2003.

[13] D. Harman, "The biologic clock: the mitochondria?," *Journal of the American Geriatrics Society*, vol. 20, no. 4, pp. 145–147, 1972.

[14] M. Valko, D. Leibfritz, J. Moncol, M. T. D. Cronin, M. Mazur, and J. Telser, "Free radicals and antioxidants in normal physiological functions and human disease," *The International Journal of Biochemistry & Cell Biology*, vol. 39, no. 1, pp. 44–84, 2007.

[15] A. Hernandez-Aguilera, A. Rull, E. Rodriguez-Gallego et al., "Mitochondrial dysfunction: a basic mechanism in inflammation-related non-communicable diseases and therapeutic opportunities," *Mediators of Inflammation*, vol. 2013, Article ID 135698, 13 pages, 2013.

[16] P. Bullon, H. N. Newman, and M. Battino, "Obesity, diabetes mellitus, atherosclerosis and chronic periodontitis: a shared pathology via oxidative stress and mitochondrial dysfunction?," *Periodontology 2000*, vol. 64, no. 1, pp. 139–153, 2014.

[17] H. Cui, Y. Kong, and H. Zhang, "Oxidative stress, mitochondrial dysfunction, and aging," *Journal of Signal Transduction*, vol. 2012, Article ID 646354, 13 pages, 2012.

[18] P. Szentesi, L. Csernoch, L. Dux, and A. Keller-Pinter, "Changes in redox signaling in the skeletal muscle with aging," *Oxidative Medicine and Cellular Longevity*, vol. 2019, Article ID 4617801, 12 pages, 2019.

[19] Z. Bagi, C. Cseko, E. Toth, and A. Koller, "Oxidative stress-induced dysregulation of arteriolar wall shear stress and blood pressure in hyperhomocysteinemia is prevented by chronic vitamin C treatment," *American Journal of Physiology. Heart and Circulatory Physiology*, vol. 285, no. 6, pp. H2277–H2283, 2003.

[20] D. Fusco, G. Colloca, M. R. Lo Monaco, and M. Cesari, "Effects of antioxidant supplementation on the aging process," *Clinical Interventions in Aging*, vol. 2, no. 3, pp. 377–387, 2007.

[21] M. M. Berger, "Can oxidative damage be treated nutritionally?," *Clinical Nutrition*, vol. 24, no. 2, pp. 172–183, 2005.

[22] M. Beppu, T. Watanabe, A. Yokota, S. Ohmori, and K. Kikugawa, "Water-soluble antioxidants inhibit macrophage recognition of oxidized erythrocytes," *Biological & Pharmaceutical Bulletin*, vol. 24, no. 5, pp. 575–578, 2001.

[23] A. Bendich and J. A. Olson, "Biological actions of carotenoids," *The FASEB Journal*, vol. 3, no. 8, pp. 1927–1932, 1989.

[24] E. J. Rhee and J. Plutzky, "Retinoid metabolism and diabetes mellitus," *Diabetes and Metabolism Journal*, vol. 36, no. 3, pp. 167–180, 2012.

[25] M. Leid, P. Kastner, R. Lyons et al., "Purification, cloning, and RXR identity of the HeLa cell factor with which RAR or TR heterodimerizes to bind target sequences efficiently," *Cell*, vol. 68, no. 2, pp. 377–395, 1992.

[26] D. J. Mangelsdorf, U. Borgmeyer, R. A. Heyman et al., "Characterization of three RXR genes that mediate the action of 9-cis retinoic acid," *Genes & Development*, vol. 6, no. 3, pp. 329–344, 1992.

[27] Q. Liu and E. Linney, "The mouse retinoid-X receptor-gamma gene: genomic organization and evidence for functional isoforms," *Molecular Endocrinology*, vol. 7, no. 5, pp. 651–658, 1993.

[28] Y. M. Lee, J. O. Lee, J. H. Jung et al., "Retinoic acid leads to cytoskeletal rearrangement through AMPK-Rac1 and stimulates glucose uptake through AMPK-p38 MAPK in skeletal muscle cells," *The Journal of Biological Chemistry*, vol. 283, no. 49, pp. 33969–33974, 2008.

[29] M. W. Sleeman, H. Zhou, S. Rogers, K. W. Ng, and J. D. Best, "Retinoic acid stimulates glucose transporter expression in L6 muscle cells," *Molecular and Cellular Endocrinology*, vol. 108, no. 1-2, pp. 161–167, 1995.

[30] M. L. Bonet, J. Ribot, and A. Palou, "Lipid metabolism in mammalian tissues and its control by retinoic acid," *Biochimica et Biophysica Acta (BBA) - Molecular and Cell Biology of Lipids*, vol. 1821, no. 1, pp. 177–189, 2012.

[31] D. C. Manolescu, A. Sima, and P. V. Bhat, "All-trans retinoic acid lowers serum retinol-binding protein 4 concentrations and increases insulin sensitivity in diabetic mice," *The Journal of Nutrition*, vol. 140, no. 2, pp. 311–316, 2010.

[32] J. Amengual, J. Ribot, M. L. Bonet, and A. Palou, "Retinoic acid treatment increases lipid oxidation capacity in skeletal

muscle of mice," *Obesity (Silver Spring)*, vol. 16, no. 3, pp. 585–591, 2008.

[33] S. Treves, R. Thurnheer, B. Mosca et al., "SRP-35, a newly identified protein of the skeletal muscle sarcoplasmic reticulum, is a retinol dehydrogenase," *The Biochemical Journal*, vol. 441, no. 2, pp. 731–741, 2012.

[34] B. Persson, Y. Kallberg, J. E. Bray et al., "The SDR (short-chain dehydrogenase/reductase and related enzymes) nomenclature initiative," *Chemico-Biological Interactions*, vol. 178, no. 1-3, pp. 94–98, 2009.

[35] A. Ruiz, E. Dror, C. Handschin et al., "Over-expression of a retinol dehydrogenase (SRP35/DHRS7C) in skeletal muscle activates mTORC2, enhances glucose metabolism and muscle performance," *Scientific Reports*, vol. 8, no. 1, p. 636, 2018.

[36] G. Cherednichenko, A. V. Zima, W. Feng, S. Schaefer, L. A. Blatter, and I. N. Pessah, "NADH oxidase activity of rat cardiac sarcoplasmic reticulum regulates calcium-induced calcium release," *Circulation Research*, vol. 94, no. 4, pp. 478–486, 2004.

[37] G. Meissner, "NADH, a new player in the cardiac ryanodine receptor?," *Circulation Research*, vol. 94, no. 4, pp. 418-419, 2004.

[38] D. B. Rodriguez-Amaya, "Quantitative analysis, in vitro assessment of bioavailability and antioxidant activity of food carotenoids—a review," *Journal of Food Composition and Analysis*, vol. 23, no. 7, pp. 726–740, 2010.

[39] T. Maoka, "Carotenoids in marine animals," *Marine Drugs*, vol. 9, no. 2, pp. 278–293, 2011.

[40] E. Ibañez, M. Herrero, J. Mendiola, and M. Castro-Puyana, "Extraction and characterization of bioactive compounds with health benefits from marine resources: macro and micro algae, cyanobacteria, and invertebrates," in *Marine Bioactive Compounds*, pp. 55–98, Springer, New York, NY, USA, 2011.

[41] S. Rivera and R. Canela, "Influence of sample processing on the analysis of carotenoids in maize," *Molecules*, vol. 17, no. 9, pp. 11255–11268, 2012.

[42] R. Kuhn and N. A. Soerensen, "The coloring matters of the lobster (*Astacus gammarus* L.)," *Angewandte Chemie*, vol. 51, no. 27, pp. 465-466, 1938.

[43] S. Boussiba, "Carotenogenesis in the green alga *Haematococcus pluvialis*: cellular physiology and stress response," *Physiologia Plantarum*, vol. 108, no. 2, pp. 111–117, 2000.

[44] A. R. Rao, H. N. Sindhuja, S. M. Dharmesh, K. U. Sankar, R. Sarada, and G. A. Ravishankar, "Effective inhibition of skin cancer, tyrosinase, and antioxidative properties by astaxanthin and astaxanthin esters from the green alga *Haematococcus pluvialis*," *Journal of Agricultural and Food Chemistry*, vol. 61, no. 16, pp. 3842–3851, 2013.

[45] A. Ali-Nehari, S.-B. Kim, Y.-B. Lee, H.-y. Lee, and B.-S. Chun, "Characterization of oil including astaxanthin extracted from krill (*Euphausia superba*) using supercritical carbon dioxide and organic solvent as comparative method," *Korean Journal of Chemical Engineering*, vol. 29, no. 3, pp. 329–336, 2012.

[46] G. Hussein, U. Sankawa, H. Goto, K. Matsumoto, and H. Watanabe, "Astaxanthin, a carotenoid with potential in human health and nutrition," *Journal of Natural Products*, vol. 69, no. 3, pp. 443–449, 2006.

[47] F. Visioli and C. Artaria, "Astaxanthin in cardiovascular health and disease: mechanisms of action, therapeutic merits, and knowledge gaps," *Food & Function*, vol. 8, no. 1, pp. 39–63, 2017.

[48] B. Capelli, S. Talbott, and L. Ding, "Astaxanthin sources: suitability for human health and nutrition," *Functional Foods in Health and Disease*, vol. 9, no. 6, p. 430, 2019.

[49] H. Miyawaki, J. Takahashi, H. Tsukahara, and I. Takehara, "Effects of astaxanthin on human blood rheology," *Journal of Clinical Biochemistry and Nutrition*, vol. 43, no. 2, pp. 69–74, 2008.

[50] M. Saito, K. Yoshida, W. Saito et al., "Astaxanthin increases choroidal blood flow velocity," *Graefe's Archive for Clinical and Experimental Ophthalmology*, vol. 250, no. 2, pp. 239–245, 2012.

[51] G. Wolf, "Retinoids and carotenoids as inhibitors of carcinogenesis and inducers of cell-cell communication," *Nutrition Reviews*, vol. 50, no. 9, pp. 270–274, 1992.

[52] B. P. Chew, J. S. Park, M. W. Wong, and T. S. Wong, "A comparison of the anticancer activities of dietary beta-carotene, canthaxanthin and astaxanthin in mice in vivo," *Anticancer Research*, vol. 19, no. 3A, pp. 1849–1853, 1999.

[53] E. Arunkumar, S. Bhuvaneswari, and C. V. Anuradha, "An intervention study in obese mice with astaxanthin, a marine carotenoid–effects on insulin signaling and pro-inflammatory cytokines," *Food & Function*, vol. 3, no. 2, pp. 120–126, 2012.

[54] N. S. Mashhadi, M. Zakerkish, J. Mohammadiasl, M. Zarei, M. Mohammadshahi, and M. H. Haghighizadeh, "Astaxanthin improves glucose metabolism and reduces blood pressure in patients with type 2 diabetes mellitus," *Asia Pacific Journal of Clinical Nutrition*, vol. 27, no. 2, pp. 341–346, 2018.

[55] J. Park, J. Chyun, Y. Kim, L. L. Line, and B. P. Chew, "Astaxanthin decreased oxidative stress and inflammation and enhanced immune response in humans," *Nutrition & Metabolism*, vol. 7, no. 1, p. 18, 2010.

[56] H. P. McNulty, J. Byun, S. F. Lockwood, R. F. Jacob, and R. P. Mason, "Differential effects of carotenoids on lipid peroxidation due to membrane interactions: X-ray diffraction analysis," *Biochimica et Biophysica Acta*, vol. 1768, no. 1, pp. 167–174, 2007.

[57] B. S. Kamath, B. M. Srikanta, S. M. Dharmesh, R. Sarada, and G. A. Ravishankar, "Ulcer preventive and antioxidative properties of astaxanthin from Haematococcus pluvialis," *European Journal of Pharmacology*, vol. 590, no. 1-3, pp. 387–395, 2008.

[58] A. M. Wolf, S. Asoh, H. Hiranuma et al., "Astaxanthin protects mitochondrial redox state and functional integrity against oxidative stress," *The Journal of Nutritional Biochemistry*, vol. 21, no. 5, pp. 381–389, 2010.

[59] S. H. Kim and H. Kim, "Inhibitory effect of astaxanthin on oxidative stress-induced mitochondrial dysfunction-a mini-review," *Nutrients*, vol. 10, no. 9, p. 1137, 2018.

[60] Y. M. Naguib, "Antioxidant activities of astaxanthin and related carotenoids," *Journal of Agricultural and Food Chemistry*, vol. 48, no. 4, pp. 1150–1154, 2000.

[61] J. P. Yuan, J. Peng, K. Yin, and J. H. Wang, "Potential health-promoting effects of astaxanthin: a high-value carotenoid mostly from microalgae," *Molecular Nutrition & Food Research*, vol. 55, no. 1, pp. 150–165, 2011.

[62] S. Hama, K. Takahashi, Y. Inai et al., "Protective effects of topical application of a poorly soluble antioxidant astaxanthin liposomal formulation on ultraviolet-induced skin

damage," *Journal of Pharmaceutical Sciences*, vol. 101, no. 8, pp. 2909–2916, 2012.

[63] S. D. Santos, T. B. Cahú, G. O. Firmino et al., "Shrimp waste extract and astaxanthin: rat alveolar macrophage, oxidative stress and inflammation," *Journal of Food Science*, vol. 77, no. 7, pp. H141–H146, 2012.

[64] M. Barros, S. Poppe, and E. Bondan, "Neuroprotective properties of the marine carotenoid astaxanthin and omega-3 fatty acids, and perspectives for the natural combination of both in krill oil," *Nutrients*, vol. 6, no. 3, pp. 1293–1317, 2014.

[65] K. Uchiyama, Y. Naito, G. Hasegawa, N. Nakamura, J. Takahashi, and T. Yoshikawa, "Astaxanthin protects β-cells against glucose toxicity in diabetic db/db mice," *Redox Report*, vol. 7, no. 5, pp. 290–293, 2013.

[66] R. G. Fassett and J. S. Coombes, "Astaxanthin: a potential therapeutic agent in cardiovascular disease," *Marine Drugs*, vol. 9, no. 3, pp. 447–465, 2011.

[67] X. Liu and T. Osawa, "Astaxanthin protects neuronal cells against oxidative damage and is a potent candidate for brain food," *Forum of Nutrition*, vol. 61, pp. 129–135, 2009.

[68] Y. P. Lu, S. Y. Liu, H. Sun, X. M. Wu, J. J. Li, and L. Zhu, "Neuroprotective effect of astaxanthin on H_2O_2-induced neurotoxicity in vitro and on focal cerebral ischemia in vivo," *Brain Research*, vol. 1360, pp. 40–48, 2010.

[69] I. Schreiber, G. Dorpholz, C. E. Ott et al., "BMPs as new insulin sensitizers: enhanced glucose uptake in mature 3T3-L1 adipocytes via PPARγ and GLUT4 upregulation," *Scientific Reports*, vol. 7, no. 1, article 17192, 2017.

[70] J. R. Jaldin-Fincati, M. Pavarotti, S. Frendo-Cumbo, P. J. Bilan, and A. Klip, "Update on GLUT4 vesicle traffic: a cornerstone of insulin action," *Trends in Endocrinology and Metabolism*, vol. 28, no. 8, pp. 597–611, 2017.

[71] S. Ishikura, P. J. Bilan, and A. Klip, "Rabs 8A and 14 are targets of the insulin-regulated Rab-GAP AS160 regulating GLUT4 traffic in muscle cells," *Biochemical and Biophysical Research Communications*, vol. 353, no. 4, pp. 1074–1079, 2007.

[72] T. T. Chiu, N. Patel, A. E. Shaw, J. R. Bamburg, and A. Klip, "Arp2/3- and cofilin-coordinated actin dynamics is required for insulin-mediated GLUT4 translocation to the surface of muscle cells," *Molecular Biology of the Cell*, vol. 21, no. 20, pp. 3529–3539, 2010.

[73] S. Rovira-Llopis, C. Banuls, N. Diaz-Morales, A. Hernandez-Mijares, M. Rocha, and V. M. Victor, "Mitochondrial dynamics in type 2 diabetes: pathophysiological implications," *Redox Biology*, vol. 11, pp. 637–645, 2017.

[74] S. Di Meo, S. Iossa, and P. Venditti, "Skeletal muscle insulin resistance: role of mitochondria and other ROS sources," *The Journal of Endocrinology*, vol. 233, no. 1, pp. R15–r42, 2017.

[75] G. N. Ruegsegger, A. L. Creo, T. M. Cortes, S. Dasari, and K. S. Nair, "Altered mitochondrial function in insulin-deficient and insulin-resistant states," *The Journal of Clinical Investigation*, vol. 128, no. 9, pp. 3671–3681, 2018.

[76] J. F. Dumas, G. Simard, M. Flamment, P. H. Ducluzeau, and P. Ritz, "Is skeletal muscle mitochondrial dysfunction a cause or an indirect consequence of insulin resistance in humans?," *Diabetes & Metabolism*, vol. 35, no. 3, pp. 159–167, 2009.

[77] T. Yamada, T. Ida, Y. Yamaoka, K. Ozawa, H. Takasan, and I. Honjo, "Two distinct patterns of glucose intolerance in icteric rats and rabbits. Relationship to impaired liver mitochondria function," *The Journal of Laboratory and Clinical Medicine*, vol. 86, no. 1, pp. 38–45, 1975.

[78] K. Paz, R. Hemi, D. LeRoith et al., "A molecular basis for insulin resistance. Elevated serine/threonine phosphorylation of IRS-1 and IRS-2 inhibits their binding to the juxtamembrane region of the insulin receptor and impairs their ability to undergo insulin-induced tyrosine phosphorylation," *The Journal of Biological Chemistry*, vol. 272, no. 47, pp. 29911–29918, 1997.

[79] R. Zhande, J. J. Mitchell, J. Wu, and X. J. Sun, "Molecular mechanism of insulin-induced degradation of insulin receptor substrate 1," *Molecular and Cellular Biology*, vol. 22, no. 4, pp. 1016–1026, 2002.

[80] J. Evans, J. Lin, and I. Goldfine, "Novel approach to treat insulin resistance, type 2 diabetes, and the metabolic syndrome: simultaneous activation of PPARα, PPARγ, and PPARδ," *Current Diabetes Reviews*, vol. 1, no. 3, pp. 299–307, 2005.

[81] J. L. Evans, B. A. Maddux, and I. D. Goldfine, "The molecular basis for oxidative stress-induced insulin resistance," *Antioxidants & Redox Signaling*, vol. 7, no. 7-8, pp. 1040–1052, 2005.

[82] V. Aguirre, T. Uchida, L. Yenush, R. Davis, and M. F. White, "The c-Jun NH_2-terminal kinase promotes insulin resistance during association with insulin receptor substrate-1 and phosphorylation of Ser^{307}," *The Journal of Biological Chemistry*, vol. 275, no. 12, pp. 9047–9054, 2000.

[83] V. Aguirre, E. D. Werner, J. Giraud, Y. H. Lee, S. E. Shoelson, and M. F. White, "Phosphorylation of Ser^{307} in insulin receptor substrate-1 blocks interactions with the insulin receptor and inhibits insulin action," *The Journal of Biological Chemistry*, vol. 277, no. 2, pp. 1531–1537, 2002.

[84] J. Ma, Y. Nakagawa, I. Kojima, and H. Shibata, "Prolonged insulin stimulation down-regulates GLUT4 through oxidative stress-mediated retromer inhibition by a protein kinase CK2-dependent mechanism in 3T3-L1 adipocytes," *The Journal of Biological Chemistry*, vol. 289, no. 1, pp. 133–142, 2014.

[85] M. Ishiki, Y. Nishida, H. Ishibashi et al., "Impact of divergent effects of astaxanthin on insulin signaling in L6 cells," *Endocrinology*, vol. 154, no. 8, pp. 2600–2612, 2013.

[86] K. T. Uysal, S. M. Wiesbrock, M. W. Marino, and G. S. Hotamisligil, "Protection from obesity-induced insulin resistance in mice lacking TNF-α function," *Nature*, vol. 389, no. 6651, pp. 610–614, 1997.

[87] H. Yaribeygi, S. Bo, M. Ruscica, and A. Sahebkar, "Ceramides and diabetes mellitus: an update on the potential molecular relationships," *Diabetic Medicine*, pp. 1–9, 2019.

[88] G. Hussein, T. Nakagawa, H. Goto et al., "Astaxanthin ameliorates features of metabolic syndrome in SHR/NDmcr-cp," *Life Sciences*, vol. 80, no. 6, pp. 522–529, 2007.

[89] Y. Ni, M. Nagashimada, F. Zhuge et al., "Astaxanthin prevents and reverses diet-induced insulin resistance and steatohepatitis in mice: a comparison with vitamin E," *Scientific Reports*, vol. 5, no. 1, article 17192, 2015.

[90] P. H. Liu, W. Aoi, M. Takami et al., "The astaxanthin-induced improvement in lipid metabolism during exercise is mediated by a PGC-1α increase in skeletal muscle," *Journal of Clinical Biochemistry and Nutrition*, vol. 54, no. 2, pp. 86–89, 2014.

[91] W. Aoi, Y. Naito, Y. Takanami et al., "Astaxanthin improves muscle lipid metabolism in exercise via inhibitory effect of oxidative CPT I modification," *Biochemical and Biophysical Research Communications*, vol. 366, no. 4, pp. 892–897, 2008.

[92] S. Soyal, F. Krempler, H. Oberkofler, and W. Patsch, "PGC-1α: a potent transcriptional cofactor involved in the pathogenesis of type 2 diabetes," *Diabetologia*, vol. 49, no. 7, pp. 1477–1488, 2006.

[93] M. Inoue, H. Tanabe, A. Matsumoto et al., "Astaxanthin functions differently as a selective peroxisome proliferator-activated receptor γ modulator in adipocytes and macrophages," *Biochemical Pharmacology*, vol. 84, no. 5, pp. 692–700, 2012.

[94] J. Yang, Y. Tan, F. Zhao et al., "Angiotensin II plays a critical role in diabetic pulmonary fibrosis most likely via activation of NADPH oxidase-mediated nitrosative damage," *American Journal of Physiology. Endocrinology and Metabolism*, vol. 301, no. 1, pp. E132–E144, 2011.

[95] C. H. Park, F. H. Xu, S. S. Roh et al., "Astaxanthin and Corni Fructus protect against diabetes-induced oxidative stress, inflammation, and advanced glycation end product in livers of streptozotocin-induced diabetic rats," *Journal of Medicinal Food*, vol. 18, no. 3, pp. 337–344, 2015.

[96] E. Manabe, O. Handa, Y. Naito et al., "Astaxanthin protects mesangial cells from hyperglycemia-induced oxidative signaling," *Journal of Cellular Biochemistry*, vol. 103, no. 6, pp. 1925–1937, 2008.

[97] B. A. Guerra and R. Otton, "Impact of the carotenoid astaxanthin on phagocytic capacity and ROS/RNS production of human neutrophils treated with free fatty acids and high glucose," *International Immunopharmacology*, vol. 11, no. 12, pp. 2220–2226, 2011.

[98] R. Otton, D. P. Marin, A. P. Bolin et al., "Astaxanthin ameliorates the redox imbalance in lymphocytes of experimental diabetic rats," *Chemico-Biological Interactions*, vol. 186, no. 3, pp. 306–315, 2010.

[99] L. Xu, J. Zhu, W. Yin, and X. Ding, "Astaxanthin improves cognitive deficits from oxidative stress, nitric oxide synthase and inflammation through upregulation of PI3K/Akt in diabetes rat," *International Journal of Clinical and Experimental Pathology*, vol. 8, no. 6, pp. 6083–6094, 2015.

[100] Y. J. Kim, Y. A. Kim, and T. Yokozawa, "Protection against oxidative stress, inflammation, and apoptosis of high-glucose-exposed proximal tubular epithelial cells by astaxanthin," *Journal of Agricultural and Food Chemistry*, vol. 57, no. 19, pp. 8793–8797, 2009.

[101] Y. Naito, K. Uchiyama, W. Aoi et al., "Prevention of diabetic nephropathy by treatment with astaxanthin in diabetic db/db mice," *BioFactors*, vol. 20, no. 1, pp. 49–59, 2004.

[102] Q. Chen, J. Tao, G. Li et al., "Astaxanthin ameliorates experimental diabetes-induced renal oxidative stress and fibronectin by upregulating connexin43 in glomerular mesangial cells and diabetic mice," *European Journal of Pharmacology*, vol. 840, pp. 33–43, 2018.

[103] X. Zhu, Y. Chen, Q. Chen, H. Yang, and X. Xie, "Astaxanthin promotes Nrf2/ARE signaling to alleviate renal fibronectin and collagen IV accumulation in diabetic rats," *Journal Diabetes Research*, vol. 2018, article 6730315, 7 pages, 2018.

[104] A. Roohbakhsh, G. Karimi, and M. Iranshahi, "Carotenoids in the treatment of diabetes mellitus and its complications: a mechanistic review," *Biomedicine & Pharmacotherapy*, vol. 91, pp. 31–42, 2017.

[105] S. K. Powers and M. J. Jackson, "Exercise-induced oxidative stress: cellular mechanisms and impact on muscle force production," *Physiological Reviews*, vol. 88, no. 4, pp. 1243–1276, 2008.

[106] M. C. Gomez-Cabrera, E. Domenech, and J. Vina, "Moderate exercise is an antioxidant: upregulation of antioxidant genes by training," *Free Radical Biology & Medicine*, vol. 44, no. 2, pp. 126–131, 2008.

[107] M. Ristow, "Unraveling the truth about antioxidants: mitohormesis explains ROS-induced health benefits," *Nature Medicine*, vol. 20, no. 7, pp. 709–711, 2014.

[108] F. G. S. Toledo, E. V. Menshikova, V. B. Ritov et al., "Effects of physical activity and weight loss on skeletal muscle mitochondria and relationship with glucose control in type 2 diabetes," *Diabetes*, vol. 56, no. 8, pp. 2142–2147, 2007.

[109] Q. He, N. Harris, J. Ren, and X. Han, "Mitochondria-targeted antioxidant prevents cardiac dysfunction induced by tafazzin gene knockdown in cardiac myocytes," *Oxidative Medicine and Cellular Longevity*, vol. 2014, Article ID 654198, 12 pages, 2014.

[110] J. M. Johnson, P. J. Ferrara, A. R. P. Verkerke et al., "Targeted overexpression of catalase to mitochondria does not prevent cardioskeletal myopathy in Barth syndrome," *Journal of Molecular and Cellular Cardiology*, vol. 121, pp. 94–102, 2018.

[111] I. G. Shabalina, M. Y. Vyssokikh, N. Gibanova et al., "Improved health-span and lifespan in mtDNA mutator mice treated with the mitochondrially targeted antioxidant SkQ1," *Aging*, vol. 9, no. 2, pp. 315–339, 2016.

[112] W. Aoi, Y. Naito, and T. Yoshikawa, "Potential role of oxidative protein modification in energy metabolism in exercise," *Sub-Cellular Biochemistry*, vol. 77, pp. 175–187, 2014.

[113] T. Polotow, C. Vardaris, A. Mihaliuc et al., "Astaxanthin supplementation delays physical exhaustion and prevents redox imbalances in plasma and soleus muscles of Wistar rats," *Nutrients*, vol. 6, no. 12, pp. 5819–5838, 2014.

[114] M. Ikeuchi, T. Koyama, J. Takahashi, and K. Yazawa, "Effects of astaxanthin supplementation on exercise-induced fatigue in mice," *Biological & Pharmaceutical Bulletin*, vol. 29, no. 10, pp. 2106–2110, 2006.

[115] P. T. Res, N. M. Cermak, R. Stinkens et al., "Astaxanthin supplementation does not augment fat use or improve endurance performance," *Medicine and Science in Sports and Exercise*, vol. 45, no. 6, pp. 1158–1165, 2013.

[116] M. Cesari, M. Pahor, B. Bartali et al., "Antioxidants and physical performance in elderly persons: the Invecchiare in Chianti (InCHIANTI) study," *The American Journal of Clinical Nutrition*, vol. 79, no. 2, pp. 289–294, 2004.

[117] J. Georges, M. H. Sharp, R. P. Lowery et al., "The effects of krill oil on mTOR signaling and resistance exercise: a pilot study," *Journal of Nutrition and Metabolism*, vol. 2018, Article ID 7625981, 11 pages, 2018.

[118] S. Z. Liu, A. S. Ali, M. D. Campbell et al., "Building strength, endurance, and mobility using an astaxanthin formulation with functional training in elderly," *Journal of Cachexia, Sarcopenia and Muscle*, vol. 9, no. 5, pp. 826–833, 2018.

[119] T. Yu, J. Dohl, Y. Chen, H. G. Gasier, and P. A. Deuster, "Astaxanthin but not quercetin preserves mitochondrial integrity and function, ameliorates oxidative stress, and reduces heat-induced skeletal muscle injury," *Journal of Cellular Physiology*, vol. 234, no. 8, pp. 13292–13302, 2019.

[120] R. J. Bloomer, A. Fry, B. Schilling, L. Chiu, N. Hori, and L. Weiss, "Astaxanthin supplementation does not attenuate muscle injury following eccentric exercise in resistance-

trained men," *International Journal of Sport Nutrition and Exercise Metabolism*, vol. 15, no. 4, pp. 401–412, 2005.

[121] L. J. Klinkenberg, P. T. Res, G. R. Haenen et al., "Effect of antioxidant supplementation on exercise-induced cardiac troponin release in cyclists: a randomized trial," *PLoS One*, vol. 8, no. 11, article e79280, 2013.

[122] M. Takami, W. Aoi, H. Terajima, Y. Tanimura, S. Wada, and A. Higashi, "Effect of dietary antioxidant-rich foods combined with aerobic training on energy metabolism in healthy young men," *Journal of Clinical Biochemistry and Nutrition*, vol. 64, no. 1, pp. 79–85, 2019.

[123] R. G. Fassett and J. S. Coombes, "Astaxanthin, oxidative stress, inflammation and cardiovascular disease," *Future Cardiology*, vol. 5, no. 4, pp. 333–342, 2009.

[124] R. J. Bloomer, "The role of nutritional supplements in the prevention and treatment of resistance exercise-induced skeletal muscle injury," *Sports Medicine*, vol. 37, no. 6, pp. 519–532, 2007.

[125] D. R. Brown, L. A. Gough, S. K. Deb, S. A. Sparks, and L. R. McNaughton, "Astaxanthin in exercise metabolism, performance and recovery: a review," *Frontiers in Nutrition*, vol. 4, p. 76, 2018.

[126] S. K. Powers, A. N. Kavazis, and K. C. DeRuisseau, "Mechanisms of disuse muscle atrophy: role of oxidative stress," *American Journal of Physiology. Regulatory, Integrative and Comparative Physiology*, vol. 288, no. 2, pp. R337–R344, 2005.

[127] S. K. Powers, A. J. Smuder, and A. R. Judge, "Oxidative stress and disuse muscle atrophy: cause or consequence?," *Current Opinion in Clinical Nutrition and Metabolic Care*, vol. 15, no. 3, pp. 240–245, 2012.

[128] S. K. Powers, A. N. Kavazis, and J. M. McClung, "Oxidative stress and disuse muscle atrophy," *Journal of Applied Physiology (Bethesda, MD: 1985)*, vol. 102, no. 6, pp. 2389–2397, 2007.

[129] S. K. Powers, "Can antioxidants protect against disuse muscle atrophy?," *Sports Medicine*, vol. 44, Supplement 2, pp. 155–165, 2014.

[130] T. Shibaguchi, Y. Yamaguchi, N. Miyaji et al., "Astaxanthin intake attenuates muscle atrophy caused by immobilization in rats," *Physiological Reports*, vol. 4, no. 15, article e12885, 2016.

[131] T. Yoshihara, Y. Yamamoto, T. Shibaguchi et al., "Dietary astaxanthin supplementation attenuates disuse-induced muscle atrophy and myonuclear apoptosis in the rat soleus muscle," *The Journal of Physiological Sciences*, vol. 67, no. 1, pp. 181–190, 2017.

[132] S. Egginton and E. Gaffney, "Tissue capillary supply–it's quality not quantity that counts!," *Experimental Physiology*, vol. 95, no. 10, pp. 971–979, 2010.

[133] M. Kanazashi, Y. Okumura, S. Al-Nassan et al., "Protective effects of astaxanthin on capillary regression in atrophied soleus muscle of rats," *Acta Physiologica (Oxford, England)*, vol. 207, no. 2, pp. 405–415, 2013.

[134] M. Kanazashi, M. Tanaka, S. Murakami et al., "Amelioration of capillary regression and atrophy of the soleus muscle in hindlimb-unloaded rats by astaxanthin supplementation and intermittent loading," *Experimental Physiology*, vol. 99, no. 8, pp. 1065–1077, 2014.

[135] T. Yoshihara, T. Sugiura, N. Miyaji et al., "Effect of a combination of astaxanthin supplementation, heat stress, and intermittent reloading on satellite cells during disuse muscle atrophy," *Journal of Zhejiang University. Science. B*, vol. 19, no. 11, pp. 844–852, 2018.

[136] T. Maezawa, M. Tanaka, M. Kanazashi et al., "Astaxanthin supplementation attenuates immobilization-induced skeletal muscle fibrosis via suppression of oxidative stress," *The Journal of Physiological Sciences*, vol. 67, no. 5, pp. 603–611, 2017.

[137] A. M. Swomley and D. A. Butterfield, "Oxidative stress in Alzheimer disease and mild cognitive impairment: evidence from human data provided by redox proteomics," *Archives of Toxicology*, vol. 89, no. 10, pp. 1669–1680, 2015.

[138] M. T. Lin and M. F. Beal, "Mitochondrial dysfunction and oxidative stress in neurodegenerative diseases," *Nature*, vol. 443, no. 7113, pp. 787–795, 2006.

[139] E. O'Donnell and M. A. Lynch, "Dietary antioxidant supplementation reverses age-related neuronal changes," *Neurobiology of Aging*, vol. 19, no. 5, pp. 461–467, 1998.

[140] J. Vina, A. Lloret, R. Orti, and D. Alonso, "Molecular bases of the treatment of Alzheimer's disease with antioxidants: prevention of oxidative stress," *Molecular Aspects of Medicine*, vol. 25, no. 1-2, pp. 117–123, 2004.

[141] E. Head, J. Rofina, and S. Zicker, "Oxidative stress, aging, and central nervous system disease in the canine model of human brain aging," *Veterinary Clinics of North America: Small Animal Practice*, vol. 38, no. 1, pp. 167–178, 2008.

[142] D. H. Lee, C. S. Kim, and Y. J. Lee, "Astaxanthin protects against MPTP/MPP+-induced mitochondrial dysfunction and ROS production *in vivo* and *in vitro*," *Food and Chemical Toxicology*, vol. 49, no. 1, pp. 271–280, 2011.

[143] W. Wu, X. Wang, Q. Xiang et al., "Astaxanthin alleviates brain aging in rats by attenuating oxidative stress and increasing BDNF levels," *Food & Function*, vol. 5, no. 1, pp. 158–166, 2014.

[144] B. Grimmig, L. Daly, M. Subbarayan et al., "Astaxanthin is neuroprotective in an aged mouse model of Parkinson's disease," *Oncotarget*, vol. 9, no. 12, pp. 10388–10401, 2018.

[145] C. Galasso, I. Orefice, P. Pellone et al., "On the neuroprotective role of astaxanthin: new perspectives?," *Marine Drugs*, vol. 16, no. 8, p. 247, 2018.

[146] E. Hwang, D. G. Lee, S. H. Park, M. S. Oh, and S. Y. Kim, "Coriander leaf extract exerts antioxidant activity and protects against UVB-induced photoaging of skin by regulation of procollagen type I and MMP-1 expression," *Journal of Medicinal Food*, vol. 17, no. 9, pp. 985–995, 2014.

[147] A. Valavanidis, T. Vlachogianni, and C. Fiotakis, "8-hydroxy-2′ -deoxyguanosine (8-OHdG): a critical biomarker of oxidative stress and carcinogenesis," *Journal of Environmental Science and Health. Part C, Environmental Carcinogenesis & Ecotoxicology Reviews*, vol. 27, no. 2, pp. 120–139, 2009.

[148] Y. R. Helfrich, D. L. Sachs, and J. J. Voorhees, "Overview of skin aging and photoaging," *Dermatology Nursing*, vol. 20, no. 3, pp. 177–83; quiz 184, 2008.

[149] H. Sies and W. Stahl, "Carotenoids and UV protection," *Photochemical & Photobiological Sciences*, vol. 3, no. 8, pp. 749–752, 2004.

[150] K. Tominaga, N. Hongo, M. Karato, and E. Yamashita, "Cosmetic benefits of astaxanthin on humans subjects," *Acta Biochimica Polonica*, vol. 59, no. 1, pp. 43–47, 2012.

[151] K. Suganuma, H. Nakajima, M. Ohtsuki, and G. Imokawa, "Astaxanthin attenuates the UVA-induced up-regulation of

matrix-metalloproteinase-1 and skin fibroblast elastase in human dermal fibroblasts," *Journal of Dermatological Science*, vol. 58, no. 2, pp. 136–142, 2010.

[152] H. S. Yoon, H. H. Cho, S. Cho, S. R. Lee, M. H. Shin, and J. H. Chung, "Supplementating with dietary astaxanthin combined with collagen hydrolysate improves facial elasticity and decreases matrix metalloproteinase-1 and -12 expression: a comparative study with placebo," *Journal of Medicinal Food*, vol. 17, no. 7, pp. 810–816, 2014.

[153] L. Phetcharat, K. Wongsuphasawat, and K. Winther, "The effectiveness of a standardized rose hip powder, containing seeds and shells of Rosa canina, on cell longevity, skin wrinkles, moisture, and elasticity," *Clinical Interventions in Aging*, vol. 10, pp. 1849–1856, 2015.

[154] S. Davinelli, M. Nielsen, and G. Scapagnini, "Astaxanthin in skin health, repair, and disease: a comprehensive review," *Nutrients*, vol. 10, no. 4, p. 522, 2018.

Hindawi
Oxidative Medicine and Cellular Longevity
Volume 2019, Article ID 2901057, 13 pages
https://doi.org/10.1155/2019/2901057

Research Article

New C-Terminal Conserved Regions of Tafazzin, a Catalyst of Cardiolipin Remodeling

Gregory A. Shilovsky,[1,2] Oleg A. Zverkov,[1] Alexandr V. Seliverstov,[1] Vasily V. Ashapkin,[2] Tatyana S. Putyatina,[3] Lev I. Rubanov,[1] and Vassily A. Lyubetsky[1]

[1]*Institute for Information Transmission Problems of the Russian Academy of Sciences (Kharkevich Institute), 127051, Russia*
[2]*Belozersky Institute of Physico-Chemical Biology, Lomonosov Moscow State University, 119991, Russia*
[3]*Faculty of Biology, Lomonosov Moscow State University, 119234, Russia*

Correspondence should be addressed to Oleg A. Zverkov; zverkov@iitp.ru

Received 21 June 2019; Accepted 16 August 2019; Published 23 October 2019

Guest Editor: Eugenia Mileykovskaya

Cardiolipin interacts with many proteins of the mitochondrial inner membrane and, together with cytochrome C and creatine kinase, activates them. It can be considered as an integrating factor for components of the mitochondrial respiratory chain, which provides for an efficient transfer of electrons and protons. The major, if not the only, factor of cardiolipin maturation is tafazzin. Variations of isoform proportions of this enzyme can cause severe diseases such as Barth syndrome. Using bioinformatic methods, we have found conserved C-terminal regions in many tafazzin isoforms and identified new mammalian species that acquired exon 5 as well as rare occasions of intron retention between exons 8 and 9. The regions in the C-terminal part arise from frameshifts relative to the full-length *TAZ* transcript after skipping exon 9 or retention of the intron between exons 10 and 11. These modifications demonstrate specific distribution among the orders of mammals. The dependence of the species maximum lifespan, body weight, and mitochondrial metabolic rate on the modifications has been demonstrated. Arguably, unconventional tafazzin isoforms provide for the optimal balance between the increased biochemical activity of mitochondria (resulting from specific environmental or nutritional conditions) and lifespan maintenance; and the functional role of such isoforms is linked to the modification of the primary and secondary structures at their C-termini.

1. Introduction

Cardiolipin (CL) is a phospholipid of mitochondrial membranes that directly interacts with several mitochondrial proteins to increase the efficiency of the respiratory chain and ADP/ATP exchange ([1] and references therein). It is also involved in protein import into mitochondria and modulates the mitochondrial retention and activity of many proteins and enzymes. CL oxidation triggers cell death and occurs in many pathologies [2]. Abnormal CL metabolism alters the structure of mitochondria including cristae loss and decreases the mitochondrial rate of divisions, fusions, and mitophagy. Altered CL metabolism can cause various forms of heart failure. These disturbances are particularly pronounced in Barth syndrome (BS), a rare X-linked genetic disorder with cardiomyopathy, skeletal myopathy, and growth delay [3]. The mutation associated with BS was mapped to the *TAZ* gene on the X chromosome [4]. More than 100 mutations in TAZ that induce BS have been reported [3]. They are scattered among all 11 exons of the gene and most of them are missense mutations or short indels, but frameshift and splicing site mutations, as well as large deletions of exons or the whole gene, also occur. No clear correlation between the mutation type and BS symptoms has been revealed.

Studies on human and animal models demonstrated that *TAZ* mutations decrease the level of mature CL and increase

that of monolyso-CL (MLCL). The MLCL/CL ratio in the blood, together with *TAZ* mutations, is the main diagnostic features of BS. The presence of the conserved motif HXXXXD (histidine and aspartic acid separated by any four amino acids) typical of glycerolipid acyltransferases pointed to the possible involvement of tafazzin in the remodeling of nascent CL. Indeed, BS patients demonstrated low linoleic acid (C18:2) incorporation into CL in contrast to other fatty acids. Moreover, the mitochondria from rat hepatocytes and human lymphoblasts realized *ex vivo* transfer of [^{14}C]linoleoyl-phosphatidylcholine to tetraoleoyl-CL, thus replacing all four acyl groups with linoleic ones [5]. Purified drosophila tafazzin efficiently transferred *in vitro* linoleic acid chains from 1-palmitoyl-2-[^{14}C]linoleoyl-phosphatidylcholine to MLCL to form CL and lysophosphatidylcholine (lysoPC, LPC).

The structure of CL is unique among phospholipids; it comprises four acyl chains derived from two molecules of phosphatidic acid linked by the central glycerol backbone [6]. In most tissues, CL has one or two dominant acyl groups, which makes it structurally uniform and molecularly symmetric [7]. Residues of unsaturated fatty acids are common dominant groups. These structural properties of mature CL forms stem from its postsynthetic modification. This remodeling starts from MLCL formation through the removal of one of four acyl groups, which is catalyzed by calcium-independent phospholipase A2 in mammals. MLCL reacetylation is mediated by three enzymes: monolysocardiolipin acyltransferase, acyl-CoA:lysocardiolipin acyltransferase, and tafazzin. The substrate specificity and specific CL remodeling remain underexplored for the first two enzymes. Tafazzin is indispensable for the maintenance of the normal composition and concentration of CL. BS induction by *TAZ* mutations indicates the importance of CL remodeling and the significance of tafazzin in mitochondrial function. Tafazzins were found in all studied eukaryotes as components of the mitochondrial intermembrane compartment [7]. The topological organization of the tafazzin molecule in mitochondria remains obscure; however, it was shown to associate with 10^5-10^6 Da multiprotein complexes. It remains unclear which proteins comprise these complexes and directly interact with tafazzin; however, this association of tafazzin with other proteins is significant for its function.

Sequence comparison of the *TAZ* gene and several of its transcripts has revealed two alternative transcription initiation sites and several splicing variants, which give rise to several tafazzin isoforms [4]. Tafazzin sequence has no explicit similarity to other known proteins; it contains two functionally important regions: a very hydrophobic sequence of 30 amino acids in the N-terminal region, apparently, a membrane anchor, and a hydrophilic domain in the central part, apparently, interacting with other proteins. The shortest tafazzin forms lack the hydrophobic region and are likely cytoplasmic proteins, while several longer variants of alternative splicing of exons 5-7 differ by the hydrophilic domain length. It is not improbable that the diversity of the hydrophilic domains modulates their affinity to different proteins. Most common isoforms are the full-length one and the one lacking exon 5. In *Drosophila*, which also has several tafazzin isoforms, they have different intracellular localization: the dominant tafazzin-A resides in mitochondria while tafazzin-B is localized in different compartments including the mitochondria, endoplasmic reticulum, and Golgi complex.

The purified recombinant tafazzin demonstrates transacylase activity towards CL and a variety of phospholipids, such as phosphatidic acid, phosphatidylcholine, phosphatidylethanolamine, phosphatidylglycerol, and phosphatidylserine, as well as their lyso-L-derivatives. The recombinant tafazzin can transfer acyl groups of 7-19 carbon atoms with 0 to 3 unsaturated double bonds. Tafazzin function is not only the conversion of a pair of phospholipids into another pair (PL1+LPL2 → LPL1+PL2) but also keeping a balance between the PL and LPL molecules. At first sight, this wide specificity of tafazzin should level the acyl composition of all phospholipids in the corresponding membrane compartments. Actually, the *in vivo* effect of tafazzin is quite specific, primarily, towards CL of the mitochondrial compartment. Apparently, the specificity of *in vivo* transacylation is largely determined by the organization of mitochondrial membranes and the availability of acyl groups rather than by the tafazzin properties. It was suggested that the major tafazzin function is to optimize the packing of phospholipids in the membranes through the thermodynamic remodeling that facilitates dynamic conformational transitions in mitochondrial membranes [7].

A deficiency of tafazzin decreases the CL concentration, alters its acyl composition, and increases the MLCL concentration. At the same time, multiprotein complexes in the inner mitochondrial membrane degrade, which can result directly from decreased CL level or indirectly from altered conformational dynamics of the membranes. Overall, this gives an insight into the origins of abnormal functional activity of mitochondria, such as decreased membrane potential, partial oxidative uncoupling, and increased oxidative stress. A further link to the phenotypic manifestations of *TAZ* mutations is not as clear. The described molecular mechanism is universal; however, the phenotypic abnormalities in BS apply to certain tissues only. For instance, morphological abnormalities in mitochondria are observed in embryonic stem cells only after their differentiation into cardiomyocytes [8]. Apparently, highly active mitochondria with high cristae density might be most sensitive to tafazzin defects. Whatever the truth, the tafazzin deficiency does not necessarily lead to defects in the mitochondrial structural organization; rather, only the proportion of defective mitochondria increases. This effect can underlie the variation of phenotypic defects in BS.

Thus, CL is a unique dimeric phospholipid specific for mitochondria, which makes it a reliable mitochondrial marker. Tissues with high oxidative capacity such as slow-twitch skeletal and cardiac muscle have high CL content ranging from 10 to 20% of the total mitochondrial phospholipids; and this is known to be critical for mitochondrial respiration and energy metabolism [9, 10]. Specifically, CL physically interacts with and activates a large number of mitochondrial proteins including most, if not all, of the inner mitochondrial membrane enzymes, along with cytochrome c and creatine kinase [11, 12]. Actually, CL can be considered as a factor integrating components of the mitochondrial respiratory chain, which provides efficient transfer of

Figure 1: The C-terminal motif of classic tafazzins (aligned to exon 11 of human FL tafazzin).

electrons and protons [11, 12]. Not only the presence of CL but also its acylation are critical for the functional activity of mitochondria. The nature of CL acyl chains can vary between tissues; however, the dominant form in the skeletal and cardiac muscles has linoleic acid (18:2n-6). A decreased proportion of this modification can interfere with the oxidase activity of cytochrome C. The main, if not the only, factor controlling the 18:2n-6 composition of CL is tafazzin, which catalyzes the transfer of 18:2n-6 from donor phospholipids such as phosphatidylcholine, thus completing CL maturation. Accordingly, mutations in the human tafazzin gene (*TAZ*) induce BS, a form of congenital myopathy featuring structural and functional abnormalities of mitochondria, cardiac and skeletal myopathy, physical load intolerance, and increased production of reactive oxygen species [13].

The tafazzin gene was first described in 1996 as a target for mutations causing BS [4, 14]. Alternative splicing of the *TAZ* primary transcript gives rise to four different experimentally observed mRNAs: full-length (FL), lacking exon 5 ($\Delta 5$), exon 7 ($\Delta 7$), or both ($\Delta 5\Delta 7$) [15]. The CL acyl chain varies between cell types and tissues in the same species. The FL and $\Delta 5$ tafazzin forms demonstrate transacylase activity but have different topology (immersion into the membrane) [16]. It remains unclear if CL remodeling is the only function of tafazzin. *TAZ* mutations decrease the synthesis of tetra-linoleoyl cardiolipin in favor of CL molecules with a different acyl composition. This change affects the structural and functional activity of mitochondria. Analysis of the patterns and proportions of tafazzin forms in the blood of BS patients and normal subjects has demonstrated, in addition to the two functional isoforms (FL and $\Delta 5$), a variety of mRNA species encoding nonfunctional protein forms.

A recent phylogenetic analysis of mitochondrial proteins in mammals and birds with significantly different maximum lifespan (MLS) [17] has demonstrated that it substantially depends on the taxon-specific numeric parameter α, which is a component of the equation of mitochondrial metabolic rate; $\mathrm{mtMR} = A \cdot M^{(B-1)/\alpha}$ (the dimension constant A will be omitted farther on). The parameter α characterizes the stability of proteins of the mitochondrial inner membrane. Another convenient index of mitochondrial metabolic rate is the basal rate of oxygen consumption per body weight per time (mtBRO_2). Disregarding the constant A, these parameters are related by the equation $\mathrm{mtMR}^{\alpha} = \mathrm{mtBRO}_2$, where $1 \le \alpha \le 8$. Overall, mtMR describes the energy requirements corresponding to species living in a particular ecological niche, while α is determined by specific amino acid composition of mitochondrial proteins and interactions between mitochondrial membrane proteins. CL, a critical integrative component of the inner membrane, should, to a large extent, determine the value of α and, hence, of species-specific MLS and mtMR. As mentioned above, acyl modification of CL by tafazzin is among the main mechanisms that control the functional activity of CL. Thus, the structural and functional properties of tafazzin can be a factor of species-specific MLS and respiratory functions of mitochondria.

Hereafter, tafazzin exons are numbered according to the FL isoform of human tafazzin (NP_000107; 292 amino acids). Without going into the description of classic tafazzins, note that their C-termini correspond to the motif shown in Figure 1, which was generated from the alignment of the C-terminal sequence of the mammalian proteins to exon 11 of the human FL tafazzin. The C-terminal sequences are aligned without deletions, and the secondary structure is preserved not only in mammals and other vertebrates but also in model protostomes (*Drosophila melanogaster*, *Caenorhabditis elegans*), fungi (*Saccharomyces cerevisiae*), etc. (see Figure 1 in [13]).

We bioinformatically analyzed the modifications in mammalian tafazzins in exons 5, 8–9, and 9–11. Specifically, the regions conserved among mammals have been identified in the C-terminal region of many isoforms of unconventional tafazzin as well as new species that acquired exon 5 in the tafazzin gene (apart from human and great apes; Hominidae). The first case tafazzins are referred to as unconventional (UTs), which are divided into two types (T1 and T2) distinguished by their motifs. The former motif results from the omission of exon 9 and a frameshift, while the second one results from intron retention between exons 10 and 11 and also a frameshift. The latter case when exon 5 is acquired is referred to as E5 tafazzins. In the rare cases, intron retention is observed between exons 8 and 9. These modifications have specific distribution among mammalian orders and correlate to the maximum lifespan and body weight as well as to the rate of mitochondrial metabolism. We propose the functional role of such changes.

2. Materials and Methods

Amino acid sequences were extracted from the RefSeq database [18] and supplemented with those from Ensembl v96 [19]. T1 isoforms of tafazzin were identified by PSI-BLAST [20] in RefSeq. The sequence ENHRADWEALQCPACARAAPGREQVSCGDSQSPD, a region of tafazzin matching in the Pacific white-sided dolphin (*Lagenorhynchus obliquidens*, isoform X5) and the narrow-ridged finless porpoise (*Neophocaena asiaeorientalis*, isoform X2), was used as the query. At the second iteration, the T1 set was supplemented only

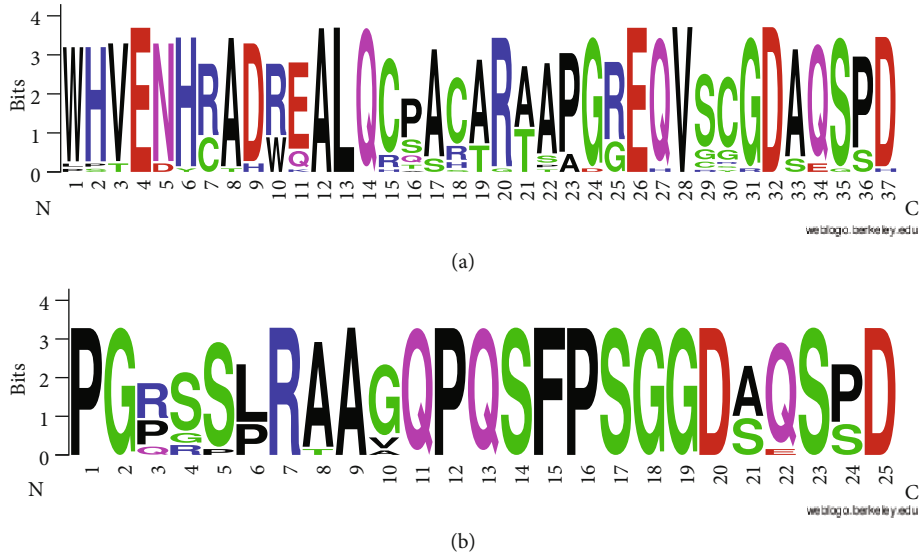

Figure 2: Motifs specific for unconventional tafazzin isoforms: (a) type 1 (T1) and (b) type 2 (T2).

by tafazzins of the naked mole-rat (NMR, *Heterocephalus glaber*) as well as additional tafazzin isoforms of the giant panda (*Ailuropoda melanoleuca*) and African bush elephant (*Loxodonta africana*); these tafazzins have a lower similarity to the query. Subsequent iterations yielded no new proteins. Eventually, 50 tafazzin sequences have been identified (listed at sheet T1 of Table S1). The *E* value cutoff was 0.005; however, the same results were obtained for the values from 0.0001 to 0.1. Hereafter, the default values were used for all unmentioned BLAST parameters.

T2 isoforms of tafazzin were identified in a similar way but using BLAST (PSI-BLAST yielded the same results). The query was the sequence PGRSSLRAAGQPQSFPSGGDSQSPD, a tafazzin region matching in the Pacific white-sided dolphin (*Lagenorhynchus obliquidens*, isoforms X1–X4) and the narrow-ridged finless porpoise (*Neophocaena asiaeorientalis*, isoform X1). The same results were obtained for *E* value cutoffs from $5 \cdot 10^{-5}$ to 10, namely, 28 tafazzins listed at sheet T2 of Table S1 together with the query, which matches all identified regions in cetaceans. The tafazzin XP_028342714 (isoform X1) of the sperm whale (*Physeter catodon*) corresponds to both T1 and T2 types. Its tafazzin XP_028342715 (X2) matches the T1 and T2 types with *E* values of 10^{-12} and $2 \cdot 10^{-5}$ and was assigned to T1. Table S1 includes a single tafazzin (XP_028342714) assigned to both T1 and T2 types.

E5 isoforms of tafazzin were identified by BLAST in RefSeq. The query was the human tafazzin region encoded by exons 4, 5, and 6 (underlined are the exon boundaries): TPAAADICFTKELHSHFFSLGKCVPVCRGAEFFQAENEGKGVLDTGRHMPGAGKRREKGDGVYQKGMDFILEKLNHGDWVHIFPE. The results remain unaltered for *E* value cutoffs from 10^{-35} to 10^{-31}. The identified proteins contain a region between exons 4 and 6 homologous to tafazzin exon 5 of apes (Hominidae, E5 tafazzins). Higher *E* values yield amino acid regions lacking the exon 5 region that cannot be assigned to E5 tafazzins. According to Table S1, E5 and T1 types do not overlap. Some species (sooty mangabey *Cercocebus atys*, green monkey *Chlorocebus sabaeus*, crab-eating macaque *Macaca fascicularis*, black snub-nosed monkey *Rhinopithecus bieti*, and African bush elephant *Loxodonta africana*) have both types, but none of their proteins belongs to both types. Thus, these three types have a single overlap (XP_028342714) for types T1 and T2, although there is no obvious reason why the loss of exon 9 cannot be combined with the acquisition of exon 5. All identified E5 tafazzins are classic (they conform to the logo in Figure 1).

For the generation of the sequence logos presented in Figure 2, a single region of each type (marked by an asterisk in Table S1) was used for each species to provide for even representation of species with a different number of tafazzin isoforms. The region most similar to the above queries for T1 or T2, respectively, was selected. Sequence logos were generated using the WebLogo service [21]. The protein secondary structures were predicted by JPred4 [22].

3. Results and Discussion

By analyzing data available in major databases, we have identified conserved C-terminal regions missing in the classic tafazzin in the amino acid sequences of mammalian tafazzin isoforms. Their motifs (sequence logos) are shown in Figures 2(a) and 2(b), and the corresponding protein sequences are presented in Table S1. This table also presents the taxonomy and Latin name of species to facilitate using their common names. Unconventional tafazzins (UTs) apply to tafazzin isoforms containing the first or the second motifs (T1 and T2).

The T1 motif was found in 23 mammalian species of 7 orders (or higher taxa): Afrotheria, Glires, Primates, Scandentia, Carnivora, Cetacea, and Artiodactyla, specifically in naked mole-rat (*Heterocephalus glaber*), Arctic ground squirrel (*Urocitellus parryii*), sooty mangabey (*Cercocebus atys*), green monkey (*Chlorocebus sabaeus*), crab-eating macaque (*Macaca fascicularis*), black snub-nosed monkey

(*Rhinopithecus bieti*), golden snub-nosed monkey (*Rhinopithecus roxellana*), Chinese tree shrew (*Tupaia belangeri chinensis*), northern fur seal (*Callorhinus ursinus*), Steller sea lion (*Eumetopias jubatus*), California sea lion (*Zalophus californianus*), Hawaiian monk seal (*Neomonachus schauinslandi*), giant panda (*Ailuropoda melanoleuca*), Pacific white-sided dolphin (*Lagenorhynchus obliquidens*), narrow-ridged finless porpoise (*Neophocaena asiaeorientalis*), sperm whale (*Physeter catodon*), zebu (*Bos indicus*), cattle (*Bos taurus*), the hybrid of the two latter (*Bos indicus* × *Bos taurus*, NCBI:txid30522), white-tailed deer (*Odocoileus virginianus*), wild boar (*Sus scrofa*), Bactrian camel (*Camelus bactrianus*), and African bush elephant (*Loxodonta africana*).

The T2 motif coincides completely in 12 species, specifically, in nearly all cetaceans and aquatic carnivores. It was found in walrus (*Odobenus rosmarus*), Weddell seal (*Leptonychotes weddellii*), Hawaiian monk seal (*Neomonachus schauinslandi*), brown and polar bears (*Ursus arctos* and *Ursus maritimus*) as well as American black bear (*Ursus americanus*, data from Ensembl), Pacific white-sided dolphin (*Lagenorhynchus obliquidens*), killer whale (*Orcinus orca*), common bottlenose dolphin (*Tursiops truncatus*), beluga whale (*Delphinapterus leucas*), narrow-ridged finless porpoise (*Neophocaena asiaeorientalis*), and sperm whale (*Physeter catodon*). It was also found in two chiropterans, black flying fox (*Pteropus alecto*) and Egyptian fruit bat (*Rousettus aegyptiacus*), as well as in a perissodactyl, white rhinoceros (*Ceratotherium simum*).

According to MobiDB [23], the conserved UT regions overlap with long disordered regions usually up to the C-terminus. These disordered regions sometimes occur in other regions of proteins but are not typical for tafazzins without the specified T1 and T2 motifs. The identified regions cannot be aligned to domains involved in enzyme activity, which gives no grounds to assume their participation in protein attachment to the mitochondrial inner membrane or being a part of the catalytic center. Similarly, disordered regions have been found at the N termini of microtubule-binding and tubulin-sequestering proteins [24].

Although RefSeq is extensive, other databases still contain proteomes missing in RefSeq. For instance, Ensembl contains the proteome of the American black bear (*Ursus americanus*) with the tafazzin containing a region matching T1; accordingly, Table S1 was supplemented with this species and the region.

In addition to the tafazzins presented in Table S1, we have found tafazzins with the C-terminal region shared in the motifs, specifically, seven C-terminal amino acids as shown in the logo (Figure 2). These can be exemplified by the North American beaver (*Castor canadensis*), whose isoforms X1, X2, and X5–X8 contain a region that partially matches both T1 and T2: VSFLPDSPKLSSVLPVPSDSQGTL AKVHEGCRPAPSLSAGGDAQSSD. The beaver can also be assigned to E5. Similarly, all isoforms (X1–X4) of the European rabbit (*Oryctolagus cuniculus*) include shortened T1 or T2; these are similar regions LPQGCGPTVSLSSGG-DAQSPH (isoforms X1 and X4), GCGPTVSLSSGGDAQSPH (X2), and LPQGCGLSSGGDAQSPH (X3), which allow us to call such proteins *shortened* UTs. Isoform X1 in naked mole-rat (*Heterocephalus glaber*) also contains the sequence GDAQGPD. Also, its T1 is represented by isoforms X2 and X3 while classic tafazzins include isoforms X4 and X5. The list of such examples goes on.

There are regions with very weak similarity to T1 or T2. For instance, isoform X1 of the Colombian white-faced capuchin (*Cebus capucinus*) is similar to T1: ALWRPDAGGAER-EAAARDRVEHRDFLAPRH; isoform X2 of the domestic sheep (*Ovis aries*) is similar to T2: VSFSLGLSSPFSLGLSSP; tafazzin of the dromedary (*Camelus dromedarius*) is similar to T2: VSSSPRQSCSCPSPSSP. To our knowledge, the capuchin has no classic tafazzin.

It is of interest that the regions GDAQSPD, GDAQSSD, GDAQSPH, GDSQSPD, GDAESPD, and GDAQGPD corresponding to the last seven positions in Figure 2 occur exclusively in unconventional tafazzins including shortened ones. Among 4 million proteins in RefSeq, there are only three exceptions, XP_007521742, XP_004712810, and XP_016049842 of European hedgehog (*Erinaceus europaeus*) and lesser hedgehog tenrec (*Echinops telfairi*), that are not tafazzins but include regions 2, 4, and 5 above. Specifically, the exact GDAQSPD sequence is present in as low as 28 mammalian proteins: 23 T1s and 5 T2s. GDSQSPD is present in 17 mammalian proteins: 4 T1s, 12 T2s, and 1 nontafazzin XP_016049842 of the hedgehog (*Erinaceus europaeus*). GDAQSSD is present in 20 mammalian proteins: 6 T1s, 8 T2s, 6 shortened UTs of the beaver (X1, X2, and X5–X8), and 1 nontafazzin XP_007521742 of the hedgehog. GDAESPD is present in 7 mammalian proteins: 4 T1s, 2 T2s, and 1 nontafazzin XP_004712810 of the tenrec (*Echinops telfairi*). GDAQSPH is present in 5 mammalian proteins: 1 T1 of Arctic ground squirrel (*Urocitellus parryii*) and 4 shortened UTs of the European rabbit (*Oryctolagus cuniculus*, X1–X4). GDAQGPD is present in 2 mammalian proteins: 2 T1s of the naked mole-rat (*Heterocephalus glaber*). RDAQSPD is present in 3 T1s of the African bush elephant (*Loxodonta africana*) and in more than a hundred nontafazzins of the family of sister chromatid cohesion protein PDS5 homolog A. Thus, these six regions largely mark unconventional tafazzins.

Hereafter, *patterns* refer to tafazzin regions specified in Materials and Methods as queries. It is natural to define the threshold segregating true T1 and T2 proteins from those with only a remote resemblance to these types. In the case of T2, at least 19 out of 25 amino acids have to match, i.e., more than 3/4. In the case of T1, it seems that true regions match at least 2/3 of the pattern (more than 22 out of 34 amino acids), although some isoforms with a lower similarity were included in the list in Table S1. For instance, there is a region with a 50% identity (17 out of 34 amino acids) in isoform X14 (XP_023396534) of the African bush elephant (*Loxodonta africana*); however, another isoform of this species (X10) used in the logo generation has more than 2/3 of matches (23 out of 34). The challenges of such a threshold definition are shown below. The prairie deer mouse (*Peromyscus maniculatus bairdii*) represented in Ensembl but not in RefSeq has a sequence matching almost a half of the first part of the T1 pattern (16 out of 34 amino acids). Such shortened T1 is typical of many rodents (the number of unconventional isoforms in RefSeq is given in

parentheses): house mouse (*Mus musculus*, 6), Gairdner's shrewmouse (*Mus pahari*, 3), Ryukyu mouse (*Mus caroli*, 2), Chinese hamster (*Cricetulus griseus*, 4), Golden hamster (*Mesocricetus auratus*, 2), lesser Egyptian jerboa (*Jaculus jaculus*, 2), and guinea pig (*Cavia porcellus*, 1). At the same time, the alignment of the region of tafazzin of the prairie deer mouse demonstrates a convincing similarity, and the absence of such tafazzins in Table S1 is due to the similarity shortness, which we consider significant. The asterisk in the prairie deer mouse sequence indicates the stop codon:

Query: ENHRADWEALQCPACARAAPGREQVSCGD-SQSPD

Subject: ENHRADREALQCTPCA*

Note that arginine at position 7 is not uncommon in mammals.

The absence of the major part of the patterns in shortened tafazzins does not allow us to assign them to UTs, although the threshold similarity length has not been defined explicitly.

In addition, new tafazzin isoforms that contain exon 5 have been found in the following orders (or higher taxa): Afrotheria, Glires, Primates, Carnivora, Cetacea, Artiodactyla, and Chiroptera. Previously, such E5 tafazzins have been found in hominids (*Homo sapiens*, *Pan paniscus*, *Pan troglodytes*, *Gorilla gorilla*, and *Pongo abelii*). Apart from these, we have identified E5 tafazzins in many Old World monkeys (Cercopithecidae): *Cercocebus atys*, *Chlorocebus sabaeus*, *Macaca fascicularis*, *M. mulatta*, *M. nemestrina*, *Mandrillus leucophaeus*, *Papio anubis*, *Theropithecus gelada*, and *Rhinopithecus bieti* as well as in the northern greater galago *Otolemur garnettii*. Occasional E5 tafazzins can be found beyond primates: in rodents (*Ochotona princeps* and *Castor canadensis*), laurasiatherians (*Pantholops hodgsonii*, *Phyllostomus discolor*, *Balaenoptera acutorostrata*, and *Puma concolor*), and afrotherians (*Loxodonta africana*). All identified E5 proteins are given in Table S1 (sheet E5).

Complementation test in yeast has demonstrated the functional activity only for the $\Delta 5$ variant, which raises the question as to why exon 5 was preserved in evolution [25]. The full-length human tafazzin proved to complement the deletion of *TAZ* gene in *Drosophila* [16]. Schlame claimed that exon 5 could be found in the *TAZ* gene only in primates [7]; however, we have found many new instances of this exon.

Figure 3 shows the number of considered species, the number of species containing each unconventional type or E5 tafazzins, and their total number per taxon (these data are given in more detail in Table S1).

In isolated cases, classic tafazzins conforming the description in Introduction preserve the intron between exons 8 and 9; such tafazzins will be referred to as CT+. Nine such cases have been found in RefSeq in the following primates: *Homo sapiens*, isoforms X2, X3, and X5 (XP_006724900, XP_016885250, and XP_024308199, respectively); bonobo (*Pan paniscus*), X2 (XP_008950941), Sumatran orangutan (*Pongo abelii*), X1 (XP_024096396), black-capped squirrel monkey (*Saimiri boliviensis*), X1, X2, and X5 (XP_010330095, XP_010330096, and XP_010330098), and chimpanzee (*Pan troglodytes*), X5, (XP_016798103). Specifically, the glycine (underlined) at the boundary of these exons, WHVGMND, is replaced with one of the following regions corresponding to a 117 bp intron insertion: GEPGDGDREMASGVGGLGLPLVPGCPAPPHVWPSVH-CAAG (human, bonobo, and chimpanzee), GEPGDGDRE-MASGVGGLGVPLVPGCPAPPHVWPSVHCAAG (orangutan), and GEPGDGDRDKASGVGSLGLPLVPGCPAPPH-VWPFVHCAAG (squirrel monkey).

Noteworthily, this intron retention exists in the human and orangutan but is missing, e.g., in the gorilla.

The exon-intron structures of the discussed tafazzin types are schematically shown in Figure 4.

As already noted, the current work is devoted to the bioinformatic study of tafazzin isoforms. Experimental verification that such tafazzin isoforms are actually expressed will be performed in a separate work.

Scatter plots for maximum lifespan (MLS, years) vs. body weight (M, kg) were generated for all classic and identified unconventional tafazzins (Figure 5). MLS data were retrieved from the AnAge database [26]. The diagram in Figure 5(a) demonstrates that species with T2 and, to a lesser extent, T1 tend towards high body weights relative to those with the classic tafazzin. Specifically, T2 is observed in the case of body weights exceeding 100 kg except large bats: Egyptian fruit bat (*Rousettus aegyptiacus*, 125 g) and black flying fox (*Pteropus alecto*, 672 g) as well as narrow-ridged finless porpoise (*Neophocaena asiaeorientalis*, 32.5 kg). T1 is observed in the case of body weights exceeding 5.5 kg with the exception of naked mole-rat (*Heterocephalus glaber*, 35 g), blind mole-rat (*Nannospalax galili*, 160 g), and tree shrew (*Tupaia chinensis*, 200 g). E5 (Figure 5(b)) is observed in the case of body weights exceeding 5.5 kg with the exception of pale spear-nosed bat (*Phyllostomus discolor*, 43 g), American pika (*Ochotona princeps*, 100 g), and northern greater galago (*Otolemur garnettii*, 1.3 kg). Similarly, MLS vs. longevity quotient (LQ) was considered (Figures 5(c) and 5(d)). T2 is characterized by a long lifespan (20 years or more even in the wild) and average LQ, while E5 features long lifespan and high (Hominidae) or average (the rest in Figures 5(c) and 5(d)) LQ. T1 has a wide range of LQ values but tends towards average LQ and long lifespan (more than 11 years).

Not much data are available on the rate of mitochondrial metabolism for the considered species. These include the data on the mitochondrial metabolic rate (mtMR) [17], basal rate of oxygen consumption (BRO_2) [27, 28], and (the most complete) mass-specific basal metabolic rate (msBMR) from the AnAge database [26] and elsewhere [29]. Several indices are available for certain species, which allowed us to reduce the available data to a single characteristic (Figure 6). The figure suggests that unconventional tafazzin isoforms focus on the optimal balance between the increased biochemical activity of mitochondria related to environmental or nutritional conditions and longevity maintenance. These unconventional tafazzins form two clusters with a significant difference in the body weight; the first one includes three artiodactyls (cattle, wild boar, and white-tailed deer; yellow squares), chimpanzee, orangutan, and human (neighboring bright-green and blue circles; according to E5 and CT+); while the second one includes the naked and blind mole-rats (yellow triangles), the microbats (Microchiroptera; 33.5 and 146 g;

Taxon					Spp.	T1	T2	E5	UT	UT+ E5
Monotremata					1					
Metatheria					4					
Eutheria	Afrotheria				6	1		1	4	5
	Euarchontoglires	Glires			24	3		2	6	9
		Primates	Cercopithecidae		12	5		9	8	19
			Hominidae		5			5		23
			Hylobatidae		1					
			Platyrrhini		4					
			Tarsiidae		1					
			Strepsirrhini		3			1		1
		Dermoptera			1					
		Scandentia			1	1			1	1
	Laurasiatheria	Carnivora	Canidae		3					
			Mustelidae		2					
			Odobenidae		1		1		1	1
			Otariidae		3	3			4	4
			Phocidae		2	1	2		4	4
			Ursidae		4	1	3		10	10
			Felidae		5			1		1
		Cetartio-dactyla	Cetacea	Mysticeti	1			1		1
				Odontoceti	7	3	6		17	17
			Ruminantia		10	4		1	14	16
			Suidae		1	1			1	1
			Camelidae		4	1			1	1
		Perissodactyla			4		1		2	2
		Chiroptera	Megachiroptera		3		2		5	5
			Microchiroptera		8			1		3
		Eulipotyphla			3					
		Pholidota			1					
		Xenarthra			1					
Total					126	24	15	22	78	124

Figure 3: Distribution of species containing each unconventional type or E5 tafazzins and their total number per taxon. The following indices are given for each taxon (left to right): total number of considered species, numbers of species with T1, T2, and E5, the total number of unconventional tafazzins, and this number supplemented with E5 tafazzins.

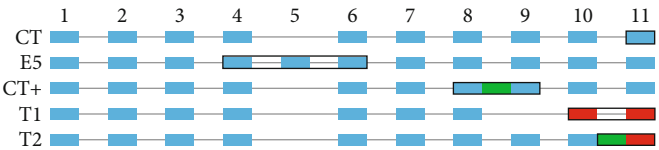

Figure 4: The exon-intron structures of the considered tafazzin types. Usual exons (i.e., as in CL) are depicted by blue rectangles, retained introns are shown in green, and frameshifted exons are shown in red. The black outlines emphasize the distinguishing features of the tafazzin types.

bright-green and bright-red diamonds), American pika (bright-green triangle), New World monkeys (squirrel monkey, blue circle above the curve; according to CT+), and northern greater galago (bright-green circles). In the second cluster, the body weight is nearly 100 times lower; however, the rate of oxygen consumption per body weight is 4-5 times higher. This is in a good agreement with the Kleiber equation $\dot{V}(O_2)/m = 3.42 \cdot m^{-0.25}$ [30] presented as a straight line in the figure. One can propose that the emergence of UTs in addition to E5 was a response to the increased mass-specific oxygen consumption considering that it is found in aquatic mammals, large bats, and white rhinoceros.

(1) Conservation of Cardiolipin Synthase and Variability of Tafazzin. Cardiolipin synthase 1 encoded by the gene CRLS1 (ENSG00000088766) in human is highly conserved. A single isoform exists in most species. The reaction catalyzed by it yields a variety of cardiolipins whose transformation is mediated by the classic and unconventional isoforms of tafazzin. One can propose that these isoforms modulate

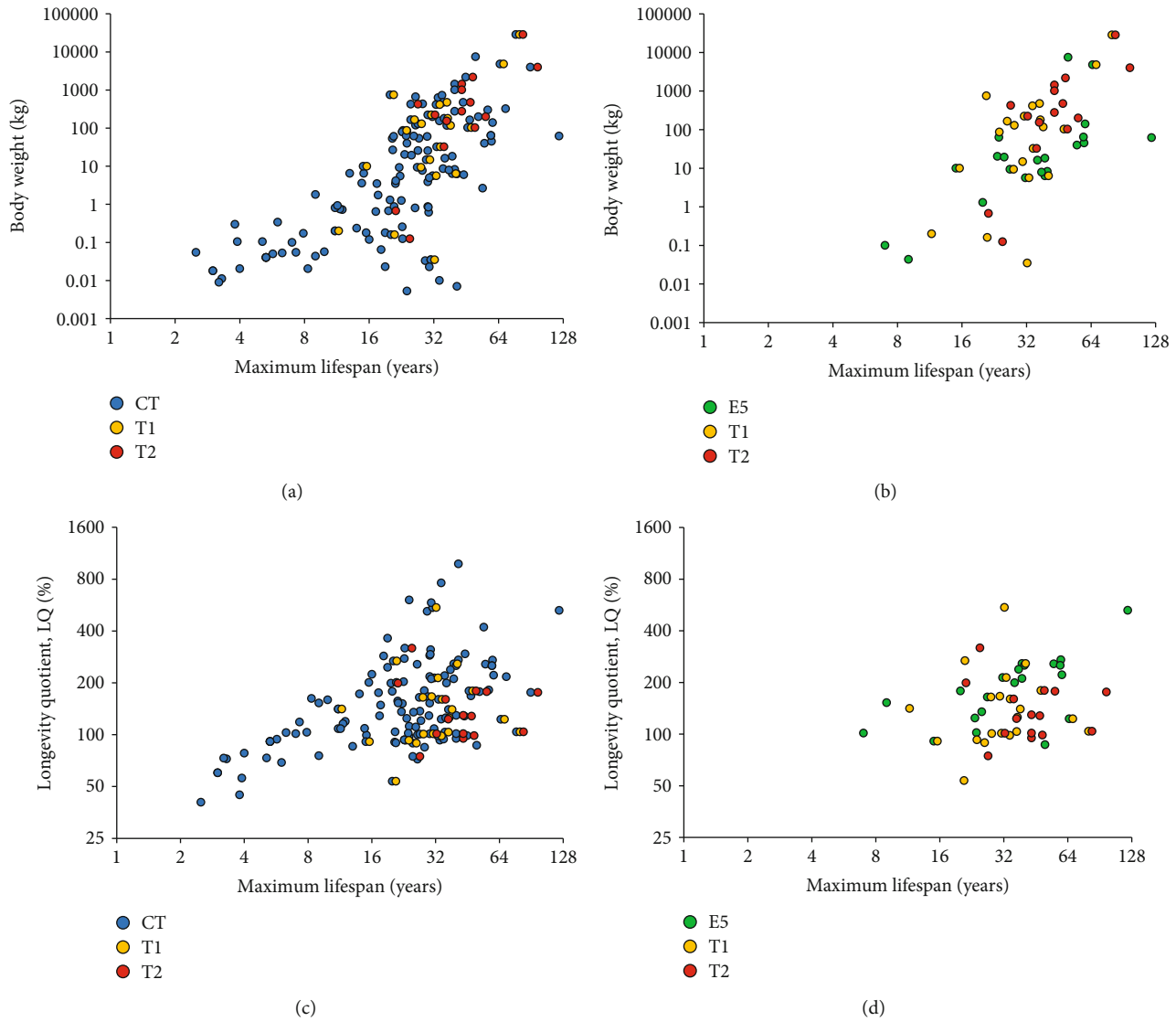

Figure 5: Distribution of mammalian tafazzins over lifespan and body weight (a, b) or longevity quotient (c, d) for classic tafazzin (CT) and unconventional T1 and T2 ones (a, c) or E5, T1, and T2 tafazzins (b, d).

the acyl composition of cardiolipins as a function of environmental conditions.

(2) The Possible Relationship between T1 and T2. In addition to the discussed above sperm whale tafazzin XP_028342715 (X2) to a different extent applying to the T1 and T2 types, there is another sperm whale protein XP_028342714 (X1) fully applying to T2 and satisfactorily applying to T1. It is the only known tafazzin with a complete T2 motif preceded at a distance of 16 amino acids by an almost complete T1 motif (lacking the terminal GDSQSPD). This isoform was assigned to both types, T1 and T2. These three isoforms illustrate a possible transition from the "intermediate" T1 type to the "new" T2 type. Specifically,

X3: ENHRADWEALQRPACARAAPGREQVSCGDSQSPD
X2: ENHRADWEALQRPACARAAPGREQVSCQPQSFPSGGDSQSPD
X1: ENHRADWEALQRPACARAAPGREQVSCEFSPRPSQSCPSPYPLCPWPPRDPGRSSLRAAGQPQSFPSGGDSQSPD.

Here, X3 is a typical T1; X2 is a T1 with insertion from T2 (turquoise); and X1 is a T1 with an insertion converting it into T2 (T2-specific motif is underlined). Apparently, the loss of exon 9 is more common than the intron fixation here. Coupled with the high number of T1 tafazzins, this points to the emergence of T2 after T1.

(3) Relationship between UT and Exons. In the classic tafazzin, the translation of exon 10 starts in phase 0 (i.e., the first exon nucleotide is the first codon nucleotide). The T1 tafazzin results from skipping exon 9 (see Figure 4) so that the spliced out region is not a multiple of three. After exon 9 splicing, the translation of exon 10 starts in phase 1 (the first nucleotide of the exon is the second nucleotide in the codon) and the first 26 amino acids of T1 motif are synthesized. The remaining 8 amino acids of the motif result from the translation of the subsequent exon eleven (also in phase 1 since the length of exon 10 is a multiple of three).

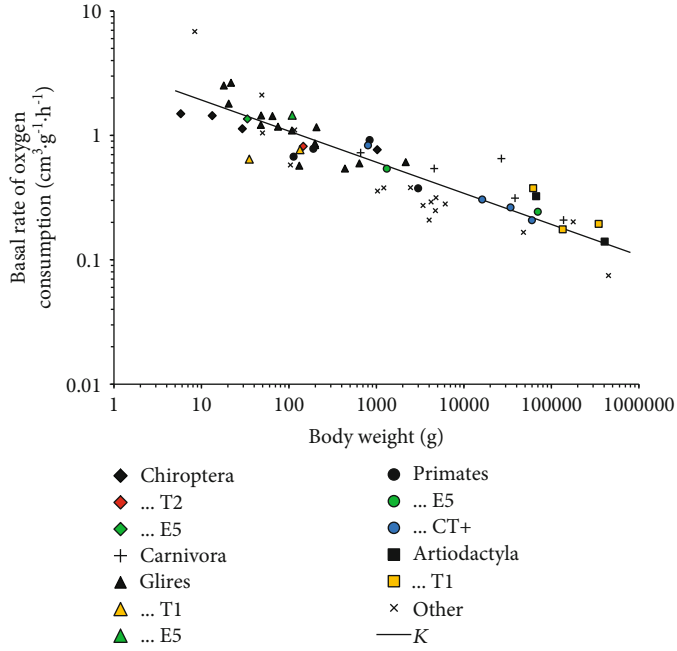

Figure 6: Oxygen consumption by mammals. Unconventional tafazzins T1 and T2 as well as E5 and CT+ are marked in yellow, bright-red, bright-green, and blue, respectively (the data for the CT+ species are from [28]). The line labeled *K* is the Kleiber relation.

This mechanism can be demonstrated on mouse tafazzin isoforms from Ensembl. The isoform ENSMUSP00000065270 corresponds to the classic tafazzin, while the other one (ENSMUSP00000134745) lacks exon 9 (ENSMUSE00000209157). In the first case, exon 10 translation yields amino acid sequence KITVLIGKPFSTLPVLERLRAENKSA; in the second case, ENHRADWEALQYTPCA, which corresponds to the onset of T1 motif. The mouse protein terminates here due to a stop codon; in the absence of it, the following sequence corresponds to T1 motif. This can be illustrated by the human FL isoform of tafazzin ENSP00000469981. After deletion of exon 9 (ENSE00003724812) from its transcript (ENST00000601016), the amino acid sequence corresponding to exon 10 and beginning of exon 11, KITVLIGKPFSALPVLERLRAENKSAVEMRKALT…, is replaced with ENHCADREALQCPACTRAAPGGEQVGCGDAESPD…, which corresponds to T1 motif. No exon 9 splicing has been reported for human; however, such proteins were experimentally demonstrated in mouse (e.g., Q810E8 in UniProt). It is not unlikely that the stop codon of the primary transcript is edited and translated as an amino acid in certain species.

Similarly, it can be shown that T2 results from intron retention between exons 10 and 11 (see Figure 4). This can be illustrated by two tafazzin isoforms of the polar bear. The first transcript (ENSUMAT00000031820), a classic tafazzin, has no introns; and translation of exons 10 and 11 generates the classic C-terminus: KITVLIGKPFSALPVLERLRAENKSAVEMRKALTDFIQEEFQRLKTQAEQLHNQLQRGR. In the second transcript (ENSUMAT00000031828), intron retention between exons 10 and 11 gives rise to the C-terminus with a typical T2 motif: KITVLIGKPFSALPVLERLRAENKSAVSCLSPLYHPPFPGLPCSCLSLSRHLQPPRAPGSSS**PGPGSPRAAVQPQSFPSGGDAQSSD**…. The sequence encoded by the retained intron is underlined and T2 motif is in bold. Notice that, similar to T1, exon 11 is translated in phase 1 rather than the natural phase 0, which explains the coincidence of the last seven amino acids in these two motifs (see Figure 2).

(4) Special Features of C-Termini of UTs. The mechanism of UT realization, i.e., the functional role of the revealed conserved C-terminal regions of tafazzin, is of great interest. In this context, it should be noted that the C-terminal secondary structure differs in UTs and classic tafazzins (CTs) (Figure 7). For instance, the house mouse CT (ENSMUSP00000065270.6) has a single long helix at the C-terminus, while in shortened UTs it is broken into two (walrus, beaver, and rabbit) or more (naked mole-rat) parts. One can propose that these C-terminal helices in UTs do not interact with the membrane since they are rich in polar amino acids. Specifically, the C-terminus of these tafazzins following the RAENKSA motif contains 2-5 times more polar amino acids, which decreases the C-terminal hydrophobicity.

(5) The Specificity of UT Taxonomic Distribution. UTs demonstrate highly uneven distribution in Euarchontoglires and Laurasiatheria. This is systemically shown in Figure 3 and briefly exemplified here. UTs are not found in monotremes and marsupials and are rare in afrotherians (1 out of 6 = 17 %); this is also true for E5. A similar UT distribution is observed in Euarchontoglires (9/51 = 18%), specifically, in Glires, Old World monkeys, and tree shrew; E5 is more common (17/51 = 33%) in the same orders and families plus hominids and lemuriform primates (Strepsirrhini). UTs are found in Laurasiatheria in a much higher proportion,

Figure 7: Secondary structure of tafazzin. Helices and extended regions predicted by JPred4 are marked green and blue, respectively. Mouse, CT; walrus, seal, bear, orca, bat, and rhino, T2; beaver, rabbit, and NMR, shortened UT where underlined regions support their assignment to UT (beaver and NMR also have different isoforms listed in Table S1). Abbreviations: mouse: NP_852657.1, isoform 2 (*Mus musculus*); walrus: XP_004414556.1, X1 (*Odobenus rosmarus*); seal: XP_006739411.1, X1 (*Leptonychotes weddellii*); orca: XP_012394911.1, X1 (*Orcinus orca*); bear: XP_026344949.1, X1 (*Ursus arctos*); bat: XP_015979168.1, X1 (*Rousettus aegyptiacus*); rhino: XP_014653014.1, X1 (*Ceratotherium simum*); beaver: XP_020040765.1, X1 (*Castor canadensis*); rabbit: XP_017194047.1, X1 (*Oryctolagus cuniculus*); NMR: XP_004875054.1, X1 (*Heterocephalus glaber*). Entirely conserved positions are labeled with asterisks.

specifically, in pinnipeds, bears, toothed whales, ruminants, swines, camelids, perissodactyls, and fruit bats, while the proportion of E5 is much lower (4/62 = 6%). Neither UT nor E5 has been found in insectivores, pangolins, and anteaters and sloths. Usually, one of the types (T1 or T2) is represented in a family excluding earless seals and bears (Carnivora) and toothed whales. T2 was found in the polar, American black, and brown bears, while their remote relative, the giant panda, has T1. T2 was also found in fruit bats but is missing in considered microbat species of the *Myotis* genus.

(6) UTs and MLS. The presence of UTs somewhat correlates with MLS as indicated by the examples below. Among long-lived rodents, unconventional T1 is found in the naked and blind mole-rats but is missing in the Damaraland mole-rat. No UTs have been found among other rodents except for the Arctic ground squirrel. Among primates, T1 was found only in certain Old World monkeys with low MLS as well as in a close relative of primates, the tree shrew (Euarchonta). Among afrotherians, T1 was found only in the African bush elephant. Among artiodactyls, T1 was found in species with both high (zebu, cattle, and Bactrian camel) and lesser MLS (white-tailed deer and wild boar). Many aquatic mammals with high MLS proved to have T1 or T2 or both. Overall, many long-lived species belong to orders where unconventional or E5 tafazzins were identified (primates, carnivores, perissodactyls, and cetartiodactyls).

(7) UTs and Body Weight. UTs demonstrate an interesting distribution across taxonomic groups as a function of body weight. Irrespective of taxonomic groups, considered mammals with body weight exceeding 1000 kg had T1 (sperm whale and elephant) or T2 (walrus, killer whale, beluga whale, and sperm whale) (Figure 3) with a single exception: no UT has been found in the common minke whale; however, the group of baleen whales remains underexplored

and its only classic tafazzin is marked as a low-quality protein in NCBI.

In the range from 500 to 1000 kg, T2 has not been found among considered species. In ruminants, T1 was found only in the cattle and zebu (livestock), which can be attributed to increased biodiversity after natural selection was replaced with artificial one, whose rate is much higher [31]. Only classic tafazzin was found in the wild yak, bison, and wild water buffalo.

Nearly a half (7/15 = 47%) of species with T2 fall into the range from 100 to 500 kg; these include cetaceans and carnivores. In tylopods, T1 was found in the domestic Bactrian camel but is missing in the wild Bactrian camel, which are considered different species [32]. This agrees with the above pattern for domestic and wild ruminants. In perissodactyls, UTs are absent in the common donkey, domesticated horse, and Przewalski's horse. Their tafazzins have RAENKSA sequence at the end of exon 10; however, the following sequences does not allow them to be assigned to T2.

In monkeys weighing less than 100 kg, T1 is found in about a half of the Old World monkeys (5/12 = 42%) with the terminal sequence GDAQSPD (except isoform X5 in the sooty mangabey *Cercocebus atys*); apparently, it competes with the classic monkey tafazzin with the exon 5 insertion. All hominids have only the classic tafazzin (with the exon 5 insertion).

UTs are found in marine carnivores with the body weight from 165 to 1012 kg, i.e., within 2- to 3-fold variation from 500 kg; the latter value corresponds to the optimal balance between heat exchange and food resources [33]. No UTs were found in mustelids and baleen whales, whose body weight differs from 500 kg by order of magnitude, which can reflect different energy expenditures related to the food resources or a different evolutionary pathway. The manatee (Afrotheria) weighing 322 kg is the exception.

(8) UTs and Evolution of Species. The relationship between UTs and evolution of species requires further analysis. However, the following observations deserve to be mentioned. No UTs were found in bats except T2 in two species that lack echolocation. Microbats followed their own evolutionary pathway resulting in decreased body size, special skills (echolocation, etc.), and improved flight performance [34]. Also, they have a higher metabolic activity owing to genes of the oxidative phosphorylation pathway and DNA repair efficiency [35]. In Old World primates, UTs are absent in hominids, T1 is found in monkeys, and both taxa have E5. UT and E5 are missing in New World monkeys. UTs are absent in lemuriformes. Apart from T1, which occurs in many mammals, more than half of marine mammals have T2. UTs have not been found in monotremes and marsupials as well as in early diverged placentals (Hoffmann's two-toed sloth and armadillo); T1 UT was found only in the African bush elephant among afrotherians. Thus, one can conclude that UTs emerged late in evolution: they are absent in monotremes (218 MYA), marsupials (169 MYA), anteaters and sloths (99 MYA), and afrotherians (94 MYA) excluding the African bush elephant and later in insectivores (81 MYA) and pangolins (74 MYA) [36].

4. Conclusions

A wide but specific distribution of tafazzin (a cardiolipin remodeler) with altered C-terminus or intron insertions across orders and other taxa was demonstrated in Euarchontoglires and Laurasiatheria. Specifically, we have found conserved regions closer to the C-terminus in many unconventional isoforms, rare cases of intron retention between exons 8 and 9, and new species that acquired exon 5 in the tafazzin gene (apart from Hominidae). The C-terminal regions result from a frameshift relative to the full-length *TAZ* transcript after skipping exon 9 or retention of the intron between exons 10 and 11. The altered ratio between tafazzin isoforms can cause severe diseases such as Barth syndrome. These alterations demonstrate specific distribution among mammalian orders. The dependence of the species maximum lifespan, body weight, and mitochondrial metabolic rate on the alterations has been demonstrated. Arguably, unconventional tafazzin isoforms provide for the optimal balance between the increased biochemical activity of mitochondria (resulting from specific environmental or nutritional conditions) and lifespan maintenance, and the functional role of such isoforms is linked to the modification of the primary and secondary structures of their C-termini.

Data Availability

All data used to support the findings of this study are included in the article and the supplementary file.

Conflicts of Interest

The authors declare that there is no conflict of interest regarding the publication of this paper.

Acknowledgments

The reported study was funded by the Russian Foundation for Basic Research (project no. 18-29-13037).

Supplementary Materials

Table S1: the sheet "species" covers the distribution of identified unconventional isoforms of tafazzin among 125 mammalian species that have an ortholog of the human tafazzin (GeneID 6901) according to Entrez Gene database [37]. Column 1 indicates taxon ID in NCBI taxonomy database [38]. Column 2 shows a brief species taxonomy within the order of mammals; column 3, species scientific name; columns T1, T2, and E5, numbers of the corresponding tafazzin isoforms identified. The sheets T1, T2, and E5 list the corresponding isoforms identified. In these sheets, column 1 indicates protein ID in RefSeq; columns 2 and 3 replicate those from the "species" sheet; column 4 specifies the isoform number; asterisk in column 5 indicates proteins used in the logo generation (Figure 2). The last column presents the

protein regions. The central part in sheet E5 contains hominid proteins where E5 was previously identified elsewhere. *(Supplementary Materials)*

References

[1] G. J. Gaspard and C. R. McMaster, "Cardiolipin metabolism and its causal role in the etiology of the inherited cardiomyopathy Barth syndrome," *Chemistry and Physics of Lipids*, vol. 193, pp. 1–10, 2015.

[2] A. Y. Mulkidjanian, D. N. Shalaeva, K. G. Lyamzaev, and B. V. Chernyak, "Does oxidation of mitochondrial cardiolipin trigger a chain of antiapoptotic reactions?," *Biochemistry (Moscow)*, vol. 83, no. 10, pp. 1263–1278, 2018.

[3] S. Ghosh, D. M. Iadarola, W. B. Ball, and V. M. Gohil, "Mitochondrial dysfunctions in Barth syndrome," *IUBMB Life*, vol. 71, no. 7, pp. 791–801, 2019.

[4] S. Bione, P. D'Adamo, E. Maestrini, A. K. Gedeon, P. A. Bolhuis, and D. Toniolo, "A novel X-linked gene, G4.5. is responsible for Barth syndrome," *Nature Genetics*, vol. 12, no. 4, pp. 385–389, 1996.

[5] Y. Xu and M. Schlame, "The turnover of glycerol and acyl moieties of cardiolipin," *Chemistry and Physics of Lipids*, vol. 179, pp. 17–24, 2014.

[6] M. Schlame, "Thematic Review Series: Glycerolipids.Cardiolipin synthesis for the assembly of bacterial and mitochondrial membranes," *Journal of Lipid Research*, vol. 49, no. 8, pp. 1607–1620, 2008.

[7] M. Schlame, "Cardiolipin remodeling and the function of tafazzin," *Biochimica et Biophysica Acta*, vol. 1831, no. 3, pp. 582–588, 2013.

[8] D. Acehan, Z. Khuchua, R. H. Houtkooper et al., "Distinct effects of tafazzin deletion in differentiated and undifferentiated mitochondria," *Mitochondrion*, vol. 9, no. 2, pp. 86–95, 2009.

[9] M. Schlame, M. Ren, Y. Xu, M. L. Greenberg, and I. Haller, "Molecular symmetry in mitochondrial cardiolipins," *Chemistry and Physics of Lipids*, vol. 138, no. 1–2, pp. 38–49, 2005.

[10] L. E. Stefanyk, N. Coverdale, B. D. Roy, S. J. Peters, and P. J. LeBlanc, "Skeletal muscle type comparison of subsarcolemmal mitochondrial membrane phospholipid fatty acid composition in rat," *The Journal of Membrane Biology*, vol. 234, no. 3, pp. 207–215, 2010.

[11] M. Schlame, D. Rua, and M. L. Greenberg, "The biosynthesis and functional role of cardiolipin," *Progress in Lipid Research*, vol. 39, no. 3, pp. 257–288, 2000.

[12] M. Schlame and M. Ren, "The role of cardiolipin in the structural organization of mitochondrial membranes," *Biochimica et Biophysica Acta*, vol. 1788, no. 10, pp. 2080–2083, 2009.

[13] A. Hijikata, K. Yura, O. Ohara, and M. Go, "Structural and functional analyses of Barth syndrome-causing mutations and alternative splicing in the tafazzin acyltransferase domain," *Meta Gene*, vol. 4, pp. 92–106, 2015.

[14] I. L. Gonzalez, "Barth syndrome: *TAZ* gene mutations, mRNAs, and evolution," *American Journal of Medical Genetics. Part A*, vol. 134A, no. 4, pp. 409–414, 2005.

[15] S. M. Kirwin, A. Manolakos, S. S. Barnett, and I. L. Gonzalez, "Tafazzin splice variants and mutations in Barth syndrome," *Molecular Genetics and Metabolism*, vol. 111, no. 1, pp. 26–32, 2014.

[16] Y. Xu, S. Zhang, A. Malhotra et al., "Characterization of tafazzin splice variants from humans and fruit flies," *The Journal of Biological Chemistry*, vol. 284, no. 42, pp. 29230–29239, 2009.

[17] Y. Kitazoe, M. Hasegawa, M. Tanaka, M. Futami, and J. Futami, "Mitochondrial determinants of mammalian longevity," *Open biology*, vol. 7, no. 10, p. 170083, 2017.

[18] N. A. O'Leary, M. W. Wright, J. R. Brister et al., "Reference sequence (RefSeq) database at NCBI: current status, taxonomic expansion, and functional annotation," *Nucleic Acids Research*, vol. 44, no. D1, pp. D733–D745, 2016.

[19] D. R. Zerbino, P. Achuthan, W. Akanni et al., "Ensembl 2018," *Nucleic Acids Research*, vol. 46, no. D1, pp. D754–D761, 2018.

[20] S. F. Altschul and E. V. Koonin, "Iterated profile searches with PSI-BLAST—a tool for discovery in protein databases," *Trends in Biochemical Sciences*, vol. 23, no. 11, pp. 444–447, 1998.

[21] G. E. Crooks, G. Hon, J. M. Chandonia, and S. E. Brenner, "WebLogo: a sequence logo generator," *Genome Research*, vol. 14, no. 6, pp. 1188–1190, 2004.

[22] A. Drozdetskiy, C. Cole, J. Procter, and G. J. Barton, "JPred4: a protein secondary structure prediction server," *Nucleic Acids Research*, vol. 43, no. W1, pp. W389–W394, 2015.

[23] D. Piovesan, F. Tabaro, L. Paladin et al., "MobiDB 3.0: more annotations for intrinsic disorder, conformational diversity and interactions in proteins," *Nucleic Acids Research*, vol. 46, no. D1, pp. D471–D476, 2018.

[24] N. I. Trushina, A. Y. Mulkidjanian, and R. Brandt, "The microtubule skeleton and the evolution of neuronal complexity in vertebrates," *Biological Chemistry*, vol. 400, no. 9, pp. 1163–1179, 2019.

[25] F. M. Vaz, R. H. Houtkooper, F. Valianpour, P. G. Barth, and R. J. A. Wanders, "Only one splice variant of the human *TAZ* gene encodes a functional protein with a role in cardiolipin metabolism," *The Journal of Biological Chemistry*, vol. 278, no. 44, pp. 43089–43094, 2003.

[26] J. P. de Magalhães and J. Costa, "A database of vertebrate longevity records and their relation to other life–history traits," *Journal of Evolutionary Biology*, vol. 22, no. 8, pp. 1770–1774, 2009.

[27] B. K. McNab, "The influence of food habits on the energetics of eutherian mammals," *Ecological Monographs*, vol. 56, no. 1, pp. 1–19, 1986.

[28] C. Ross, "Basal metabolic rate, body weight and diet in primates: an evaluation of the evidence," *Folia Primatologica*, vol. 58, no. 1, pp. 7–23, 1992.

[29] V. M. Savage, J. F. Gillooly, W. H. Woodruff et al., "The predominance of quarter-power scaling in biology," *Functional Ecology*, vol. 18, no. 2, pp. 257–282, 2004.

[30] M. Kleiber, *The Fire of Life*, John Wiley, New York, New York, USA, 1961.

[31] P. D. Gingerich, "Rates of evolution: effects of time and temporal scaling," *Science*, vol. 222, no. 4620, pp. 159–161, 1983.

[32] E. Mohandesan, R. R. Fitak, J. Corander et al., "Mitogenome sequencing in the genus Camelus reveals evidence for purifying selection and long-term divergence between wild and domestic Bactrian camels," *Scientific Reports*, vol. 7, no. 1, p. 9970, 2017.

[33] W. Gearty, C. R. McClain, and J. L. Payne, "Energetic tradeoffs control the size distribution of aquatic mammals," *Proceedings*

of the National Academy of Sciences of the United States of America, vol. 115, no. 16, pp. 4194–4199, 2018.

[34] G. Zhang, C. Cowled, Z. Shi et al., "Comparative analysis of bat genomes provides insight into the evolution of flight and immunity," *Science*, vol. 339, no. 6118, pp. 456–460, 2013.

[35] Y. Y. Shen, L. Liang, Z. H. Zhu, W. P. Zhou, D. M. Irwin, and Y. P. Zhang, "Adaptive evolution of energy metabolism genes and the origin of flight in bats," *Proceedings of the National Academy of Sciences of the United States of America*, vol. 107, no. 19, pp. 8666–8671, 2010.

[36] N. M. Foley, M. S. Springer, and E. C. Teeling, "Mammal madness: is the mammal tree of life not yet resolved?," *Philosophical Transactions of the Royal Society B: Biological Sciences*, vol. 371, no. 1699, p. 20150140, 2016.

[37] D. Maglott, J. Ostell, K. D. Pruitt, and T. Tatusova, "Entrez Gene: gene-centered information at NCBI," *Nucleic Acids Research*, vol. 39, no. Database, pp. D52–D57, 2011.

[38] S. Federhen, "The NCBI Taxonomy database," *Nucleic Acids Research*, vol. 40, no. D1, pp. D136–D143, 2012.

Hindawi
Oxidative Medicine and Cellular Longevity
Volume 2019, Article ID 1232146, 11 pages
https://doi.org/10.1155/2019/1232146

Research Article

Zinc-Induced SUMOylation of Dynamin-Related Protein 1 Protects the Heart against Ischemia-Reperfusion Injury

Xiyun Bian,[1] Jingman Xu,[2] Huanhuan Zhao,[3] Quan Zheng,[1] Xiaolin Xiao,[1] Xiaofang Ma,[1] Yanxia Li,[1] Xinping Du,[4] and Xiaozhi Liu[1]

[1]*Central Laboratory, The Fifth Central Hospital of Tianjin, Tianjin 300450, China*
[2]*Medical Research Center, North China University of Science and Technology, Tangshan 063000, China*
[3]*Department of Physiology and Pathophysiology, Tianjin Medical University, 300070 Tianjin, China*
[4]*Department of Cardiology, The Fifth Central Hospital of Tianjin, Tianjin 300450, China*

Correspondence should be addressed to Xinping Du; xpdu2012@163.com and Xiaozhi Liu; lxz7997@126.com

Received 29 April 2019; Accepted 13 June 2019; Published 22 July 2019

Guest Editor: Konstantin Lyamzaev

Background. Zinc plays a role in mitophagy and protects cardiomyocytes from ischemia/reperfusion injury. This study is aimed at investigating whether SUMOylation of Drp1 is involved in the protection of zinc ion on cardiac I/R injury. *Methods*. Mouse hearts were subjected to 30 minutes of regional ischemia followed by 2 hours of reperfusion (ischemia/reoxygenation (I/R)). Infarct size and apoptosis were assessed. HL-1 cells were subjected to 24 hours of hypoxia and 6 hours of reoxygenation (hypoxia/reoxygenation (H/R)). Zinc was given 5 min before reperfusion for 30 min. SENP2 overexpression plasmid (Flag-SENP2), Drp1 mutation plasmid (Myc-Drp1 4KR), and SUMO1 siRNA were transfected into HL-1 cells for 48 h before hypoxia. Effects of zinc on SUMO family members were analyzed by Western blotting. SUMOylation of Drp1, apoptosis and the collapse of mitochondrial membrane potential ($\Delta\Psi$m), and mitophagy were evaluated. *Results*. Compared with the control, SUMO1 modification level of proteins in the H/R decreased, while this effect was reversed by zinc. In the setting of H/R, zinc attenuated myocardial apoptosis, which was reversed by SUMO1 siRNA. Similar effects were observed in SUMO1 KO mice exposed to H/R. In addition, the dynamin-related protein 1 (Drp1) is a target protein of SUMO1. The SUMOylation of Drp1 induced by zinc regulated mitophagy and contributed to the protective effect of zinc on H/R injury. *Conclusions*. SUMOylation of Drp1 played an essential role in zinc-induced cardio protection against I/R injury. Our findings provide a promising therapeutic approach for acute myocardial I/R injury.

1. Introduction

Myocardial ischemia-reperfusion (I/R) injury causes a variety of serious consequences, including ventricular fibrillation, heart rupture, and sudden death. Currently, there are few effective interventions to protect the heart against ischemia-reperfusion injury [1]. Sheng et al. [2] found that levels of zinc decreased in cardiomyocytes during reperfusion and zinc ion is one of the essential trace elements for the body. Zinc was involved in the regulation of more than 100 proteases, structural stability of cell membranes and organelles, and regulation of signaling pathways in various pathophysiological processes [3]. Moreover, the levels of various zinc transporters maintain zinc homeostasis during reoxygenation. Protein levels of ZnT1, ZnT2, ZnT5, and ZnT9 decreased, and protein levels of Zip2, Zip7, Zip13, and Zip14 increased [4]. These indicated that endogenous zinc ions played an important role in myocardial ischemia-reperfusion injury. Similarly, isolated rat hearts treated with exogenous zinc ions during reperfusion reduced the infarct size of the heart through some kinase pathways, and rat cardiomyocytes H9c2 treated with zinc ions during reoxygenation also reduced myocardial cell damage [5]. It is indicated that exogenous zinc ions also protect the myocardium from I/R or H/R damage. However, the exact protection mechanism of zinc ions needs to be further explored.

In the past ten years, a number of studies have shown that SUMOylation is involved in determining the fate of perfused

heart [6, 7]. Currently, there are five mammalian SUMO paralogues (SUMO1, SUMO2, SUMO3, SUMO4, and SUMO5). The primary structural homology of SUMO1, SUMO2, and SUMO3 proteins is nearly 50%, and the homology of SUMO2 and SUMO3 proteins is about 97%. The structure of SUMO4 and SUMO5 is different from the other three SUMO proteins, and they have not been widely observed in mammalians [8, 9]. SUMO4, lacking of C-terminal processing, results in its inability to conjugate to lysine residues in target proteins [10]. SUMOylation is a dynamic reversible process and can be mediated by the SENP family. There are seven mammalian SENPs, including SENP1, SENP2, SENP3, SENP5, SENP6, SENP7, and SENP8. Of these, SENP8 shows a specificity against ubiquitin-like Nedd8 protein and does not reverse SUMOylation. Other SENPs have a different specificity for SUMOs. SENP1 and SENP2 have a broad specificity for SUMO1 and SUMO2/3, while SENP3 and SENP5 favour the removal of SUMO2, and SENP6 and SENP7 have less effect on SUMO2/3 monomer than poly-SUMO of SUMO2/3 [11]. The SUMO conjugation pathway is important for the development of a wide variety of human diseases such as brain ischemia and tumorigenesis [12–14]. Previous work also indicated that SUMOs targeting the proteins contribute to a number of human cardiovascular disease, such as valvular abnormalities, ischemic heart disease, cardiac hypertrophy, and idiopathic cardiomyopathy [15]. In animals subjected to heart I/R, SUMO1 conjugations were shown to be inactivated [16]. However, it is unclear, under these conditions, whether and how SUMO modification is involved in the protection of zinc ions against cardiac I/R injury.

Dynamin-related protein (Drp) 1 is a key protein for mitochondrial fission. It consists of four parts: GTP-binding, middle, insert B, and C-terminal GTPase effector (GED) domains. A variety of posttranscriptional modifications contribute to the regulation of Drp1 activity, such as phosphorylation, ubiquitination, SUMOylation, and S-nitrosylation, and SUMOylation appears to exert a role in the regulation of Drp1 activity [17, 18]. Studies have reported the removal of SUMO2/3 from Drp1 mediated by SENP3 and SENP5 and the removal of SUMO1 from Drp1 through SENP2 [6, 19, 20]. However, there is no evidence indicating a direct involvement of SUMOylation of Drp1 in the protection of zinc against cardiac I/R injury.

The aim of our study is to determine whether (1) the SUMOylation of Drp1 contributes to the progression of myocardial I/R injury and how it contributes to the protection of zinc preconditioning and (2) zinc preconditioning can induce mitophagy via regulating Drp1 SUMOylation in the heart.

2. Methods

This study conforms to the NIH Guide for the Care and Use of Laboratory Animals (NIH publication No. 85–23, revised 1996).

2.1. Chemicals and SUMO1 KO Mice. $ZnCl_2$ and N,N,N′, N′- tetrakis-(2-pyridylmethyl) ethylenediamine (TPEN) was purchased from Sigma (St. Louis, MO, USA). SUMO1 KO animals were graciously made available by Professor Wei Yang and Huaxin Sheng (Duke University, Durham, North Carolina, USA) [7]. Wild-type C57Bl/6J mice were purchased from the Military Medical Science Academy Laboratory, Beijing, China.

2.2. Perfusion of Isolated Rat Hearts. Mice ($n = 6$/group) were anesthetized with isoflurane (300 mg/kg, intraperitoneal). After the mice were anesthetized, the PE-90 cannula with internal and external core structure was used for tracheal intubation. Inserted into the upper part of the tracheal bifurcation, pull out the inner core, intubate the ventilator, adjust the tidal volume of the mouse to maintain 250-300 ml/min, and adjust the respiratory rate to 110-130 times/min. The body temperature was maintained at 36.5-37°C using an infrared body temperature heater. The mice were fixed in the right lateral position, and a transverse incision was made from the left axilla. Open the thoracic cavity to expose the left ventricle and the left atrial appendage from the fourth or fifth intercostal space. Using the 7-0 lossless suture from the lower edge of the left atrial appendage about 2 mm through the myocardium surface to the side of the pulmonary artery cone, the ends of the suture were passed through a small piece of soft vinyl tubing to form a snare. Regional ischemia was induced by fixing the snare to the heart by clamping a hemostat. After 30 min of ischemia, the hearts were reperfused for 120 min by releasing the hemostat. Zinc (100 μg/kg) was given 5 min before reperfusion for 30 min.

2.3. Measurement of IS. After 2 h of I/R, the left anterior descending artery was ligated, and 1 ml of 2% Evans blue dye (Sigma-Aldrich, St. Louis, MO) was injected from the abdominal aorta. After the heart turned blue, the perfusion was stopped and the heart washed thoroughly with normal saline to distinguish between nonrisk areas and area at risk (AAR). Remove the heart and store in a refrigerator at -20°C for 2 h. After the heart is frozen and fixed, cut a slice of about 1 mm from the apex, a total of 4 pieces. The heart was incubated in 1% triphenyltetrazolium chloride (TTC, Sigma-Aldrich, St. Louis, MO) at 37°C for 20 minutes to distinguish the infarct area (white, IS) from the risk area (red). The sections were fixed in 10% paraformaldehyde for 2 h to distinguish the stained areas from the unstained areas. The area of nonrisk areas, area at risk, and infarcted areas was analyzed by ImageJ software (National Institutes of Health, Bethesda, MD). The percentage of infarct size was calculated as IS/AAR × 100%.

2.4. Hypoxia/Reoxygenation of Cardiac Cells. Mouse atrial myocyte cell line HL-1 was obtained from the American Type Culture Collection (ATCC, Manassas, VA) and cultured in Claycomb Medium (Sigma, San Francisco, USA) with 10% fetal bovine serum (FBS) (Invitrogen, Carlsbad, CA) and 1‰ streptomycin at 37°C in the 5% CO_2-95% air atmosphere. After cells grow to a density of 90%, digest with 0.25 mM trypsin, dilute to different densities, and inoculate them in different well plates, such as 6-well plates (5.6×10^4 cells/well), 96-well plates (2×10^3 cells/well), and confocal plates (2×10^4 cells/plate). For hypoxia/reoxygenation (H/R) experiments, cells were cultured in low-glucose

DMEM (Invitrogen, Carlsbad, CA) with free FBS and were placed in a hypoxic chamber (Coylab, Grass Lake, MI) and cultured with 95% N_2/5% CO_2 at 37°C for 24 h. During 6 h of reoxygenation, HL-1 cells were incubated in DMEM containing 10% FBS at 37°C in the 5% CO_2-95% air atmosphere.

2.5. Plasmid Construction, siRNA Synthesis, and Transient Transfection into HL-1 Cells. Full-length cDNAs for mouse SUMO1, UBC9, SENP2, and Drp1 were obtained by RT-PCR using total RNA extracted from HL-1 cells, and their sequences were confirmed by BigDye sequencing (Applied Biosystems). SUMO1, UBC9, SENP2, and Drp1 full-length cDNAs were subcloned into the mammalian expression plasmid pcDNA3.1 (Life Technologies) harboring a HA, Flag, Myc tag at the C-terminus, respectively. Lysines 532, 535, 558, and 568 of Drp1 were replaced with leucine (Myc-Drp1 4KR) using the site-directed gene mutagenesis kit (Beyotime). siRNA oligonucleotides were synthesized by Sigma. The sequences were as follows: negative control siRNA: 5′-GAT CCG AAT TGC CAC AAC AGG GTC GTG TTC AAG AGA ATCA CAT CTT CTT CCT CCA TTC TTT TTTG-3′; SUMO1 siRNA: 5′-GAT CCG CCT TCA TAT TAC CCT CTC CTT TCA AGA GAA GGA GAG GGT AAT ATG AAG GCT TTT TTG-3′. The empty vectors, the target plasmid, negative control siRNA, and SUMO1 siRNA were transiently transfected into HL-1 cells using lipofectamine 2000 reagent (Invitrogen, Carlsbad, CA) according to the manufacturer's instructions. All experiments were conducted for 48 h after transfection.

2.6. Confocal Imaging of Mitochondrial Membrane Potential. The mitochondrial membrane potential ($\Delta\Psi$m) was measured by JC-10 (Solarbio, Beijing, China), the mitochondrial membrane fluorescent dye. HL-1 cells were incubated with JC-10 according to the manufacturer's instructions. The fluorescence changes were detected with a laser scanning confocal microscope. The maximum excitation wavelength of JC-10 monomer is 515 nm and the maximum emission wavelength is 529 nm (green); the maximum excitation wavelength of JC-10 polymer is 585 nm, and the maximum emission wavelength is 590 nm (red).

2.7. Measurement of Reactive Oxygen Species. HL-1 cells were stained with 2,7-dichlorodihydrofluorescein diacetate (DCFH-DA,10 μM/l) (Solarbio, Beijing, China) for 20 minutes in Claycomb Medium with free FBS. The cells were washed three times with serum-free medium and were directly observed by confocal microscopy with serum-free cultures, using 488 excitation light and 525 emission light to capture green fluorescence.

2.8. Western Blotting. After protein sample extraction, the concentration was consistently applied in an equal volume of 30 μg and electrophoresed on 10-12% polyacrylamide gel. The protein was transferred to polyvinylidene fluoride membranes, blocked with 5% skim milk for 90 min, and incubated with the primary antibody at 4°C overnight. Primary antibodies included anti-SUMO1 (ab11672; Abcam, Cambridge, MA), anti-UBC9 (ab75854; Abcam, Cambridge, MA), anti-Bcl2 (ab692; Abcam, Cambridge, MA), anti-Bax (ab32503; Abcam, Cambridge, MA), anti-caspase3 (ab13847; Abcam, Cambridge, MA), anti-active caspase-3 antibody (ab2302; Abcam, Cambridge, MA), anti-Tom20 antibody (ab56783; Abcam, Cambridge, MA), anti-Tim23 antibody (ab116329; Abcam, Cambridge, MA), anti-Drp1 antibody (ab184247; Abcam, Cambridge, MA), anti-LC3B antibody (ab51520; Abcam, Cambridge, MA), anti-p62 antibody (ab56416; Abcam, Cambridge, MA), and anti-GAPDH antibody (ab128915; Abcam, Cambridge, MA). Primary antibodies were recovered and incubated with the secondary antibody for 1 h at room temperature. The membranes were visualized with the enhanced chemiluminescence reagents (Millipore, Boston, MA).

2.9. Immunoprecipitation. HL-1 cells were immunoprecipitated with antibodies to either SUMO1 or Drp1 using the Pierce™ Crosslink Magnetic IP/Co-IP Kit (88805, Thermo Fisher, Waltham, Massachusetts, USA) according to the manufacturer's instructions. The samples were then subjected to the standard Western blotting techniques and the membranes probed, respectively, with antibodies to Drp1 and SUMO1.

2.10. Experimental Protocols. Mouse hearts were subjected to 30 min of regional ischemia, followed by 2 h of reperfusion. The mice were treated with zinc (100 μg/kg; Sigma, St. Louis, MO, USA) via the tail vein 5 min before reperfusion for 30 min. HL-1 cells were exposed to 1% O_2 with Claycomb Medium for 24 h followed by 6 h of reoxygenation. Zn^{2+} chelator N,N,N′,N′-tetrakis-(2-pyridylmethyl) ethylenediamine (TPEN, 20 μM) (Sigma-Aldrich, St. Louis, MO) was given 2 h after transfection with the vector or plasmid for 48 h.

2.11. Statistical Analysis. Data are expressed as mean ± SEM and were obtained from 5 to 10 separate experiments. Statistical significance was determined using the Student t-test or one-way ANOVA followed by Tukey's test. A value of $P < 0.05$ was considered as statistically significant.

3. Results

3.1. Effects of Zinc on SUMO Family Proteins under Normoxic and H/R Conditions. Researches have reported that SUMOs play an important role in cerebral ischemia and cardiac ischemia. We have previously shown that zinc protects the heart against ischemia-reperfusion injury in isolated rat hearts and H9c2, so we investigate whether SUMO family proteins are involved in the protective effect of zinc on myocardial ischemia-reperfusion injury. As shown in Figures 1(a)–1(e) ($n = 6$), compared with the control group, H/R injury significantly decreased the SUMO1 conjugation of proteins. However, H/R injury did not affect the SUMO2/3 conjugation. Furthermore, the levels of SENP2, SENP5, and SENP7 decreased, whereas zinc reversed the effect of H/R on SUMO1, SENP2, SENP5, and SENP7. Under the normoxic conditions, zinc also downregulated SENP5 and SENP7 levels but did not have an effect on SUMO1 conjugation and SENP2 protein. Interestingly, the sole SUMO ligase UBC9 was also expressed at lower levels in the setting of

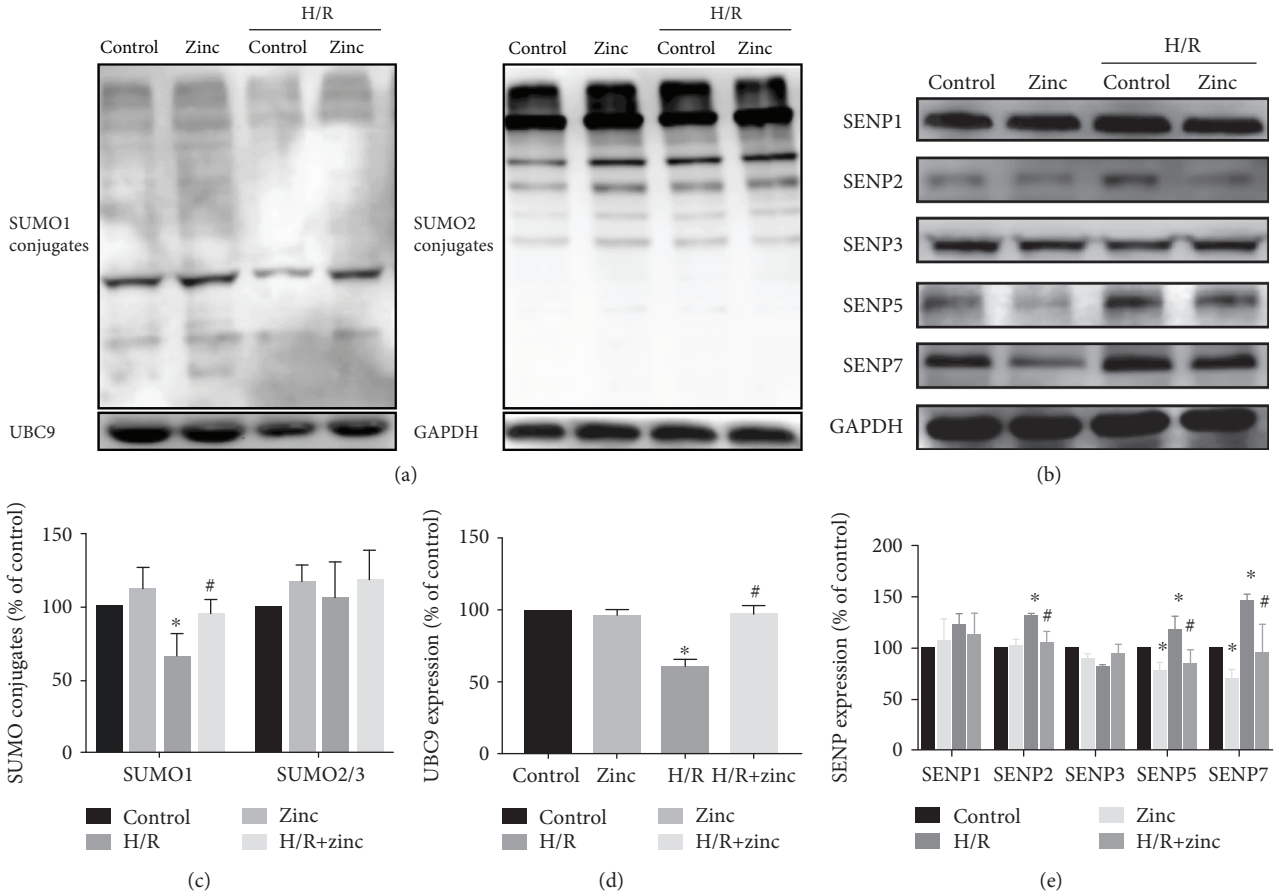

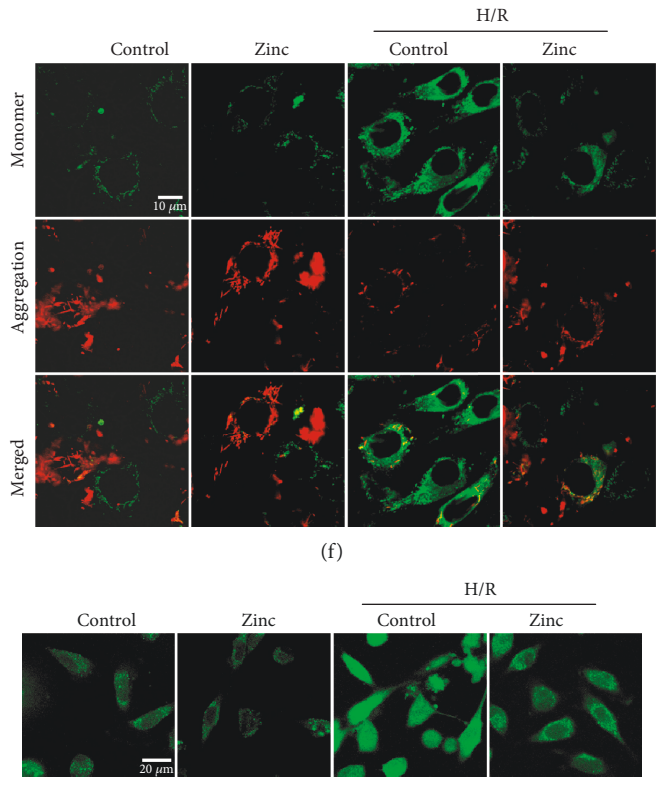

Figure 1: Continued.

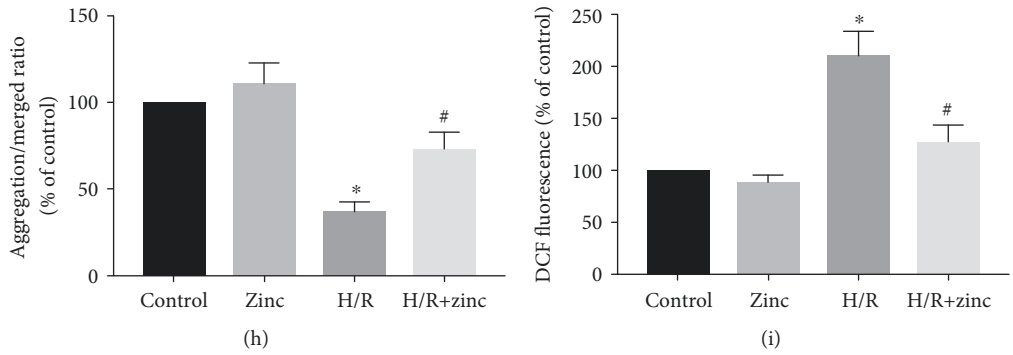

Figure 1: Effects of zinc on SUMO family members under physiological and H/R conditions. Compared with the control group, SUMO1 modification level of proteins and UBC9 in the H/R group decreased. The levels of SENP2, SENP5, and SENP7 decreased, while zinc (5 μM) reversed the changes of SUMO1 and SENP2, SENP5, and SENP7 (a–e, $n = 6$). Compared with the H/R group, the aggregation/monomer ratio stained with JC-1 was reversed by zinc. Scale bar: 10 μm (f, h; $n = 10$). Zinc inhibited H/R-induced increase of ROS detected by DCFH-DA. Scale bar: 20 μm (g, i; $n = 10$). $^{*}P < 0.05$ vs. control; $^{\#}P < 0.05$ vs. H/R. H/R: hypoxia/reoxygenation.

ischemia/reperfusion, which was reversed by zinc. Together, these data suggest that SUMO1 conjugation and SENP2 levels are highly regulated by zinc in the setting of H/R injury but not under normoxic conditions. At the same time, H/R caused a loss of $\Delta\Psi$m indicated by the decrease in the red (aggregate)/green (monomer) ratio and increased cellular ROS detected by DCF fluorescence intensity, which was reversed by zinc (Figures 1(f)–1(i), $n = 10$).

3.2. SUMO1 Contributes to the Protective Effect of Zinc on H/R Injury. To examine if zinc protects cardiac cells from H/R injury via SUMO1, we determined the effect on the cleaved caspase3/caspase3 ratio, the Bcl2/Bax ratio, and the ratio of the JC-1 aggregation/monomer. As shown in Figures 2(a)–2(d) ($n = 6$), compared with the H/R group, zinc attenuated myocardial apoptosis by reducing the cleaved caspase3/caspase3 ratio but increasing the Bcl2/Bax ratio, which were reversed by SUMO1 siRNA and overexpressing SENP2. Similarly, compared with the H/R group, zinc increased the JC-1 ratio at reoxygenation, which was again abrogated by SUMO1 siRNA and overexpressing SENP2 (Figures 2(e) and 2(f), $n = 7$). These data suggest that SUMO1 contributes to the protective effect of zinc on H/R injury.

3.3. Zinc Protects the Heart against I/R Injury through SUMO1 in Isolated Mouse. To probe if elevated SUMO1 conjugation has an effect on the protective role of zinc, the SUMO1 knockout mice were subjected to 30 min regional ischemia followed by 2 h reperfusion. As shown in Figure 3(a) ($n = 5$), we observed variable decrease in the SUMO1 conjugations in the SUMO1 KO mice. The effects of zinc on IS and apoptosis were assessed in the WT and SUMO1 KO mice hearts. Compared to I/R, zinc reduced IS, and this effect of zinc was abolished by SUMO1 knockout (Figures 3(b) and 3(c), $n = 6$). In addition, zinc attenuated myocardial apoptosis by reducing the cleaved caspase3 ratio but increasing the Bcl2/Bax ratio, which were reversed by SUMO1 knockout (Figures 3(d)–3(f), $n = 5$).

3.4. Zinc Regulates the SUMOylation of Drp1. Drp1 is a substrate of SUMO modification, so we test whether the protective role of zinc on I/R injury is dependent on Drp1 SUMOylation. Consistent with this, endogenous Drp1 interacts with SUMO1 in HL-1 cells and zinc treatment enhanced its interaction with SUMO1 (Figures 4(a) and 4(b), $n = 5$). To fully confirm the critical role of zinc on Dpr1 SUMO1-ylation, we made a non-SUMOylation Drp1 by mutating the four accepter lysines to arginines (Drp1 4KR). Compared to the zinc group, the SUMO1, UBC9, and Drp1 cotransfection increased the Drp1 SUMO1-ylation, which was abrogated by Drp1 4KR (Figures 4(c) and 4(d), $n = 5$). These data demonstrated that zinc regulates the Drp1 SUMO1-ylation.

3.5. Zinc Increased Mitophagy through SUMOylation of Drp1. Previous reports suggested that Drp1 is downstream of the PINK1 signaling pathway. We have previously found that zinc induced autophagy via the PINK1 pathway; therefore, we next investigated whether SUMOylation of Drp1 induced by zinc could regulate mitophagy. As shown in Figure 5(a) ($n = 7$), compared to the H/R group, zinc increased the colocalization of GFP-LC3 and TOM20, which was reversed by Drp1 4KR, indicating that zinc might induce mitophagy through Drp1 SUMOylation. Similar findings were obtained in further studies using Western blotting; compared to the H/R group, zinc significantly increased the ratio of LC3-II/I but significantly downregulated levels of p62 and mitochondrial marker proteins TOM20 and TIM23 (Figures 5(b)–5(d), $n = 5$), which was reversed by Drp1 4KR. Further experiments showed that the selective zinc chelator TPEN suppressed the increase in LC3-II/I and decrease in TOM20 and TIM23 induced by Drp1 overexpression (Figure 5(e), $n = 5$).

3.6. SUMOylation of Drp1 Contributes to the Protective Effect of Zinc on H/R Injury. To test whether zinc prevents H/R injury through Drp1 SUMOylation, we determined the change of $\Delta\Psi$m by detecting the ratio of the JC-1 aggregate/monomer. Compared to the H/R group, zinc increased the JC-1 ratio, which was suppressed by Drp1 4KR (Figures 6(a) and 6(c), $n = 5$). The DCF analysis showed that, compared to the H/R group, zinc decreased the DCF

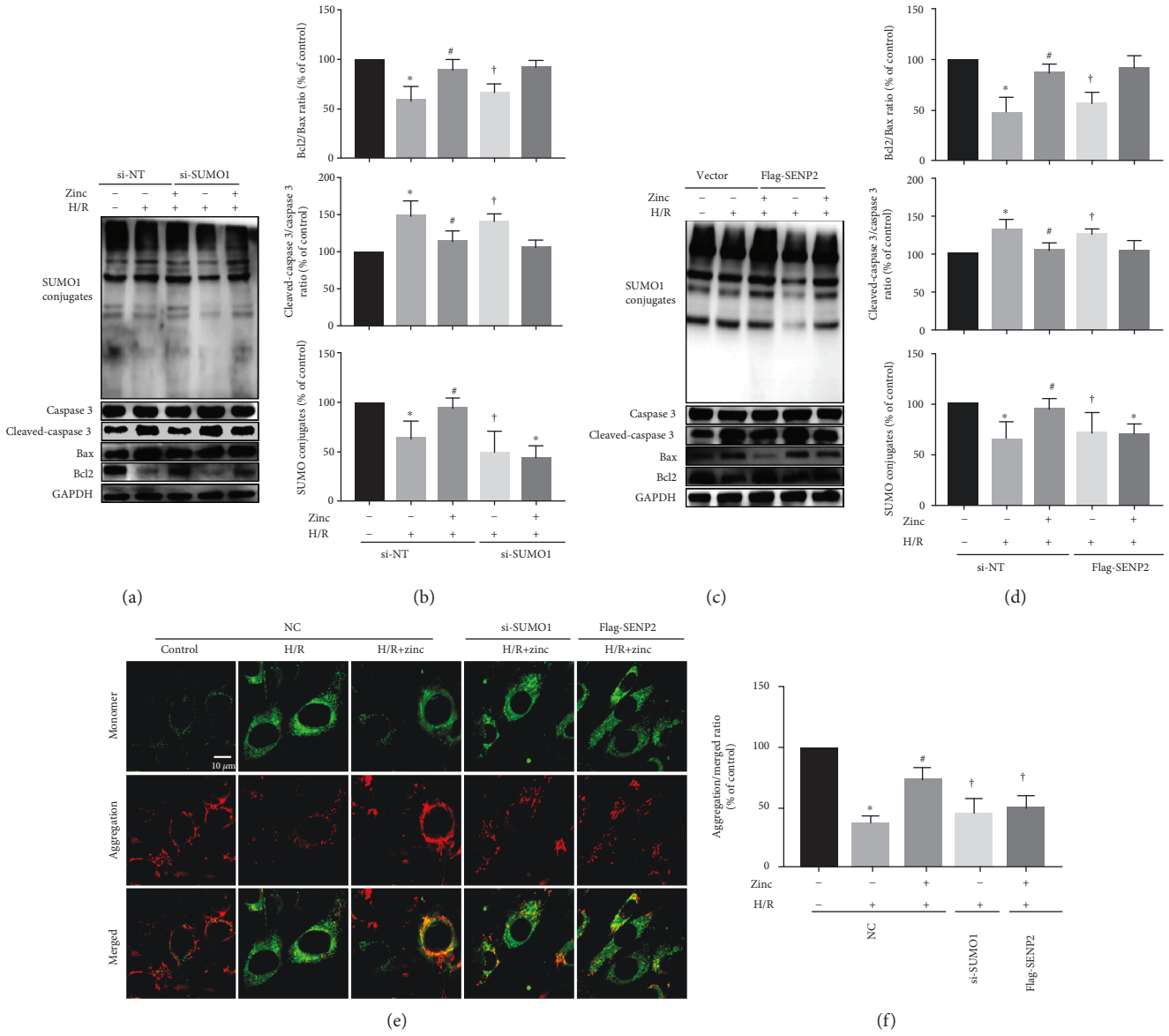

Figure 2: SUMO1 and SENP2 play an important role in the cardioprotective effect of zinc on H/R injury. Compared with the H/R group, zinc attenuated apoptosis by increasing the Bcl2/Bax ratio and decreasing the cleaved caspase3/caspase3 ratio, which were abolished by SUMO1 siRNA (a, b; $n = 6$) and overexpressed with SENP2 (c, d; $n = 6$). Compared with the H/R group, zinc inhibited the decrease of mitochondrial membrane potential detected by JC-1, which was abolished by SUMO1 siRNA (a, b; $n = 6$) and overexpressed with SENP2 (e, f; $n = 7$). Scale bar: 10 μm. $^{*}P < 0.05$ vs. control; $^{\#}P < 0.05$ vs. H/R. $^{\dagger}P < 0.05$ vs. H/R+zinc. H/R: hypoxia/reoxygenation; NC: negative control.

fluorescence intensity, which could be also abrogated by Drp1 4KR (Figures 6(b) and 6(d), $n = 5$).

4. Discussion

In this study, we have confirmed that SUMOylation of Drp1 plays an important role in the protective effect of zinc on H/R injury. When the heart suffers from I/R, SUMO1 conjugates are inactivated, zinc induced mitophagy via increasing Drp1 SUMO1-ylation. Mitophagy induced by Drp1 SUMOylation cleared damaged mitochondria, controlled mitochondrial quality, and prevented ROS generation, which improves myocardial function and reduces myocardial I/R damage.

Zinc is discovered in almost all biological tissues as one of the essential trace elements for the physiological and catalytic functions of the body [21]. Previous studies have reported that zinc is involved in myocardial differentiation and regeneration, arrhythmia, cardiac ischemia and reperfusion, and cardiac transplantation recovery [22]. Zinc given at reperfusion could reduce infarct size indirectly through signal factors, or directly as a signal molecule [23, 24]. Zinc is involved in cardioprotection indirectly through changing kinase activity, such as PI3K/Akt, ERK, glycogen synthase kinase 3β (GSK-3β), or by regulating the second messenger. For example, zinc alters intracellular second messenger cAMP activity by stimulating the activity of cyclic nucleotide phosphodiesterases (PDEs) [23, 25–27]. In addition, zinc is

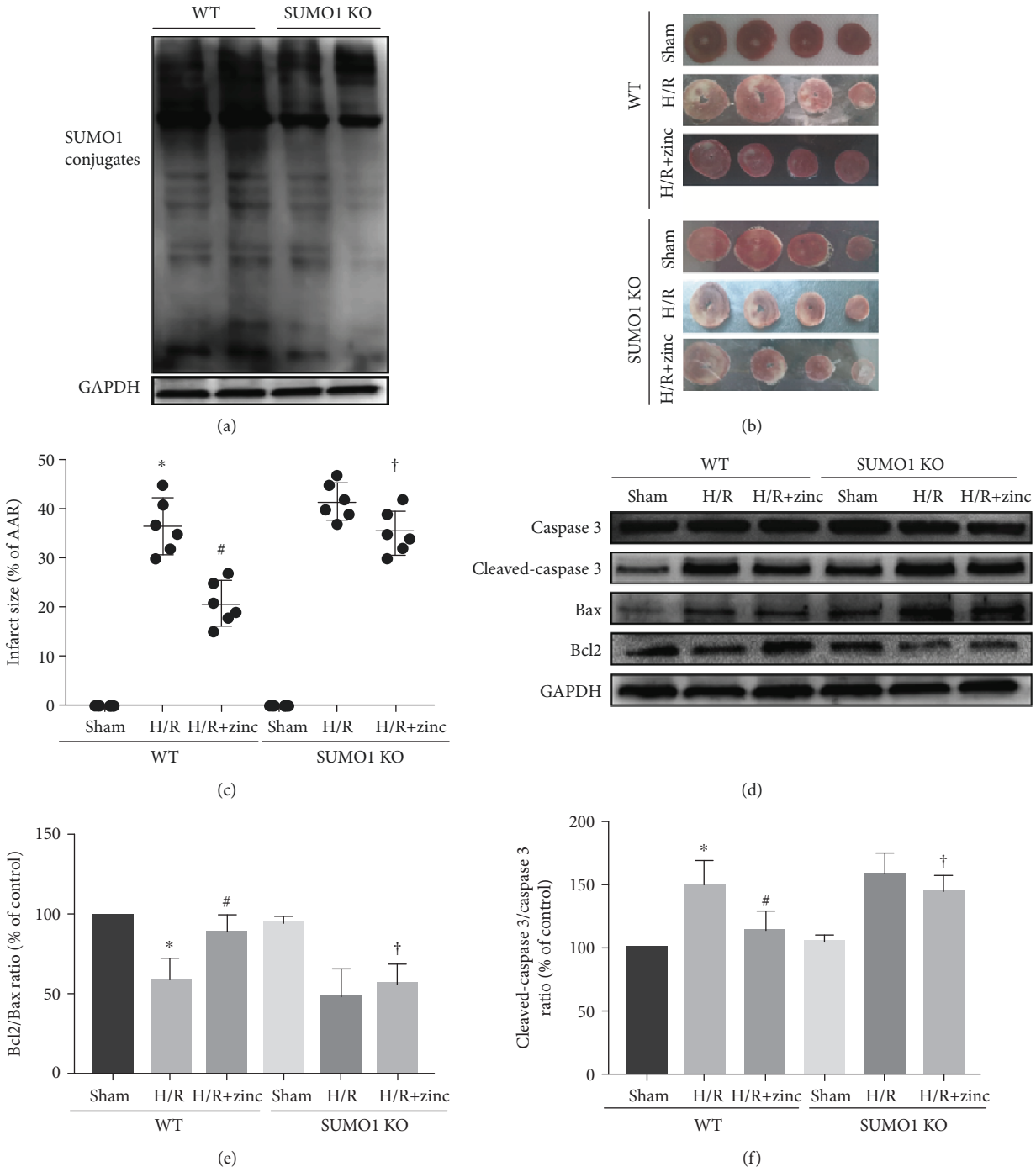

Figure 3: Effect of SUMO1 on zinc preconditioning-mediated myocardial injury reduction at the end of reperfusion in a Langendorff local I/R model. Compared to WT mice, the level of SUMOylation of proteins in the myocardium of SUMO1 KO mice decreased (a, $n = 5$). SUMO1 KO canceled the effect of zinc on attenuating myocardial infarct size (b, c; $n = 6$). Compared with the I/R group, zinc attenuated apoptosis by increasing the Bcl2/Bax ratio (d, e; $n = 5$) and decreasing the cleaved caspase3/caspase3 ratio (d, f; $n = 5$), which were abolished by SUMO1 KO. $^{*}P < 0.05$ vs. control; $^{\#}P < 0.05$ vs. I/R. $^{\dagger}P < 0.05$ vs. I/R+zinc. AAR indicates area at risk; I/R: ischemia/reperfusion; SUMO1 KO: SUMO1 knockout.

tightly linked to the cardioprotective effect through directly acting as intracellular signaling molecules [24]. In this context, we firstly reported that zinc increased the proteins of SUMOylation and decreased the levels of SENP2, SENP5, and SENP7. What is more, zinc given at reperfusion could protect mitochondria by increasing SUMO1 and decreasing the level of SENP2. SUMO1 knockout in mice heart significantly reversed the cardioprotective effect of zinc in the setting of H/R.

Although the global SUMO1 conjugations were significantly decreased at reperfusion, it is noteworthy to identify the target protein of SUMOylation modification.

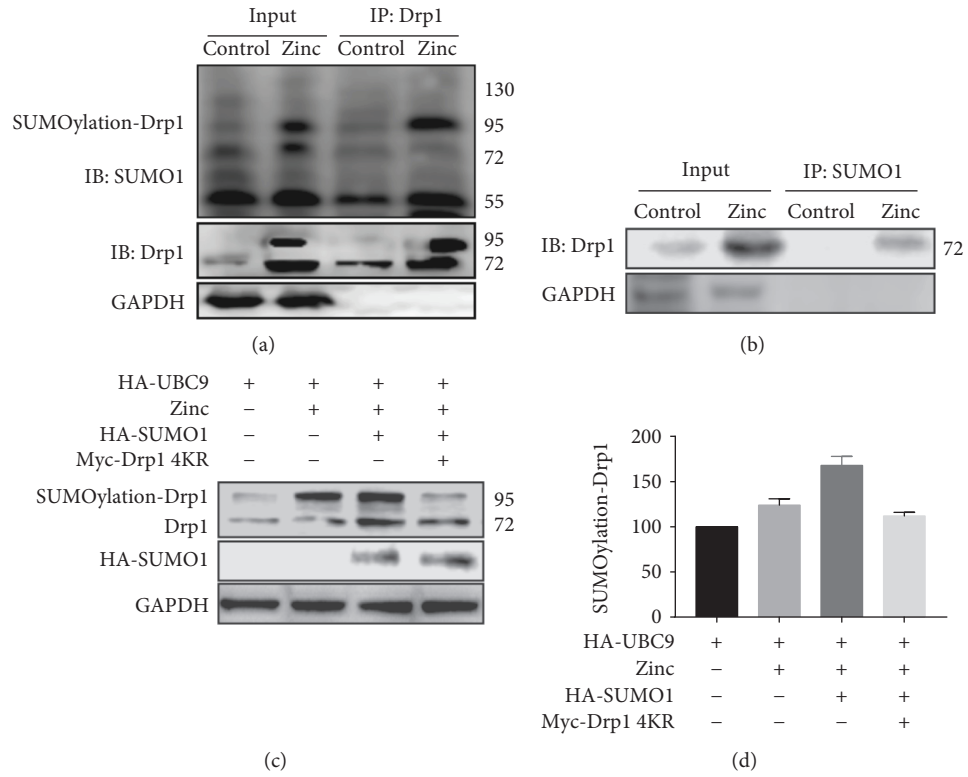

Figure 4: SUMOylation of Drp1 induced by zinc. Immunoprecipitation-immunoblot analyses examined the conjugation between Drp1 and SUMO1. Compared with the control group, zinc increased Drp1 SUMOylation (a, b; $n = 5$). Mutating four accepter lysines to arginines (Drp1 4KR) in cultured cardiomyocytes reduced zinc-induced Drp1 SUMOylation (c, d; $n = 5$). $^{*}P < 0.05$ vs. zinc; $^{\#}P < 0.05$ vs. zinc+HA-SUMO1.

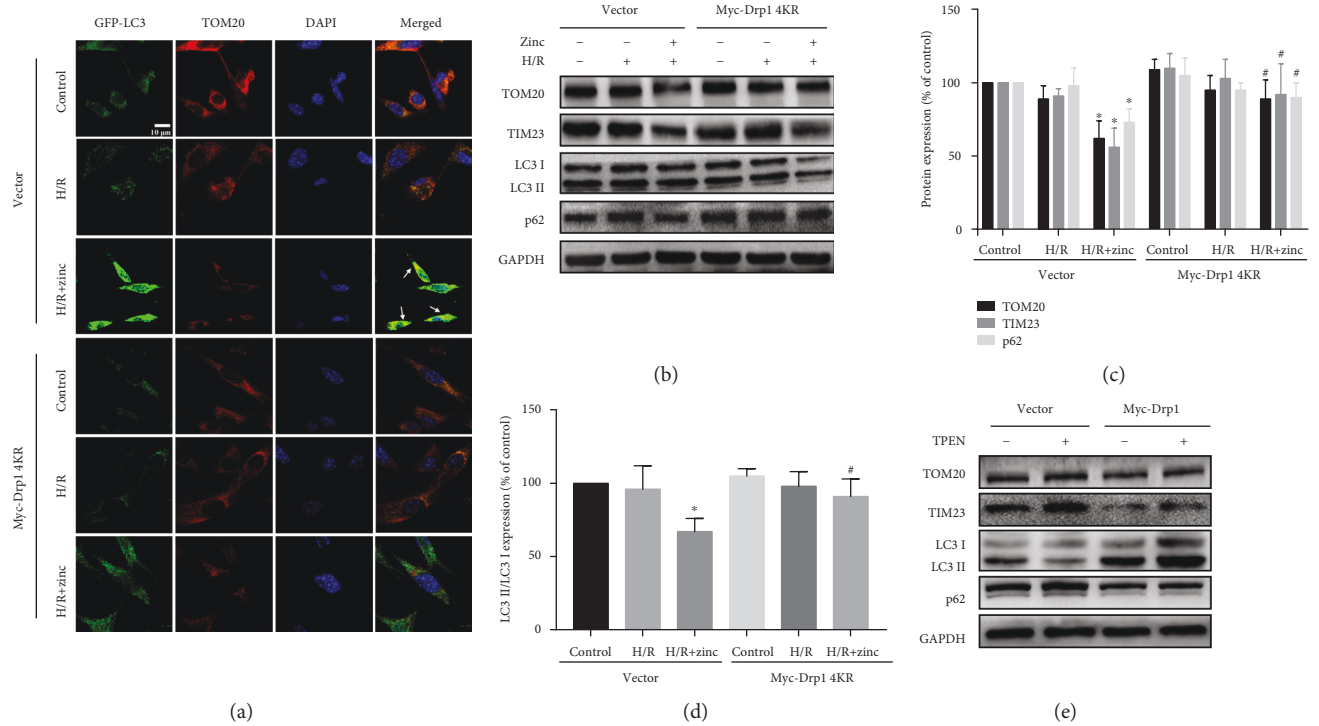

Figure 5: The role for Drp1 SUMO1-ylation in zinc-induced mitophagy. Confocal images of GFP-LC3 (green) and TOM20 (red). Increased LC3 was colocalized with TOM20 (a, $n = 7$). Effects of $ZnCl_2$ on TOM20, TIM23, p62, and LC3 levels were inhibited by Myc-Drp1 4KR and Myc-Drp1 (b–e; $n = 5$). $^{*}P < 0.05$ vs. H/R (Vector); $^{\#}P < 0.05$ vs. H/R+$ZnCl_2$ (Vector).

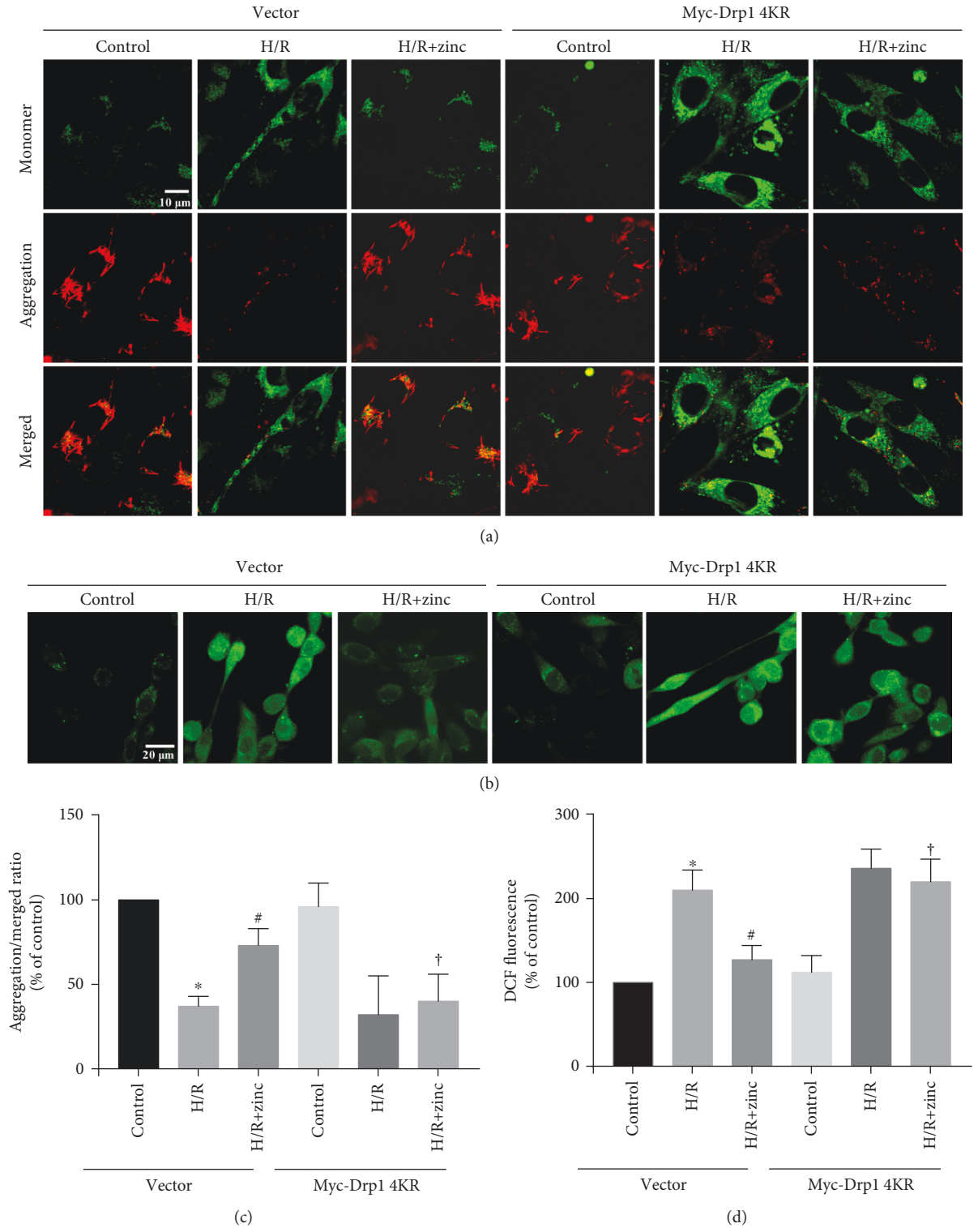

Figure 6: Effect of Myc-Drp1 4KR on zinc-mediated mitochondria protection in H/R-induced HL-1 cells. Compared with the H/R group, the aggregation/monomer ratio stained with JC-1 was reversed by zinc, which was abolished by Myc-Drp1 4KR (a, c; $n = 5$). Zinc inhibited H/R-induced increase of ROS, which was abolished by Myc-Drp1 4KR (b, d; $n = 5$). $^{*}P < 0.05$ vs. H/R (Vector); $^{\#}P < 0.05$ vs. H/R+$ZnCl_2$ (Vector).

Mitochondria is the main source of superoxide generation under pathophysiological status in cardiomyocytes and mitochondria cleavage and fusion homeostasis plays an important role in I/R injury. Drp1 is a key protein necessary for mitochondrial division [28]. It has been reported that Drp1 SUMO2/3-ylation plays a cytoprotective role in the brain OGD model. SENP3 specifically cleaves SUMO2/3 from Drp1 and reduces apoptosis [29]. In contrast to the apoptotic effects reported for SUMO1 conjugation, Prudent et al. [30] reported that Drp1 SUMO1-ylation

induced mitochondria division by recruiting Drp1 to mitochondria, leading to cell apoptosis. SENP5 overexpression mediated deSUMOylation of Drp1 and rescues Drp1 SUMO1-ylation-induced mitochondrial fragmentation. Consistent with this model, Jiang et al. discovered that Drp1 SUMO1-ylation increased the mitochondrial division, leading to neurodegeneration. In this model, SENP2 has an impact on the deSUMOylation of Drp1 [20]. Our data indicated that zinc has an adaptive protective response to I/R injury. Drp1 and its specific SENP may play different roles, which depend on the state of the cells and the animal models. Future research will be warranted to resolve these issues.

Drp1 was an important factor regulating mitochondrial division in cardiovascular disease [31]. Joshi et al. [31] have shown that endogenous Drp1 can bind to Bcl-1/Bcl-xL under physiological and I/R stress conditions. Bcl-1/Bcl-xL is an endogenous inhibitor of the autophagy-inducing factor Beclin1. Consistent with this, Drp1 knockout suppressed autophagy by increasing the conjugation of Beclin1 and Bcl-1/Bcl-xL, which resulted in mitochondrial dysfunction and cardiomyocyte apoptosis. Similarly, our finding showed that zinc induced mitophagy by increasing SUMOylation of Drp1, which led to damaged mitochondrial clearance and prevention of ROS generation in the setting of cardiac I/R. Although it is the first time to report such a protective mechanism of zinc, a mass of questions remain to be future researched.

In summary, this study demonstrated that SUMOylation of Drp1 played an essential role in zinc-induced cardioprotection against I/R injury. SUMOylation of Drp1 caused by zinc increased mitophagy at reperfusion as a result of prevention of ROS and myocardial injury. SUMO1, as a posttranslational modification factor, mediates the action of zinc through Dpr1, which provides a new insight into the mechanisms underlying cardioprotection of zinc. We believe that our findings certainly warrant further investigations for application in the clinical setting.

Data Availability

All the data used to support the findings of this study are available from the corresponding authors upon request.

Conflicts of Interest

The authors declare that they have no conflicts of interest.

Authors' Contributions

Xiyun Bian and Jingman Xu contributed equally to the study.

Acknowledgments

The present study was supported by the National Natural Science Foundation of China (Grant no. 81700324), the Hebei Provincial Natural Science Foundation (Grant no. H2018209378), and the Tianjin Natural Science Foundation (Grant no. 18JCQNJC12800).

References

[1] S. E. Boag, E. Andreano, and I. Spyridopoulos, "Lymphocyte communication in myocardial ischemia/reperfusion injury," *Antioxidants & Redox Signaling*, vol. 26, no. 12, pp. 660–675, 2017.

[2] M. Sheng, G. Zhang, J. Wang et al., "Remifentanil induces cardio protection against ischemia/reperfusion injury by inhibiting endoplasmic reticulum stress through the maintenance of zinc homeostasis," *Anesthesia & Analgesia*, vol. 127, no. 1, pp. 267–276, 2018.

[3] J. Adulcikas, S. Sonda, S. Norouzi, S. Sohal, and S. Myers, "Targeting the zinc transporter ZIP7 in the treatment of insulin resistance and type 2 diabetes," *Nutrients*, vol. 11, no. 2, p. 408, 2019.

[4] G. Zhang, M. Sheng, J. Wang et al., "Zinc improves mitochondrial respiratory function and prevents mitochondrial ROS generation at reperfusion by phosphorylating STAT3 at Ser^{727}," *Journal of Molecular and Cellular Cardiology*, vol. 118, pp. 169–182, 2018.

[5] X. Bian, T. Teng, H. Zhao et al., "Zinc prevents mitochondrial superoxide generation by inducing mitophagy in the setting of hypoxia/reoxygenation in cardiac cells," *Free Radical Research*, vol. 52, no. 1, pp. 80–91, 2018.

[6] Y. Shimizu, J. P. Lambert, C. K. Nicholson et al., "DJ-1 protects the heart against ischemia–reperfusion injury by regulating mitochondrial fission," *Journal of Molecular and Cellular Cardiology*, vol. 97, pp. 56–66, 2016.

[7] J. Karhausen, J. D. Bernstock, K. R. Johnson et al., "Ubc9 overexpression and SUMO1 deficiency blunt inflammation after intestinal ischemia/reperfusion," *Laboratory Investigation*, vol. 98, no. 6, pp. 799–813, 2018.

[8] V. Tiwari, "Post-translational modification of ESKAPE pathogens as a potential target in drug discovery," *Drug Discovery Today*, vol. 24, no. 3, pp. 814–822, 2019.

[9] H. J. Zhou, Z. Xu, Z. Wang, H. Zhang, M. Simons, and W. Min, "SUMOylation of VEGFR2 regulates its intracellular trafficking and pathological angiogenesis," *Nature Communications*, vol. 9, no. 1, p. 3303, 2018.

[10] Y. Y. Li, H. Wang, X. X. Yang et al., "*Small ubiquitin-like modifier 4 (SUMO4)* gene M55V polymorphism and type 2 diabetes mellitus: a meta-analysis including 6,823 subjects," *Frontiers in Endocrinology*, vol. 8, p. 303, 2017.

[11] K. Kunz, T. Piller, and S. Muller, "SUMO-specific proteases and isopeptidases of the SENP family at a glance," *Journal of Cell Science*, vol. 131, no. 6, 2018.

[12] J. D. Bernstock, W. Yang, D. G. Ye et al., "SUMOylation in brain ischemia: patterns, targets, and translational implications," *Journal of Cerebral Blood Flow & Metabolism*, vol. 38, no. 1, pp. 5–16, 2018.

[13] M. P. C. Mulder, R. Merkx, K. F. Witting et al., "Total chemical synthesis of SUMO and SUMO-based probes for profiling the activity of SUMO-specific proteases," *Angewandte Chemie International Edition*, vol. 57, no. 29, pp. 8958–8962, 2018.

[14] Z. Zhang, J. Du, S. Wang et al., "OTUB2 promotes cancer metastasis via hippo-independent activation of YAP and TAZ," *Molecular Cell*, vol. 73, no. 1, pp. 7–21.e7, 2019.

[15] L. Mendler, T. Braun, and S. Muller, "The ubiquitin-like SUMO system and heart function: from development to disease," *Circulation Research*, vol. 118, no. 1, pp. 132–144, 2016.

[16] Y. Du, P. Liu, T. Xu et al., "Luteolin modulates SERCA2a leading to attenuation of myocardial ischemia/ reperfusion injury via sumoylation at lysine 585 in mice," *Cellular Physiology and Biochemistry*, vol. 45, no. 3, pp. 883–898, 2018.

[17] M. J. Boyer and S. Eguchi, "A cytoskeletal anchor connects ischemic mitochondrial fission to myocardial senescence," *Science Signaling*, vol. 11, no. 556, article eaav3267, 2018.

[18] J. M. Henley, R. E. Carmichael, and K. A. Wilkinson, "Extranuclear SUMOylation in neurons," *Trends in Neurosciences*, vol. 41, no. 4, pp. 198–210, 2018.

[19] C. Guo, K. A. Wilkinson, A. J. Evans, P. P. Rubin, and J. M. Henley, "SENP3-mediated deSUMOylation of Drp1 facilitates interaction with Mff to promote cell death," *Scientific Reports*, vol. 7, no. 1, article 43811, 2017.

[20] J. Fu, H. M. I. Yu, S. Y. Chiu et al., "Disruption of SUMO-specific protease 2 induces mitochondria mediated neurodegeneration," *PLoS Genet*, vol. 10, no. 10, article e1004579, 2014.

[21] T. Hara, T. A. Takeda, T. Takagishi, K. Fukue, T. Kambe, and T. Fukada, "Physiological roles of zinc transporters: molecular and genetic importance in zinc homeostasis," *The Journal of Physiological Sciences*, vol. 67, no. 2, pp. 283–301, 2017.

[22] S. Zhong and R. A. Khalil, "A disintegrin and metalloproteinase (ADAM) and ADAM with thrombospondin motifs (ADAMTS) family in vascular biology and disease," *Biochemical Pharmacology*, vol. 164, pp. 188–204, 2019.

[23] H. Mnatsakanyan, R. S. i. Serra, P. Rico, and M. Salmerón-Sánchez, "Zinc uptake promotes myoblast differentiation via Zip7 transporter and activation of Akt signalling transduction pathway," *Scientific Reports*, vol. 8, no. 1, article 13642, 2018.

[24] D. S. Chu, "Zinc: a small molecule with a big impact on sperm function," *PLoS Biology*, vol. 16, no. 6, article e2006204, 2018.

[25] B. Pochwat, A. Rafało-Ulińska, H. Domin, P. Misztak, G. Nowak, and B. Szewczyk, "Involvement of extracellular signal-regulated kinase (ERK) in the short and long-lasting antidepressant-like activity of NMDA receptor antagonists (zinc and Ro 25-6981) in the forced swim test in rats," *Neuropharmacology*, vol. 125, pp. 333–342, 2017.

[26] E. Tuncay, Y. Olgar, A. Durak, S. Degirmenci, C. V. Bitirim, and B. Turan, "β3-adrenergic receptor activation plays an important role in the depressed myocardial contractility via both elevated levels of cellular free Zn^{2+} and reactive nitrogen species," *Journal of Cellular Physiology*, vol. 234, no. 8, pp. 13370–13386, 2019.

[27] J. Y. Koh, H. N. Kim, J. J. Hwang, Y. H. Kim, and S. E. Park, "Lysosomal dysfunction in proteinopathic neurodegenerative disorders: possible therapeutic roles of cAMP and zinc," *Molecular Brain*, vol. 12, no. 1, p. 18, 2019, Article ID 30866990, 15 pages.

[28] T. Cao, S. Fan, D. Zheng et al., "Increased calpain-1 in mitochondria induces dilated heart failure in mice: role of mitochondrial superoxide anion," *Basic Research in Cardiology*, vol. 114, no. 3, p. 17, 2019.

[29] C. Guo, K. L. Hildick, J. Luo, L. Dearden, K. A. Wilkinson, and J. M. Henley, "SENP3-mediated deSUMOylation of dynamin-related protein 1 promotes cell death following ischaemia," *The EMBO Journal*, vol. 32, no. 11, pp. 1514–1528, 2013.

[30] J. Prudent, R. Zunino, A. Sugiura, S. Mattie, G. C. Shore, and H. M. McBride, "MAPL SUMOylation of Drp1 stabilizes an ER/mitochondrial platform required for cell death," *Molecular Cell*, vol. 59, no. 6, pp. 941–955, 2015.

[31] A. U. Joshi, A. E. Ebert, B. Haileselassie, and D. Mochly-Rosen, "Drp1/Fis1-mediated mitochondrial fragmentation leads to lysosomal dysfunction in cardiac models of Huntington's disease," *Journal of Molecular and Cellular Cardiology*, vol. 127, pp. 125–133, 2019.